Iron- and Copper-catalyzed Borylation of Alkyl and Aryl Halides and B–B Bond Activation and NHC Ring-expansion Reactions of the Diboron(4) Compound Bis(ethylene glycolato)diboron (B_2eg_2)

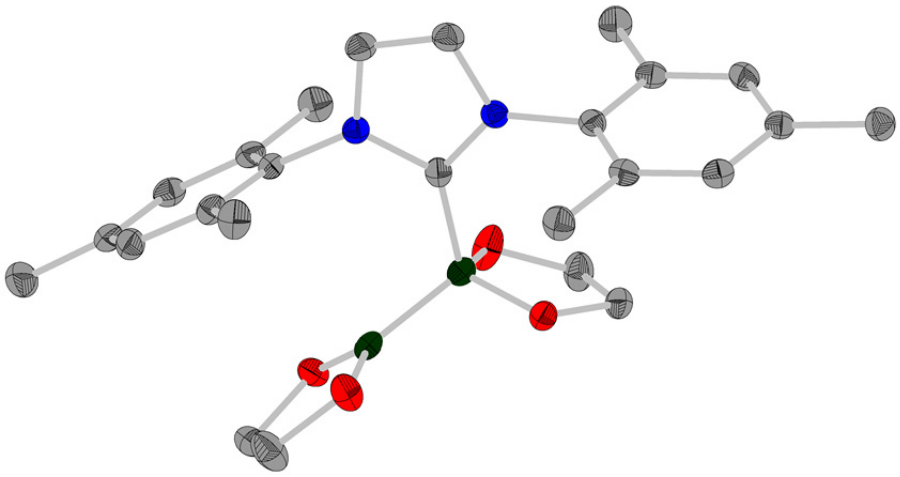

Dissertation zur Erlangung des naturwissenschaftlichen Doktorgrades der Julius-Maximilians-Universität Würzburg

vorgelegt von

Martin Eck

aus Suhl

Würzburg 2017

Eingereicht bei der Fakultät für Chemie und Pharmazie

am: _____

Gutachter der schriftlichen Arbeit

1. Gutachter: Prof. Dr. Todd B. Marder

2. Gutachter: Prof. Dr. Udo Radius

Prüfer des öffentlichen Promotionskolloquiums

1. Prüfer: Prof. Dr. Todd B. Marder

2. Prüfer: Prof. Dr. Udo Radius

3. Prüfer: _____

Datum des öffentlichen Promotionskolloquiums

am: _____

Doktorurkunde ausgehändigt

am: _____

Die Experimente zur vorliegenden Arbeit wurden in der Zeit von März 2012 bis Juli 2016 am Institut für Anorganische Chemie der Julius-Maximilians-Universität Würzburg in Betreuung von Prof. Dr. Todd B. Marder durchgeführt.

AFFIDAVIT

I hereby confirm that my thesis entitled “Iron- and Copper-catalyzed Borylation of Alkyl and Aryl Halides and B–B Bond Activation and NHC Ring-expansion Reactions of the Diboron(4) Compound Bis(ethylene glycolato)diboron (B_2eg_2)” is the result of my own work. I did not receive any help or support from commercial consultants. All sources and / or materials applied are listed and specified in the thesis.
Furthermore, I confirm that this thesis has not yet been submitted as part of another examination process either in identical or in similar form.

EIDESSTATTLICHE ERKLÄRUNG

Hiermit erkläre ich an Eides statt, die Dissertation “Iron- and Copper-catalyzed Borylation of Alkyl and Aryl Halides and B–B Bond Activation and NHC Ring-expansion Reactions of the Diboron(4) Compound Bis(ethylene glycolato)diboron (B_2eg_2)” eigenhändig, d.h. insbesondere selbstständig und ohne Hilfe eines kommerziellen Promotionsberaters angefertigt und keine anderen als die von mir angegebenen Quellen und Hilfsmittel verwendet zu haben.
Ich erkläre außerdem, dass die Dissertation weder in gleicher noch in ähnlicher Form bereits in einem anderen Prüfungsverfahren vorgelegen hat.

Würzburg, den

Ingo Eck

****1st November 1962 – †22nd March 1984***

Loved and Unforgotten

ACKNOWLEDGEMENT

I want to thank Prof. Todd B. Marder for the opportunity to do my PhD thesis under his supervision. I also want to thank him for the infinite support he gave me in any situation. I will never forget the meetings, conferences and parties we joined and the fun we had together. However, there were also tough situations during the last five years during which I asked him for advice, and he always had good advice for me. I am very happy that I have had the chance to meet Todd and I highly appreciate his knowledge as scientist and even more his humanity. This combination made him the mentor I always was looking for. Moreover, I want to thank sincerely his wife, Anne, for her great support as well. I will be forever grateful for this! It was an honor and a great pleasure to work in the Marder group, and I am happy to be a part of the family as well as of the boron community.

Furthermore, I want to thank Prof. Dr. Udo Radius for the fruitful discussions, advice and the great help I got in general, and especially while writing the manuscript of our paper. In addition, I want to point out the fantastic collaboration we have with his working group. I highly appreciate the unique spirit of the Radius group, and will keep the memories forever.

I want to thank Dr. Christian Kleeberg for the great time and fruitful discussions we had at the Euroboron 6 conference in Warsaw (2013) and for his suggestions regarding the copper chemistry.

I want to thank two persons who had a very great impact on my research and who helped me a lot: Dr. Sabrina Würtemberger-Pietsch and Antonius Eichhorn. I highly appreciate the discussions with Sabrina and Toni on synthesis as well as on chemical theory and paper writing. I thank Toni very much for having carried out all but two of the crystal structure determinations in this thesis and for the time sacrificed from his own thesis research. I thank Drs. Andreas Lorbach and Katharina Edkins (nee Fucke) for carrying out the other two structure determinations.

I want to thank my best friend Thomas Steffenhagen, whom I have known since 1998, and who convinced me to study chemistry. Our paths crossed multiple times during the last 15 years and I highly appreciate his friendship and humanity.

Furthermore, I want to thank Dr. Stephan Wagner for his help with the quantitation by GC-MS, his general support, and for teaching me how to use and maintain the GC-MS systems.

I want to thank sincerely Dr. Rüdiger Bertermann for his extensive assistance with recording and assigning the solid-state NMR spectra, as well as advice on other NMR issues, during my time as PhD student. I also want to thank Marie-Luise Schäfer for recording the many low temperature NMR spectra.

Moreover, I want to thank Christoph Mahler for carrying out the HRMS measurements, and for general support in the laboratory.

I want to thank the bachelor students I supervised for their assistance with some of the syntheses; Regina Wirth (University of Würzburg, Würzburg, Germany), Maxim K. Lang (University of Texas at Austin, TX, USA) and Chow Chun Fai (City University of Hong Kong, HK).

I want to thank my colleagues from laboratory 120 for the great atmosphere and the team spirit in our small lab area: Dr. Emily Neeve, Lujia Mao, Stefanie Griesbeck and Matthias Ferger.

Special thanks to Dr. Jörn Nitsch, Dr. Shubhankar Kumar Bose, Dr. Robert M. Edkins, Dr. Andreas Lorbach, Charlotte Scheufler, Roberto Molteni, Nicola Schwenk, Jens Seufert, Marco Stanoppi, Benjamin Hupp, Markus Gernert, Dr. Johannes Brand, Florian Rauch, Laura Kuehn, Julia Merz, Dr. Daniel Sieh, Florian Kerner, Jan Maier, Carolin Sieck, Dr. David Schmidt, Dr. Qing Ye, Julia Schuster, Sabine Lorenzen, Helga Dietrich, Patricia Schmidt, Eleonore Klaus, Stefanie Ziegler, Manfred Reinhart, Michael Ramold, Alfred Schertzer, Alois Ruf, Berthold Fertig, Wolfgang Obert, Cornelia Walter, Liselotte Michels, Sabine Timmroth for their infinite help.

I want to thank all people from the following working groups: AK Prof. Todd B. Marder, AK Prof. Udo Radius, AK Prof. Maik Finze, AK Prof. Holger Braunschweig for making my time in the Institute enjoyable.

I want to thank my family, my wife Claudia and my daughter Daria for the infinite support.

LIST OF PUBLICATIONS

The publication listed below is partly reproduced in this dissertation with permission from the Royal Society of Chemistry. The table itemizes to what extent the different sections of the paper have been reproduced, and at which position in this work.

Publication	Position
M. Eck, S. Würtemberger-Pietsch, A. Eichhorn, J. H. Berthel, R. Bertermann, U. S. Paul, H. Schneider, A. Friedrich, C. Kleeberg, U. Radius, T. B. Marder, *Dalton Trans* **2017**, *46*, 3661-3680.	Chapter Two 1 1.1 1.2 2.1 2.2 2.2.1 2.2.2.2 2.2.3.2 2.2.3.4 2.2.4 2.2.4.1 2.2.4.2

Further publications:

2015:

D. Scharnagel, A. Müller, F. Prause, M. Eck, J. Goller, W. Milius, M. Breuning, *Chem. Eur. J.* **2015**, *21*, 12488-12500.

LIST OF ABBREVIATIONS

AIBN	Azobisisobutyronitrile
ALS	Automatic liquid handling system
APCI	Atmospheric pressure chemical ionization
Ar	Aryl
ASAP	Atmospheric solids analysis probe
BNCT	Boron neutron capture therapy
bpy	2,2'-Bipyridine
brine	Sodium chloride solution
cat	Catecholato
cat.	Catalyst
COD	1,5-Cyclooctadiene
COE	Cyclooctene
Cp*	1,2,3,4,5-Pentamethylcyclopentadienyl
Cy	Cyclohexyl
Cy_2Im	1,3-Bis(cyclohexyl)imidazolin-2-ylidene
DFT	Density functional theory
diglyme	1-Methoxy-2-(2-methoxyethoxy)ethane
DIPE	Diisopropyl ether
Dipp	2,6-Diisopropylphenyl
$Dipp_2Im$	1,3-Bis-(2,6-diisopropylphenyl)imidazolin-2-ylidene
DMA	Dimethylacetamide
DME	Dimethoxyethane
DMF	Dimethylformamide
dmpe	1,2-Bis(dimethylphosphino)ethane
dppbz	1,2-Bis(diphenylphosphino)benzene
dppe	1,2-Bis(diphenylphosphino)ethane
dppf	1,1'-Bis(diphenylphosphino)ferrocene
dppp	1,3-Bis(diphenylphosphino)propane
dtbpy	4,4'-Di-*tert*-butyl-2,2'-bipyridine
eg	Ethylene glycolato

EI	Electron impact ionization
equiv	Equivalents
GC	Gas chromatography
h	Hour
Hex	Hexyl
HPLC	High performance liquid chromatography
HRMS	High-resolution mass spectrometry
iPr_2Im	1,3-(Diisopropyl)imidazolin-2-ylidene
iPr_2Im^{Me}	1,3-(Diisopropyl-4,5-dimethyl)imidazolin-2-ylidene
LIFDI	Liquid injection field desorption ionization
lit.	Literature
m	Multiplet
MAS	Magic-angle spinning
Me_2Im^{Me}	1,2,3,4-(Tetramethyl)imidazolin-2-ylidene
Mes_2Im	1,3-Bis-(2,4,6-trimethylphenyl)imidazolin-2-ylidene
Mes	Mesityl
MHz	Megahertz
min	Minute
MS	Mass spectrometry
MSD	Mass selective detector
MTBE	Methyl *tert*-butyl ether
neop	Neopentyl glycolato
NHC	*N*-heterocyclic carbene
NMR	Nuclear magnetic resonance
nPr_2Im	1,3-(Di-*n*-propyl)imidazolin-2-ylidene
OD	Outer diameter
phen	1,10-Phenanthroline
pin	Pinacolato
prim	Primary
pybox	2,6-Bis[(4S)-(−)-isopropyl-2-oxazolin-2-yl]pyridine
RER	Ring-expansion reaction
RF	response factor
RT	Room temperature
s	Singlet

sec	Secondary
t	Triplet
TEEDA	*N,N,N',N'*-tetraethylethylenediamine
temp.	Temperature
tert	Tertiary
THF	Tetrahydrofuran
TLC	Thin layer chromatography
TMEDA	*N,N,N',N'*-tetramethylethylenediamine
TMS	Trimethylsilyl
TON	Turnover number
UV	Ultraviolet
xantphos	4,5-Bis(diphenylphosphino)-9,9-dimethyl-xanthene

ABSTRACT

Organoboronate esters, especially arylboronates, are extremely useful reagents in organic synthesis. They can be used in Suzuki-Miyaura and other cross-coupling reactions, and the boronate can be converted into virtually any functional group. Thus, the challenge is to develop new ways to prepare boronate esters, using inexpensive metals with the lowest toxicity possible. While direct borylation of C–H bonds is very attractive, selectivity is predominantly determined by steric effects. Thus, alternative routes are still required, such as the borylation of C–X bonds. Therefore, the first part of this thesis covers a detailed investigation of the potential of iron-catalyzed borylation reactions with alkyl halides as substrates and B_2pin_2 as the borylation reagent.

Studies of the copper mediated borylation reactions of aryl halides were performed, including the screening of substrates and alkoxy bases as well as extensive ligand-screening. Investigations were undertaken using Cu-nanoparticles, which might be involved in this catalytic reaction. Furthermore, Cu-phosphine complexes were synthesized as catalyst precursors, and unsuccessful attempts were made to isolate Cu-boryl species which are key intermediates in this catalysis.

The second part of this thesis covers a detailed study on the diboron(4) compounds bis(ethylene glycolato)diboron (B_2eg_2), tetrakis(dimethylamino)diboron ($B_2(NMe_2)_4$), and tetramethoxydiboron ($B_2(OMe)_4$) and their reactivity with backbone unsaturated *N*-heterocyclic carbenes (NHCs) of different steric demand. Depending on the nature of the NHC used, Lewis-acid/Lewis-base adducts or NHC ring-expansion products stemming from B–B and C–N bond activation were observed. The corresponding NHC adducts and NHC ring-expanded products were isolated and characterized *via* solid-state and solution NMR spectroscopy and single-crystal X-ray diffraction. In general, B–B bond and C–N bond activation was observed at low temperature for B_2eg_2. The reactivity strongly depends on steric effects of the NHCs, as well as on their Lewis-basicity and the Lewis-acidity of the diboron(4) compound.

The results provide profound insight into the reactivity of these diboron(4) reagents with the nowadays ubiquitous NHCs, the stability of the corresponding NHC adducts and on B–B activation using Lewis-bases in general. It is demonstrated that B–B

bond activation may be triggered even at temperatures as low as -40 °C to -30 °C without any metal species involved. For example, the reactions of B_2eg_2 with sterically less demanding NHCs such as Me_2Im^{Me} and iPr_2Im in solution led to the corresponding ring-expanded products at low temperatures. Furthermore, boronium $[L_2B(OR)_2]^+$ and borenium $[LB(OR)_2]^+$ cations have been observed from the reaction of the bis-borate B_2eg_3 with the NHCs iPr_2Im and Me_2Im^{Me}, which led to the conclusion that the activation of bis-borates with NHCs (or Lewis-bases in general) might be a facile and simple route to access boron cations. Both boron-based nucleophiles and electrophiles are important for applications in organic synthesis.

TABLE OF CONTENTS

CHAPTER ONE

-

Catalysis

“Why did I decide to undertake my doctorate research in the exotic field of boron hydrides? As it happened, my girlfriend, Sarah Baylen, soon to become my wife, presented me with a graduation gift, Alfred Stock's book, The Hydrides of Boron and Silicon. I read this book and became interested in the subject. How did it happen that she selected this particular book? This was the time of the Depression. None of us had much money. It appears she selected as her gift the most economical chemistry book ($2.06) available in the University of Chicago bookstore. Such are the developments that can shape a career.”

Prof. Herbert C. Brown (1912-2004), Nobel Lecture 1979

CHAPTER ONE
-
Catalysis

1 Introduction

1.1 Historical development of alkoxy diboron(4) compounds: in 50 years from insignificant to indispensable

In 1925, Stock *et al.*[1] reported on the first observation of a reductive B-B coupling of BCl_3 to the tetrahalide B_2Cl_4, *via* an electrical arc discharge between zinc electrodes, and thus, a new group of very reactive and useful diboron(4) reagents was introduced. In particular, alkoxy derivatives of diborane(4) (Figure 1) became very important compounds for organic synthesis and have been extensively developed over the past 50 years.[2-9] B_2H_4 (**1**) and the tetrahalides (**2**), B_2X_4 (X = F, Cl, Br, I),[10] have some restrictive properties which limit their application in borylation reactions. While the parent diborane(4) (**1**) requires stabilization by Lewis base ligands such as phosphines[11,12] or amines,[12] the tetrahalides (**2**), except B_2F_4, have low thermal stability and are challenging to handle and difficult to prepare. In addition, tetraorganodiborane(4) (**3**) compounds, B_2R_4, are only stable with bulky R groups such as *t*Bu, CH_2*t*Bu or mesityl.[13-17] However, it has been shown that the most useful and stable derivatives of diborane(4) are those in which good *π*-donor groups (e.g. amido = NR_2 or alkoxy = OR) are used.

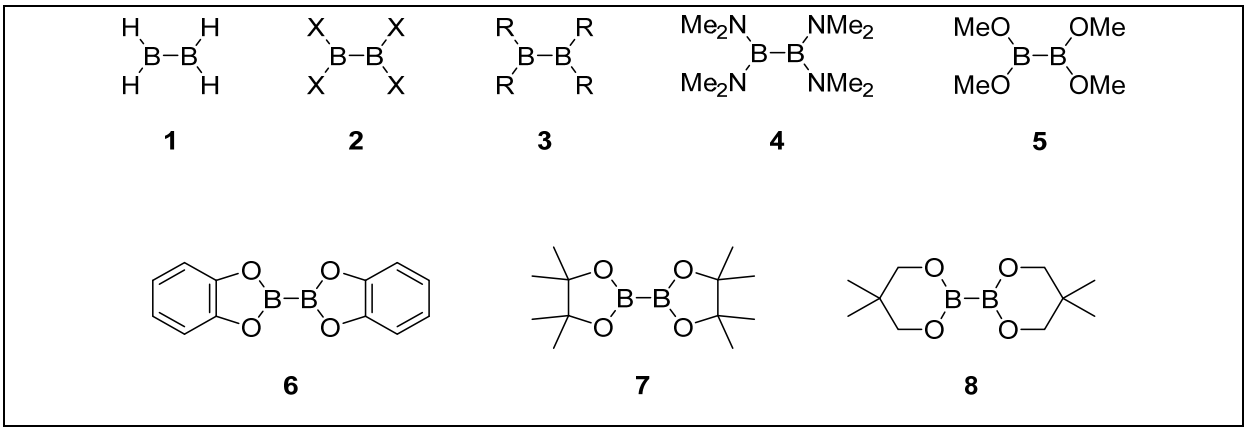

Figure 1. Derivatives of diborane(4).

In 1960, the U.S. Borax research group[18-21] synthesized the first prototypes $B_2(NMe_2)_4$ (**4**) and $B_2(OMe)_4$ (**5**), with compound **4** becoming the primary starting material for many diborane(4) derivatives due to its thermal stability and high-yielding synthesis. In 1968, Welch and Shore[22] reported new heteronuclear diboron ring systems, for example, B_2cat_2 (**6**). These novel compounds were prepared from reactions of $B_2(NMe_2)_4$ (**4**) or B_2Cl_4 (**2**) with selected diols such as catechol. In 1984, Nöth's group[15] published the synthesis and the single-crystal structure of B_2pin_2 (**7**), and the first "basic toolkit" of modern alkoxy diboron reagents was established. Further extension of novel ring systems were carried out by Norman, Marder and co-workers[23,24] in 1994 with their development of B_2neop_2 (**8**, Figure 1). Moreover, in 2001, Marder's group[25] observed the first transition metal-catalyzed, reductive coupling of pinacolborane to B_2pin_2 (**7**) and, in 2011, Braunschweig *et al.*[26,27] developed a more efficient transition metal-catalyzed synthesis of B_2cat_2 and B_2pin_2.

While the first high yielding syntheses of thermally stable diborane(4) derivatives were reported in 1960,[18-20] it took over three decades before application of alkoxy diboron reagents in organic synthesis was developed. The most widely used reagent in borylation reactions is B_2pin_2 (**7**) due to its overall stability towards air and hydrolysis, which simplifies reaction setups, isolation and purification of products. Currently, B_2pin_2 (**7**) is commercially available from many suppliers (e.g. AllyChem, BASF, Boron Molecular, Frontier Scientific, Sigma-Aldrich) in both small and bulk quantities.

A breakthrough for its application was the first platinum-catalyzed diboration of alkynes (**9**) using bis(pinacolato)diboron (**7**) reported by Miyaura's group in 1993 (Scheme 1).[28-30]

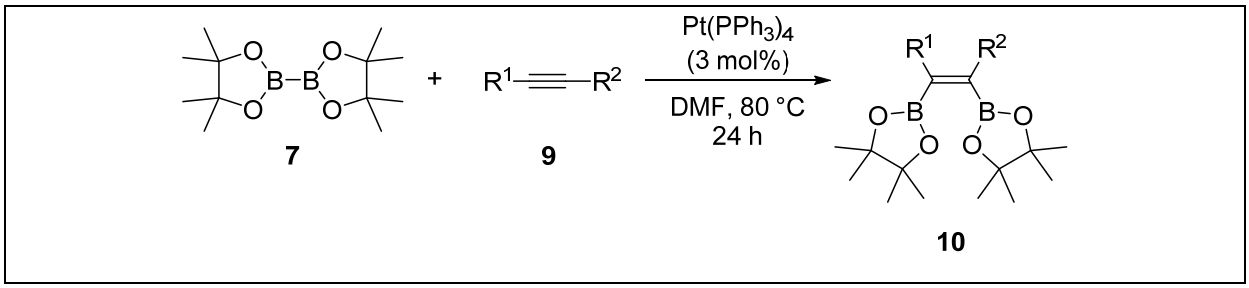

*Scheme 1. Miyaura's platinum-catalyzed diboration of alkynes (**9**).*

In 1995, Miyaura *et al.* greatly expanded the application of **7** when they published the first palladium-catalyzed cross-coupling reaction of **7** with aryl halides (**11**) to give aryl boronates (**12**, Scheme 2).[29,31]

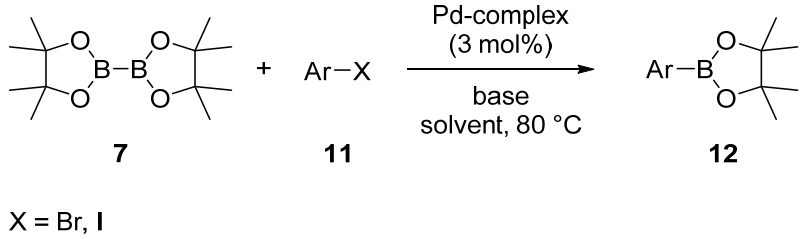

*Scheme 2. Miyaura's palladium-catalyzed borylation of aryl halides (**11**).*

Now, alkoxy diboron(4) compounds, above all B_2pin_2 (**7**), represent extremely useful borylation reagents to synthesize organoboron derivatives. Further historical developments of transition metal-catalyzed borylation reactions are described in detail in the following paragraphs.

1.2 Development of C–H and C–X borylation reactions

1.2.1 Direct C–H borylation

1.2.1.1 First aromatic C–H borylation

The first iridium-promoted C–H borylation of arenes was reported in 1993 by Marder's group.[32] When the synthesis of [Ir(η^6-aryl)(Bcat)$_3$] from [Ir(η^5-C_9H_7)(COD)] and excess HBcat (catechol borane) was performed in toluene as well as other aromatic solvents such as benzene and benzene-d_6, the corresponding borylated solvents were detected in trace quantities as side products by GC-MS analysis.

In 1999, Smith and co-workers[33] developed a catalytic aromatic C–H borylation reaction with HBpin (**23**) using an iridium-Cp* complex and an alkylphosphine ligand. Further studies strongly improved the catalyst performance. A maximum turnover number (TON) of ~ 4500 was obtained using the [Ir(η^5-C_9H_7)(COD)] complex in conjunction with the ligand 1,2-bis(dimethylphosphino)ethane (dmpe, **24**, Scheme 3).[34]

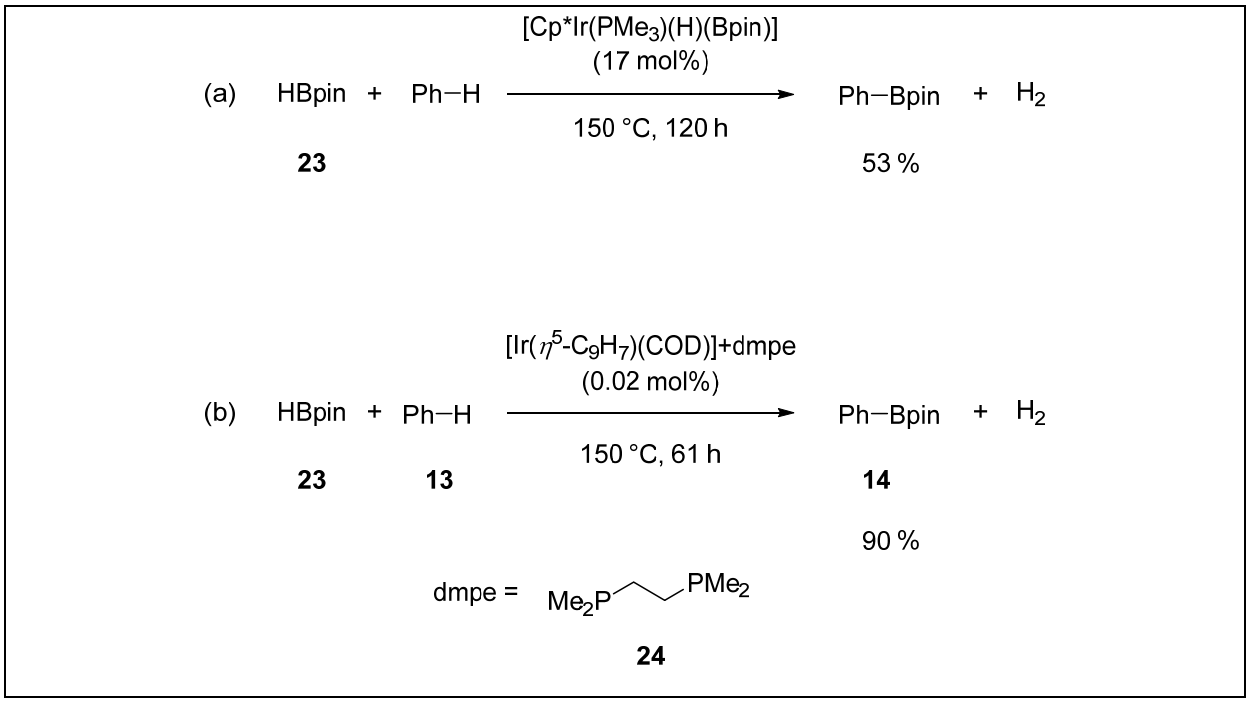

Scheme 3. Iridium-catalyzed C–H borylations reported by Smith and co-workers.

Under Smith's conditions, the selectivity for the borylation of 1,3-disubstituted arenes was determined by steric effects rather than by electronic properties of the substituents, and borylation occurred at the *meta*-position of the aryl substrates.

In 2002, Hartwig, Ishiyama, Miyaura and co-workers[35] reported a more efficient catalyst system for the C–H borylation of arenes (**25**), using a combination of commercially available $[IrCl(COD)]_2$ complex and 2,2'-bipyridine (**26**) as the ligand (Scheme 4).

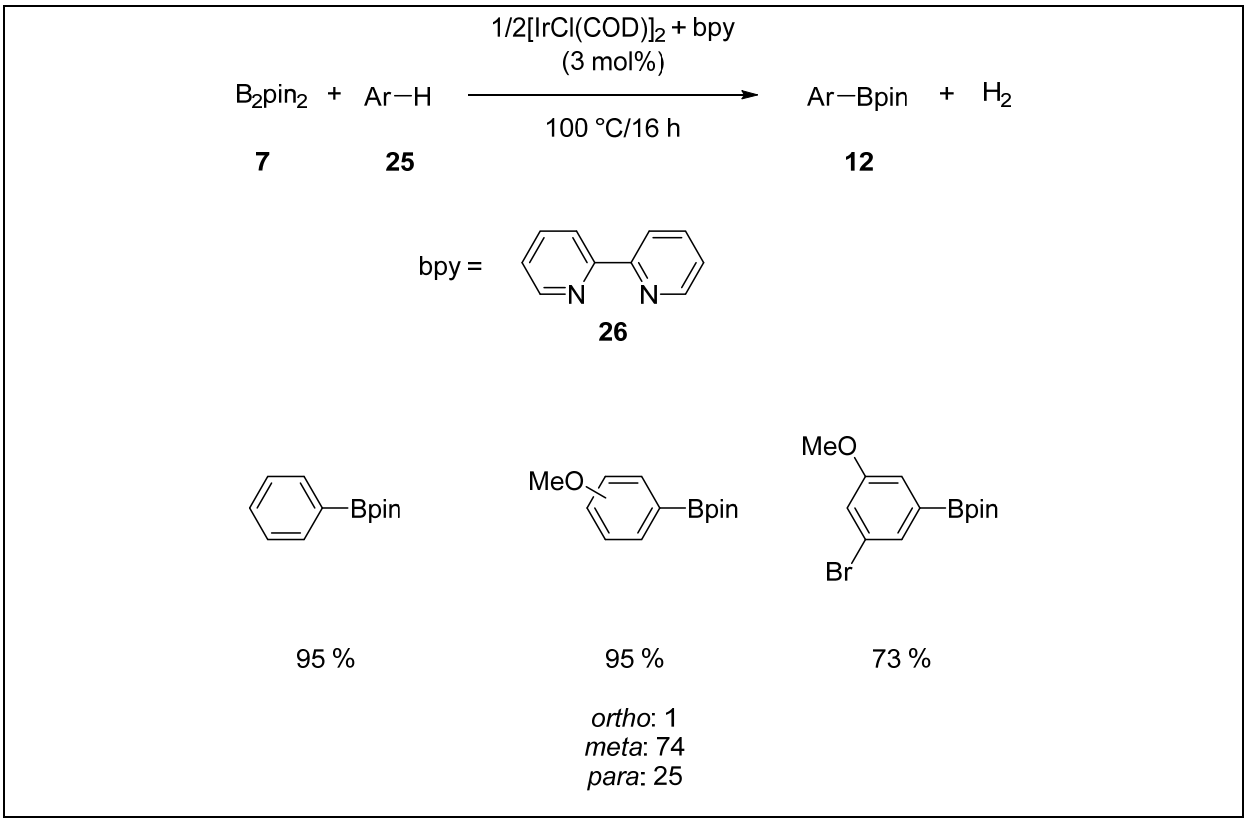

Scheme 4. Iridium-catalyzed aromatic C–H borylation reported by Hartwig and co-workers.

Independent of the electronic nature of the substrates, monosubstituted arenes were borylated at the *meta*- and *para*-positions in statistical ratios of ~ 2:1, whilst the *ortho*-borylated product was generally not observed, likely because steric effects prevent *ortho*-borylation. Under Hartwig's conditions, 1,3-disubstituted arenes were predominantly borylated at the *meta*-position. A maximum turnover number (TON) of ~ 8000 was achieved using $[IrCl(COE)_2]_2$ combined with 4,4'-di-*tert*-butyl-2,2'-bypyridine (dtbpy).

Mechanistic studies were undertaken and resulted in the isolation of an active intermediate $[Ir(dtbpy)(COE)(Bpin)_3]$.[35] Dissolving this iridium tris-boryl complex in C_6D_6 at room temperature gave three equivalents of borylated arene, which underlined the catalytic activity of $[Ir(dtbpy)(COE)(Bpin)_3]$, even though once the first borylation takes place, the tris-boryl complex no longer exists. The reactivity of

[Ir(dtbpy)(COE)(Bpin)$_3$] is quite similar to the reactions of tris(boryl)Ir(III) complexes reported by both Marder[32] and Smith.[34]

Hartwig and co-workers[35,36] proposed a mechanism involving an iridium(III)–iridium(V) cycle in a two-step process supported by a theoretical study of Sakaki *et al*.[37] (Scheme 5).

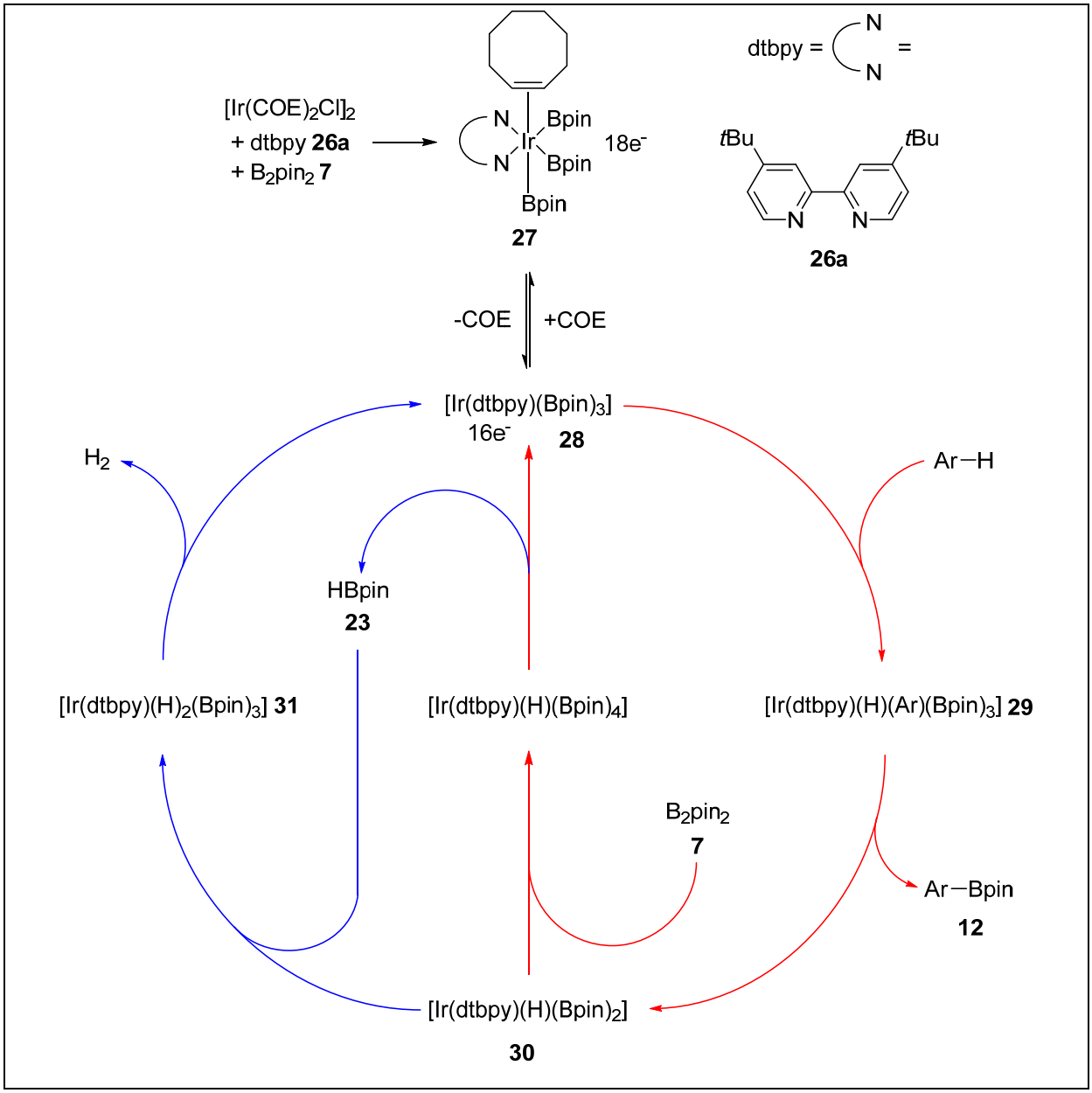

*Scheme 5. Proposed mechanism for the iridium-catalyzed aromatic C–H borylation by B$_2$pin$_2$ (**7**) (two-step process: 1st cycle = fast borylation with B$_2$pin$_2$ (**7**) and 2nd cycle = slow borylation with HBpin (**23**).*

Firstly, [Ir(COE)$_2$Cl]$_2$, dtbpy (**26a**) and B$_2$pin$_2$ (**7**) react to form *in situ* the 18-electron tris(boryl)iridium(III) complex (**27**). Then **27** converts, *via* dissociation of the COE ligand, to the 16-electron [Ir(III)(dtbpy)(Bpin)$_3$] complex (**28**), followed by oxidative

addition of the substrate to generate the iridium(V) species **29** and then reductive elimination to form a bis(boryl)Ir(III)hydride complex (**30**). Subsequently, oxidative addition of B_2pin_2 (**7**) and reductive elimination of HBpin (**23**) occurs to regenerate intermediate **28**. The second cycle is the slower borylation process starting with the oxidative addition of HBpin (**23**) to give the possible intermediate **31** followed by reductive elimination of hydrogen to regenerate the 16-electron tris(boryl)Ir(III) complex (**28**).[35-40]

1.2.1.2 First aliphatic C–H borylation

The first transition metal-catalyzed aliphatic C–H borylation *via* photochemical activation of a rhenium-Cp* species was reported by Hartwig's group[41] in 1999. The reaction of B_2pin_2 (**7**) and *n*-pentane (**32**) catalyzed by [Cp*Re(CO)$_3$] (**33**) in a CO atmosphere (202 kPa) and mediated by irradiation with a mercury arc lamp (450 W, Hanovia) resulted in the respective *n*-pentyl boronate (**34**, Scheme 6).

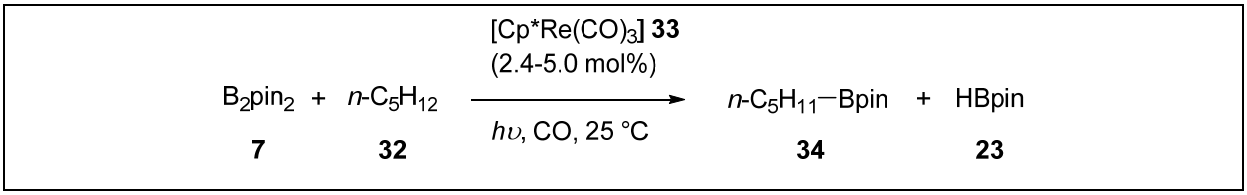

Scheme 6. Rhenium-catalyzed aliphatic C–H borylation reported by Hartwig and co-workers.

A proposed mechanism for the catalytic cycle starts with the photochemical dissociation of CO from **33** and oxidative addition of B_2pin_2 (**7**) to [Cp*Re(CO)$_2$] to give the bis(boryl)rhenium complex (**35**). This is followed by C–H activation and simultaneous dissociation of CO to form intermediate **36** before the alkyl boronate is produced by reductive elimination (Scheme 7).

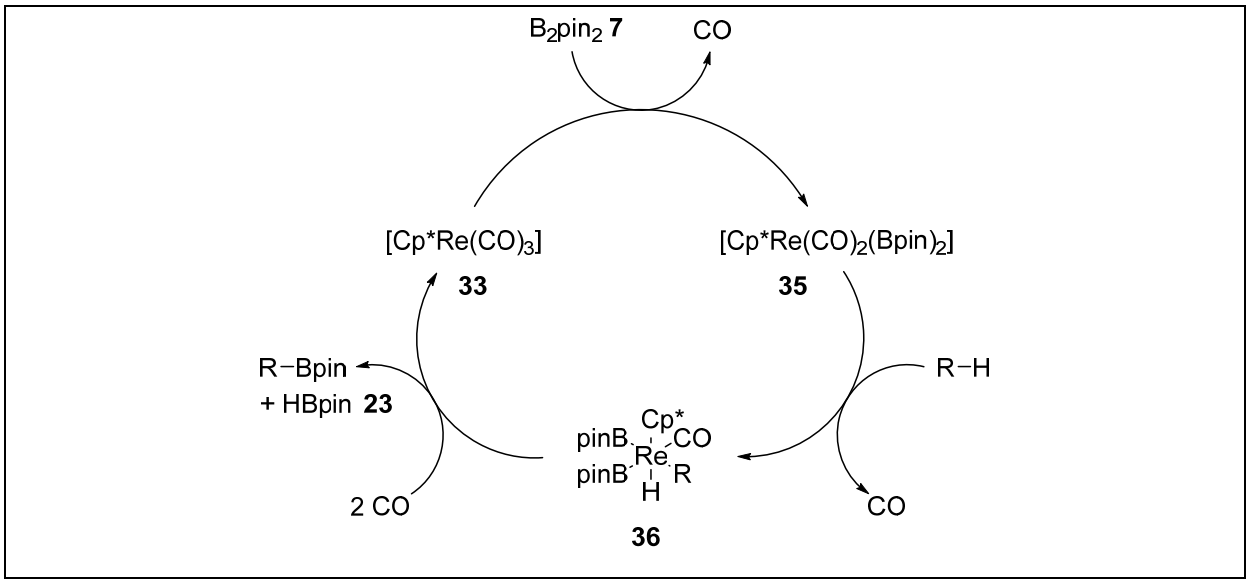

*Scheme 7. Proposed mechanism for the photochemical Re-catalyzed aliphatic C–H borylation with B_2pin_2 (**7**).*

Interestingly, HBpin (**23**) is generated but does not participate in the catalytic cycle because it decomposed to pinB–O–Bpin.[38,39,41]

1.2.2 C–X borylation

1.2.2.1 Palladium-catalyzed borylation

In 1995, Miyaura's group[31] reported the first one-pot borylation reaction of aryl halides with B_2pin_2 (**7**, Scheme 2).

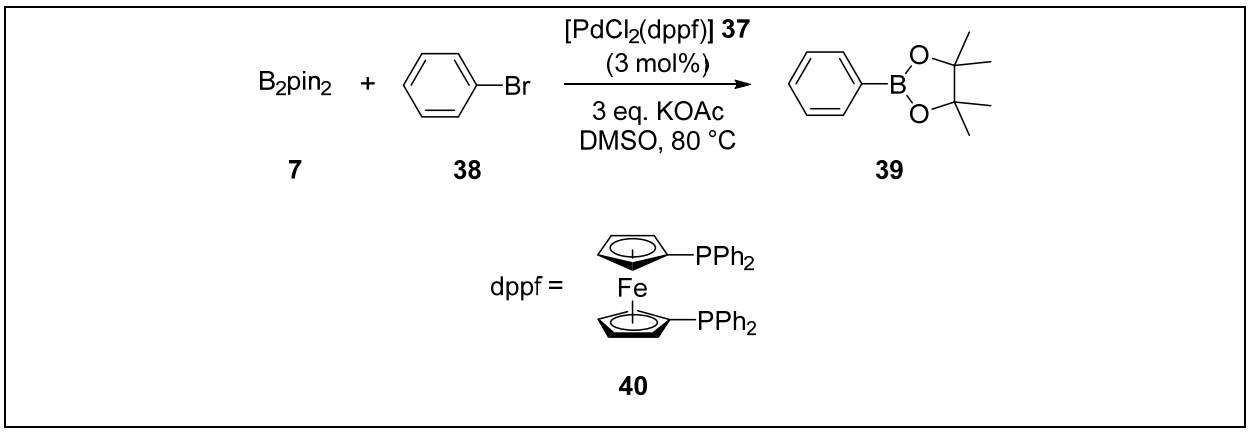

Scheme 8. Palladium-catalyzed aromatic C–X borylation reported by Miyaura and co-workers.

The palladium-catalyzed C–B cross-coupling reaction conditions were optimized to use [$PdCl_2$(dppf)] (**37**) as pre-catalyst, KOAc as base and bromobenzene (**38**) as substrate at 80 °C (Scheme 8). Other bases, such as K_3PO_4 and K_2CO_3, were applied in the borylation reaction, but resulted in a significant amount of homo-

coupled side product, because the relative ease of transmetallation of B_2pin_2 (**7**) versus ArBpin (**39**) depends on the applied base. Therefore, the best results were obtained with KOAc, giving both high yields and high selectivity for the desired product. It was observed that the reaction rate was affected by the polarity of the solvents; the reaction was accelerated by an increase in the solvent polarity, with DMSO ≥ DMF > dioxane > toluene. The palladium catalyst (**37**) achieved the best results in the cross-coupling reactions of B_2pin_2 (**7**) and bromobenzene derivatives independent of the electronic nature of substituents. On the other hand, the $Pd(PPh_3)_4$-catalyzed borylation of substrates with an electron-donating group such as 4-bromoanisole, resulted in a 62% yield of the respective arylboronate and an 8% yield of unexpected phenylboronate. This side product could be formed by the borylation of a phenyl group on the triphenylphosphine ligand. Other group 10 triphenylphosphine-based catalysts, such as $[Pt(PPh_3)_4]$ or $[Ni(PPh_3)_4]$, did not show any catalytic activity. The scope of the $[PdCl_2(dppf)]$-catalyzed borylation of aryl halides by B_2pin_2 (**7**) is shown in Figure 2.

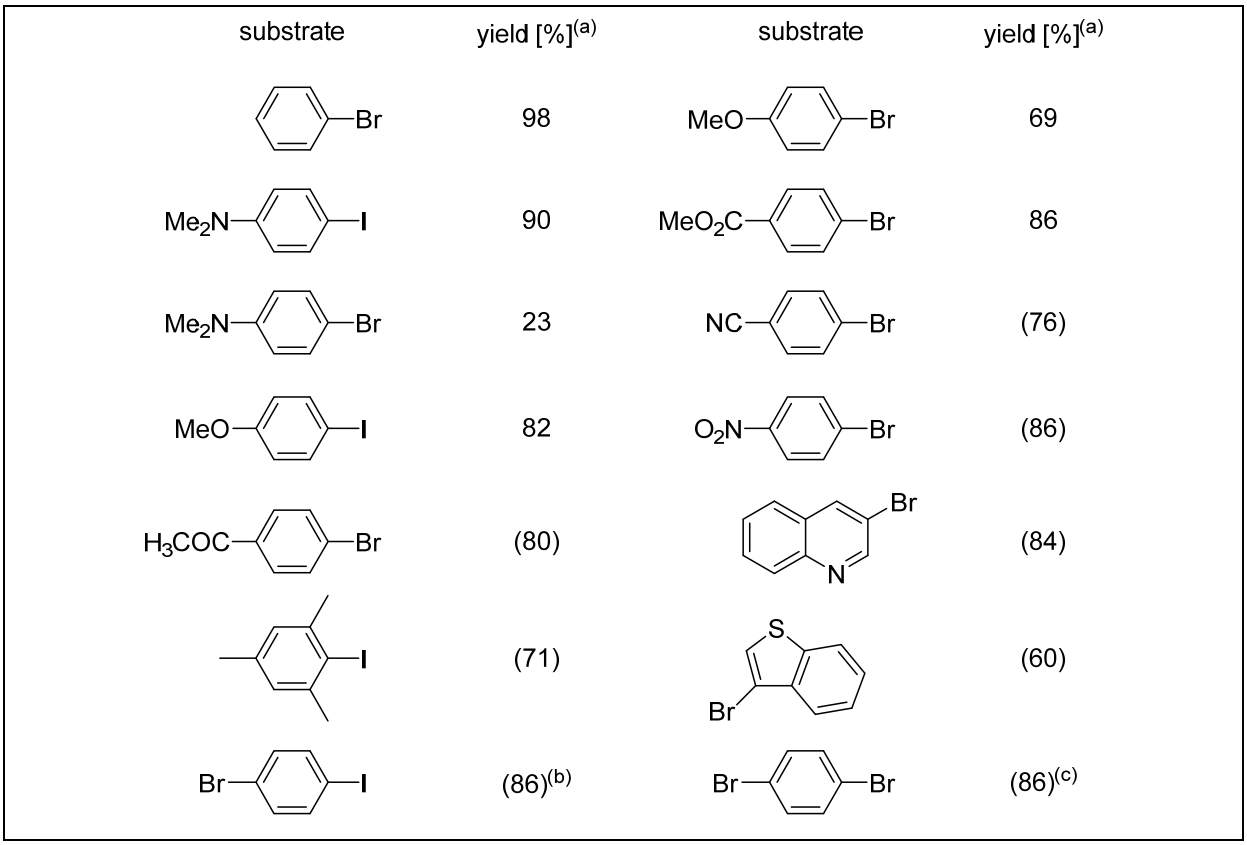

*Figure 2. Substrates of the palladium-catalyzed borylation with B_2pin_2 (7): (a) yields of respective arylboronates determined by GC, with isolated yields in parentheses; (b) 1.0 equiv of B_2pin_2 (**7**), yield of (4-bromophenyl)boronate; (c) 2.2 equiv of B_2pin_2 (**7**), yield of diboronic ester.*

The reaction rate of the C–B coupling was shown to be faster for iodide than for bromide substrates. Furthermore, it was observed that the reaction conditions tolerated sterically hindered substrates and various functional groups such as esters, ketones or nitriles.

A mechanism for the palladium-catalyzed borylation of aryl halides by B_2pin_2 (**7**) was proposed (Scheme 9). Starting with an oxidative addition of the substrate (**11**) to the Pd(0) complex **41** to form a Pd(II) intermediate (**42a**), transmetalation *via* the acetoxypalladium(II) species (**43a**) yields the Pd(II)-boryl complex **45a**. Subsequent reductive elimination results in the aryl boronate **12** and regeneration of the Pd(0) complex **41**.

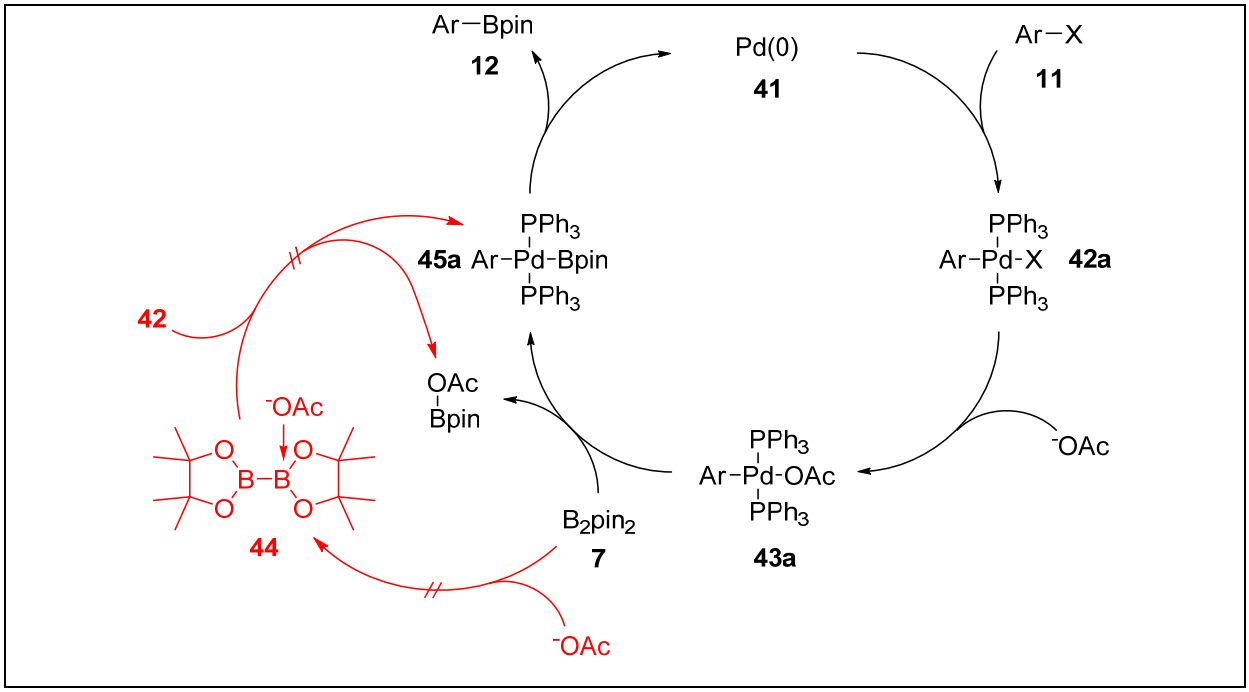

*Scheme 9. Proposed mechanism for the Pd-catalyzed C–X borylation with B_2pin_2 (**7**).*

To support the suggested mechanism, stoichiometric reactions were carried out to form the acetoxypalladium(II) complex **43a**, which showed high reactivity towards B_2pin_2 (**7**). Furthermore, there was no evidence for the formation of an organoborane-base adduct (**44**), which could potentially transmetalate with the Pd(II) intermediate **42a**. Therefore, the transmetalation between the acetoxypalladium(II) complex **43a** and B_2pin_2 (**7**) is apparently involved in the catalytic cycle.

Inspired by Miyaura's results,[31] Masuda and co-workers[42] established a borylation reaction of aryl iodides and bromides, in the presence of [$PdCl_2$(dppf)] (**37**), a tertiary amine, and HBpin (**23**) as the boron source (Scheme 10). At the time, this route

seemed preferable as **23** was readily available and B_2pin_2 was just beginning to be commercialized at a relatively high price.

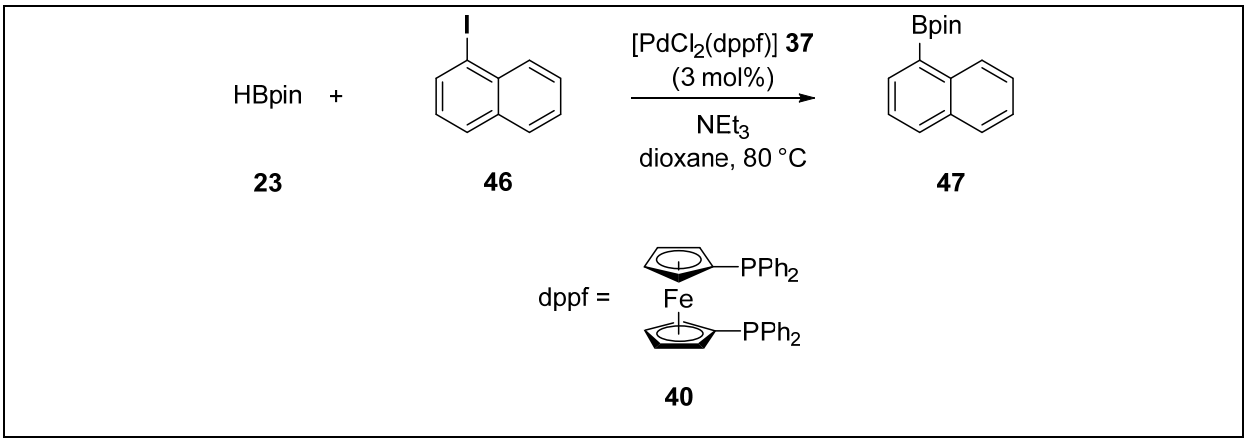

Scheme 10. Palladium-catalyzed aromatic C–X borylation reported by Masuda and co-workers.

The authors proposed an oxidative addition of the aryl halide to the Pd(0) complex **41** followed by transmetallation with HBpin (**23**). It was proposed that the transmetallation step involved a boryl anion salt (**43b**) formed from NEt_3 and HBpin (**23**) (Scheme 11).[43]

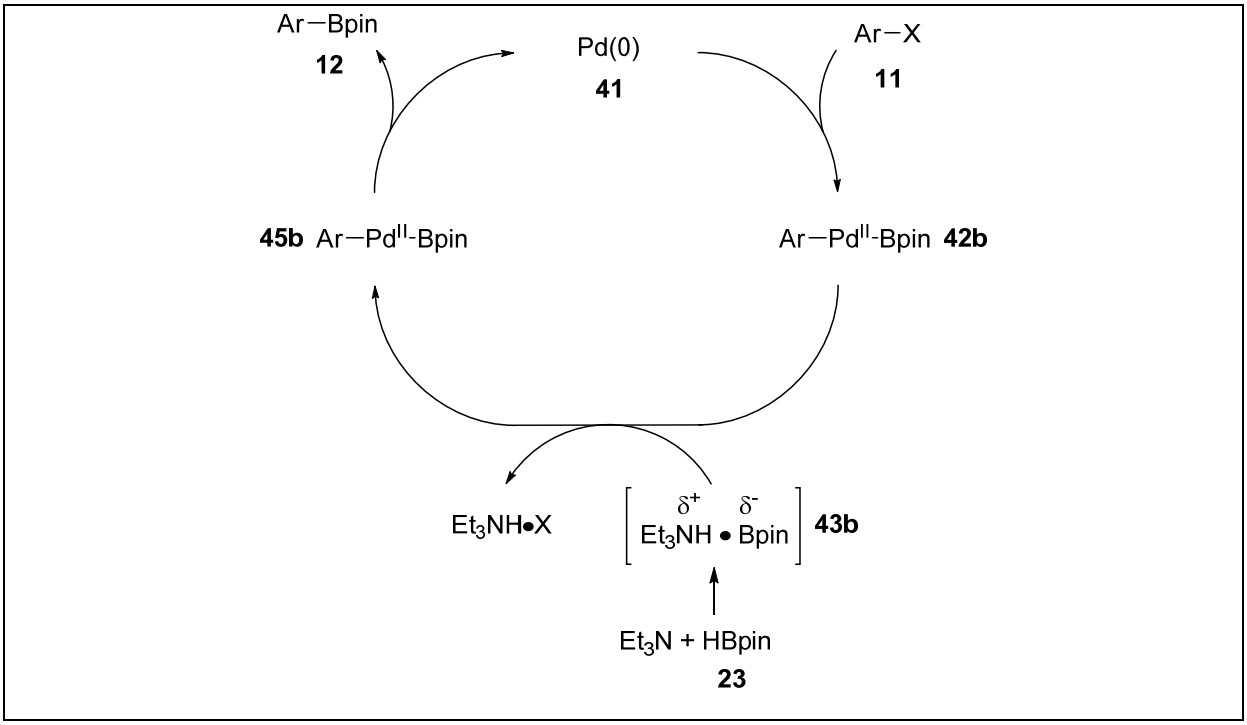

*Scheme 11. Proposed mechanism for the Pd-catalyzed C–X borylation with HBpin (**23**) by Masuda and co-workers.*

This mechanism was refuted by DFT calculations of Lin, Marder and co-workers[44] which supported a σ-bond metathesis between HBpin (**23**) and a cationic 14-electron palladium(II)aryl species (**43c**), as the borylation step (Scheme 12).

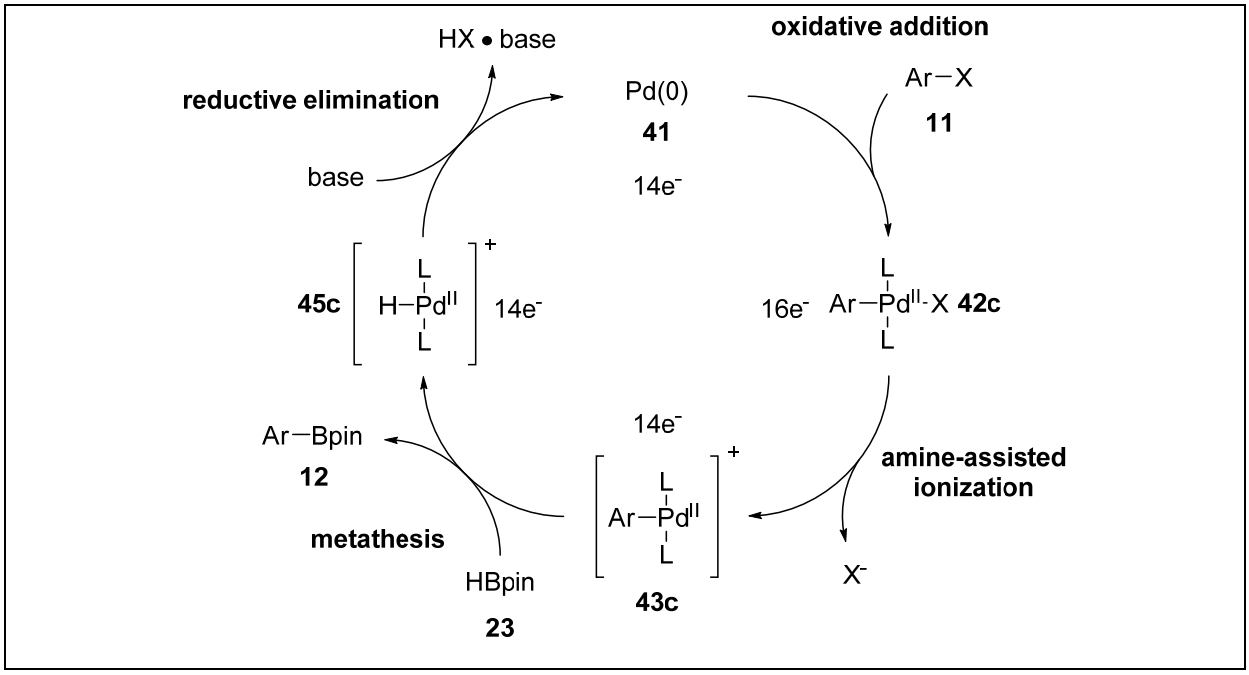

*Scheme 12. Proposed mechanism for the Pd-catalyzed C–X borylation with HBpin (**23**) by Lin, Marder and co-workers.*

Shortly afterwards, Miyaura and co-workers[45] extended the substrate scope to aryl chlorides and, in 2002, Fürstner's group[46] published the first synthesis of aryl boronates from aryl chlorides catalyzed by a palladium/imidazolium salt system (Scheme 13).

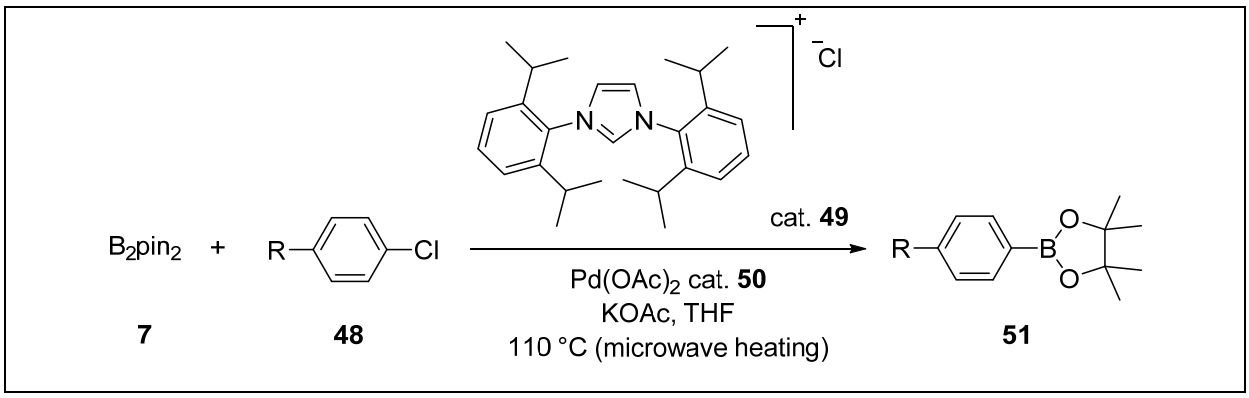

Scheme 13. Palladium-catalyzed aromatic C–X borylation reported by Fürstner and co-workers.

1.2.2.2 Copper-catalyzed borylation

In 2006, Zhu and Ma[47] reported the first copper-catalyzed borylation of aryl iodides by HBpin (**23**). The reaction conditions were optimized to use CuI as pre-catalyst, THF as the solvent and sodium hydride (NaH) as the base (Scheme 14).

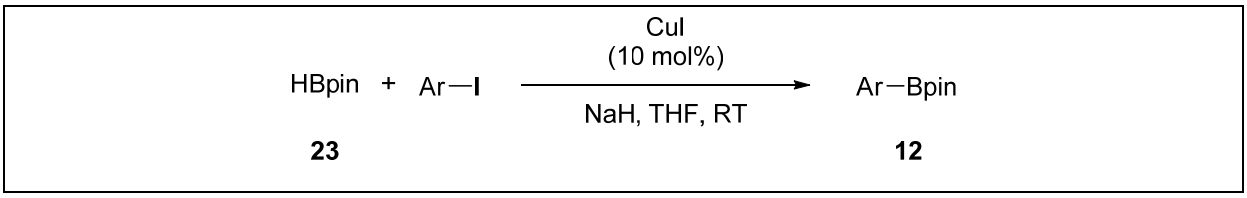

Scheme 14. Cu-catalyzed aromatic C–I borylation reported by Zhu and Ma.

Other bases, for example NEt_3, KO*t*Bu and Cs_2CO_3, were investigated but resulted in poor yields. Only the use of NaH as base showed good conversion, especially at room temperature. The scope of the reaction was limited to aryl iodides and a small range of functional groups was tolerated. Furthermore, it was observed that bulky groups did not affect the borylation reaction.

Based on the proposed mechanism of Miyaura and co-workers[31] for the palladium-catalyzed borylation of aryl halides, Zhu and Ma suggested an oxidative addition of aryl iodide to CuI to give a Cu(III) species (**52**). This is followed by transmetallation of HBpin (**23**) with the assistance of NaH. Afterwards, reductive elimination takes place *via* intermediate **53** to regenerate the catalyst and yield the desired aryl boronate **12** (Scheme 15).

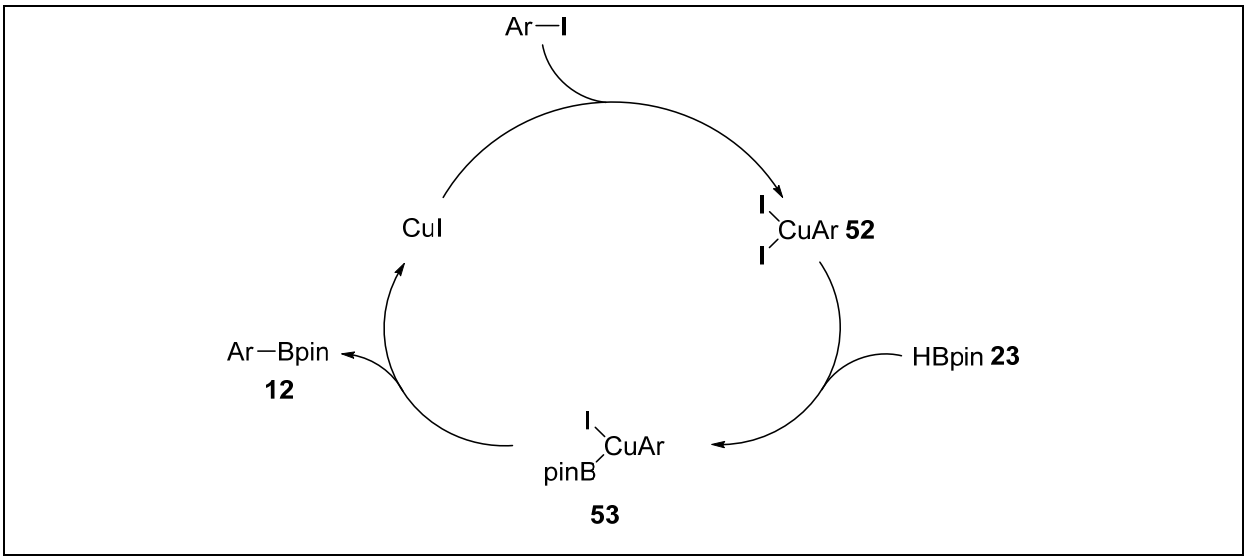

*Scheme 15. Proposed mechanism for the Cu-catalyzed aromatic C–I borylation by HBpin (**23**).*

Inspired by Zhu and Ma's copper-catalyzed borylation of aryl iodides, in 2009, Marder and co-workers[48] reported a robust copper-catalyzed borylation of aryl halides with B_2pin_2 (**7**). The reaction conditions were optimized to use CuI as pre-catalyst, P(*n*Bu)$_3$ as ligand, KO*t*Bu as base, THF as solvent and 4-iodotoluene as substrate at room temperature (Scheme 16).

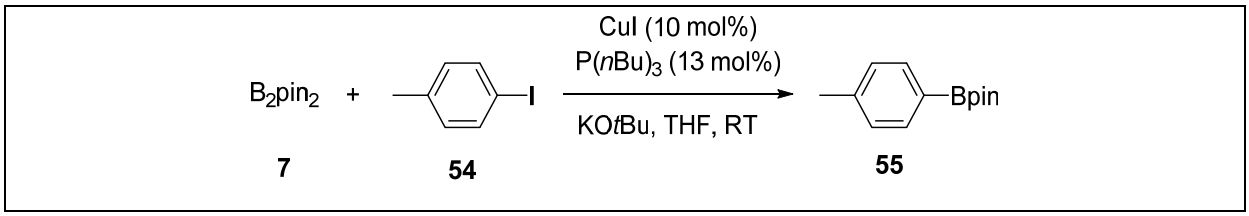

Scheme 16. Copper-catalyzed aromatic C–X borylation reported by Marder and co-workers.

Furthermore, different bases, copper sources, phosphine ligands, solvents and reaction conditions were screened to assess the scope and limitations of this reaction. Increasing the temperature to 60 °C, or the use of microwave heating, accelerated the reaction rate dramatically. The use of weaker bases such as KOAc or K_2CO_3 resulted in no conversion of the substrate, either under standard conditions, at higher temperatures or with microwave heating. Other solvents with increasing polarity such as toluene, THF, MTBE, MeCN, DMF and MeOH were also tested. Moderate conversions in toluene and MeCN were observed as solubility issues of KO*t*Bu or the *in situ* formed adduct of B_2pin_2 (**7**) and KO*t*Bu could affect the yield, while no conversion was observed in MeOH.[49,50]

A broad scope of aryl halides was screened and a wide range of aryl iodides and bromides were converted into the respective aryl boronates in good to excellent yields. It was observed that the borylation reaction shows excellent conversion independent of the nature of the halide (Br, I) and tolerates many substituents, although there are some restrictions concerning the functional group reactivity at present. For example, aryl chlorides did not show any conversion and substrates containing an ester group such as a methyl ester underwent transesterification as a side reaction.

Mechanistic studies proposed a C–B bond-formation step by σ-bond metathesis of the copper(I) boryl complex **56** and the aryl halide through an "oxidatively added transition state" followed by transmetallation *via* the copper(I) alkoxy complex **58** to regenerate the catalyst (Scheme 17).

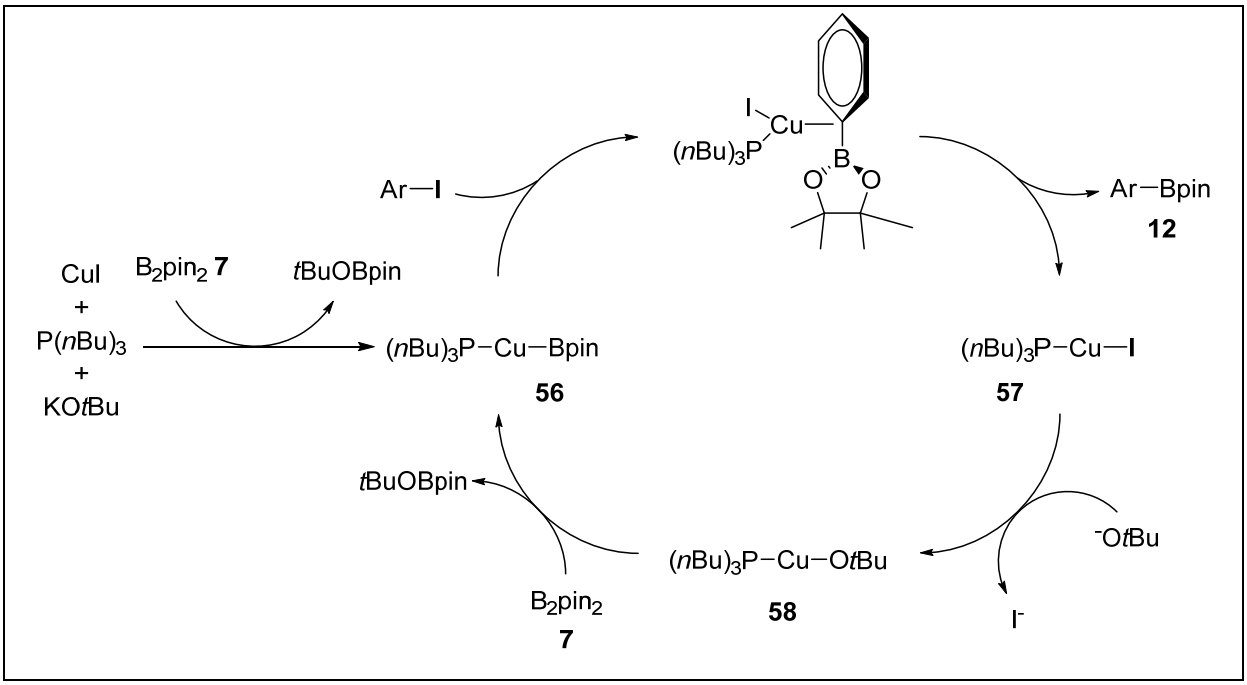

*Scheme 17. Proposed mechanism for the Cu-catalyzed aromatic C–X borylation by B_2pin_2 (**7**).*

In summary, Marder and co-workers[48] showed a facile catalytic process for the borylation of aryl halides with good functional group tolerance, including electron-rich and bulky bromides. This reaction, under mild conditions and using an inexpensive metal (Cu) and ligand (P(nBu)$_3$), provides a cost-effective alternative to the normally employed palladium-catalyzed borylation reactions of Miyaura and co-workers[31] or Masuda and co-workers.[42] Based on the results of Marder's group,[48] in 2012 Yan and co-workers[51] published a ligand-free copper-catalyzed borylation of aryl halides and, in 2014, Kiatisevi *et al.*[52] reported on a Pd/Cu system to borylate aryl iodides under atmospheric conditions.

Furthermore, in 2012, Marder, Liu, Steel and co-workers reported the first copper-catalyzed borylation of primary (*prim*) and secondary (*sec*) alkyl halides by B_2pin_2 (**7**). The reaction conditions were optimized to use CuI as pre-catalyst, PPh_3 as ligand, LiOMe as base and DMF as solvent, whereas chlorides and tosylates typically required the use of Bu_4NI as an additive (Scheme 18).

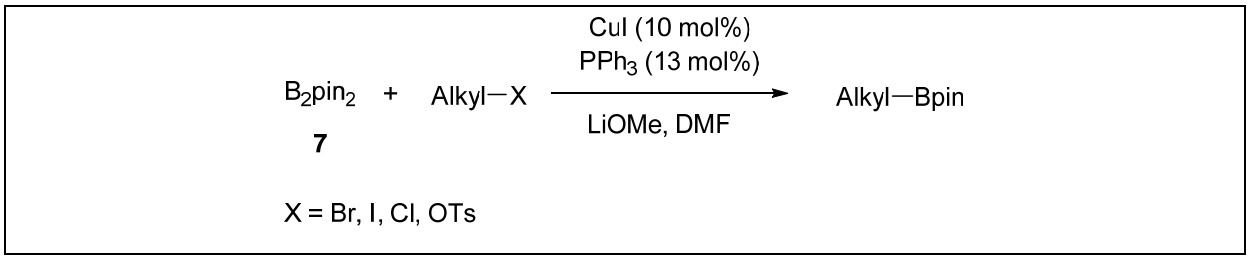

Scheme 18. Copper-catalyzed aliphatic C–X borylation reported by Marder and co-workers.

This borylation reaction tolerated a wide range of functional groups such as esters, nitriles, ethers, ketones, olefins, amides and silyl esters.

In 2012, Ito and co-workers[53] published a copper-catalyzed borylation of alkyl halides in the presence of CuCl as pre-catalyst, Xantphos as ligand and KO*t*Bu as base (Scheme 19).

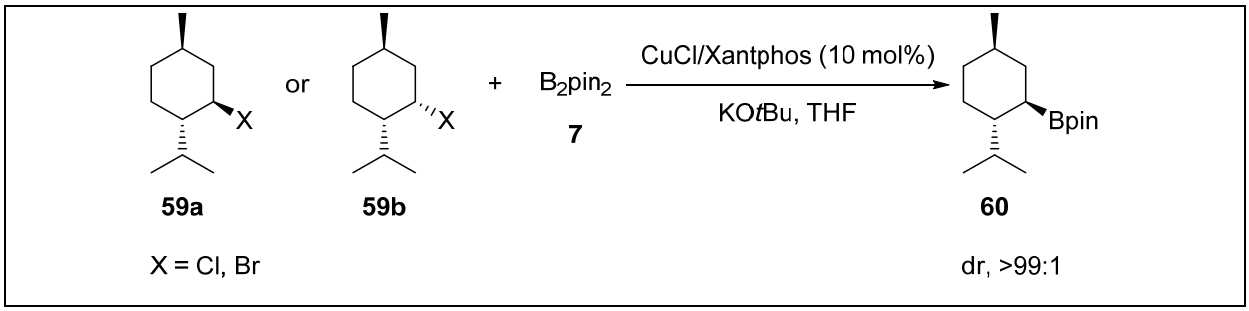

Scheme 19. Copper-catalyzed C–X borylation, with excellent diastereoselectivity, reported by Ito and co-workers.

The first copper-nanoparticle-catalyzed borylation of alkyl bromides was reported in 2014 by Chung *et al.*[54] (Scheme 20) who suggested a radical pathway for the borylation which was supported by ring opening experiments.

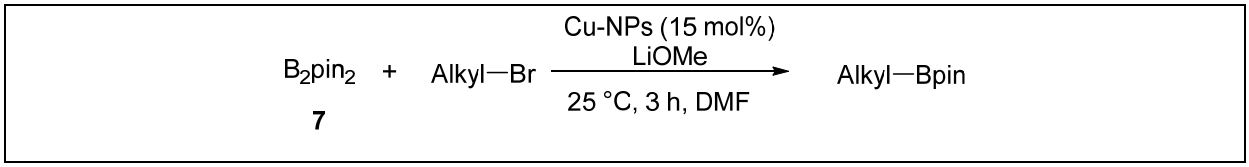

Scheme 20. Copper-nanoparticle-catalyzed borylation, reported by Chung and co-workers

1.2.2.3 Nickel-catalyzed borylation

In 2012, Fu and co-workers[55] reported a nickel-pybox catalyst system, which was able to carry out the borylation of a broad range of primary, secondary and tertiary alkyl halides by B_2pin_2 (**7**). Fu's group showed that $NiBr_2$•diglyme as pre-catalyst, the

pybox ligand (**61**), KOEt as base and DIPE/DMA as solvent at room temperature gave good yields of the desired product (Scheme 21).

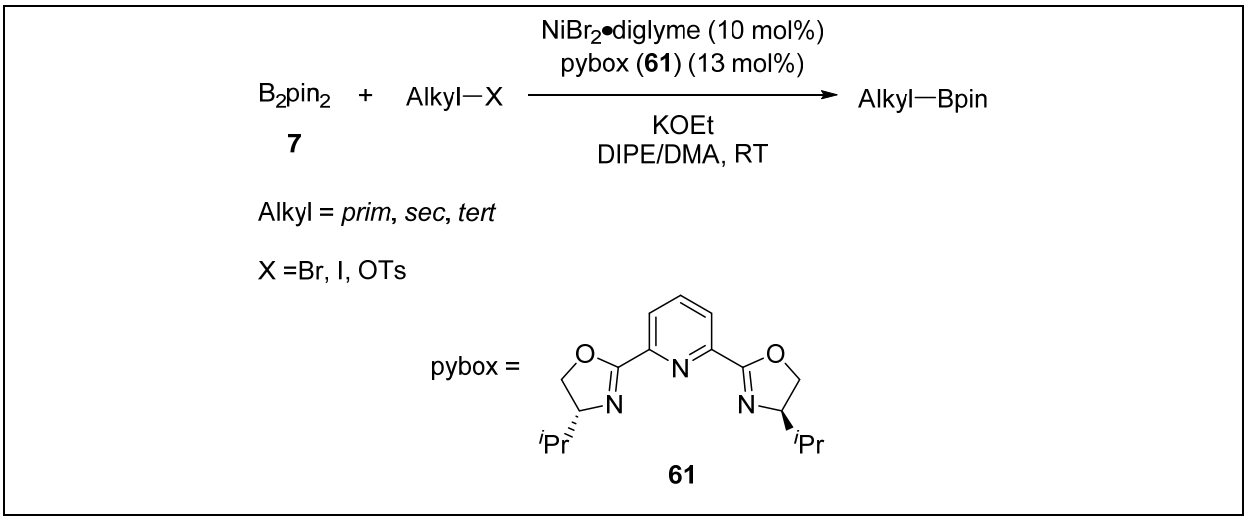

Scheme 21. Nickel-catalyzed tertiary C–X borylation reported by Fu and co-workers.

A catalytic cycle involving a radical mechanism was proposed using evidence from mechanistic studies and general observations from the borylation reactions (Scheme 22). Reactivity increases with the number of substituents (*prim* < *sec* < *tert*). This mechanism was supported by DFT calculations of Lin and Marder *et al.*[56]

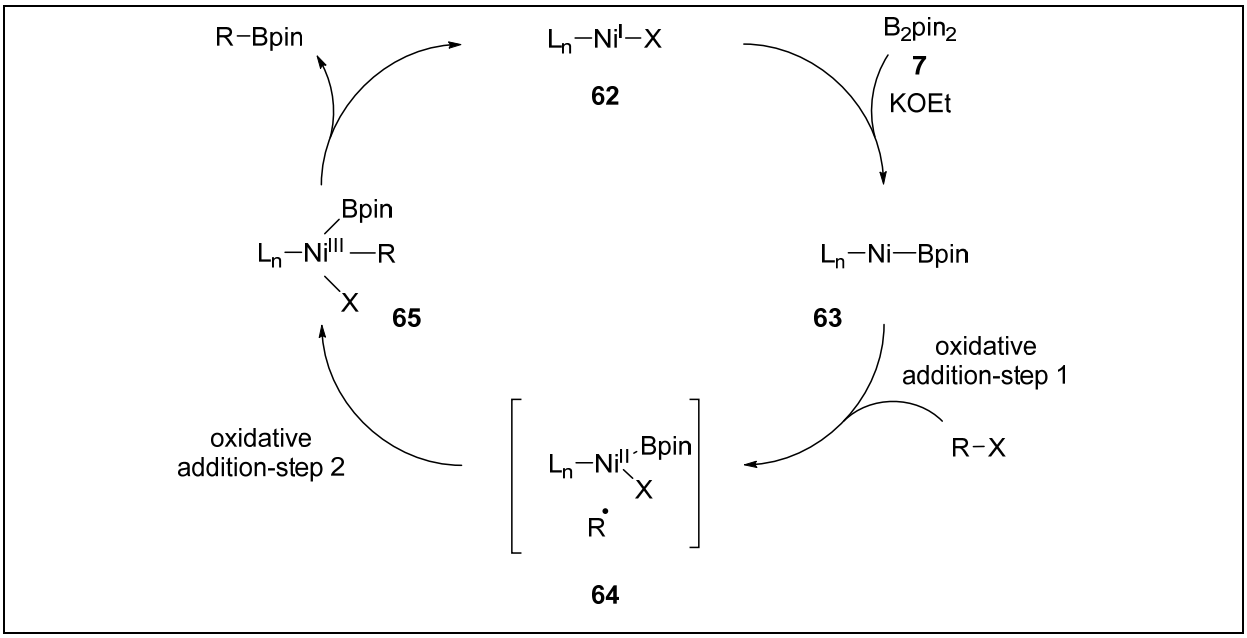

*Scheme 22. Proposed mechanism for the Ni-catalyzed tertiary C–X borylation by B_2pin_2 (**7**).*

This umpolung process shows good tolerance to functional groups and opens an accessible route to selective borylation reactions of tertiary alkyl halides to synthesize a broad range of the respective alkyl boronates.

Moreover, further transition metal-catalyzed borylation reactions of alkyl halides, were reported by Liu and co-workers[57] (nickel and palladium), Gong and co-workers[58] (nickel) and Biscoe and co-workers[59] (palladium).

1.2.2.4 Zinc-catalyzed borylation

In 2013, Uchiyama *et al*.[60] published the first zinc-catalyzed borylation of aryl halides using pyrophoric diethyl zinc as precursor, proposed to proceed *via* a borylzincate species as intermediate (Scheme 23).

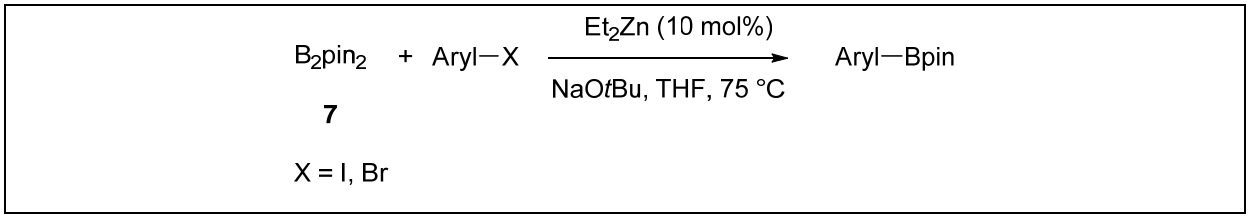

Scheme 23. Zinc-catalyzed, aromatic C–X borylation reported by Uchiyama and co-workers.

In 2014, Marder and co-workers[61] published a group 12 transition metal-catalyzed borylation reaction of *prim*, *sec* and *tert* alkyl halides with B_2pin_2 (**7**) as the diboron reagent in the presence of the abundant, non-precious metal zinc. The reaction conditions were optimized using bromocyclohexane (**66**) as substrate, $ZnCl_2$ as pre-catalyst, a Mes_2Im ligand (**67**), KO*t*Bu as base and MTBE as solvent at room temperature (Scheme 24).

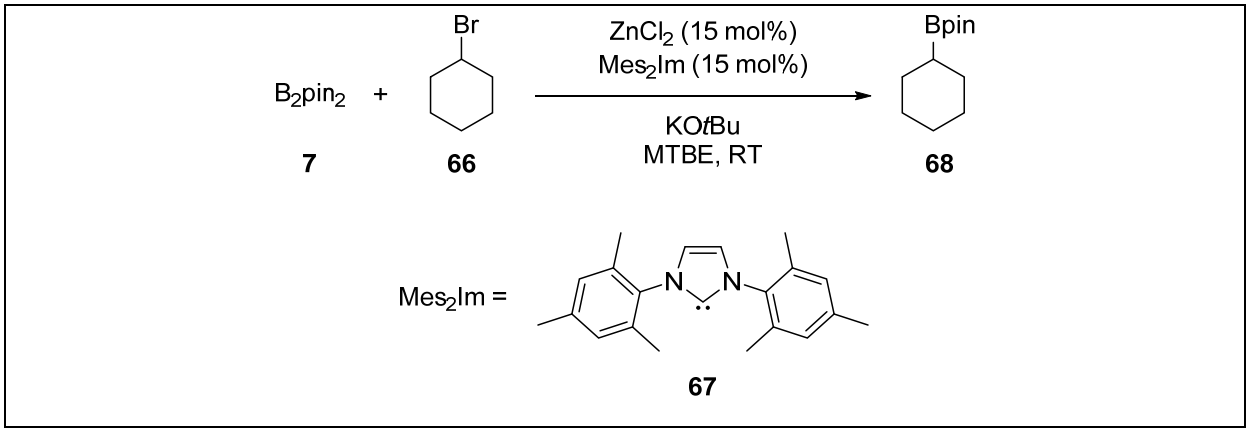

Scheme 24. Zinc-catalyzed, aliphatic C–X borylation reported by Marder and co-workers.

Other bases such K_2CO_3 and KOEt were applied in the borylation reaction but resulted in limited or no conversion of substrate to the respective alkyl boronate. Different zinc sources were also screened, for example $ZnBr_2$, ZnI_2, but no improvement in reactivity was observed. No activity was shown when zinc dust was

utilized in the reaction. The reaction is moderately sensitive to air and water and gives versatile access to a broad range of *prim*, *sec* and limited *tert* alkyl boronates on a gram scale. Moreover, B_2pin_2 (**7**) can be substituted by B_2neop_2 (**8**) to yield the corresponding borylated compounds.

The mechanism is still under investigation, but a NHC-zinc complex might play a role to activate the diboron reagent forming a zinc boryl complex, which facilitates the borylation of the alkyl halides. All experimental observations, including ring-opening and ring-closing reactions, indicate that the borylation might occur *via* a radical pathway, suggesting that the borylation reaction involves a one-electron process. This proposal was supported by test reactions with an excess of a radical scavenger (9,10-dihydroanthracene), which prevents the reaction from taking place.

Thus, Marder and co-workers developed a versatile, accessible route to primary, secondary, and some tertiary alkyl boronates under mild conditions (room temperature) using the abundant and less toxic (than palladium or nickel) metal zinc and an inexpensive NHC-ligand to constitute a cost effective borylation reaction, which complements and expands the copper-, palladium- and nickel-catalyzed borylation of alkyl halides.

Furthermore, in 2014, Marder and co-workers[62] also reported a zinc-catalyzed, route to access aryl boronates, using B_2pin_2 (**7**) and a zinc-NHC complex as pre-catalyst (Scheme 25). In 2015, they showed an alternative version of a zinc-catalyzed dual C–X and C-H borylation of aryl halides using a Zn(II)/dtbpy catalyst system.[63]

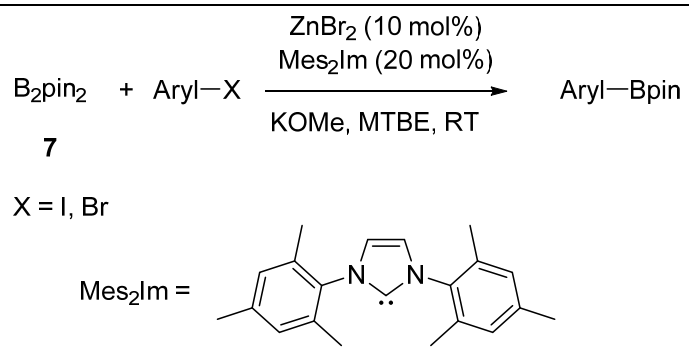

Scheme 25. Zinc-catalyzed, aromatic C–X borylation reported by Marder and co-workers.

1.2.2.5 Iron-catalyzed borylation

In 2014, Cook and co-workers,[64] reported the first iron-catalyzed borylation of alkyl electrophiles under mild conditions (Scheme 26). In the presence of $Fe(acac)_3$ as pre-catalyst, TMEDA and using water-sensitive ethylmagnesiumbromide as additive, and B_2pin_2 (**7**), they were able to borylate both unactivated and activated alkyl bromides (*prim*, *sec*), whereas the borylation of alkyl chlorides and tosylates provided only trace yields. The presence of the Grignard reagent in this reaction was required to activate the B_2pin_2 (**7**) and to reduce the iron(III) to a low valent state.

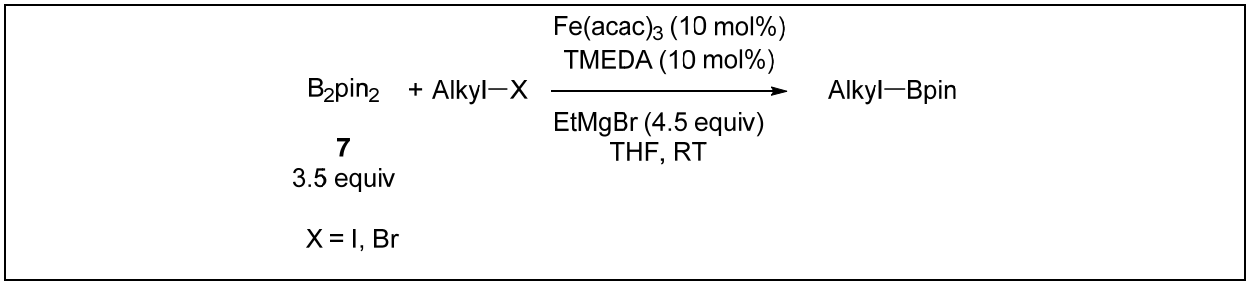

Scheme 26. Iron-catalyzed, aliphatic C–X borylation reported by Cook and co-workers.

Moreover, in 2014, Bedford *et al.*,[65] independently and almost simultaneously with Cook *et al.*,[64] developed an iron-catalyzed borylation of alky, allyl and aryl halides (Scheme 27).

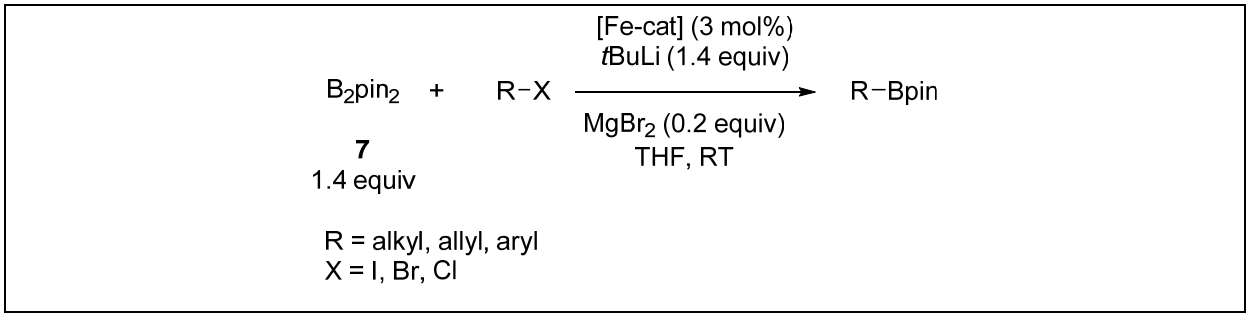

Scheme 27. Iron-catalyzed, C–X borylation reported by Bedford and co-workers.

This catalysis, also required the use of a strong reductant (Li*t*Bu) to activate the B_2pin_2 (**7**) via the formation of a borate anion (**69**), which was supported by ^{11}B and ^{1}H NMR spectroscopy. They also isolated and structurally characterized an iron(I) boryl complex (**70**), although it was shown not to be an active catalyst for the borylation reaction (Figure 3).

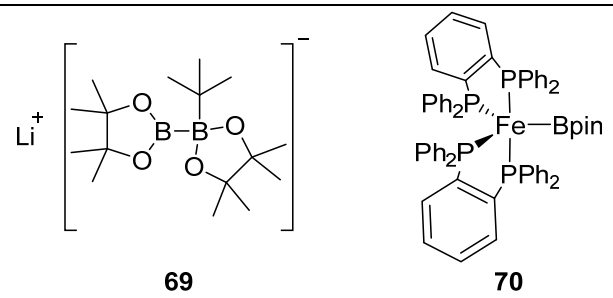

*Figure 3. Borate anion (**69**) and iron(I) boryl complex (**70**).*

1.2.2.6 Cobalt-catalyzed borylation

In 2016, Huang and co-workers[66] reported a cobalt-catalyzed borylation of aryl halides and pseudohalides (Scheme 28), which resulted in the corresponding arylboronates in good to excellent yields; even electron rich aryl chlorides gave the desired products in moderate yields, under mild conditions. Mechanistic studies included radical-scavenger and radical-clock experiments. Whereas the radical scavengers decreased the yields, the radical clock experiments, monitored by NMR spectroscopy, showed no evidence for the formation of the radical cyclization product.

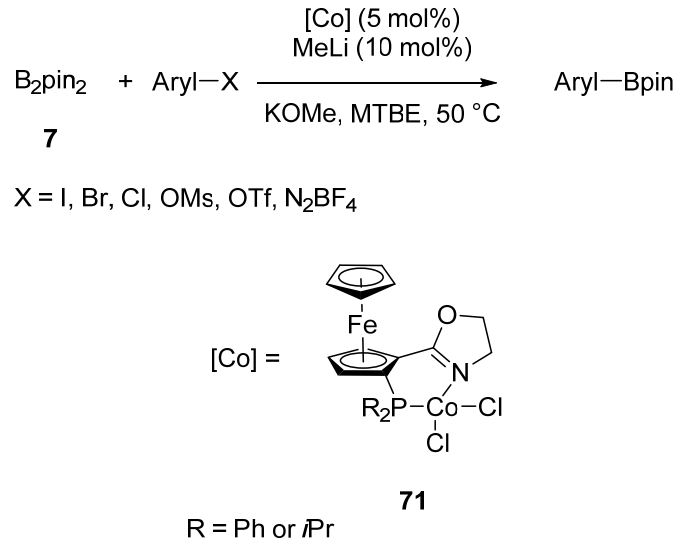

Scheme 28. Cobalt-catalyzed, aromatic C–X borylation reported by Huang and co-workers.

1.2.2.7 Manganese-catalyzed borylation

The first manganese-catalyzed borylation of unactivated alkyl chlorides was reported in 2016 by Cook and Atack (Scheme 29).[67] While the borylation of the chloro-substrates resulted in good yields, the system requires the strong reductant EtMgBr as additive. Preliminary mechanistic studies suggested a stepwise, oxidative radical process to be involved.

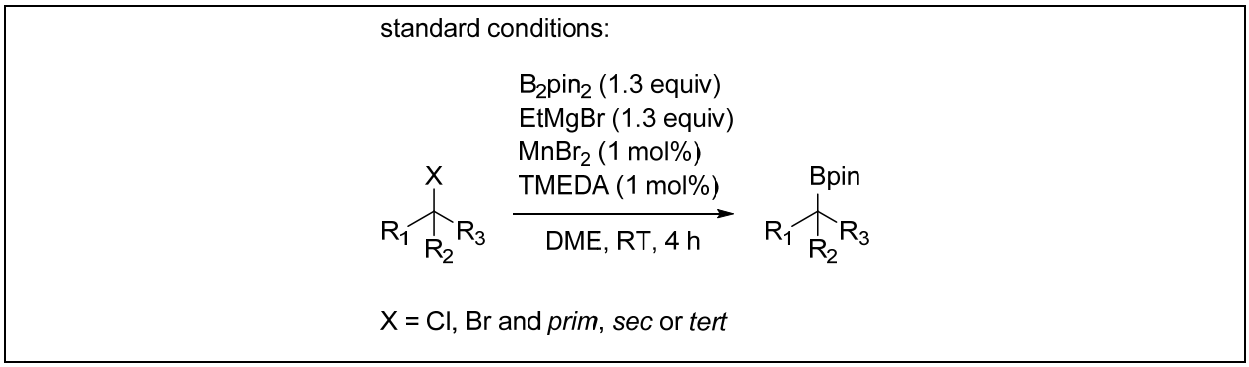

Scheme 29. Manganese-catalyzed borylation reported by Cook and Atack.

1.2.2.8 Transition metal-free borylation

In 2012, Ito *et al.*[68] reported a transition metal-free borylation of aryl-, alkenyl- and alkyl halides *via* a formal nucleophilic boryl substitution with a silylborane-alkoxy base system (Scheme 30). This facile route to the corresponding boronic esters resulted in high yields and showed a good functional group tolerance. Later the substrate scope of alky- and alkenyl halides was extended , and it was shown that heteroaryl halides could also be borylated with this method.[69,70] Mechanistic studies proposed a carbanion-mediated pathway for the boryl substitution, this was supported by DFT calculations.[71]

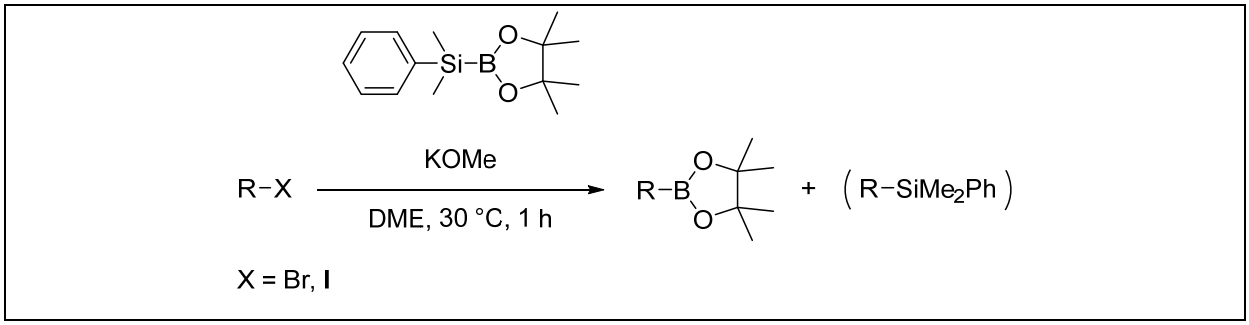

Scheme 30. Transition metal-free borylation reported by Ito and co-workers.

1.2.2.9 Metal-free borylation

In 2013, Zhang *et al*.[72] published the first metal-free borylation of aryl iodides which is promoted by cesium carbonate in methanol (Scheme 31). So far, this protocol works well for activated aryl iodides, whereas the borylation of unactivated substrates furnished only poor yields. Mechanistic studies support neither a copper-catalyzed pathway nor a radical mediated process being involved.

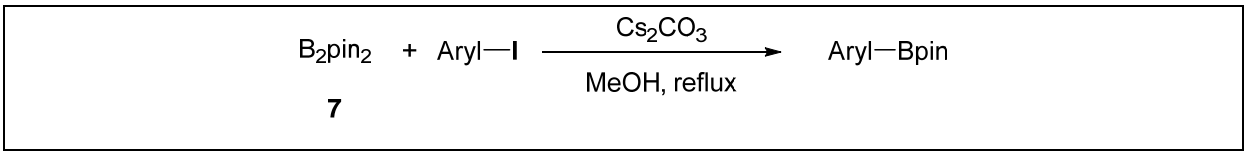

Scheme 31. Metal-free aromatic C–I borylation reported by Zhang and co-workers.

2 Motivation

Boronic acid derivatives, such as organoboronate esters, are extremely useful reagents, which are widely employed as intermediates in organic synthesis, in functional molecules or polymers, and as ^{10}B carriers in boron neutron capture therapy (BNCT) for the treatment of malignant brain tumors, and directly in biologically active compounds.[73] In particular, aryl boronate esters are utilized in Suzuki-Miyaura[74-76] and other cross-coupling reactions. These have become among the most important reagents in organic chemistry as boronate esters can be converted into virtually any functional group, resulting in access to a range of complex organic frameworks (Figure 4).[29,38,39]

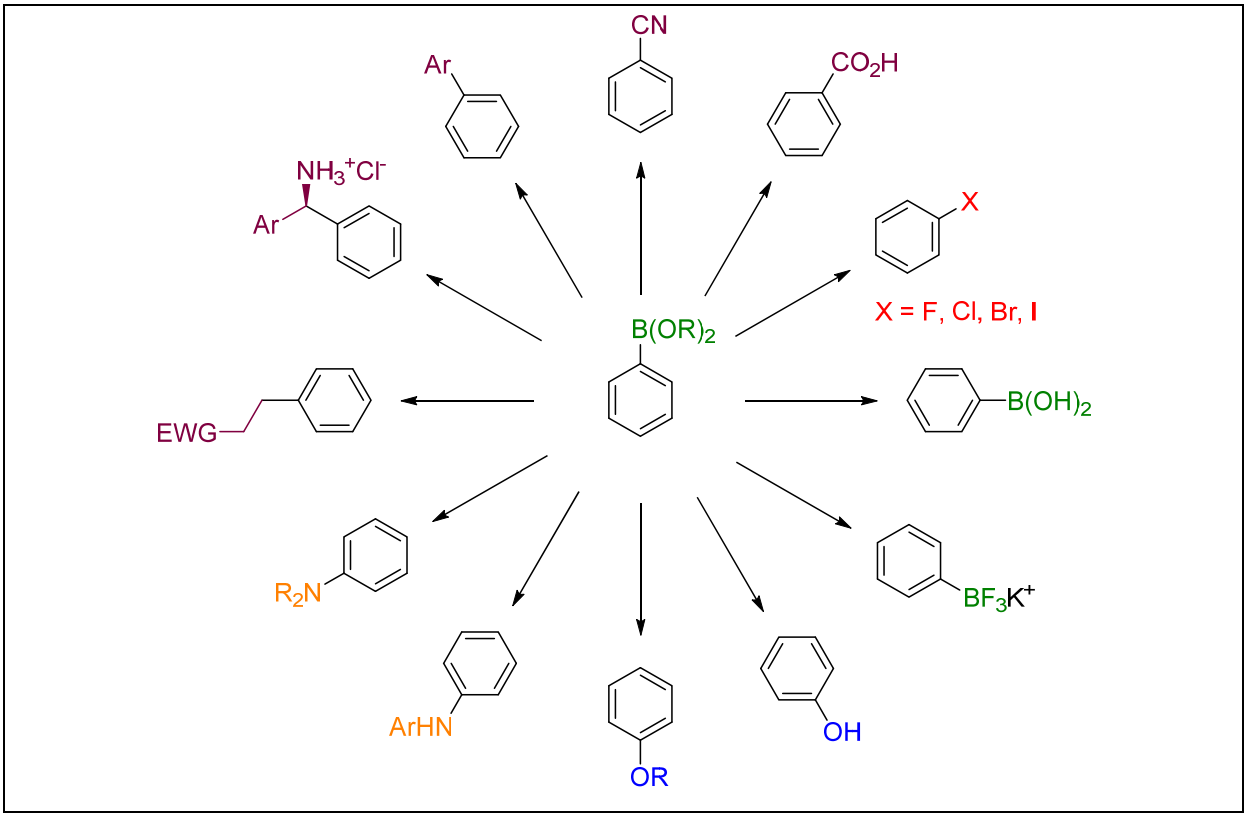

Figure 4. Conversions of aryl boronates to various functionalized aryl derivatives.

Classically, the preparation of organoboronate esters is based on the reaction of trialkylborates with Grignard- or lithium reagents or on hydroboration protocols. These routes are severely limited due to functional group reactivity of the substrates and preparative difficulties, although they are commonly applied in large scale synthesis.[38] Therefore, the challenge is to develop new ways to prepare boronate esters such as transition metal-catalyzed borylation of alkyl- or aryl halides,[77] using

inexpensive metals with the lowest toxicity possible. While direct borylation of C–H bonds is very attractive,[38,39] steric effects predominantly determine selectivity. Recent developments of the Cu-catalyzed[47,48,51-54,78] borylation of C–X bonds in both aryl- and alkyl halides under mild conditions and with inexpensive ligands, represent a major advantage over palladium[31,42,52,57,59] (expensive) and nickel[55,57,79] (toxic) systems. Even electron-rich and sterically hindered aryl bromides were suitable substrates, as were primary and secondary alkyl halides and pseudo-halides, including iodides, bromides, chlorides, and tosylates.

Therefore, it is also desirable to develop new borylation catalysts based on even less expensive, low toxicity metals, such as iron, zinc, cobalt and manganese.[60-62,66,67] Alkoxy diboron compounds,[9] above all B_2pin_2 (**7**), represent extremely useful borylation reagents to synthesize organoboron derivatives and it is desirable to extend their applications.

3 Results and discussion

3.1 Iron-catalyzed borylation

3.1.1 Borylation of 1-bromohexane and bromocyclohexane

The Fe-catalyzed borylation of 1-bromohexane (**72**) and bromocyclohexane (**66**) has been investigated using $FeCl_2$ and $FeCl_3$ as pre-catalysts in combination with various ligands (Scheme 32 and Figure 5).

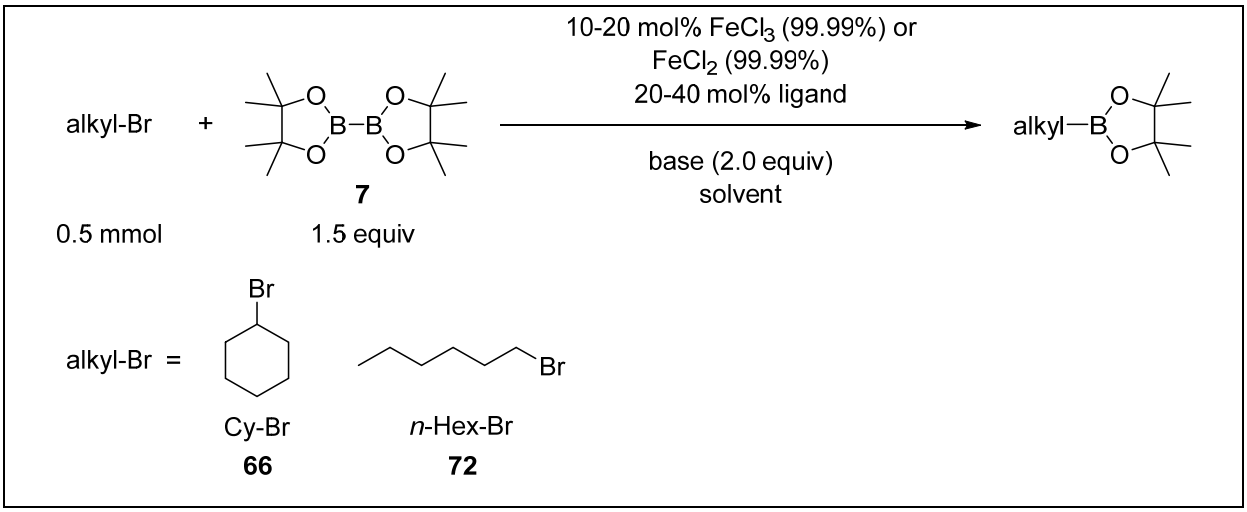

*Scheme 32. Fe-catalyzed borylation of 1-bromohexane or (**72**) and bromocyclohexane (**66**) using either iron(II)- or iron(III) chloride as the pre-catalyst.*

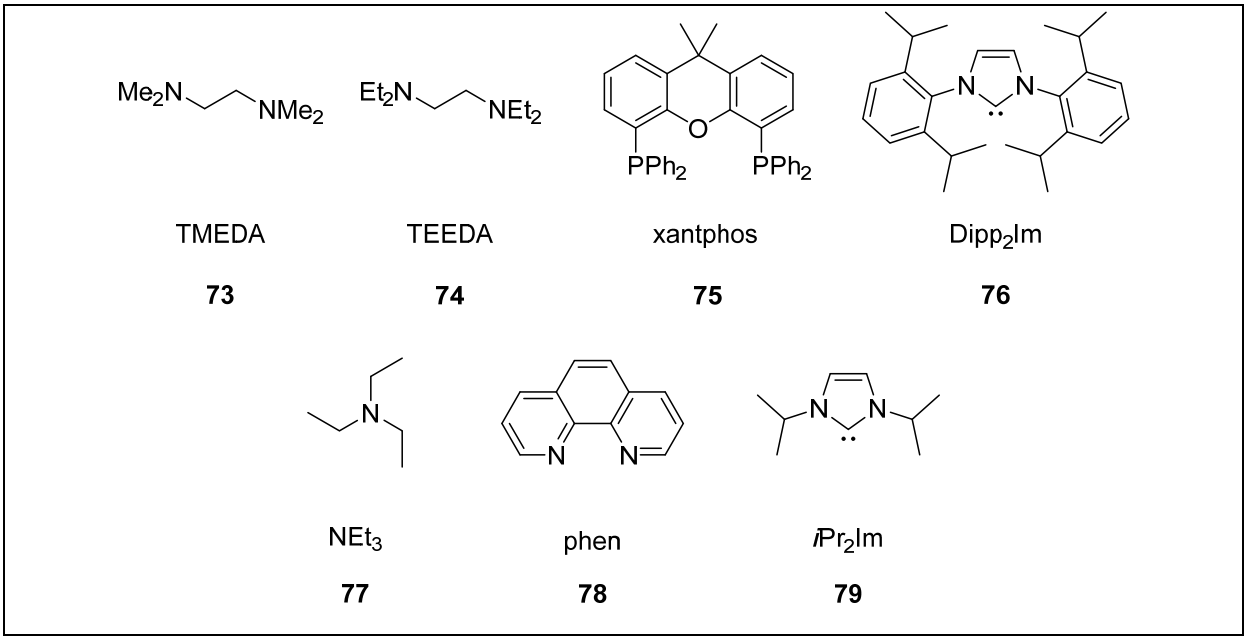

Figure 5. Ligands used in the Fe-catalyzed borylation reactions.

The first reactions were performed under following conditions: $FeCl_3$ (10 mol%) as pre-catalyst, TEEDA (20 mol%, **74**) as ligand, LiO*t*Bu (2 equiv) as base, THF (1 mL) as solvent and **72** (1 equiv) as substrate (Chart 1, Table 1).

Under these conditions, different issues were observed: first, the reaction mixture became sometimes a gel, which strongly affected the stirring and the homogeneity, and second, the poor solubility of LiO*t*Bu in THF decreased the performance of the reaction. Considering these problems, different parameters were changed to attempt to improve the performance. Thus, the ratio of $FeCl_3$ to TEEDA (**74**) as well as the reaction temperatures were varied, and a scale-up of the reaction was also performed.

*Chart 1. Corresponding to Table 1: Fe-catalyzed borylation of 1-bromohexane (**72**).*

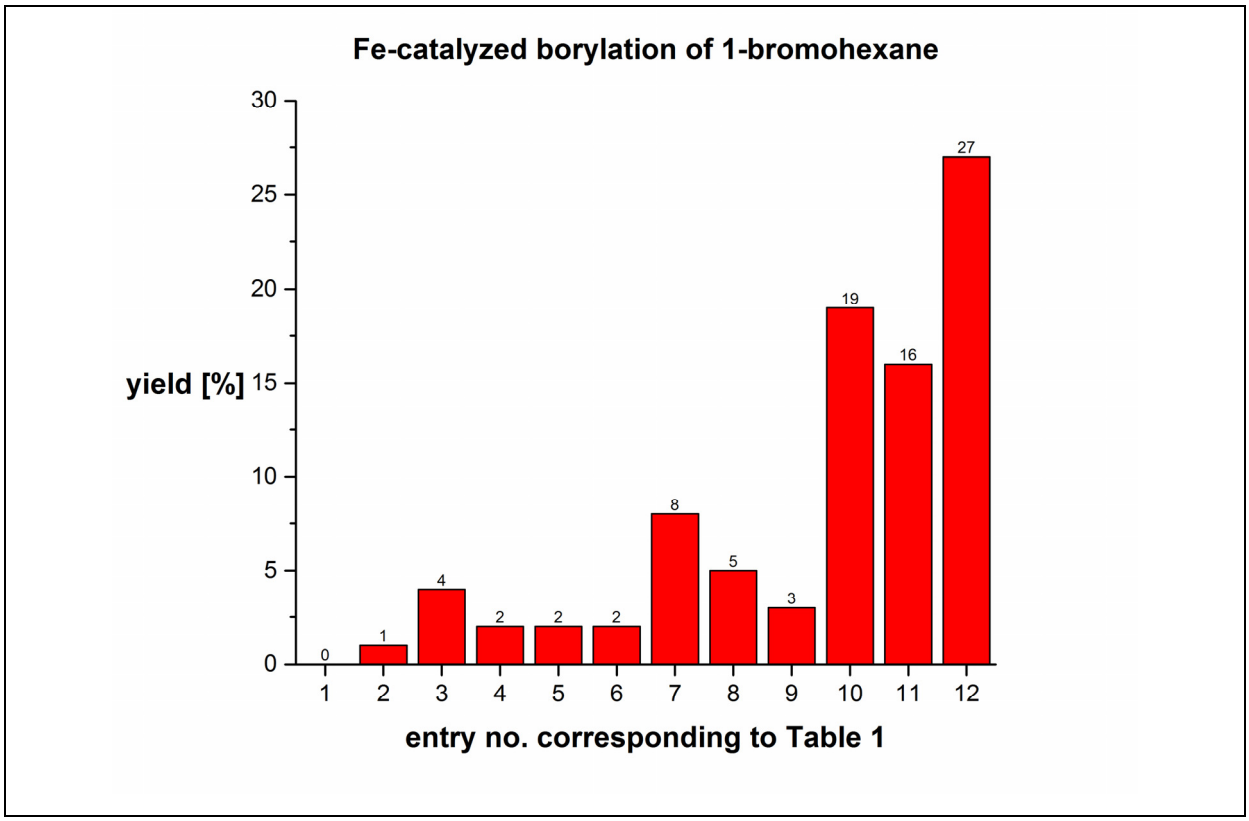

*Table 1. Fe-catalyzed borylation of 1-bromohexane[(a)] (**72**).*

entry	$FeCl_3$(99.99%) [mol%]	TEEDA [mol%]	base [2 equiv]	THF [mL]	temp. [°C]	time [hrs]	yield [%][(b)]
1	10	10	LiO*t*Bu	2	50	24	trace
2	10	10	LiO*t*Bu	2	50	24	1
3	10	10	LiO*t*Bu	2	50	24	4[(c)]
4	10	20	LiO*t*Bu	1	40	24	2
5	10	20	LiO*t*Bu	2	50	24	2[(c)]
6	10	20	LiO*t*Bu	2	60	24	2[(d)]
7	15	20	LiO*t*Bu	1	40	24	8
8	15	20	LiO*t*Bu	2	50	24	5[(c)]
9	15	20	LiO*t*Bu	2	60	24	3[(d)]
10	20	20	LiO*t*Bu	1	40	24	19
11	20	20	LiO*t*Bu	2	50	16	16±4[(c,e)]
12	**20**	**20**	**LiO*t*Bu**	**2**	**50**	**24**	**27[(c)]**

(a) scale: 0.5 mmol substrate, 1.5 equiv B_2pin_2 (**7**) and 2.0 equiv LiO*t*Bu; (b) the product yields were determined by GC-MS; (c) scale: 1.2 mmol substrate, 1.5 equiv B_2pin_2 (**7**) and 2.0 equiv LiO*t*Bu; (d) scale: 0.5 mmol substrate, 1.2 equiv B_2pin_2 (**7**) and 1.5 equiv LiO*t*Bu; (e) average yield of three reactions under exact the same conditions.

After screening different conditions, the Fe-catalyzed borylation of **72** continuously resulted in poor yields of the desired product. Therefore, further test reactions were performed with alternative ligands (e.g. phosphines and amines), but showed no improvement of the yield of the borylation (Table 2).

*Table 2. Fe-catalyzed borylation of 1-bromohexane[(a)] (**72**) with other ligands.*

entry	$FeCl_3$ [mol%]	ligand [20 mol%]	base [2 equiv]	THF [mL]	temp. [°C]	time [hrs]	yield [%][(b)]
1	20	xantphos	LiO*t*Bu	2	50	16	4
2	20	NEt_3	LiO*t*Bu	3	50	24	5[(c)]
3	20	phen	LiO*t*Bu	3	50	24	trace[(c)]

(a) scale: 1.2 mmol substrate, 1.5 equiv B_2pin_2 (**7**) and 2.0 equiv LiO*t*Bu; (b) the product yields were determined by GC-MS; (c) scale: 1.2 mmol substrate, 1.1 equiv B_2pin_2 (**7**) and 1.5 equiv LiO*t*Bu.

A screening with TMEDA (**73**) as the ligand, was performed but did not show any improvement (Table 3).

*Table 3. Fe-catalyzed borylation of 1-bromohexane[(a)] (**72**) with TMEDA (**73**) as ligand under different reaction conditions.*

entry	$FeCl_3$ [mol%]	TMEDA [mol%]	base [2 equiv]	solvent [mL]	temp. [°C]	time [hrs]	yield [%][(b)]
1	10	-	LiO*t*Bu	THF	45	24	-
2	**20**	**20**	**LiO*t*Bu**	**THF**	**50**	**16**	**12[(c)]**
3	20	40	LiO*t*Bu	THF	75	20	trace[(c,d)]
4	10	20	LiO*t*Bu	toluene	50	24	trace[(e,f)]
5	20	40	KOMe	MTBE	45	72	2
6	10	20	KOMe	MTBE	45	96	4

(a) scale: 0.5 mmol substrate, 1.5 equiv B_2pin_2 (**7**) and 2.0 equiv base; (b) the product yields were determined by GC-MS; (c) scale: 1.2 mmol substrate, 1.5 equiv B_2pin_2 (**7**) and 2.0 equiv LiO*t*Bu; (d) microwave heating; (e) scale: 0.5 mmol substrate, 1.1 equiv B_2pin_2 (**7**) and 1.5 equiv LiO*t*Bu; (f) scale: 0.6 mmol substrate, 1.5 equiv B_2pin_2 (**7**) and 2.0 equiv LiO*t*Bu.

Due to the poor yields (max. 27%, Table 1) in the borylation of **72**, with a maximum turnover number (TON) of ~ 1, the reactions were classified as semi-stoichiometric and not catalytic. In order to check and improve the borylation reaction performance the substrate was changed to bromocyclohexane (**66**) and different reaction conditions of the Fe-catalyzed borylation were screened (Chart 2, Table 4).

*Chart 2. Corresponding to Table 4: Fe-catalyzed borylation of bromocyclohexane (**66**).*

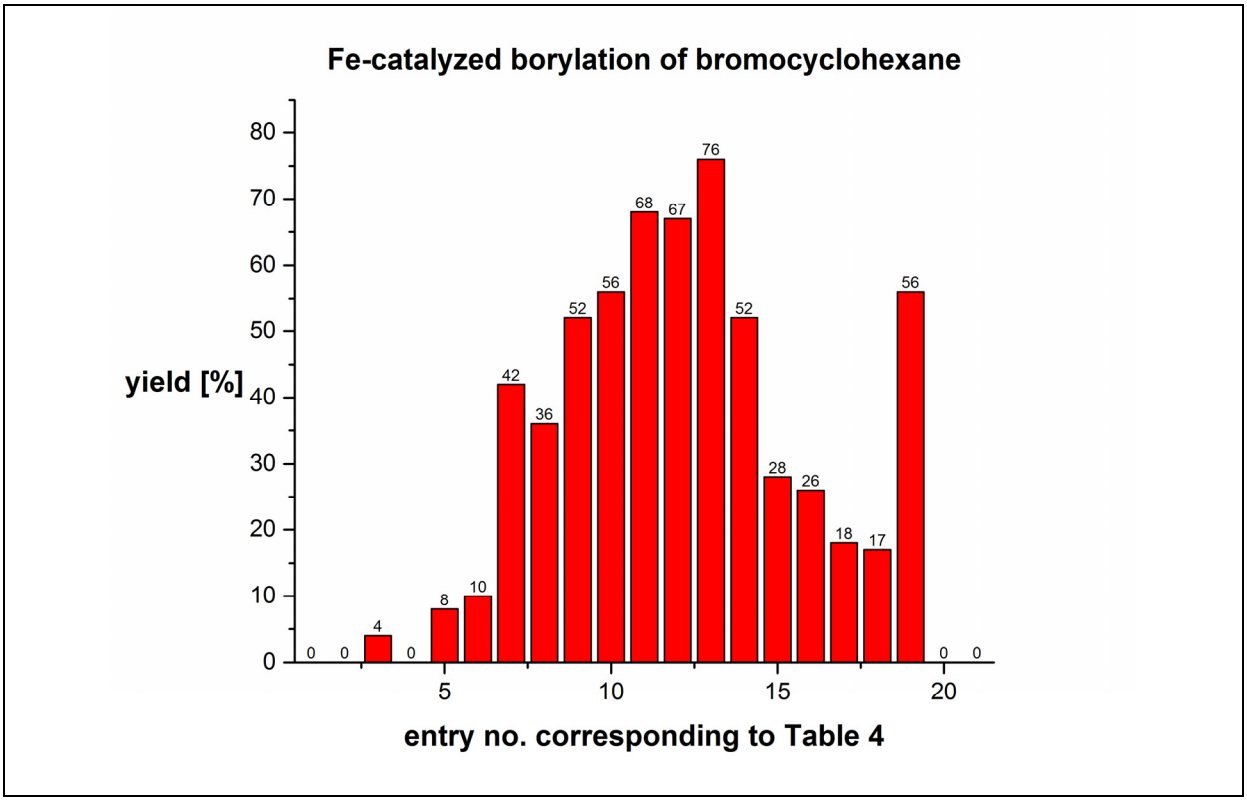

*Table 4. Screening of Fe-catalyzed borylation of bromocyclohexane[(a)] (**66**) with TMEDA (**73**) as ligand.*

entry	$FeCl_3$ [mol%]	TMEDA [mol%]	base [2 equiv]	solvent [5 mL]	temp. [°C]	time [hrs]	yield [%][(b)]
1	20	20	LiO*t*Bu	THF	45	24	trace
2	20	40	LiO*t*Bu	MTBE	45	96	trace
3	20	20	KO*t*Bu	THF	45	24	4
4	20	20	KO*t*Bu	MTBE	45	24	-
5	20	20	KOMe	THF	45	24	8
6	20	40	KOMe	THF	45	24	10
7	10	20	KOMe	MTBE	45	96	42
8	20	20	KOMe	MTBE	45	24	36
9	20	20	KOMe	MTBE	45	96	52
10	20	40	KOMe	MTBE	45	48	56
11	20	40	KOMe	MTBE	45	96	68
12	20	40	KOMe	MTBE	45	96	67
13	**20**	**40**	**KOMe**	**MTBE**	**45**	**96**	**76**
14	20	40	KOMe	MTBE	RT	96	52
15	**20**	**40**	**KOMe**	**MTBE**	**RT**	**96**	**28[(c)]**
16	20	40	KOMe	MTBE	45	96	26[(d)]
17	20	40	KOMe	MTBE	45	120	18[(d)]
18	20	40	KOMe	MTBE	60	72	17
19	20	40	KOMe	Et_2O	45	72	56
20	20	40	KOMe	EtOH	45	24	-[(e)]
21	20	40	KOMe	MeCN	45	24	-

(a) scale: 0.5 mmol substrate, 1.5 equiv B_2pin_2 (**7**) and 2.0 equiv base; (b) the product yields were determined by GC-MS; (c) isolated yield, scale: 100 mmol substrate, 1.5 equiv B_2pin_2 (**7**) and 2.0 equiv KOMe; (d) scale: 0.5 mmol substrate, 1.5 equiv KOMe and 1.5 equiv B_2pin_2 (**7**), MTBE (3 mL); (e) KOMe was more soluble in ethanol, but generated the ethoxy anion $[EtO]^-$ which reacted with B_2pin_2 and formed EtO-Bpin.

The reactions gave moderate to good yields (Chart 2, Table 4, entries 7-14) with a maximum turnover number (TON) of ~ 4 (Chart 2, Table 4, entry 13). The optimal reaction conditions were determined to be: TMEDA (**73**) as ligand, KOMe as base, MTBE or Et_2O as solvent and a runtime of 96 h at 45 °C. In a large scale reaction (100 mmol substrate) under these conditions, the cyclohexyl boronic ester was isolated in 28% yield (Chart 2, Table 4, entry 15). Nevertheless, there are still issues to consider, such as the long runtime of 96 hours. Therefore, further test reactions were performed to check how dilution, a radical initiator (AIBN), or a radical

scavenger (9,10-dihydroanthracene) affected the runtime and the yield of the desired product (Table 5).

*Table 5. Fe-catalyzed borylation of bromocyclohexane[(a)] (**66**) with TMEDA (**73**) as ligand and AIBN or 9,10-dihydroanthracene as additive.*

entry	$FeCl_3$ [mol%]	TMEDA [mol%]	base [2 equiv]	solvent [5 mL]	temp. [°C]	time [hrs]	yield [%][(b)]
1	20	40	KOMe	MTBE	45	72	-[(c)]
2	20	40	KOMe	MTBE	45	96	-[(d)]
3	20	40	KOMe	MTBE	45	24	-[(e)]
4	20	40	KOMe	MTBE	90	1	trace[(e,f)]
5	20	40	KOMe	MTBE	90	4	trace[(e,f)]
6	**20**	**40**	**KOMe**	**MTBE**	**90**	**4**	**-[(f,g)]**

(a) scale: 0.5 mmol substrate, 1.5 equiv B_2pin_2 (**7**) and 2.0 equiv KOMe; (b) the product yields were determined by GC-MS; (c) 15 mL solvent, reaction too dilute, no conversion of starting material observed; (d) reaction performed with radical scavenger (9,10-dihydroanthracene); (e) reaction performed with radical initiator (AIBN); (f) microwave heating; (g) no internal standard added, complete conversion of starting material, product was detected, no quantitation; for subsequent quantitation, see below.

In the reactions with both the radical scavenger and the radical initiator it was observed that the performance of the borylation of bromocyclohexane (**66**) was strongly decreased. (Table 5).

Further reactions were carried out at 90 °C (microwave heating) to take the initiating temperature of AIBN into account, but no improvements were observed (Table 5, entries 4 and 5). However, a microwave-heated (90 °C) test reaction without additive showed complete conversion of starting material (Table 5, entry 6). Accordingly, a screening of microwave-heated Fe-catalyzed borylation reactions of **66** was performed (Table 6). The runtime was reduced to 4 hours and the reactions gave moderate yields, whereas the “classically” oil bath heated reactions did not show any conversion of the starting material under the same reaction conditions and runtime.

*Table 6. Microwave-heated, Fe-catalyzed borylation of bromocyclohexane[(a)] (**66**) with TMEDA (**73**) as ligand.*

entry	$FeCl_3$ [mol%]	TMEDA [mol%]	base [2 equiv]	solvent [5 mL]	temp. [°C]	time [hrs]	yield [%][(b)]
1	20	20	KOMe	MTBE	70	2	-[(c)]
2	**20**	**40**	**KOMe**	**MTBE**	**90**	**4**	**40±8[(c,d)]**
3	20	40	KOMe	MTBE	90	5	27[(c)]
4	20	40	KOMe	MTBE	90	10 min	7[(c)]
5	20	40	KOMe	THF	90	1.5	trace[(c)]
6	20	40	KOMe	MTBE	90	4	-[(e)]

(a) scale: 0.5 mmol substrate, 1.5 equiv B_2pin_2 (**7**) and 2.0 equiv KOMe; (b) the product yields were determined by GC-MS; (c) microwave heating; (d) average yield of three reactions under the exact same conditions; (e) two reactions were "classically" heated in an oil bath, and no conversion of starting material was observed.

In further experiments, different ligands were screened for the Fe-catalyzed borylation of **66** (Table 7). In addition, $FeCl_2$ was used as iron source to see if the oxidation state of the iron made a difference, but no improvement was observed (Table 8).

*Table 7. Fe-catalyzed borylation of bromocyclohexane[(a)] (**66**) with different ligands*

entry	$FeCl_3$ [mol%]	ligand [mol%]	base [2 equiv]	solvent [5 mL]	temp. [°C]	time [hrs]	yield [%][(b)]
1	**20**	**$Dipp_2Im$ [20]**	**KOMe**	**MTBE**	**90**	**4**	**33[(c)]**
2	20	$Dipp_2Im$ [40]	KOMe	MTBE	45	96	18
3	20	*i*Pr_2Im [30]	KOMe	MTBE	90	2	trace[(c)]
4	20	*i*Pr_2Im [30]	KOMe	THF	90	4	trace[(c)]
5	20	xantphos [40]	KOMe	MTBE	45	96	19

(a) Scale: 0.5 mmol substrate, 1.5 equiv B_2pin_2 (**7**) and 2.0 equiv KOMe; (b) the product yields were determined by GC-MS; (c) microwave heating.

*Table 8. Fe-catalyzed borylation of bromocyclohexane[(a)] (**66**) with $FeCl_2$ as pre-catalyst and different ligands*

entry	$FeCl_2$ [mol%]	ligand [mol%]	base [2 *equiv*]	solvent [5 mL]	temp. [°C]	time [hrs]	yield [%][(b)]
1	20	$Dipp_2Im$ [40]	KOMe	THF	45	48	7
2	20	$Dipp_2Im$ [40]	KOMe	THF	90	4	11[(c)]
3	20	TMEDA [40]	KOMe	THF	45	48	8

(a) Scale: 0.5 mmol substrate, 1.5 equiv B_2pin_2 (**7**) and 2.0 equiv KOMe; (b) the product yields were determined by GC-MS; (c) microwave heating.

3.1.2 Conclusion (Fe-catalyzed borylation)

In conclusion, the Fe-catalyzed borylation reactions gave poor yields for the *prim* substrate and moderate to good yields for the *sec* substrate. Taking into account that the reactions with a radical initiator or a radical scavenger both decreased the yield, and effectively shut down the reaction, a radical process might be involved but this was not be proven. The mechanism of the borylation is not yet clear.

Several issues, such as the poor solubility of the base, strongly affected the reaction performance. Disappointingly, at this stage, the Fe-catalyzed borylation of *prim* and *sec* alkyl halides cannot compete with other catalysts such as copper-, nickel- or zinc based systems at this time. However, the best results are sorted by ligand and are summarized in Chart 3 and Table 9.

*Chart 3. Corresponding to Table 9: Fe-catalyzed borylation of 1-bromohexane (**72**) and bromo-cyclohexane (**66**).*

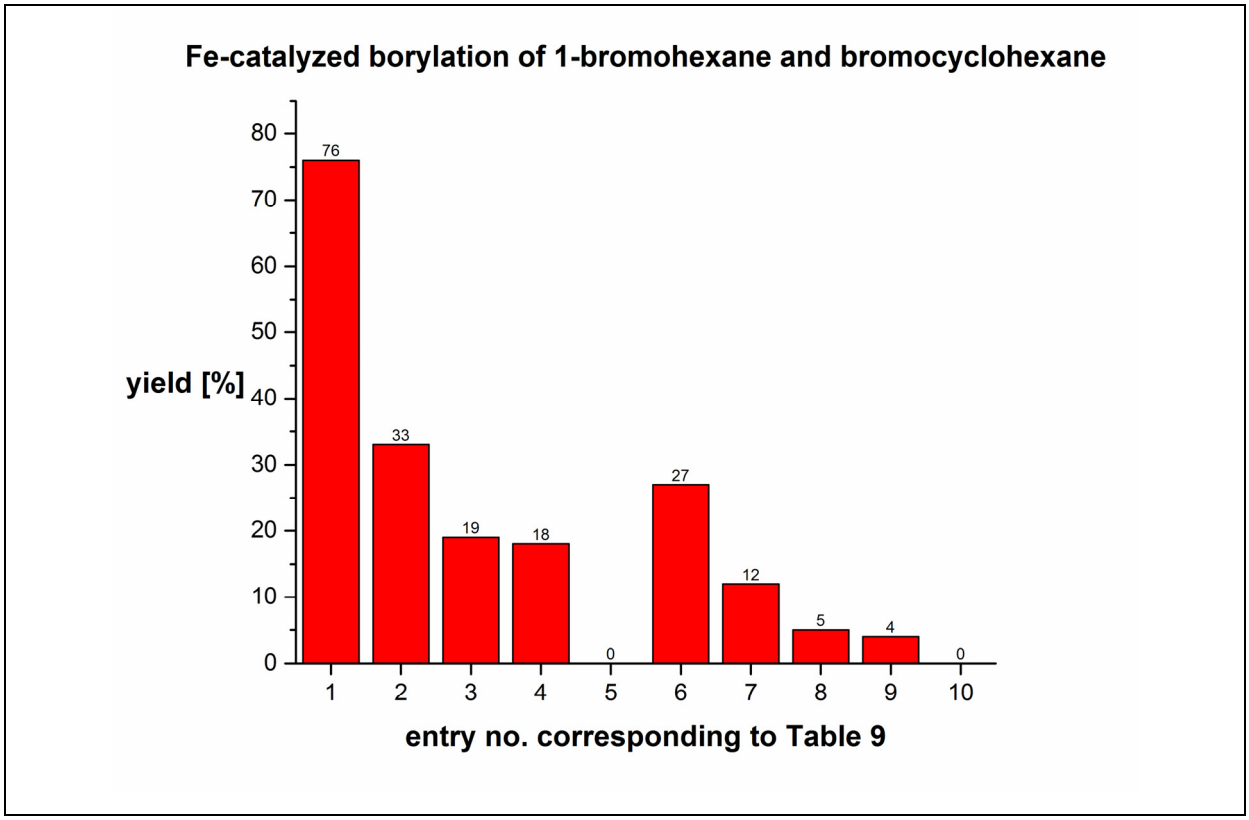

*Table 9. Fe-catalyzed borylation of 1-bromohexane (**72**) and bromocyclohexane (**66**): best results sorted by ligand.*

entry	substrate	$FeCl_3$ [mol%]	ligand [mol%]	base	solvent	temp. [°C]	time [hrs]	yield [%][(a)]
1	Cy-Br	20	TMEDA [40]	KOMe	MTBE	45	96	76
2	Cy-Br	20	$Dipp_2Im$ [20]	KOMe	MTBE	90	4	33[(b)]
3	Cy-Br	20	xantphos [40]	KOMe	MTBE	45	96	19
4	Cy-Br	20	$Dipp_2Im$ [40]	KOMe	MTBE	45	96	18
5	Cy-Br	20	iPr_2Im [30]	KOMe	THF	90	4	trace[(b)]
6	*n*-Hex-Br	20	TEEDA [20]	LiO*t*Bu	THF	50	24	27
7	*n*-Hex-Br	20	TMEDA [20]	LiO*t*Bu	THF	50	16	12
8	*n*-Hex-Br	20	NEt_3 [20]	LiO*t*Bu	THF	50	24	5
9	*n*-Hex-Br	20	xantphos [20]	LiO*t*Bu	THF	50	16	4
10	*n*-Hex-Br	20	phen [20]	LiO*t*Bu	THF	50	24	trace

(a) The product yields were determined by GC-MS; (b) Microwave heating.

Recently reported Fe-catalyzed borylation reactions[64,65] require a large amount of alkoxy diboron compound and a strong reductant, such as organolithium or Grignard reagents as additive to perform the borylation in moderate to good yields. Thus, this approach does not seem to be the best, given the classical synthesis of boronate esters by reaction of Grignard or organolithium reagents with suitable boron compounds, because functional group tolerance is still an issue. In addition, the quantaties of additive and alkoxy diboron compound required in these Fe-catalyzed borylation reactions are not attractive from an economic point of view.

3.2 Copper-catalyzed borylation

In the recently reported Cu-catalyzed borylation of aryl halides, Kleeberg, Lin and Marder *et al.*[48] demonstrated a very facile route to aryl boronic esters (Scheme 33).

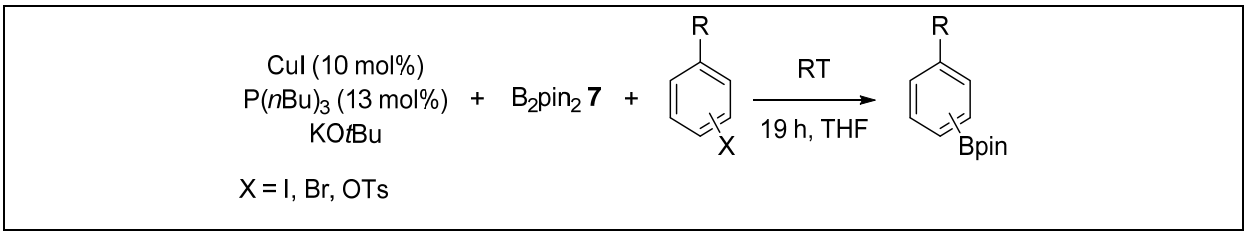

Scheme 33. Copper-catalyzed aromatic C–X borylation.

The application of simple and inexpensive starting materials (e.g. CuI, KO*t*Bu, P(*n*Bu)$_3$, B_2pin_2) for the borylation reactions under mild conditions, was a great advantage compared to Miyaura's Pd-catalyzed borylation,[31] which was the first transition metal catalyzed borylation of aryl-X and the best choice at this time. It also was an very good alternative to the classical routes to aryl boronates (*via* Grignard or organo lithium reagents).

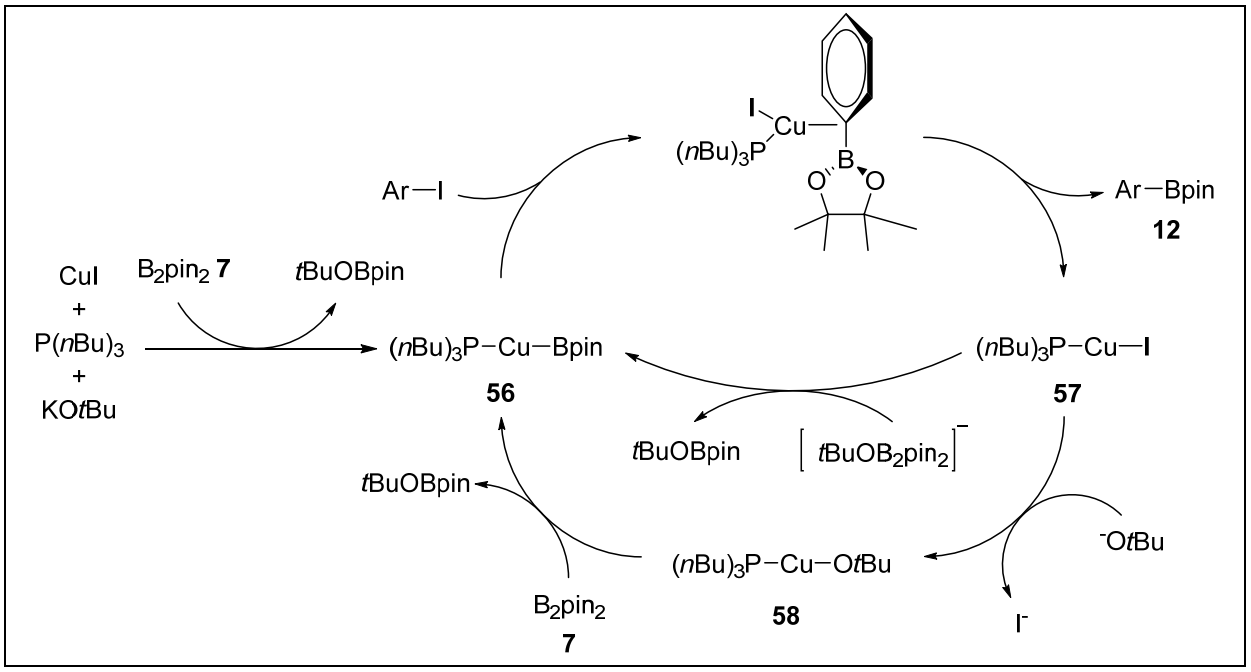

Scheme 34. Proposed mechanism for the Cu-catalyzed borylation of aryl halides.

As, the B–B bond activation and the reactivity of Lewis base adducts of alkoxy diboron(4) compounds as nucleophiles was reported,[80] the originally proposed mechanism for the Cu-catalyzed borylation of aryl halides, by Kleeberg, Lin and Marder *et al.,*[48] *via* a Cu-alkoxy complex **58** (Scheme 34; see also chapter one, 1.2.2.2, Scheme 17) can be modified. The Cu-boryl complex **56** might be also formed directly by transmetalation of the Cu-phosphine complex **57** with an adduct of tBuO$^-$ and B_2pin_2.

Whereas the performance of the Cu-catalysis was very good for electron poor and electron rich iodides, bromides and tosylates, with a great tolerance to many functional groups, some substrates with more or less intolerant functional groups (e.g. nitriles, esters and nitro compounds) were still challenging concerning side reactions such as transesterification and hydrodehalogenation. Therefore, further ligands, bases and substrates were screened to investigate the scope of this catalysis and to identify the issues with some substrates.

3.2.1 Ligand screening

Under the standard conditions of Kleeberg and Marder *et al.*[48], as different σ-donor, π-acceptor ligands, with more or less sterical demand,[81] as well as chelating ligands, were tested for the Cu-catalyzed borylation of 4-iodotoluene, 4-bromotoluene and 4-chlorotoluene (Scheme 35).

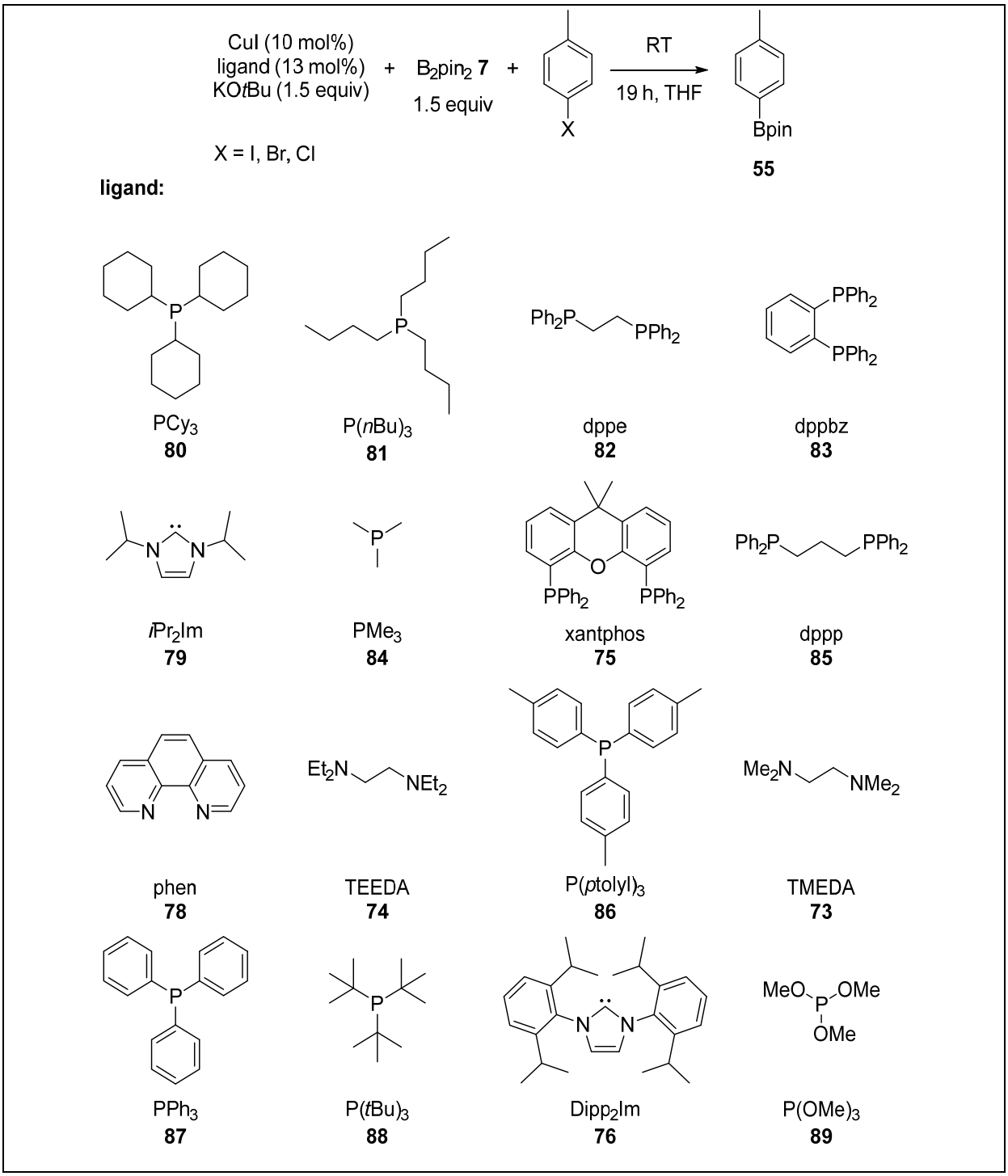

Scheme 35. Ligand screening; Cu-catalyzed aromatic C–X borylation of 4-iodo-,4-bromo- and 4-chlorotoluene.

For the borylation of 4-iodotoluene (Table 10, Chart 4), the ligands PCy_3 and $P(nBu)_3$ gave very good yields up to 92% (entries 1-2), whereas dppe, dppbz, iPr_2Im, PMe_3, xantphos and dppp resulted in good yields of about 68% (entries 3-8). The less effective ligands phen, TEEDA, $P(ptolyl)_3$, TMEDA, PPh_3, $P(tBu)_3$, $Dipp_2Im$ and $P(OMe)_3$ gave about 20% yield. Coincident with a decreasing yield of the borylated product, increasing hydrodehalogenation was observed (entries 9-16). Moreover, the conversion of the starting material was not complete using the ligands dppp, TEEDA, TMEDA and $Dipp_2Im$.

Table 10. Ligand screening for the Cu-catalyzed borylation of 4-iodotoluene.[(a)]

entry	ligand	starting material [%][(b)]	hydrodehalogenation [%][(b)]	yield [%][(b)]
1	PCy_3	-	6	92
2	$P(nBu)_3$	-	6	75
3	dppe	-	22	69
4	dppbz	-	14	69
5	iPr_2Im	-	6	68
6	PMe_3	-	25	68
7	xantphos	-	27	68
8	dppp	34	28	43
9	phen	-	20	32
10	TEEDA	13	56	29
11	$P(ptolyl)_3$	-	55	27
12	TMEDA	13	70	26
13	PPh_3	-	60	20
14	$P(tBu)_3$	-	69	7
15	$Dipp_2Im$	56	27	3
16	$P(OMe)_3$	1	38	3

(a) standard conditions: 10 mol% CuI, 13 mol% ligand, 1.5 equiv KO*t*Bu, 1.5 equiv B_2pin_2, 459 µmol substrate; (b) The yields were determined by GC-MS.

Chart 4. Corresponding to Table 10, ligand screening for the Cu-catalyzed borylation of 4-iodotoluene.

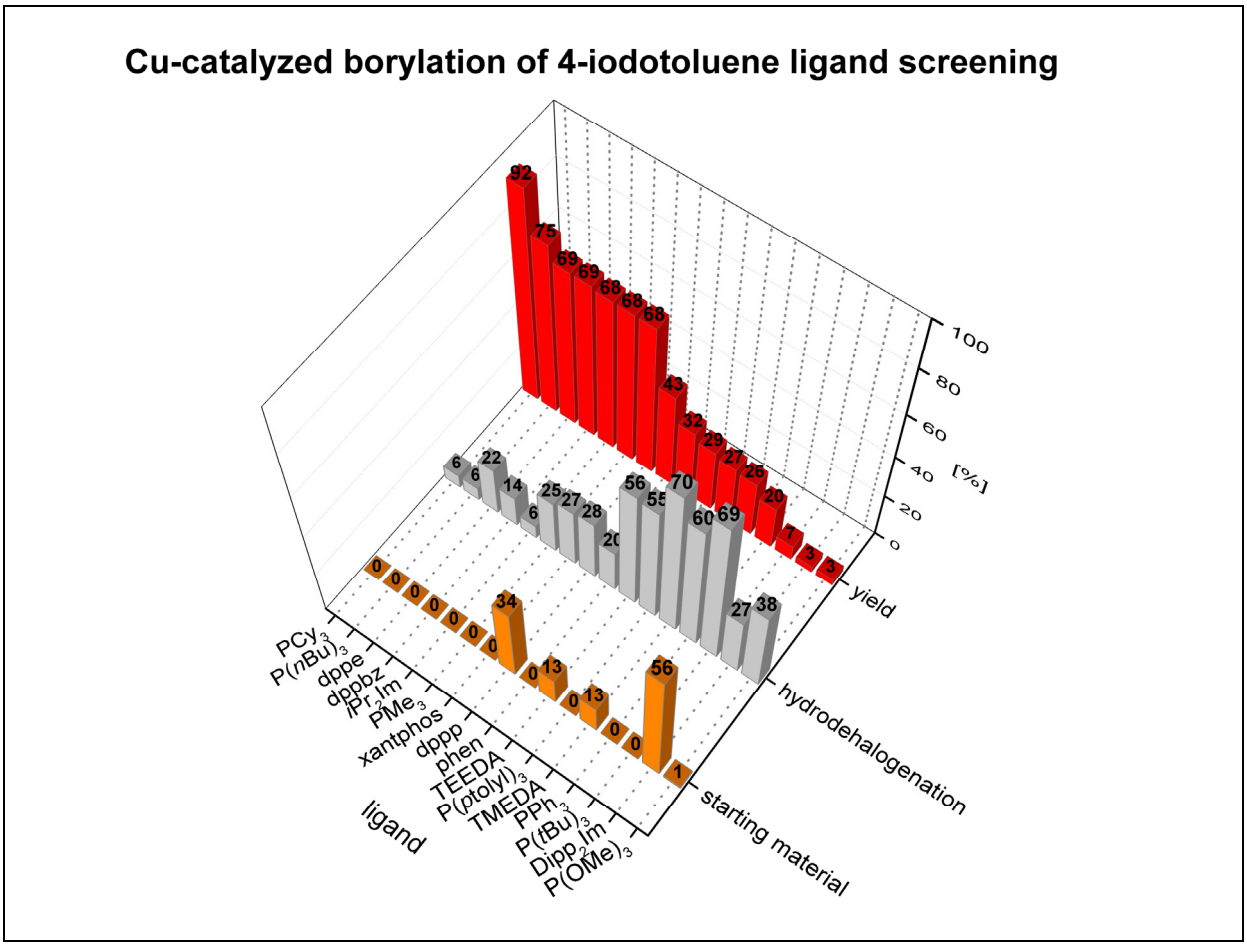

PCy_3, dppbz, dppp and $P(nBu)_3$ were also effective for the borylation of 4-bromotoluene (Table 11, Chart 5) and resulted in yields up to 73% (entries 1-4) whereas, PMe_3, xantphos, dppe and $P(tBu)_3$ were less efficient (entries 5-8), and phen, TEEDA, $P(ptolyl)_3$, TMEDA, PPh_3 and $P(OMe)_3$ were essentially inactive (entries 9-14). For all reactions, hydrodehalogenation was observed as well, and increased when the formation of the borylated product decreased, respectively, and the starting material was not converted completely.

For the Cu-catalyzed borylation of 4-chlorotoluene, none of the ligands were effective and no conversion of the substrate to any product was observed.

Table 11. Ligand screening for the Cu-catalyzed borylation of 4-bromotoluene[(a)]

entry	ligand	starting material [%][(b)]	hydrodehalogenation [%][(b)]	yield [%][(b)]
1	PCy_3	-	21	73
2	dppbz	17	11	45
3	dppp	-	40	40
4	$P(nBu)_3$	-	41	35
5	PMe_3	-	67	14
6	xantphos	68	11	10
7	dppe	72	6	8
8	$P(tBu)_3$	59	17	5
9	phen	54	22	1
10	TEEDA	94	5	0
11	$P(ptolyl)_3$	78	7	0
12	TMEDA	93	7	0
13	PPh_3	75	8	0
14	$P(OMe)_3$	78	10	0

(a) standard conditions: 10 mol% CuI, 13 mol% ligand, 1.5 equiv KO*t*Bu, 1.5 equiv B_2pin_2, 459 µmol substrate; (b) The yields were determined by GC-MS.

Chart 5. Corresponding to Table 11, ligand screening for the Cu-catalyzed borylation of 4-bromotoluene.

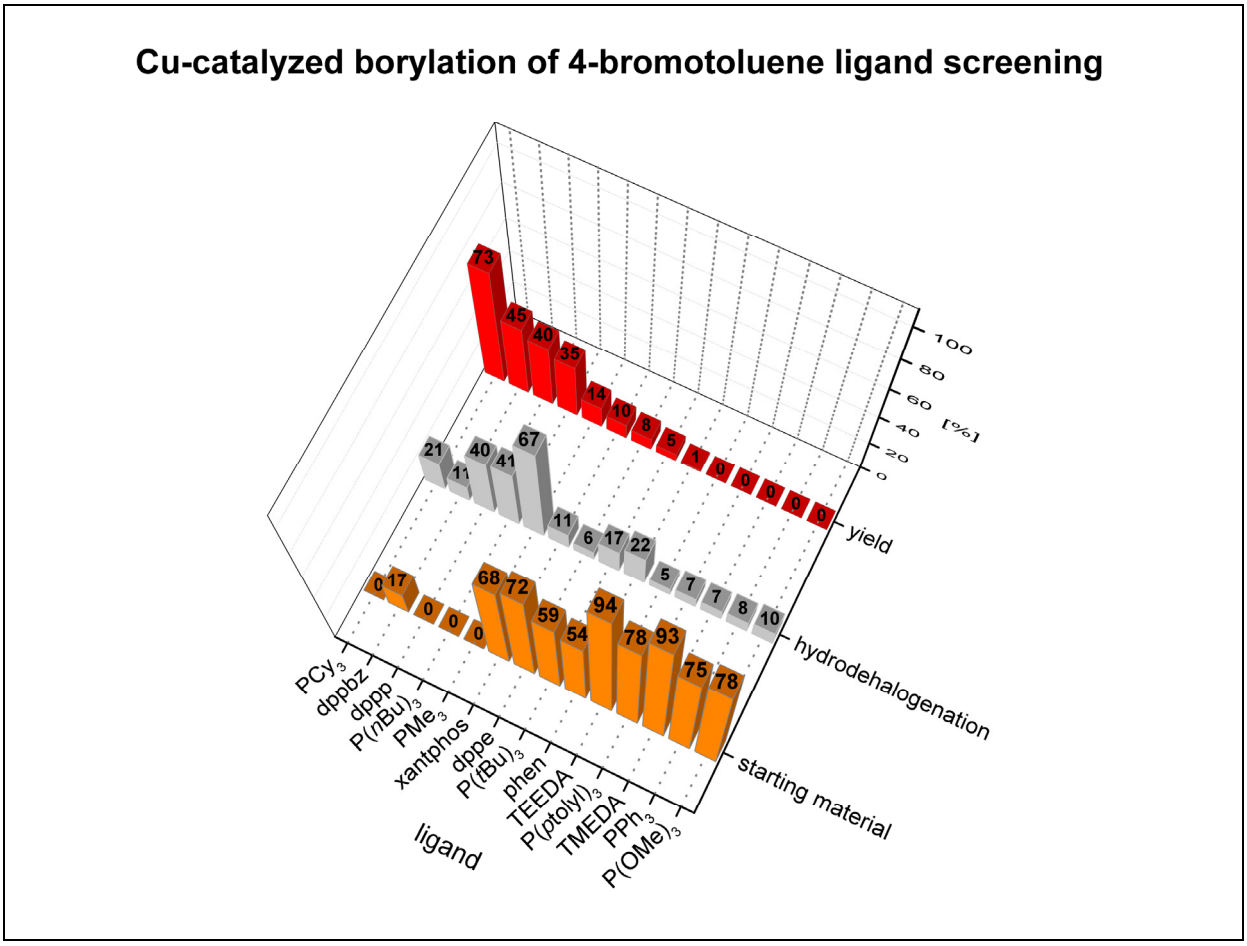

For the borylation of 4-iodotoluene and 4-bromotoluene, the use of monodentate phosphine ligands resulted in moderate to very good yields and, dependent on the basicity of the phosphine, the yield increased, with one exception, namely the bulky P(*t*Bu)$_3$ for which steric effects might be stronger than electronic effects (Table 12).

Table 12. Basicity of monodentate phosphine ligands and the resulting yields of the Cu-catalyzed borylation of 4-iodotoluene and 4-bromotoluene.[(a)]

entry	ligand	pk_a	4-Iodotoluene yield [%][(b)]	4-bromotoluene [%][(b)]
1	P(*t*Bu)$_3$	12.2[82]	7	5
2	PCy$_3$	9.70[83]	92	73
3	P(*n*Bu)$_3$	8.43[83]	75	35
4	PMe$_3$	8.65[83]	68	14
5	P(*p*tolyl)$_3$	4.46[84]	27	0
6	PPh$_3$	2.73[83]	20	0
7	P(OMe)$_3$	0.83[84]	3	0

(a) standard conditions: 10 mol% CuI, 13 mol% ligand, 1.5 equiv KO*t*Bu, 1.5 equiv B_2pin_2, 459 µmol substrate; (b) The yields were determined by GC-MS.

Chelating phosphine ligands showed good yields as well; even though they are lower in basicity, a combination of electronic and steric effects (bite angle) might affect the performance of the borylation reaction (Table 13).

Table 13. Cheating phosphine ligands and the resulting yields of the Cu-catalyzed borylation of 4-iodotoluene and 4-bromotoluene.[(a)]

entry	ligand	pk_a1[85]	natural bite angel[86] P-M-P [°]	4-Iodotoluene yield [%][(b)]	4-bromotoluene [%][(b)]
1	dppe	3.86	85	69	8
2	dppbz	4.50	83	69	45
3	xantphos	n.a.	107[(c)]	68	10
4	dppp	2.91	91	43	40

(a) standard conditions: 10 mol% CuI, 13 mol% ligand, 1.5 equiv KO*t*Bu, 1.5 equiv B_2pin_2, 459 µmol substrate; (b) The yields were determined by GC-MS. (c) flexibility range 97° to 135°; see ref.[86]

In Chart 6 and Chart 7, the yields for the borylation of 4-iodo- and 4-bromotoluene as well as the corresponding hydrodehalogenation are shown in comparison.

Chart 6. Ligand screening for the Cu-catalyzed borylation of aryl halides in comparison.

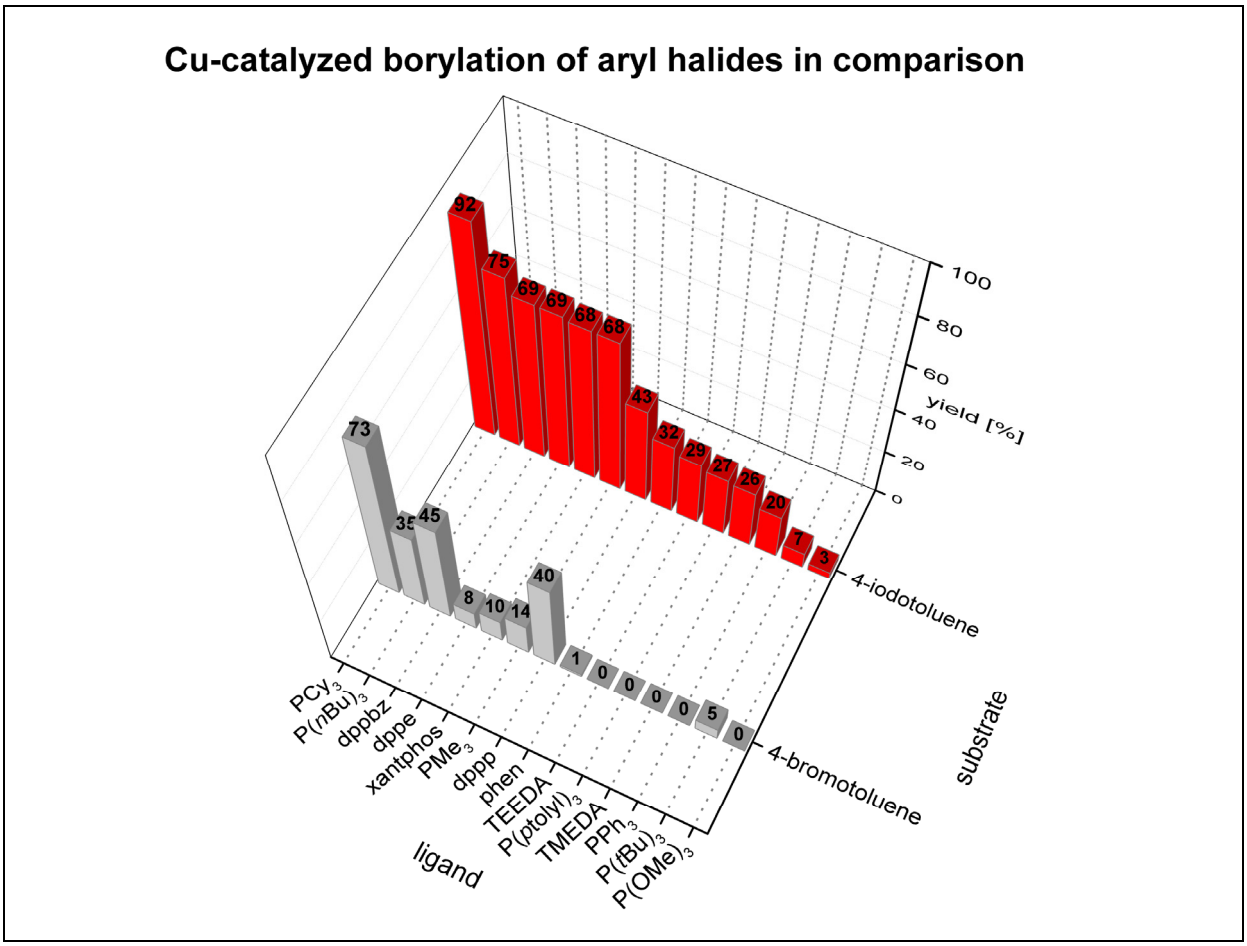

Chart 7. Hydrodehalogenation during ligand screening for the Cu-catalyzed borylation of aryl halides.

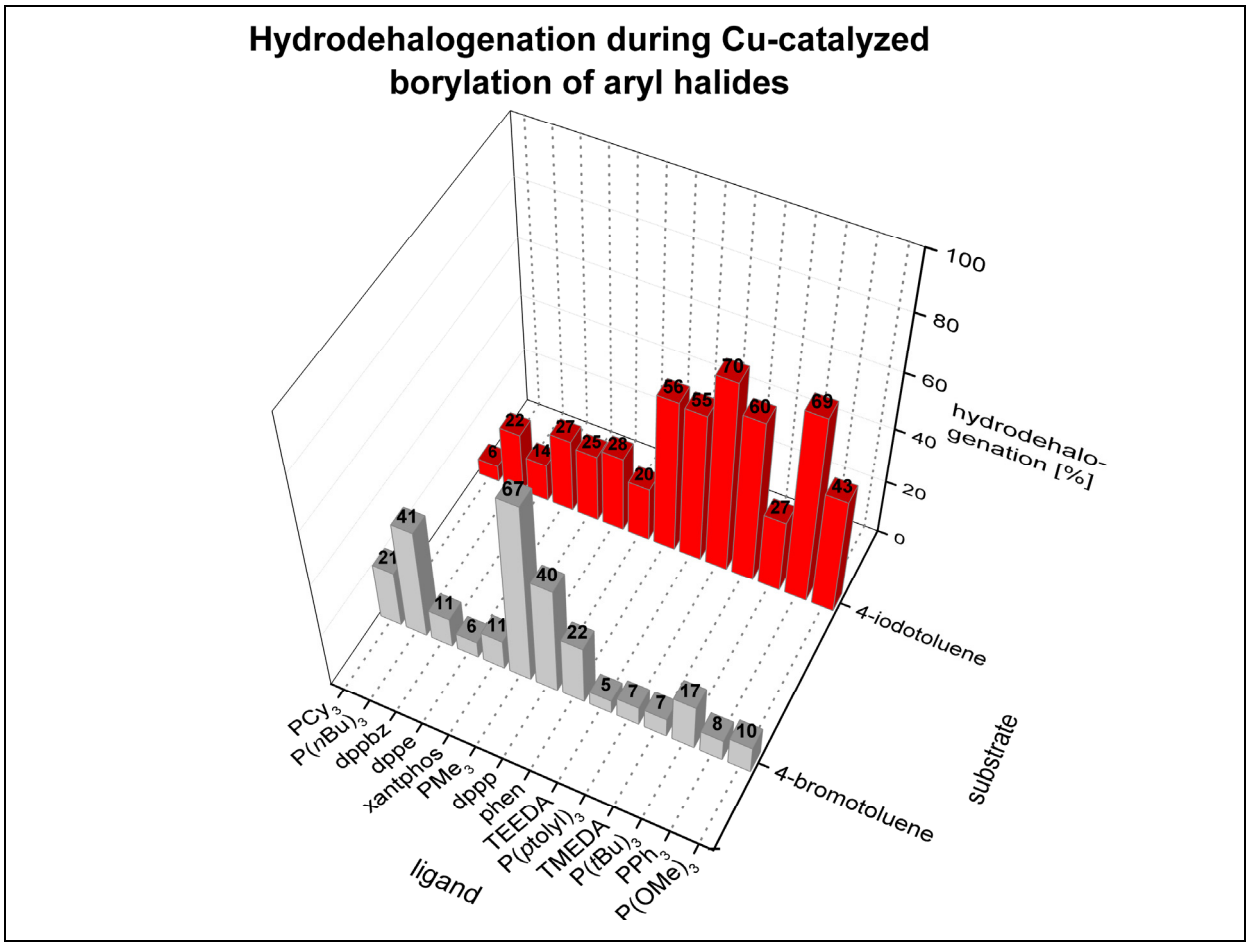

3.2.2 Base screening

The base screening was performed under the standard conditions of Kleeberg and Marder *et al.*[48] to check the influence on the reaction performance of different bases (Scheme 36).

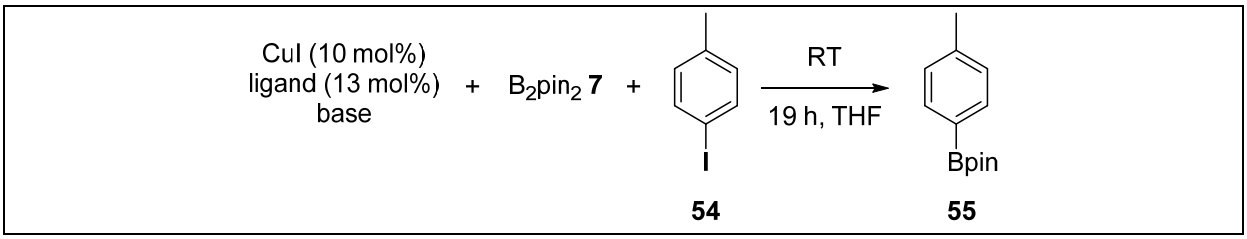

Scheme 36. Base screening; Cu-catalyzed borylation of 4-iodotoluene.

For almost all applied alkoxy bases, the Cu-catalyzed borylation resulted in more or less 100% conversion of the substrate 4-iodotoluene (Table 14, Chart 8). The *t*BuO$^-$ and MeO$^-$ bases showed good to very good conversions of up to 100% (entries 1,3-7) exept for LiOMe, which gave a poor conversion of 12%. The different solubility of the bases, as well as the solubility of the presumably formed alkoxy diboron(4) base adduct,[48,49,80,87] might be the reason for this observation, whereas the basicity is quite consistent. The carbonate bases showed only trace conversion (entry 8) or no reaction at all (entry 9). While a metal free borylation of aryl iodides with Cs_2CO_3 in MeOH was recently reported,[72] an addition of MeOH to the reactions with carbonates did not result in a significant increase in conversion. The lower basicity of the carbonates, compared to the other alkoxy bases used, might be the reason for the poor performance in those cases (entries 8 and 9), and the concentration of methanol in THF could affect the reaction as well, because the carbonate should function as a co-base to push the equilibrium towards the methoxide which then would be the stronger base.

Table 14. Base screening; Cu-catalyzed borylation of 4-iodotoluene[(a)]

entry	base	pk_a[(b)]	Conversion of 4-Iodotoluene [%][(c)]
1	KOMe	15.21	100
2	LiOMe	15.21	12
3	NaOMe	15.21	94
4	KOEt	15.85	89
5	KO*t*Bu	16.54	100
6	LiO*t*Bu	16.54	100
7	NaO*t*Bu	16.54	73
8	Cs_2CO_3	10.33	2
9	Li_2CO_3	10.33	0

(a) standard conditions: 10 mol% CuI, 13 mol% ligand, 1.5 equiv base, 1.5 equiv B_2pin_2, 459 µmol substrate; (b) pk_a values (relative to H_2O) of the corresponding acid; entries 1-7 see ref.[88] entries 8-9 see ref.[89] (c) The conversion was determined by GC-MS from the raw ratio of the peak areas for 4-MeC_6H_4I and 4-MeC_6H_4Bpin.

Chart 8. Base screening; Cu-catalyzed borylation of 4-iodotoluene.

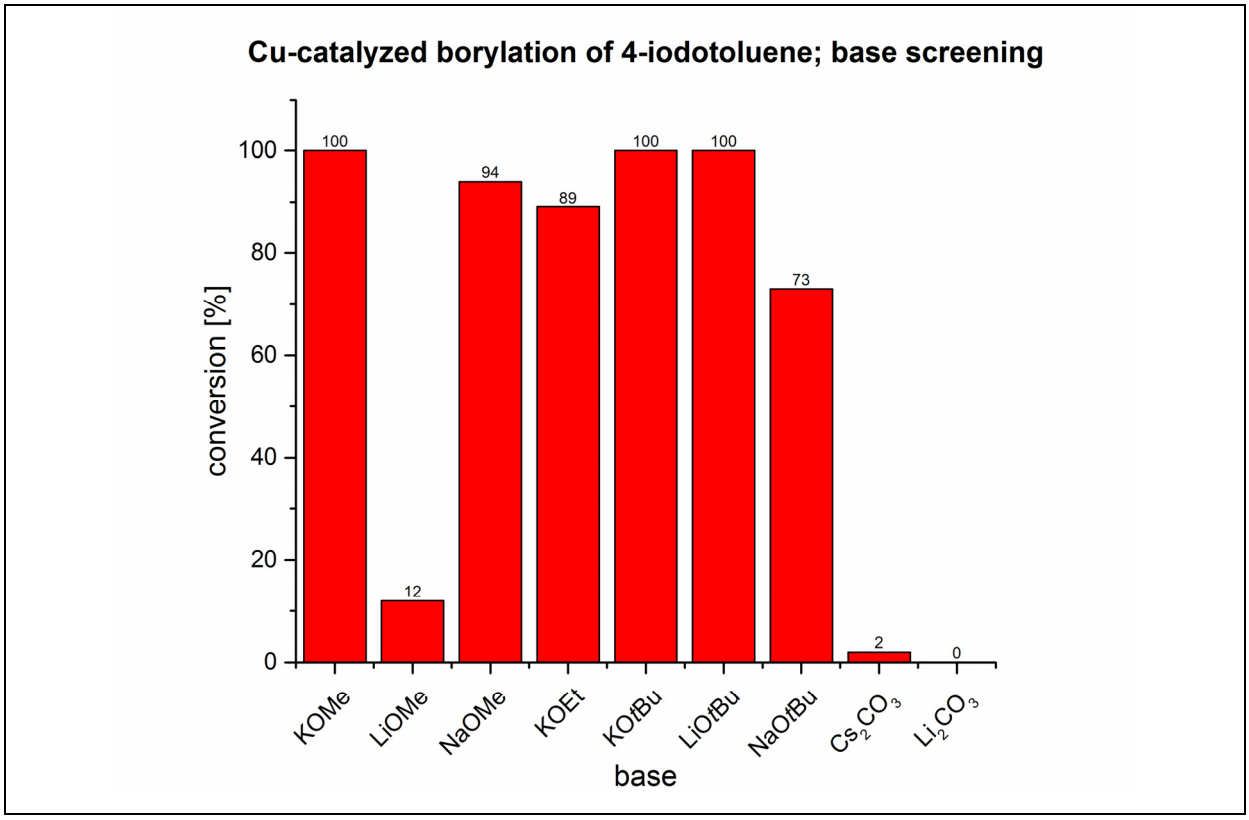

3.2.3 Substrate screening

Xantphos ligands are very useful in transition metal-catalyzed reactions such as hydroformylation (e.g. Rh-catalyzed) or cross-coupling reactions (e.g. Ni- or Pd-catalyzed)[86,90-92] as well as in recently reported Cu-catalyzed[53] borylation reactions. Due to the huge flexibility in chelating the metal (bite angle range 97° - 135°)[86] it seems to be a very powerful ligand in catalysis.

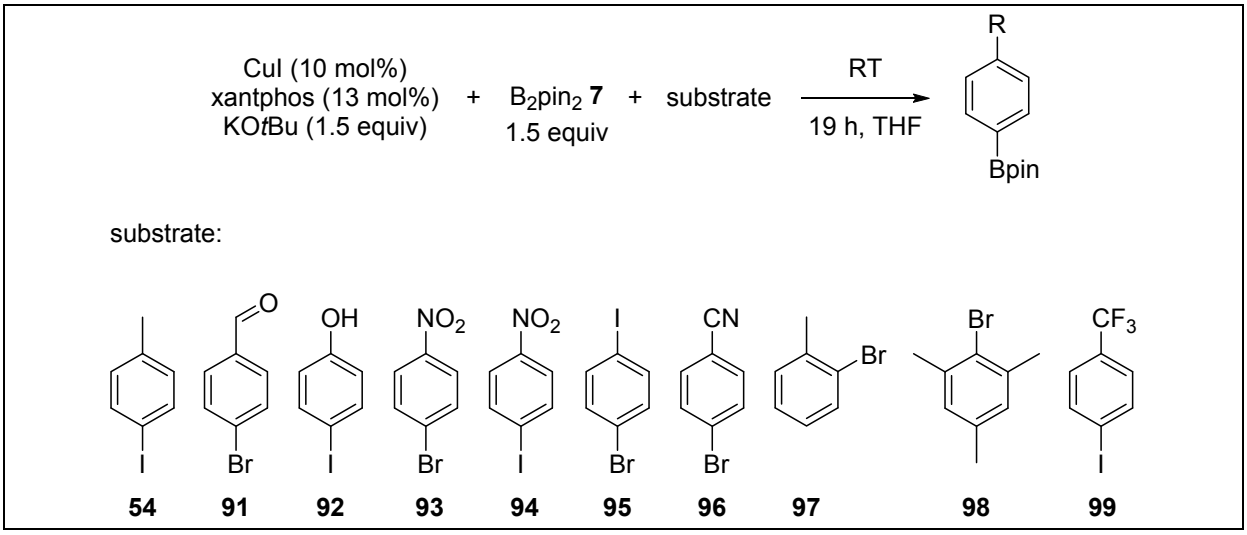

Scheme 37. Substrate screening; Cu-catalyzed borylation of aryl halides.

Therefore, substrate screening for the Cu-catalyzed borylation of aryl halides, was carried out with xantphos as the ligand using substrates which could not be borylated in good yields, or for which no borylation or unknown side products were observed under the standard conditions of Kleeberg, Lin and Marder *et al.*[48] (Scheme 37).

The Cu-catalyzed borylation of compounds **54**, **97** and **99** with xantphos as the ligand showed quite similar conversions to the corresponding borylated product as were observed with P(*n*Bu)$_3$ as the ligand (Table 15, entries 1, 8, 10, Chart 9). However, the conversion for substrates **95**, **96** and **97** were about 30% worse than under the standard conditions (entries 6-8). Moreover, 41% of the 4-bromobenzaldehyde (**91**) could be converted to the borylated product using xantphos, while no conversion was observed for P(*n*Bu)$_3$ (entry 2). The starting materials containing a nitro functional group (entries 4 and 5) could not be borylated *via* Cu-catalysis with xantphos or with other phosphine ligands.

Table 15. Substrate screening; Cu-catalyzed borylation of aryl halides.[(a)]

entry	substrate	P(*n*Bu)$_3$ conversion [%][(b)]	xantphos conversion [%][(b)]
1	4-iodotoluene **54**	100	97
2	4-bromobenzaldehyde **91**	0	41
3	4-iodophenol **92**	0	0
4	1-bromo-4-nitrobenzene **93**	0	0
5	1-iodo-4-nitrobenzene **94**	0	0
6	1-bromo-4-iodobenzene **95**	87[(c)]	54[(c)]
7	4-bromobenzonitrile **96**	48	19
8	2-bromotoluene **97**	100	78
9	2-bromomesitylene **98**	94	7
10	4-iodobenzotrifluoride **99**	100	100

(a) standard conditions: 10 mol% CuI, 13 mol% ligand, 1.5 equiv KO*t*Bu, 1.5 equiv B_2pin_2, 459 µmol substrate; (b) the conversion was determined by GC-MS from the raw ratio of the peak areas for the substrate and the corresponding borylated product. (c) *p*-bromo-C_6H_4-Bpin.

Chart 9. Substrate screening; Cu-catalyzed borylation of aryl halides.

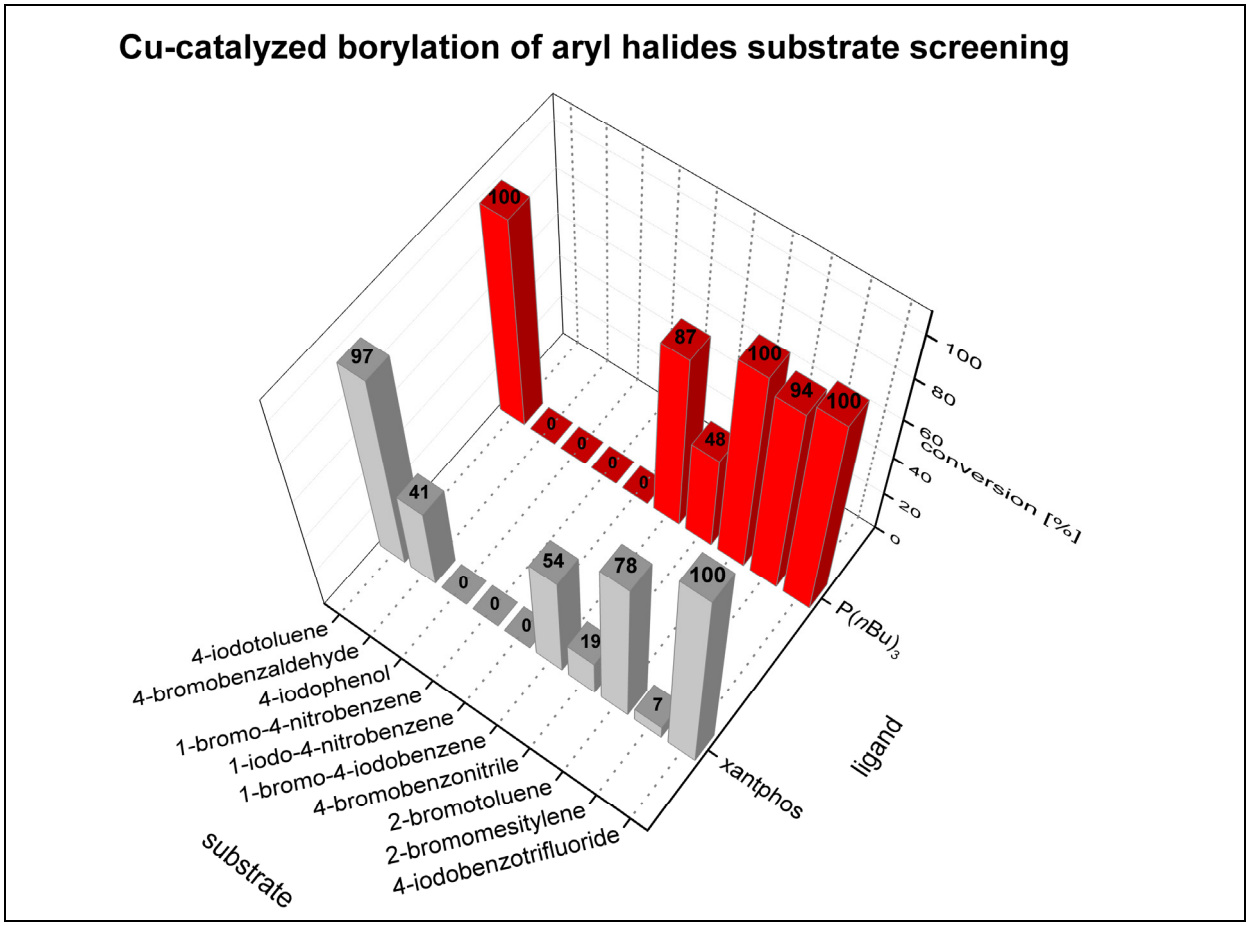

The borylation reaction of 1-bromo-4-nitrobenzene (**94**) did not result in the corresponding borylated product. Instead, a reductive N=N coupling[93] reaction occurred which was identified as the main reaction (Scheme 38, Figure 6).

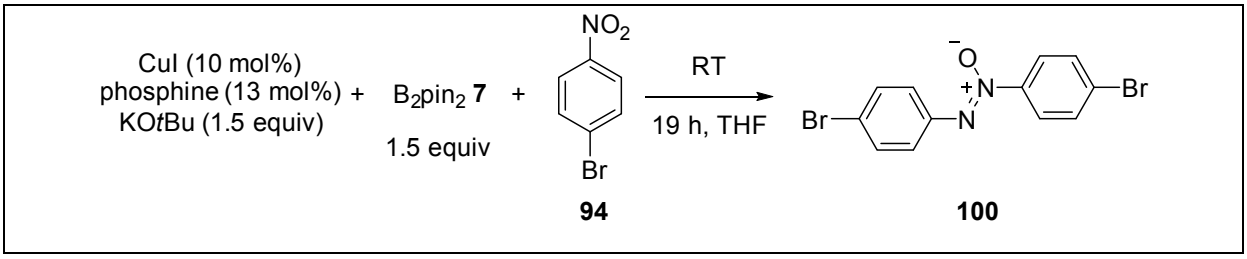

Scheme 38. Cu-catalyzed, reductive N-N coupling reaction of nitro aryl halides.

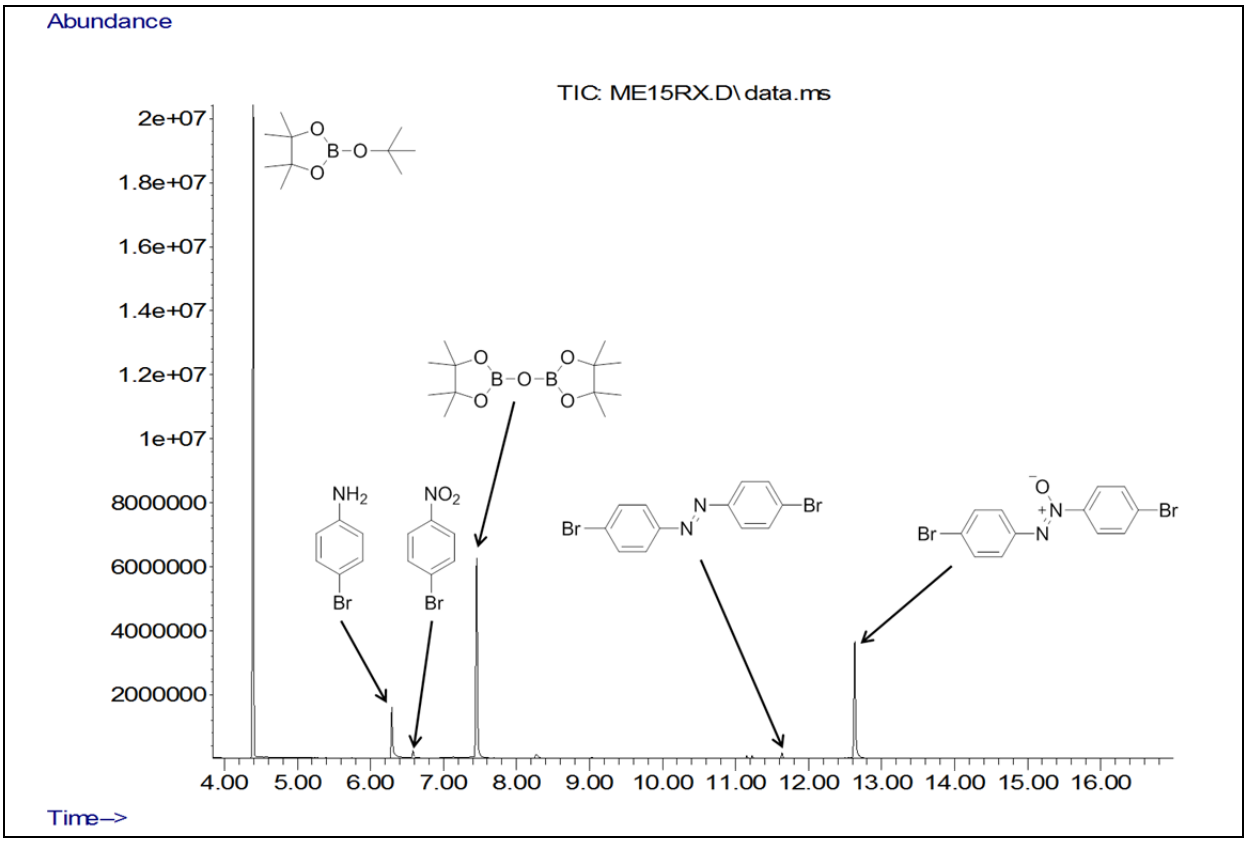

Figure 6. Cu-catalyzed, reductive N=N coupling reaction of nitro aryl halides; B_2pin_2 as reductant; total ion chromatogram of the reaction mixture.

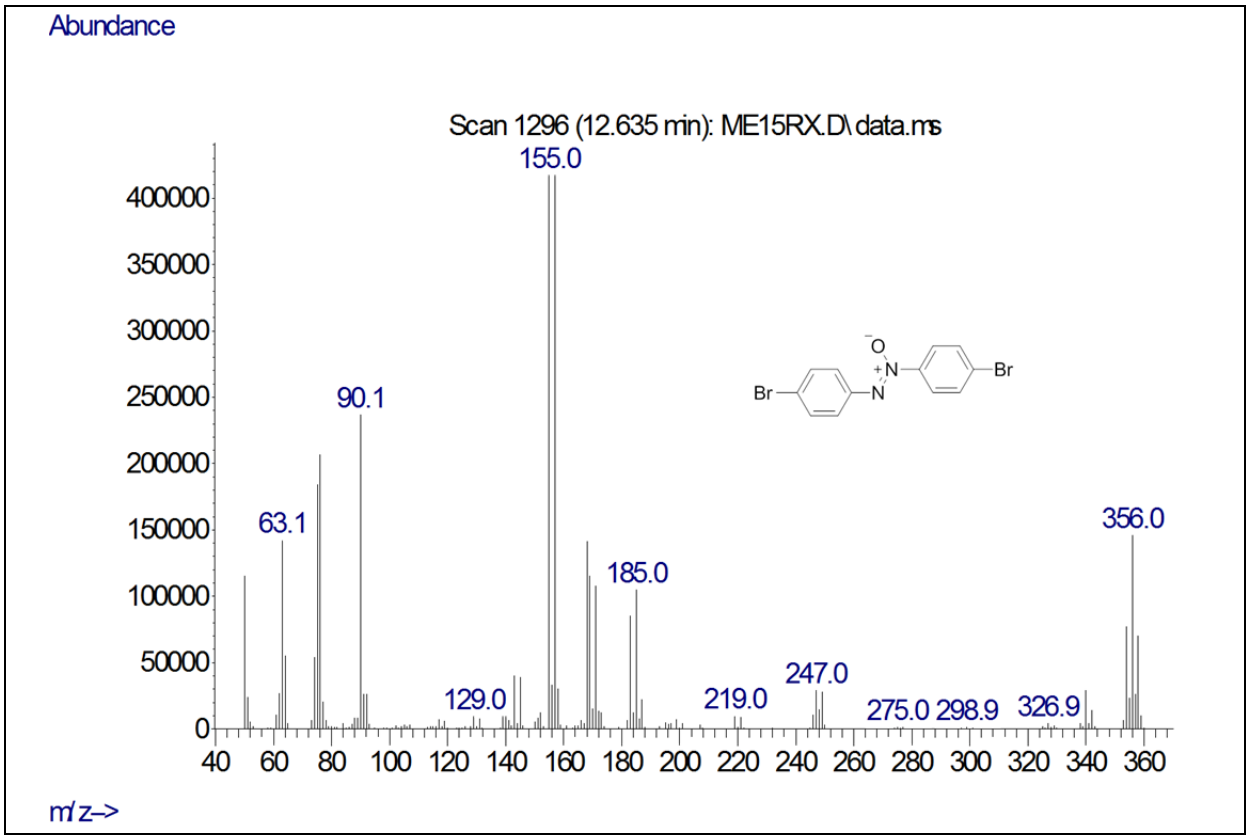

*Figure 7. Cu-catalyzed, reductive N-N coupling reaction of nitro aryl halides; B_2pin_2 as reductant; mass spectrum of 4,4'-dibromoazoxybenzene (**100**).*

In this case, the alkoxy diboron(4) compound reduced the nitro group to the *p*-bromo-aniline derivative, the reduction products coupled to give 4,4'-dibromoazoxybenzene (Figure 7, Scheme 39) and the diboron(4) compound was oxidized to the corresponding B–O–B species (Figure 6 and Figure 8). The same results were also observed for the 1-iodo-4-nitrobenzene substrate (**93**).

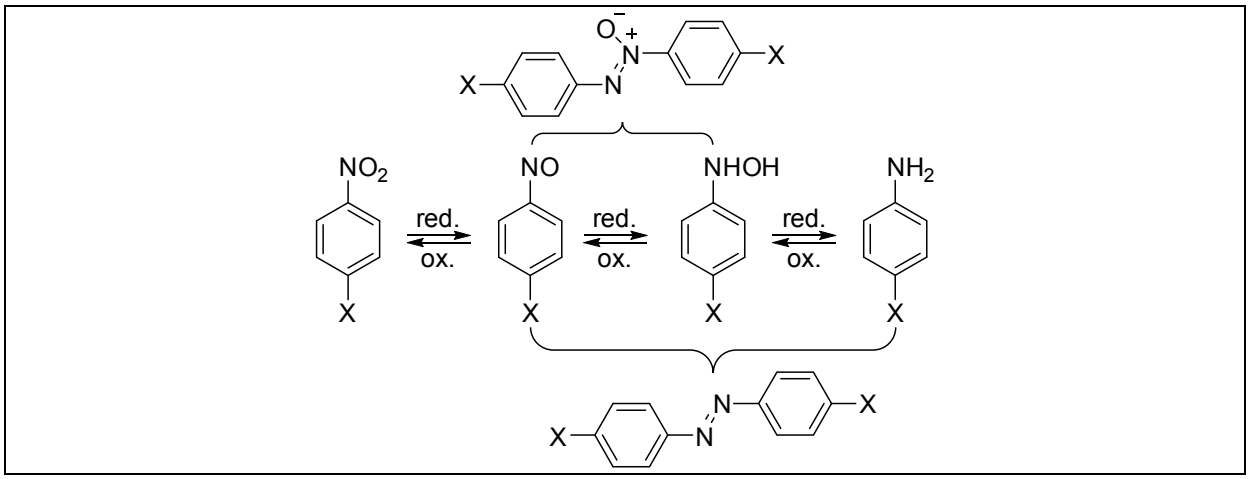

Scheme 39. B_2pin_2 as reductant; proposed pathway[93] for reductive N=N coupling of nitro aryl halides.

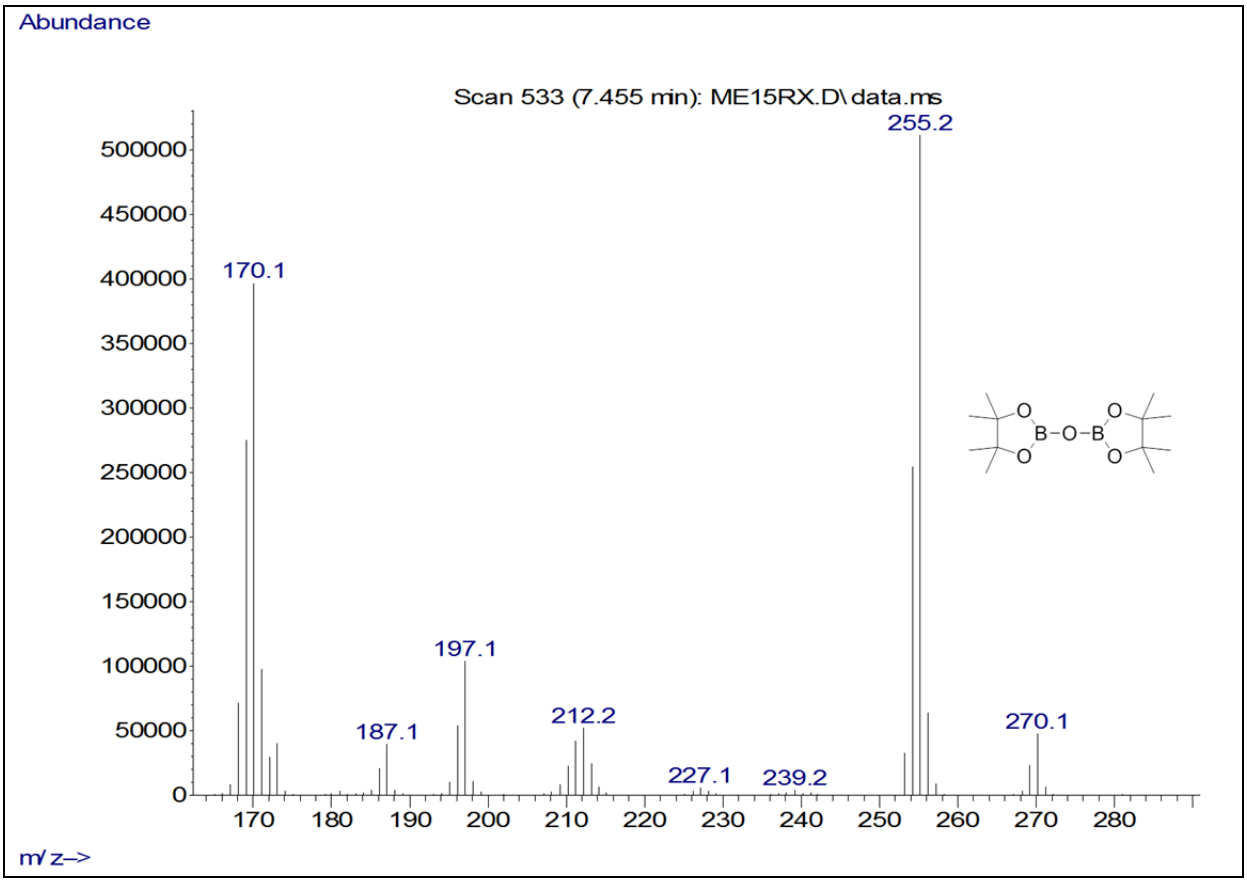

Figure 8. Cu-catalyzed, reductive N-N coupling reaction of nitro aryl halides; B_2pin_2 as reductant; mass spectrum of the oxidized B_2pin_2; pinB–O–Bpin.

The 4,4'-dibromoazoxybenzene (**100**) could be isolated in moderate 43% yield and was characterized by ^{1}H NMR spectroscopy, GC-MS and high resolution mass spectrometry. The literature known molecular structure of compound **100** was also confirmed by single-crystal X-ray diffraction (Figure 9).

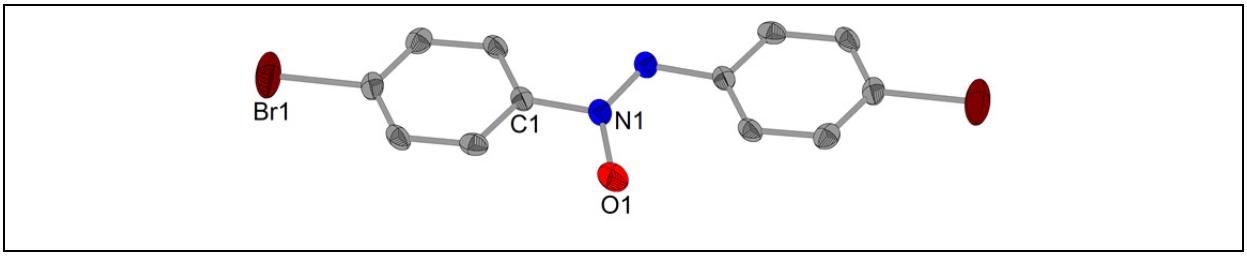

*Figure 9. Single-crystal structure of compound **100**; protons are omitted for clarity, the oxygen O1 is disordered with 50% occupancy.*

Reacting the 4,4'-dibromoazoxybenzene (**100**) in a separate Cu-catalyzed borylation reaction, resulted in complete reduction to the corresponding 4,4'-dibromoazo-benzene and no borylation of the halide was observed at all.

3.2.4 Borylation of 4-iodotoluene with copper-nanoparticles

As Kleeberg, Lin and Marder *et al.*[48] observed the formation of Cu-nanoparticles in their reported copper catalyzed borylation of aryl halides, it is still not clear whether they play a role in the Cu-catalyzed borylation reaction. Moreover, recently, Chung *et al.*[54] and Xu *et al.*[94] reported on Cu(0)-nanoparticle and CuO-nanoparticle-catalyzed borylations of alkyl bromides, respectively.

Therefore, Cu(0)-nanoparticles were synthesized accordingly a literature procedure[95] and were screened for the borylation of 4-iodotoluene (Scheme 40).

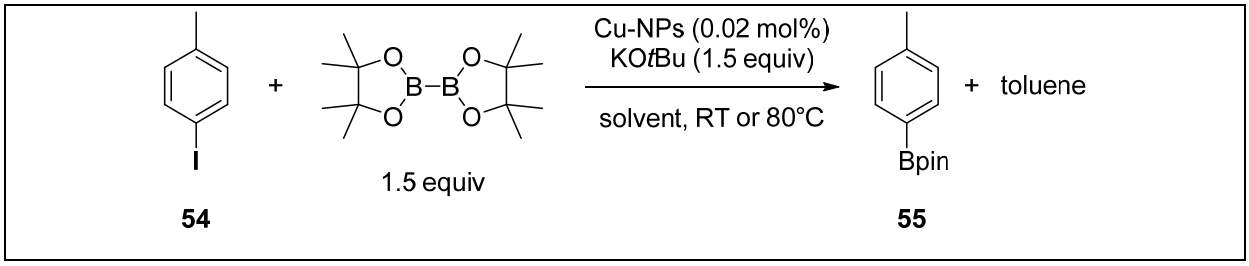

Scheme 40. Cu-nanoparticle catalyzed borylation of 4-iodotoluene.

The Cu-nanoparticles generated, only showed activity at elevated temperatures (Table 16, entries 1-5) and promoted the hydrodehalogenation rather than the borylation reaction. At room temperature, the Cu-NPs were inactive for both (entries 6 and 7).

Table 16. Cu-nanoparticle catalyzed borylation of 4-iodotoluene.[(a)]

entry	catalyst [mol%]	time	temp. [°C]	solvent	starting material [%][(b)]	hydrodehalo-genation [%][(b)]	yield [%][(b)]
1	Cu-NPs [0.02]	25 min	60	DMF	62	21	12[(c)]
2	Cu-NPs [0.02]	35 min	80	DMF	45	31	18[(c)]
3	Cu-NPs [0.02]	45 min	80	DMF	7	60	22[(c)]
4	Cu-NPs [0.15]	45 min	80	DMF	0	59	25[(c)]
5	Cu-NPs [0.02]	18 h	80	DMF	0	74	21
6	Cu-NPs [0.02]	18 h	RT	DMF	90	0	0
7	Cu-NPs [0.02]	18 h	RT	THF	98	0	0

(a) standard conditions: Cu-NPs, 1.5 equiv KO*t*Bu, 1.5 equiv B_2pin_2, 459 µmol substrate; (b) the yields were determined by GC-MS; (c) microwave heating.

The reaction in THF at room temperature (entry 7) might indicate that the Cu(0)-NPs should not affect the borylation of aryl halides under the standard conditions of

Kleeberg, Lin and Marder *et al.*;[48] nevertheless, the mechanism for the hydrodehalogenation is still unclear.

Bearing in mind that Lei *et al.*[96] recently reported on phenyl radical formation from aryl bromides promoted by *t*BuO$^-$ and 1,10-phenantroline in DMF, one might consider a radical pathway involved in the Cu-catalyzed borylation of aryl halides as well. Therefore, a radical scavenger experiment was performed. Addition of 9,10-dihydroanthracene (1.1 equiv) did not shut down the borylation, and the formation of anthracene was not observed (Figure 10), hence a radical process involved in the Cu-catalyzed borylation of Kleeberg, Lin and Marder *et al.*[48] might be ruled out.

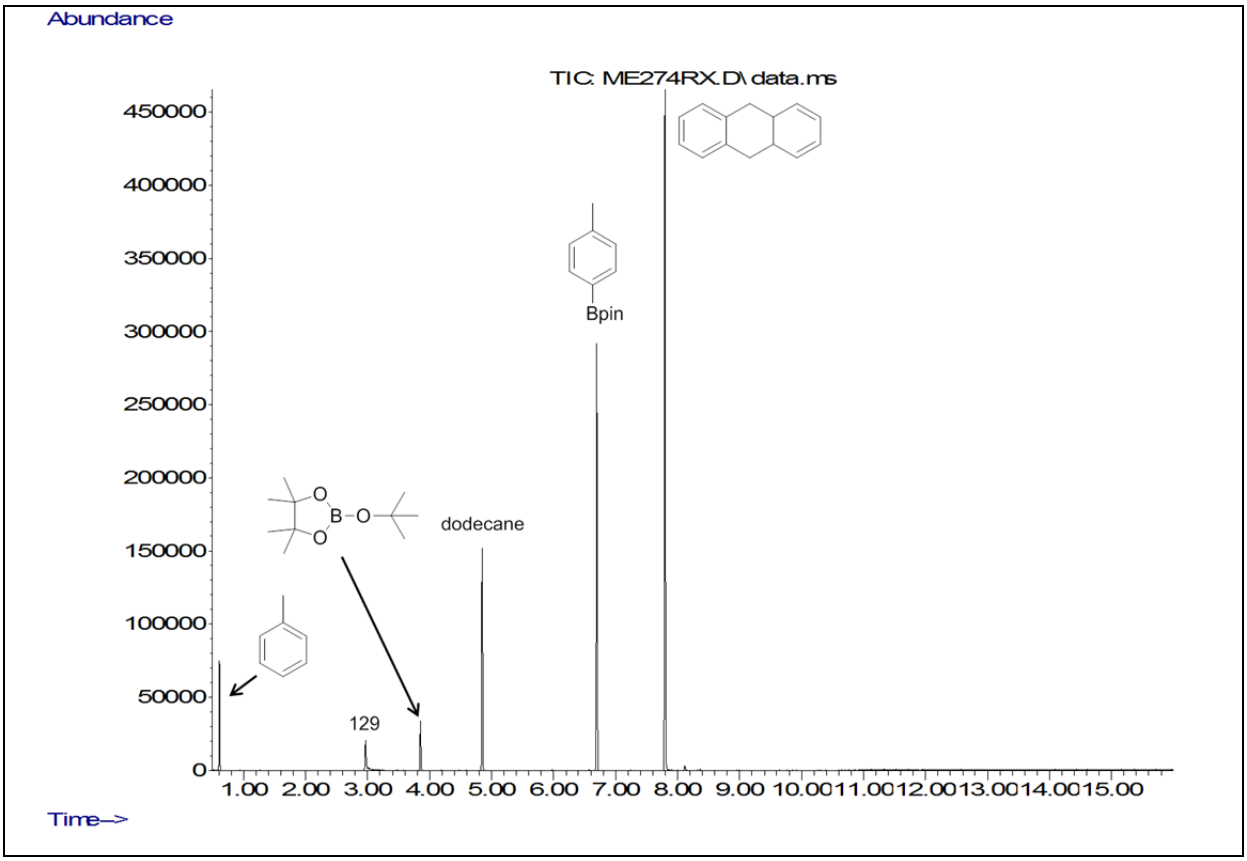

Figure 10. Cu-catalyzed borylation of 4-iodotoluene with 9,10-dihydroanthracen as radical scavenger additive.

3.2.5 Precursors for copper boryl complexes

Since 2005, when Sadighi *et al.*[97] reported on the first successful isolation of a NHC-Cu-boryl complex, only few examples of Cu-boryl complexes were successfully isolated and reported (Figure 11).[98-100] However, due to their high reactivity it is still very challenging to prepare and isolate Cu-boryl complexes, especially with ligands other than NHCs such as phosphines.

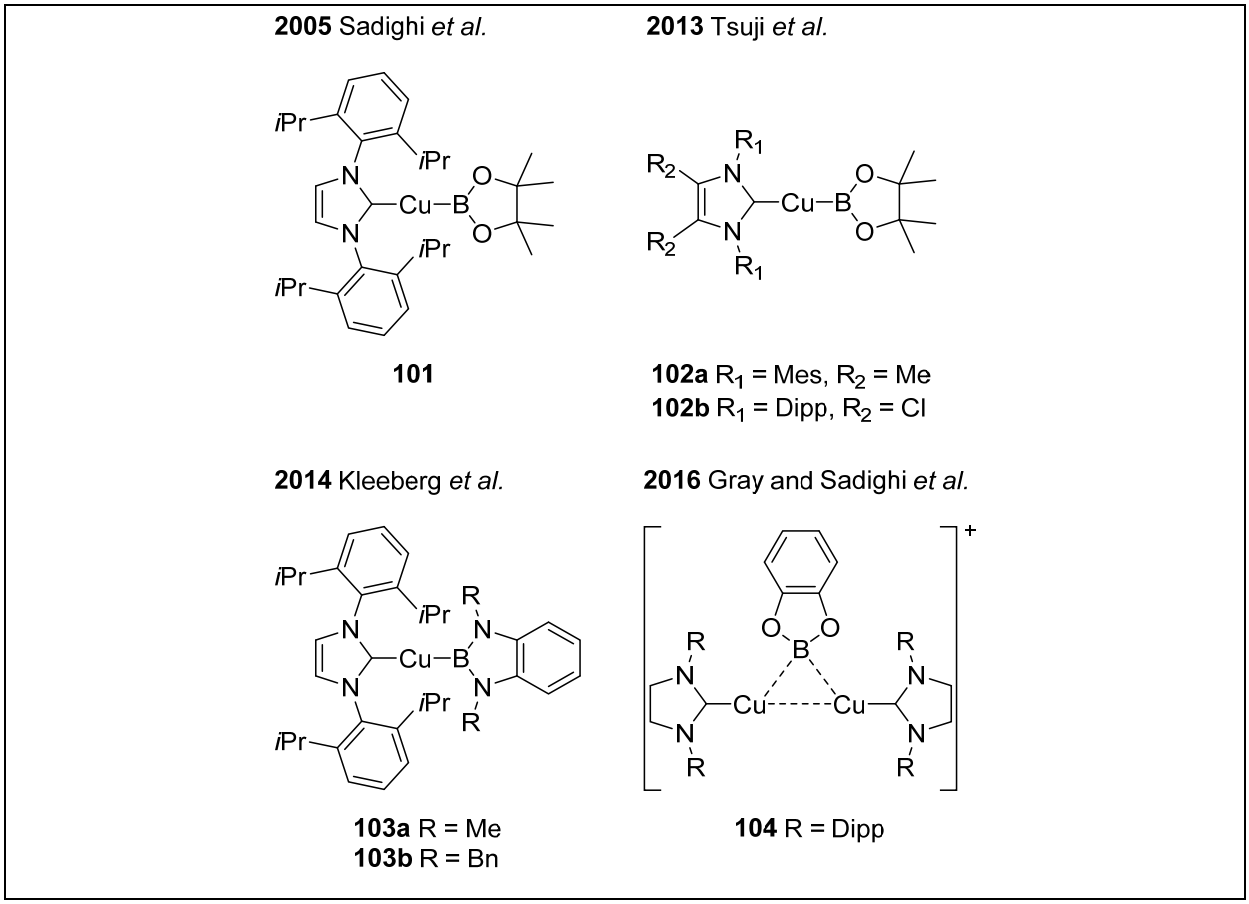

Figure 11. Recently reported NHC-Cu-boryl complexes.

Phosphine-Cu-boryl complexes, and indeed Cu-boryl complexes in general, are of great interest concerning their role as intermediates in the catalysis.

Therefore, different copper complexes were prepared as precursors for the synthesis of the corresponding Cu-boryl complexes. The [Cu(O*t*Bu)][101] tetramer **105**, the four mononuclear Cu-phosphine complexes, [(xantphos)CuX][102,103] **106**, [(dppbz)CuCl] **108**,[104,105] and the trigonal planar $[(PCy_3)_2CuBr]$[106,107] **107** as well as the dinuclear Cu-phosphine complex $[(PCy_3)Cu(\mu\text{-}I_2)Cu(PCy_3)]$[106,107] **109**. Thus, complexes with both chelating and non-chelating phosphine ligands were examined (Figure 12).

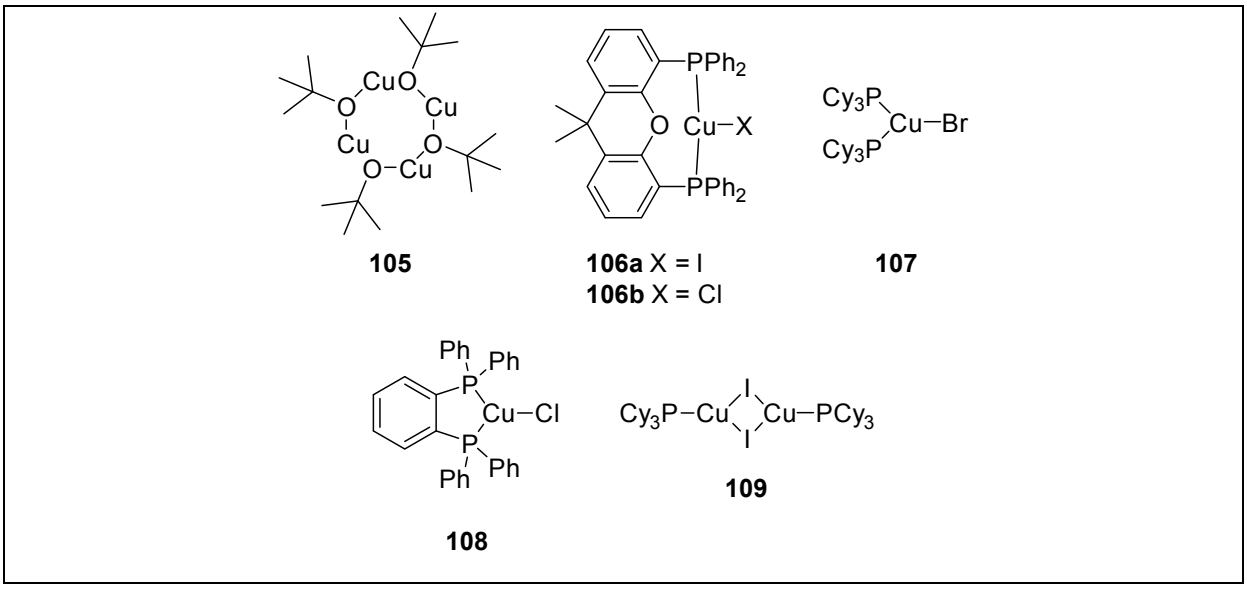

Figure 12. Cu-complexes as precursors for the synthesis of the corresponding Cu-boryl complexes.

Compounds **105** – **109** were isolated and characterized by ^{1}H and/or $^{31}P\{^{1}H\}$ NMR spectroscopy and/or high resolution mass spectrometry. X-ray diffraction studies of single-crystals of compound **107** confirmed the literature known molecular structure of the mononuclear complex $[(PCy_3)_2CuBr]$[107] (Figure 13).

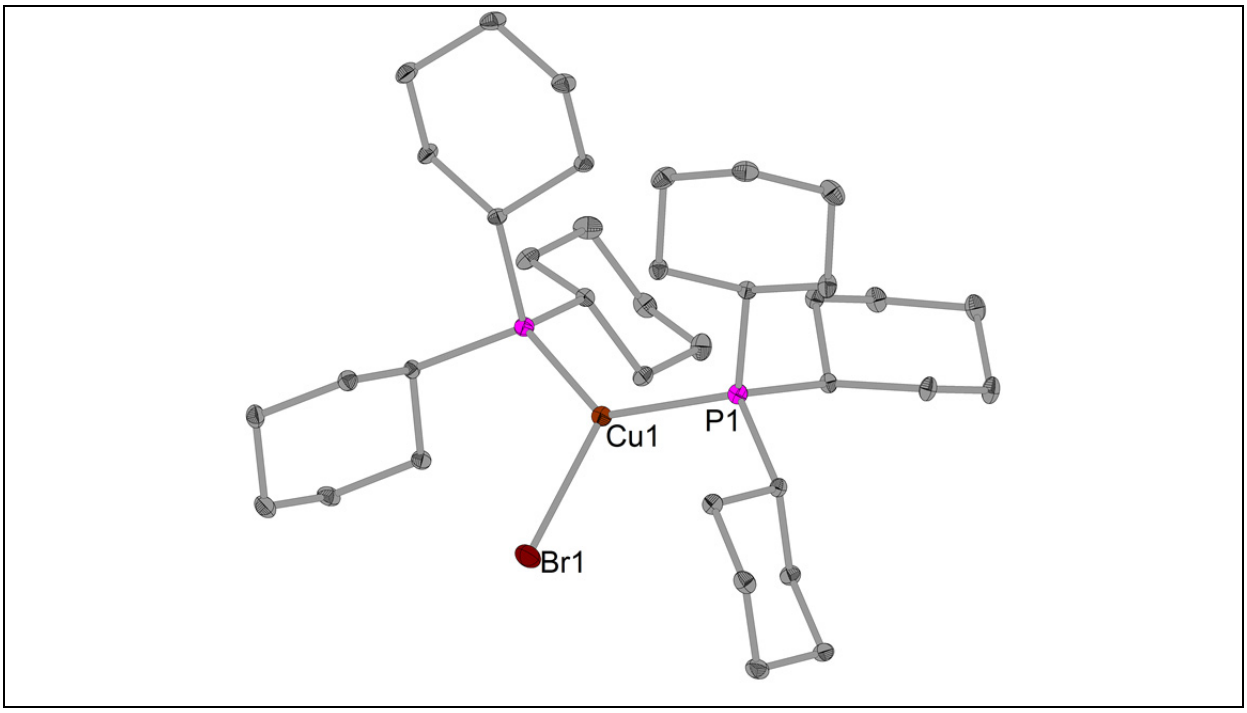

*Figure 13. Molecular structure of compound **107**; hydrogens are omitted for clarity.*

Interestingly, the solution $^{31}P\{^{1}H\}$ NMR spectrum of the complex [(dppbz)CuCl] **108** displayed the formation of two species (Figure 14), one for the Cu-complex **108** with a resonance at -18.4 ppm (br),[105] and a second one for the homoleptic Cu-complex

[Cu(dppbz)$_2$][Cl] at 8.30 ppm (br).[108] While the the ^{31}P{^{1}H} NMR spectrum showed two compounds, the HRMS-ASAP only provided evidence for the mononuclear complex [(dppbz)CuCl] **108**. However, if there were two compounds present in the solid state as well, they could not be separated. Moreover, formation of the dinuclear Cu-complex [(dppbz)Cu(μ-Cl$_2$)Cu(dppbz)][105] cannot be ruled out, but neither the NMR investigations nor the HRMS provided evidence for a dinuclear complex.

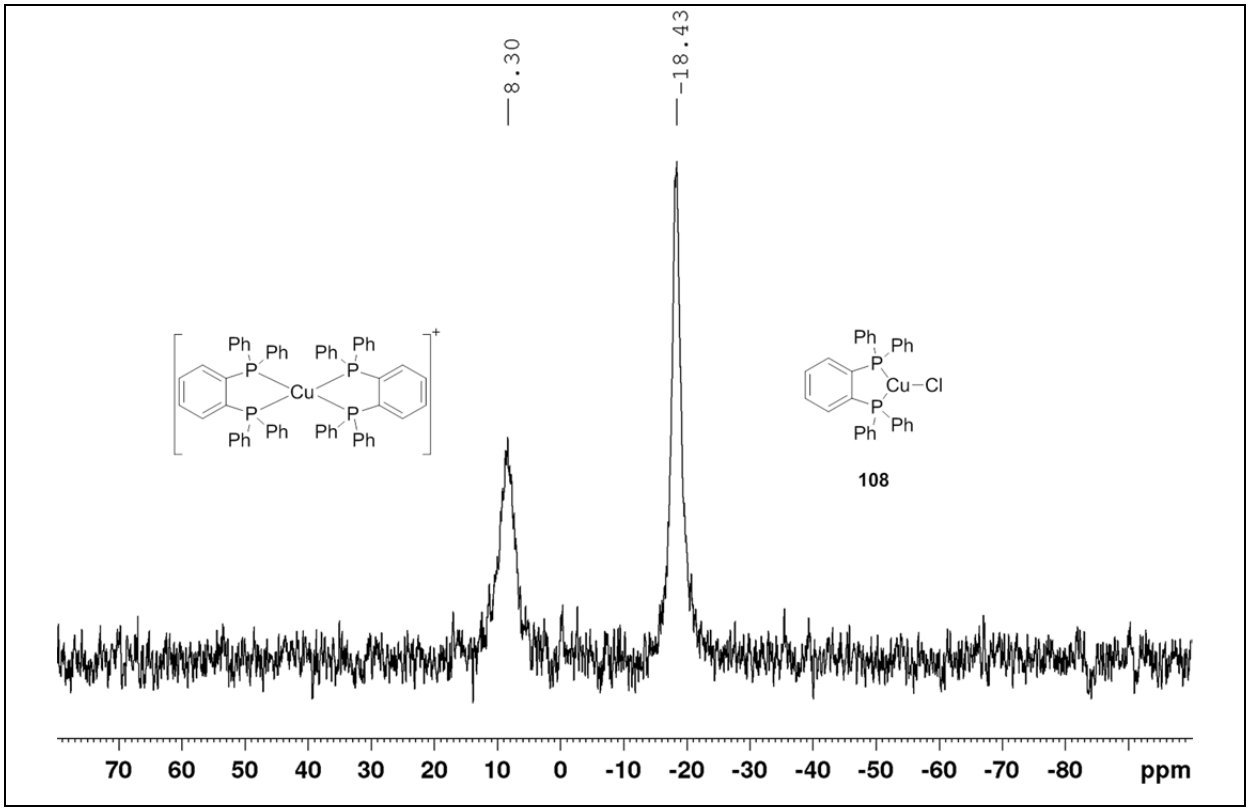

Figure 14. ^{31}P{^{1}H} NMR spectrum of compound [(dppbz)CuCl] ***108****.*

Furthermore, in collaboration with Dr. Emily C. Neeve, the precursors were reacted with the methoxide adduct of B$_2$pin$_2$ ([K(18-crown-6)][(B$_2$pin$_2$)OMe]). Unfortunately, due to the presumably high reactivity, the related Cu-boryl complexes could not be isolated. However, the low temperature *in situ* ^{11}B{^{1}H} NMR spectra of the reaction of complex [(PCy$_3$)Cu(μ-I$_2$)Cu(PCy$_3$)] **109** with the adduct [K(18-crown-6)][(B$_2$pin$_2$)OMe] (ratio 1:2), displayed the transformation of the alkoxy adduct (Figure 15).

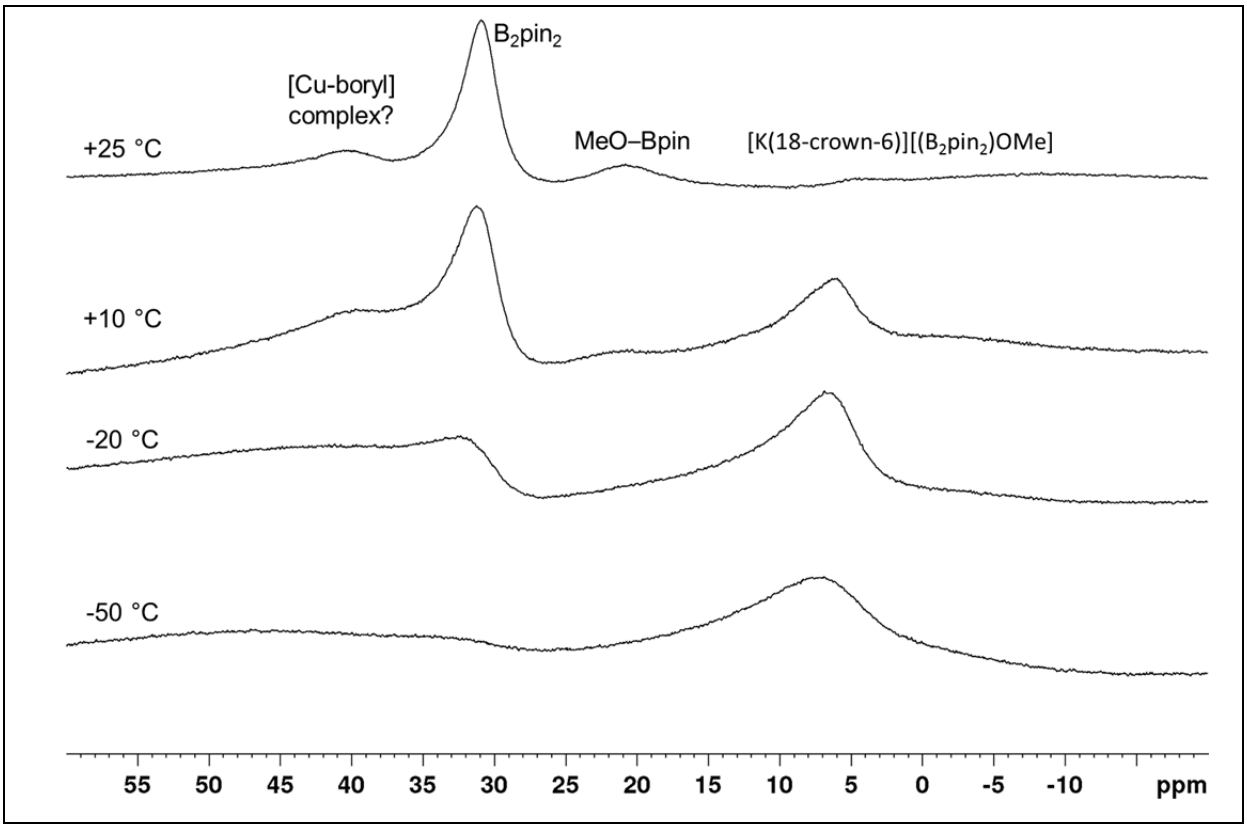

Figure 15. $^{11}B\{^1H\}$ NMR of the reaction (ratio 1:2) of [(PCy$_3$)Cu(μ-I$_2$)Cu(PCy$_3$)] ***109*** and *[K(18-crown-6)][(B$_2$pin$_2$)OMe] in d$_8$-THF (96 MHz, at various temperatures).*

While at -50 °C only the [K(18-crown-6)][(B$_2$pin$_2$)OMe] adduct was observed (7.00 ppm, vbr), at room temperature the formation of B$_2$pin$_2$ and MeO–Bpin (20.9 ppm, br) occurred.[80] Furthermore, a new broad peak appeared at 40.5 ppm (Figure 16), and is quite similar to that of the [NHC-Cu-Bpin] complex reported by Sadighi *et al.,*[97] which shows a $^{11}B\{^1H\}$ NMR signal at 41.7 ppm (in C$_6$D$_6$). Therefore, this observation might indicate that a [Cu-boryl] species formed. This is also supported by the observation of the decreasing $^{11}B\{^1H\}$ NMR signal of the [K(18-crown-6)][(B$_2$pin$_2$)OMe] adduct (Figure 15), reported by Kleeberg, Lin and Marder *et al.*,[80] which shows, at room temperature two signals, one broad peak at 5.80 ppm and one very broad peak at 37.5 ppm (in d$_8$-THF at 25 °C).

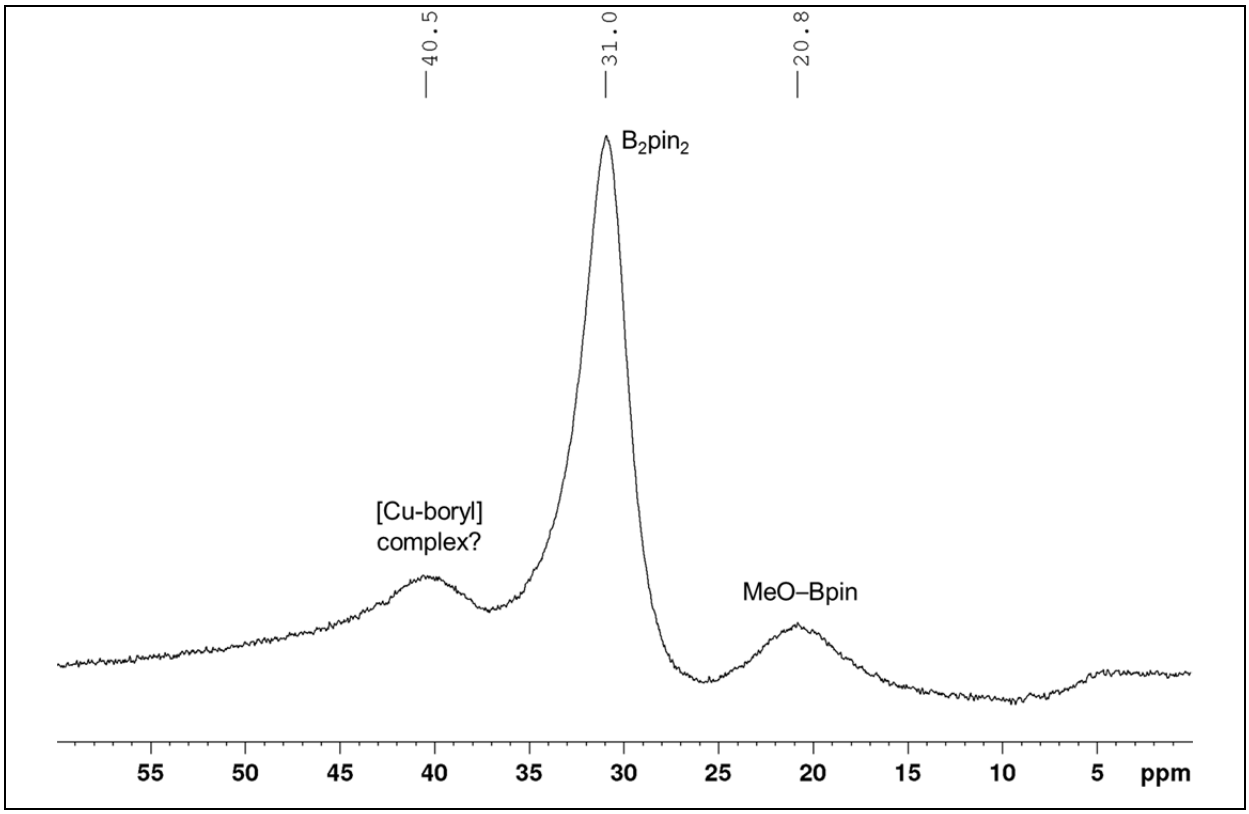

Figure 16. $^{11}B\{^1H\}$ NMR spectrum of the reaction (ratio 1:1) of $[(PCy_3)Cu(\mu\text{-}I_2)Cu(PCy_3)]$ ***109*** and *$[K(18\text{-crown-}6)][(B_2pin_2)OMe]$ in d_8-THF (96 MHz, at 25 °C).*

3.2.6 Conclusion (Cu-catalyzed borylation)

In conclusion, the Cu-catalyzed borylation reactions of 4-iodotoluene and 4-bromotoluene gave moderate to very good yields. The steric demand of the phosphine and its basicity both played a key role for the performance of the reaction, whereas using chelating phosphine ligands, which are less basic, resulted in moderate yields. In this case, a combination of electronic and steric (bite angle) effects might control the performance.

The screening of different alkoxy bases showed the importance of solubility of the base itself or of the presumably formed base adduct of the diboron(4) compound, while the basicity of the bases used was quite constant.

Substrate screening resulted in a lack of improvement of the borylation, but a side reaction for nitro group-containing aryl halides as substrates was identified as an elegant route for reductive (B_2pin_2 as reductant) N=N coupling to give azo-arenes. From a chemical point of view, thus is very interesting. However, concerning the literature[109] known abundance of alternative methods to reduce the nitro group for N=N coupling reactions, B_2pin_2 might have too high a cost to be used as a reducing

reagent, especially if there is a very cheap alternative, for example, the Béchamp reduction (Fe/HCl).[110]

Investigations on Cu-NPs showed no activity for borylation of aryl halides at room temperature, or a radical process to be involved in the Cu-catalysis of Kleeberg, Lin and Marder *et al.*[48].

All attempts to isolate phosphine-Cu-boryl complexes, unfortunately failed, but a presumably formed Cu-boryl species was observed in an *in situ* $^{11}B\{^{1}H\}$ NMR experiment.

CHAPTER TWO

-

B_2eg_2

Bis(ethylene glycolato)diboron

“There is life in the old dog yet”

CHAPTER TWO
-
Reactivity of bis(ethylene glycolato)diboron B_2eg_2

1 Introduction and Motivation

This section is slightly modified and reproduced from ref.[111] with permission from the Royal Society of Chemistry.

In 1997, Marder, Norman *et al.* reported the first metal-catalyzed (platinum) 1,4-diborylation of α,β-unsaturated compounds, subsequently termed "β-borylation".[112,113] Since the initial report, the β-borylation of α,β-unsaturated compounds has received more and more attention,[49,114-129] mostly employing Cu-based catalysts; Zhao, Marder Lin and co-workers reported DFT studies of the mechanisms of both the Pt[122] and Cu[123] catalytic cycles. (Scheme 41).

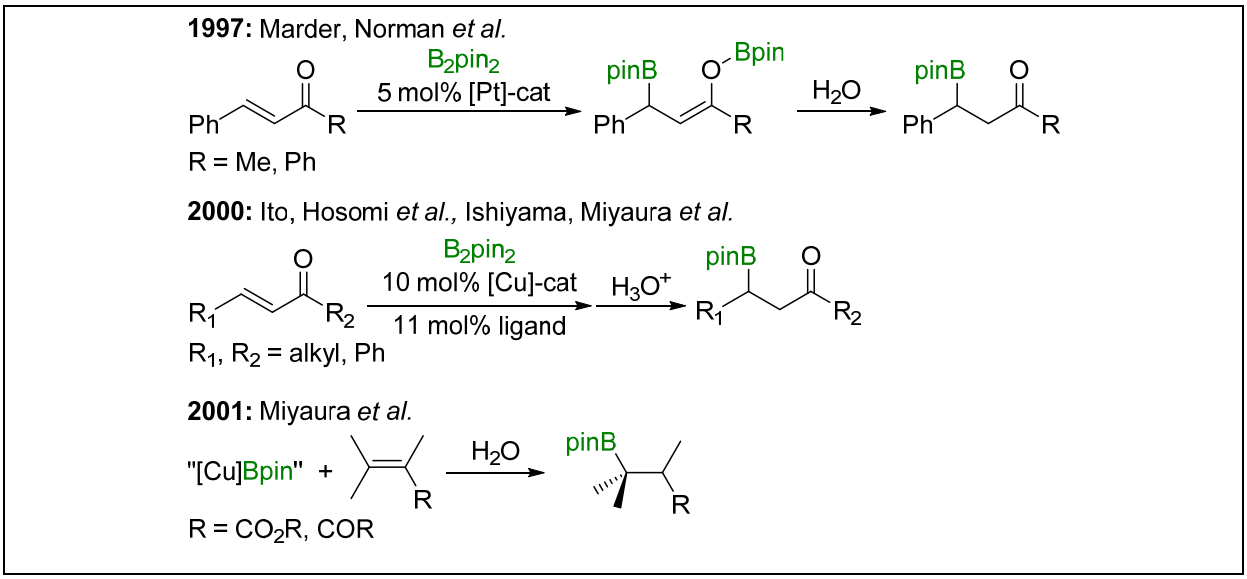

Scheme 41. Examples of reported β-borylation reactions.

Over the last decade, however, β-borylation has also been accomplished without any transition metal catalyst by using Lewis-bases as organocatalysts. It is believed that adducts of the Lewis-base with the diboron(4) compound play a major role in these reactions.

1.1 Lewis base adducts of diboron(4) compounds

Combinations of Lewis-basic NHCs and Lewis-acidic boranes can lead to classical Lewis acid/base complexes. In the last few years, it has emerged that such complexes can exhibit very interesting reactivity. In 2009, Hoveyda *et al.*[130-133] reported the application of NHCs as organocatalysts in the β-borylation of α,β-unsaturated compounds with the diboron(4) reagent B_2pin_2 as the boron source (Scheme 42).

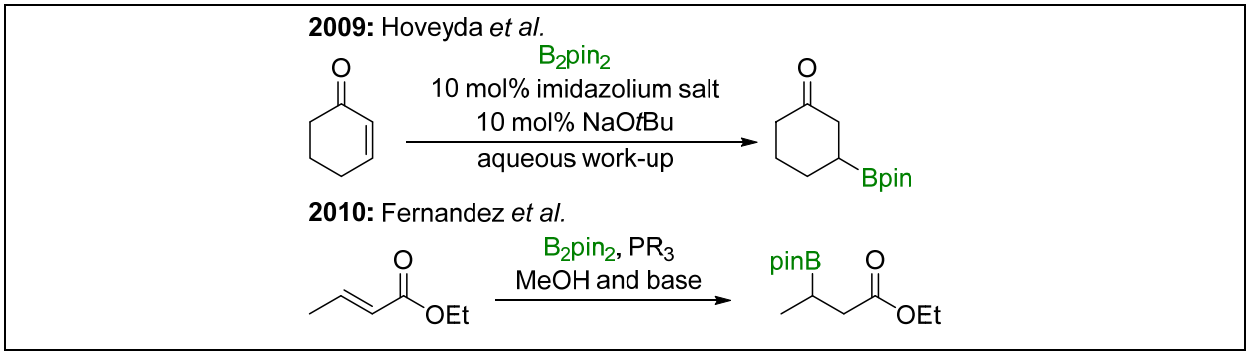

Scheme 42. Examples of reported, transition metal-free β-borylation reactions.

They suggested the formation of NHC-diboron adducts as intermediates (Figure 17, middle).[68,80,87,134-146] Thus, the first metal-free β-borylation reaction was reported to proceed *via* activation of the B–B bond of the diboron(4) compound with an *in situ*-formed NHC (Cy_2Im).[130,131] Hoveyda *et al.* proposed a mechanism including B–B bond activation *via* coordination of the *in situ* formed NHC to B_2pin_2 to give a mono-NHC adduct. Nevertheless, the originally NMR data reported by Hoveyda and co-workers were incorrect and the observed $^{11}B\{^1H\}$ NMR signals (at 4.5 and 6.3 ppm) did not match the expected region for a sp^2-sp^3 diboron adduct (sp^3-B ≤ 20 ppm, sp^2-B ≥ 20 ppm).[131] Later, in 2012, the system was investigated in detail by Kleeberg, Lin, Marder *et al.* (Figure 17),[147] and they reported the synthesis of the mono-NHC adduct B_2pin_2•Cy_2Im, which was fully characterized *via* single-crystal X-ray diffraction, and solid-state and temperature-dependent NMR spectroscopy. Kleeberg, Lin, Marder and co-workers showed that the $^{11}B\{^1H\}$ NMR signals of this mono-NHC adduct are assigned at 2.4 (sp^3-B) and 37.2 ppm (sp^2-B) at 5 °C. Furthermore, at room temperature the boron resonances were broadened due to a dynamic exchange process in solution, as the system is near the coalescence temperature.

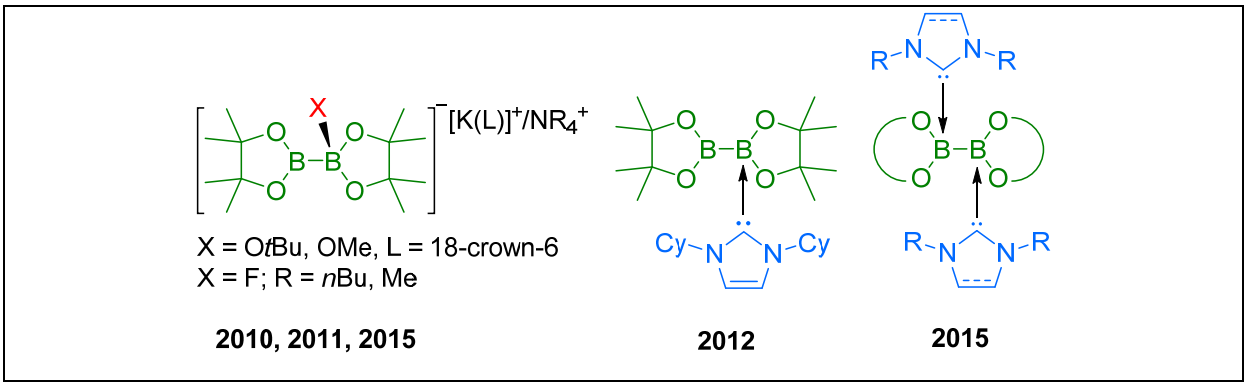

Figure 17. Recently reported and structurally characterized anionic and neutral sp^2-sp^3 and sp^3-sp^3 diboron adducts by Kleeberg, Radius and Marder et al.

In 2010, Kleeberg, Radius and Marder *et al*. reported the synthesis and characterization of anionic sp^2-sp^3 diboron adducts of the type $[B_2pin_2(OR)]K$ and $[B_2pin_2(F)][NR_4]$ (Figure 17, left).[80,148,149] They also demonstrated that these adducts can be used as boron sources in borylation reactions with aryl iodides and diazonium salts.[80] Fernández *et al.* have also employed such species, formed *in situ*, as boryl nucleophiles.[49,50,117-120,150-156]

1.2 NHC ring-expansion reactions (RER)

In 2012, Radius *et al*. reported the ring-expansion reaction (RER) of NHCs using different silanes to form six-membered heterocyclic rings.[157] In the same year, Hill *et al.*[158,159] discovered the formation of a heterocycle containing beryllium as the heteroatom from an NHC RER.[158] Afterwards, Rivard *et al.*,[160] Inoue *et al.*[161] and Stephan *et al.*[162] showed that these six-membered heterocyclic rings could also be obtained using different boron compounds, as the heteroatom inserted into the C–N bond of the NHC. Furthermore, several theoretical investigations were reported on the mechanism of NHC ring-expansion reactions.[163-169]

Additionally, it was shown that RERs are applicable to diboron(4) compounds. In 2014, Marder and co-workers observed a related ring-expansion product in conjunction with their studies of Zn-catalyzed alkyl halide borylations.[61] Thus, the reaction of $[Zn(Mes_2Im)Cl_2]$ with B_2pin_2 and KO*t*Bu yielded a six-membered heterocyclic ring *via* insertion of the Zn atom into the C–N bond of the NHC and migration of a Bpin moiety to the former carbene carbon atom (Figure 18, left). In addition, a further Bpin moiety inserts into the C–N bond of a second N-heterocyclic carbene ligand.

In 2015, Ingleson, Radius, Marder and co-workers reported NHC ring-expansion reactions of B_2cat_2 and B_2neop_2 as the diboron compound with the NHCs Me_2Im^{Me} or nPr_2Im (Figure 18, centre and right).[170] The reactions yielded the ring-expanded products by insertion of a $B(OR)_2$ moiety into the C–N bond of the carbene with the second $B(OR)_2$ bound *exo* to the former carbene-C atom.

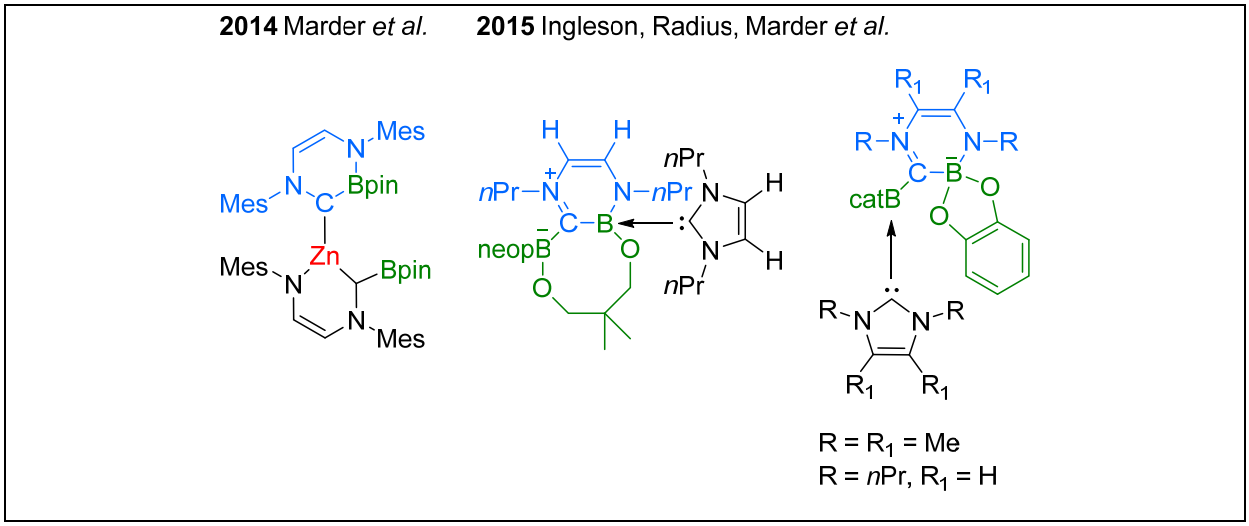

Figure 18. NHC-ring-expanded products containing zinc and diboron(4) compounds.

In the case of B_2cat_2, one boron atom is stabilized by a second equivalent of the NHC. In the case of B_2neop_2, one neopentylglycolato substituent ringopens and binds to the second boron atom forming an 8-membered heterocyclic ring. As a result, the second NHC coordinates to stabilize the boron atom in the six-membered ring (Figure 18, right).[170],[171]

Furthermore, Radius, Marder *et al.* reported the reactions of catecholborane (HBcat) with unsaturated and saturated NHCs as well as $CAAC^{Me}$, and have shown that the outcome of this reaction depends critically on the carbene used.[172] Mono-NHC adducts of the type HBcat•NHC (NHC = nPr_2Im, iPr_2Im, iPr_2Im^{Me}, and $Dipp_2Im$) were obtained from the stoichiometric reactions of HBcat with unsaturated NHCs. In contrast, the reaction of $CAAC^{Me}$ with HBcat yielded the B-H "oxidative addition" product, $CAAC^{Me}$(H)Bcat *via* insertion of the carbene-carbon atom into the B-H bond. Finally, at room temperature, the backbone saturated NHC $Dipp_2SIm$ reacted to give an NHC ring-expanded product featuring a six-membered –B–C=N–C=C–N-ring, *via* C-N bond cleavage and hydride migration from two HBcat molecules to the former carbene-carbon atom.

Increasing interest in the application of Lewis acid/base-adducts of diboron(4) compounds shows the rapidly growing importance of the diboron(4) reagents in both metal-catalyzed and metal-free synthetic transformations,[9] and for applications in organo-catalysis.[49,50,72,114-133,150-156,173] This fact warrants a proper and accurate description of their true structures, and a detailed study of NHC-adducts of different diboron(4)[15,18,20,22-24,174,175] compounds and their Lewis base-triggered B–B bond activation.

2 Results and Discussion

This section (except 2.2.2; 2.2.2.1; 2.2.3; 2.2.3.1; 2.2.3.3, 2.2.5, 2.3 and 2.4) is slightly modified and reproduced from ref.[111] with permission from the Royal Society of Chemistry.

2.1 $B_2(NMe_2)_4$ "The Origin"

Due to its thermal stability and high yielding synthesis,[18] tetrakis(dimethylamino)-diboron(4) **4** is used as the primary starting material for the synthesis of many diboron(4) derivatives.[15,18,20,22-24,174,175] The Lewis acidity of compound **4** is strongly degraded because of π-bonding of the N-lone pairs to the empty p-orbitals on the B-atoms. As a result, $B_2(NMe_2)_4$ is thermally stable, and neither adduct formation nor indeed any reactivity was observed with NHCs.

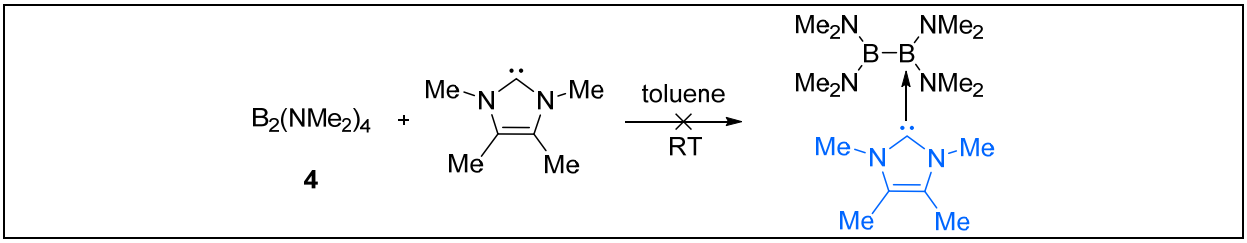

Scheme 43. Reaction of $B_2(NMe_2)_4$ with one equivalent of Me_2Im^{Me}.

For example, the *in situ* $^{11}B\{^1H\}$ NMR spectrum of the reaction of compound **4** with the sterically less demanding and highly reactive NHC, Me_2Im^{Me} (Scheme 43) does not show any significant shift indicative of adduct formation or further ring-expansion reaction (Figure 19).

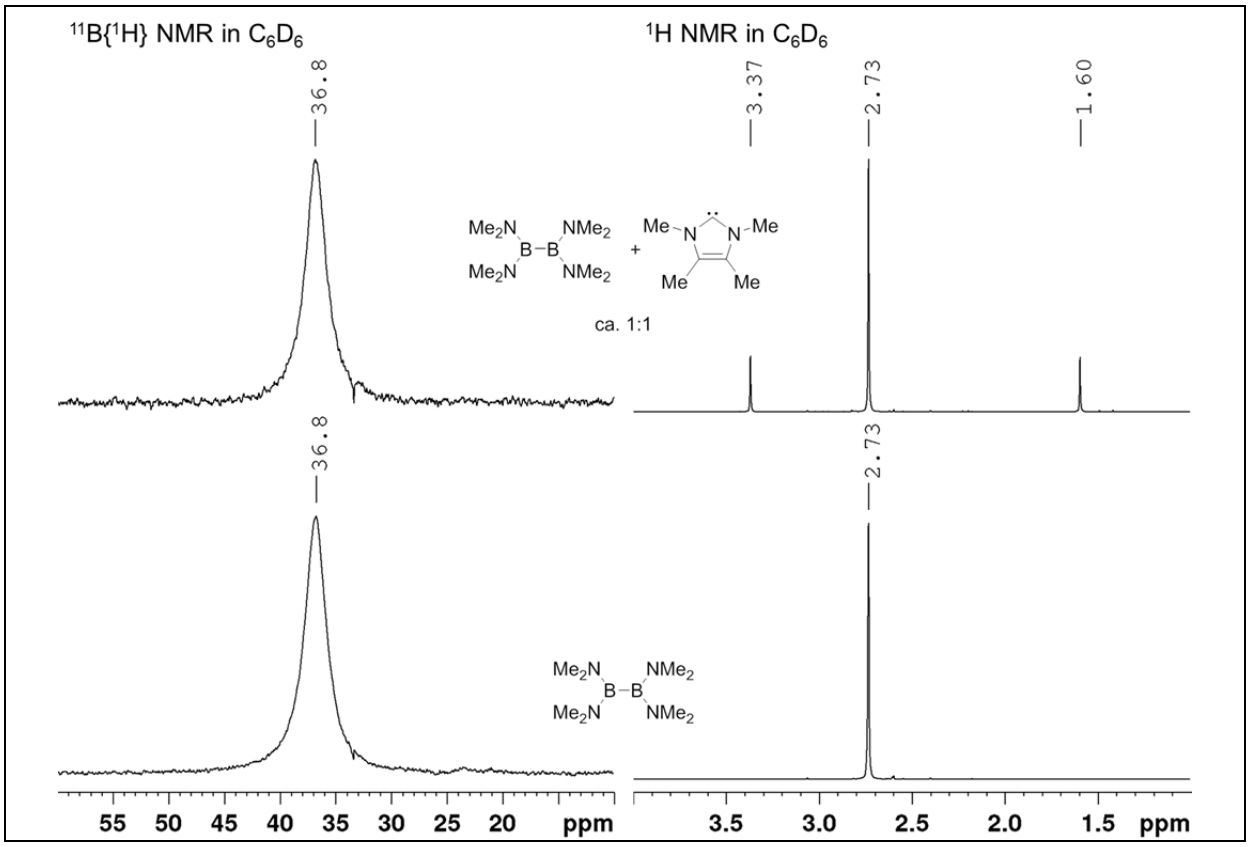

Figure 19. $^{11}B\{^1H\}$ NMR spectrum of compound **4** (bottom left) and the reaction mixture with Me_2Im^{Me} (top left) in C_6D_6 (64 MHz, 25 °C); ^1H NMR spectrum of compound **4** (bottom right) and the reaction mixture with Me_2Im^{Me} (top right) in C_6D_6 (200 MHz, 25 °C).

2.2 Bis(ethylene glycolato)diboron B_2eg_2 "The Old Dog"

In 2015, Ingleson, Radius and Marder *et al.* reported some ring-expansion reactions of the diboron(4) compounds B_2cat_2 and B_2neop_2,[170] and have shown that the RERs of B_2cat_2 with the NHCs *n*Pr_2Im and Me_2Im^{Me} occur at higher temperatures. In contrast, they have observed the ring expanded product of B_2neop_2 with *n*Pr_2Im even at room temperature. Moreover, they have shown that the reactions of B_2cat_2 **6** with *i*Pr_2Im and $Dipp_2Sim$ also require higher temperatures to afford ring-expansion products, while the reactions of B_2neop_2 **8** with the sterically less demanding NHCs Me_2Im and Me_2Im^{Me} resulted in the ring-expanded products at room temperature. The resulting compounds have only a limited stability in solution due to the high reactivity of the smaller NHCs.

This leads to the question about the role of the steric demand of the backbone of the diboron(4) compound as well, and prompted us to examine reactions of the potentially more reactive diboron reagent bis(ethylene glycolato)diboron(4) (B_2eg_2; **110**) with sterically demanding and less demanding NHCs.

2.2.1 Synthesis of B_2eg_2 "The Old Dog"

Therefore, B_2eg_2, **110** was synthesized *via* a literature procedure[20,22] from the reaction of $B_2(NMe_2)_4$ **4** with ethylene glycol ($HOCH_2CH_2OH$) and $HCl{\bullet}Et_2O$, and was isolated in 48% yield (Scheme 44).

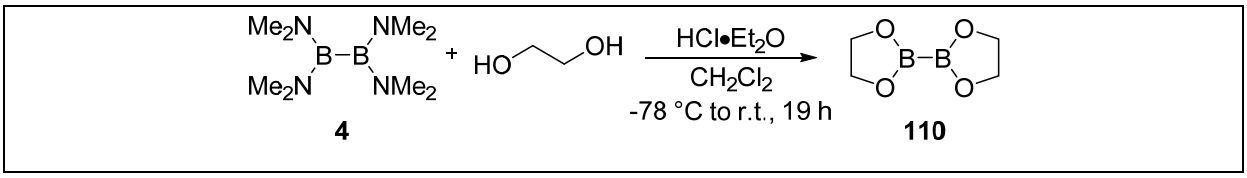

*Scheme 44. Synthesis of bis(ethylene glycolato)diboron(4) (B_2eg_2; **110**).*

Compound **110** was obtained as a colorless crystalline solid and was characterized using NMR spectroscopy and high resolution mass spectrometry. The ^1H NMR signal occurs at 3.50 ppm, and a $^{13}C\{^1H\}$ resonance is observed at 65.3 ppm. The $^{11}B\{^1H\}$ NMR spectrum shows a resonance at 31.5 ppm (for NMR spectra, see appendix A2). The $^{11}B\{^1H\}$ NMR signals of selected diboron(4) compounds are listed in Table 17 for comparison.

Table 17. $^{11}B\{^1H\}$ NMR (64 MHz, C_6D_6, RT) signals of selected diboron(4) compounds.[(a)]

	B_2neop_2	B_2cat_2	$B_2(OMe)_4$	B_2eg_2	B_2pin_2	$B_2(NMe_2)_4$
$^{11}B\{^1H\}$ signal [ppm]	28.7	30.9	31.0	31.4[(b)]	31.4	36.8

(a) See appendix A1 for spectra; (b) $^{11}B\{^1H\}$ NMR (96 MHz, C_6D_6, RT)

The recently reported[111] molecular structure of B_2eg_2 **110** shows a virtually planar molecule, crystallizing in the space group $P2_1/c$ with an inversion center and with half a molecule in the asymmetric unit. The range of the B–B bond length (1.704(3) Å)[111] is quite similar compared to the bond lengths found for B_2pin_2 (1.707(5) Å)[111] and B_2neop_2 (1.712(3) Å).[111] Compared to the B–B bond length of $B_2(NMe_2)_4$ (1.735(3) Å)[111] it is significantly shorter, and compared to B_2cat_2 (1.678(3) Å),[24] noticeably longer.

2.2.2 Scrambling of the boron substituents "The Old Dog's Siblings"

It is well known and reported in the literature that the formation of spiro- or other bis-borates as side products, can occur when using alkoxy diboron(4) compounds. Also, the addition of Lewis bases to diboron(4) compounds or to boranes such as HBcat an ClBcat may lead to scrambling of the boron substituents. To study the reactivity of B_2eg_2 with NHCs it was required to know what the NMR shifts of the spiro-borate $[Beg_2]^-$ and the bis-borate B_2eg_3 are.[111,147,170,172,176,177]

2.2.2.1 Spiro-borate $[Beg_2]^-$ "The Old Dog's Sister"

To assign the NMR shift of $[Beg_2]^-$, a simple reaction was performed according to the literature, which was monitored by *in situ* NMR spectroscopy (Scheme 45, Figure 20).[178]

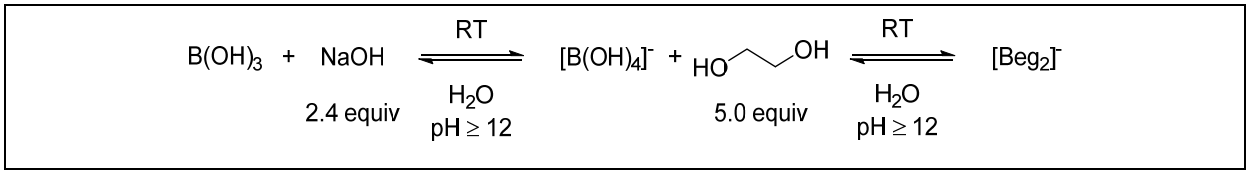

Scheme 45. Reaction of boric acid with NaOH and ethylene glycol.

Boric acid and an excess of sodium hydroxide were dissolved in water to form the tertrahydroxyborate $[B(OH)_4]^-$. The equilibrium is pH dependent and completely on the borate side at a pH ≥ 12. The $^{11}B\{^1H\}$ NMR signal for boric acid in H_2O is at 19.3 ppm and the signal for $[B(OH)_4]^-$ at 1.61 ppm, up-field shifted and in the expected region of four-coordinated boron species. To the solution of the tetrahydroxborate, an excess of ethylene glycol was added and the formation of the mixed borate $[egB(OH)_2]^-$ and the spiro-borate $[Beg_2]^-$ was observed, for which the equilibrium is concentration and pH dependent. The $^{11}B\{^1H\}$ NMR showed a resonance at 5.49 ppm for $[egB(OH)_2]^-$ and at 9.30 ppm for $[Beg_2]^-$ (Figure 20). So, the NMR shift of $[Beg_2]^-$ should be expected to be in the region of ca. 10.0 ppm, and indeed, this shift can differ slightly depending on the counter-ion.

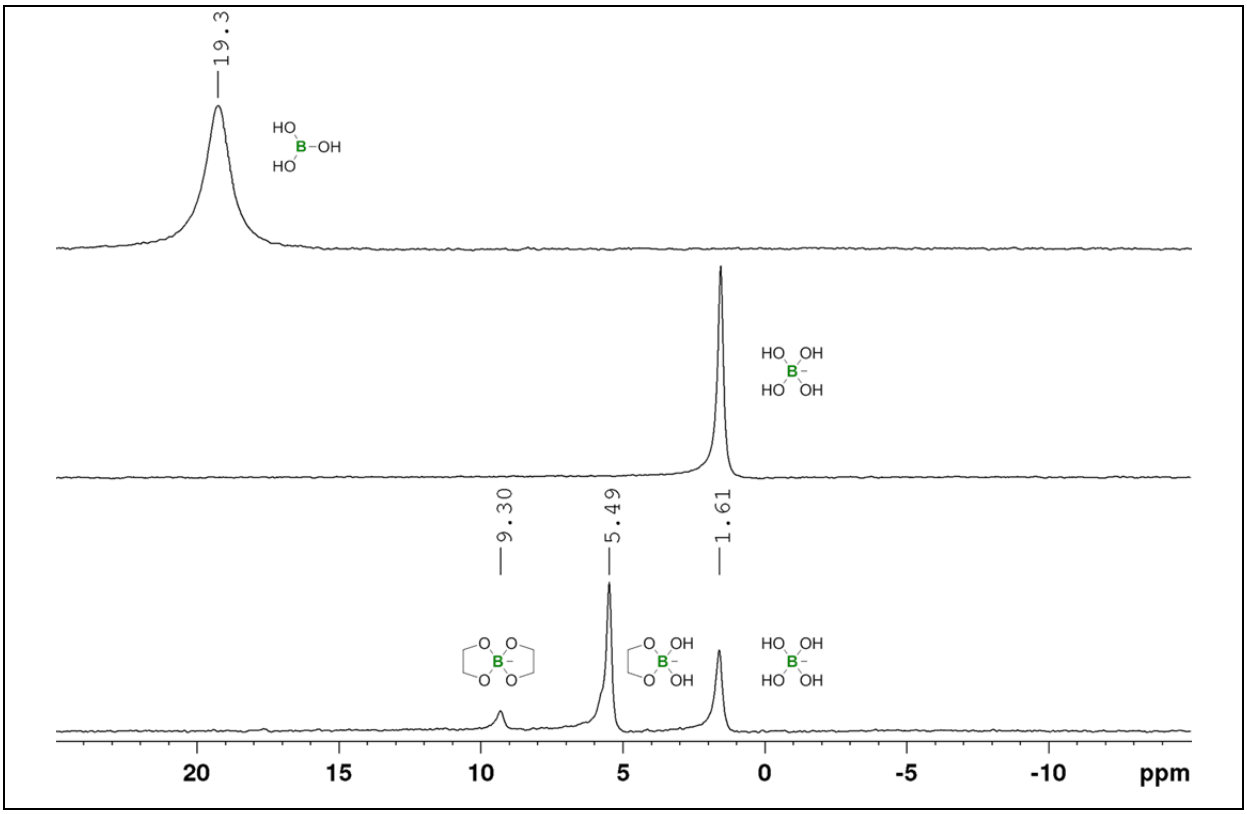

Figure 20. $^{11}B\{^1H\}$ *NMR spectra of boric acid (top), a mixture of boric acid with an excess of NaOH forming the tertrahydroxyborate* $[B(OH)_4]^-$ *anion (middle) and a mixture of the tertrahydroxyborate with ethylene glycol forming the corresponding borates (bottom) in* H_2O *(64 MHz, 25 °C).*

2.2.2.2 B_2eg_3 tris(ethylene glycolato)diboron "The Old Dog's Brother"

Due to the poor quality of commercially purchased (Sigma-Aldrich) BH_3•THF, tris(ethylene glycolato)diboron (B_2eg_3 **111**) was synthesized according the literature by the reaction of freshly prepared BH_3•THF with ethylene glycol and obtained in 35% yield over 2 steps (Scheme 46).[179-182]

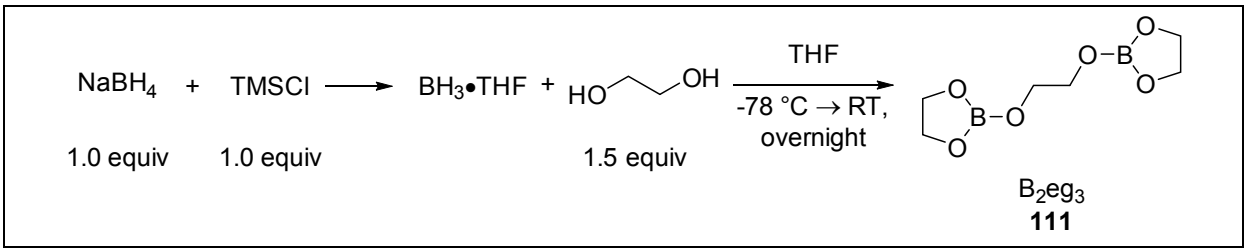

Scheme 46. Synthesis of tris(ethylene glycolato)diboron (B_2eg_3*,* ***111****).*

The ^{11}B NMR spectrum of the freshly prepared BH_3•THF showed the characteristic signal (quartet) at -0.17 ppm, whereas the commercially purchased batch already indicated decomposition of the borane (Figure 21).

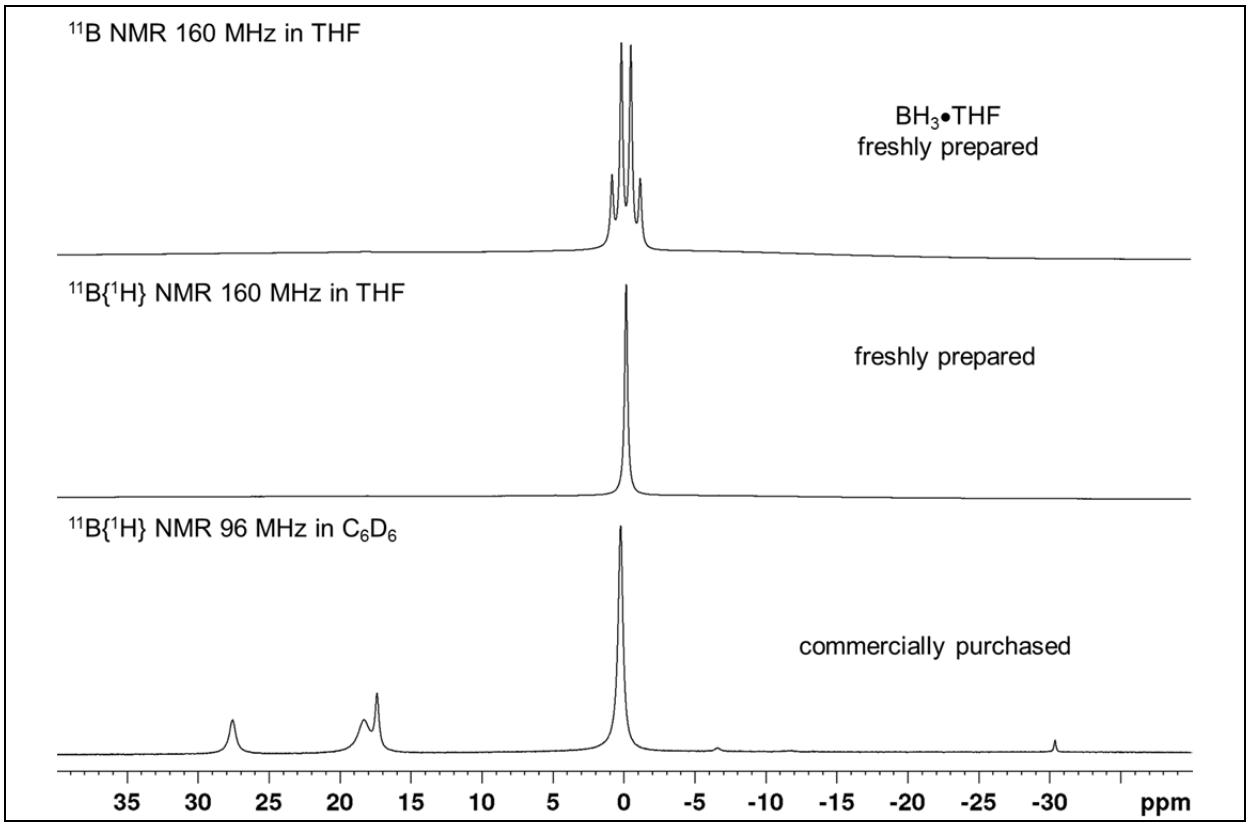

Figure 21. ^{11}B and $^{11}B\{^1H\}$ NMR spectra of BH_3•THF.

The reaction of the THF borane with ethylene glycol was also monitored *via* $^{11}B\{^1H\}$ NMR spectroscopy (Figure 22).

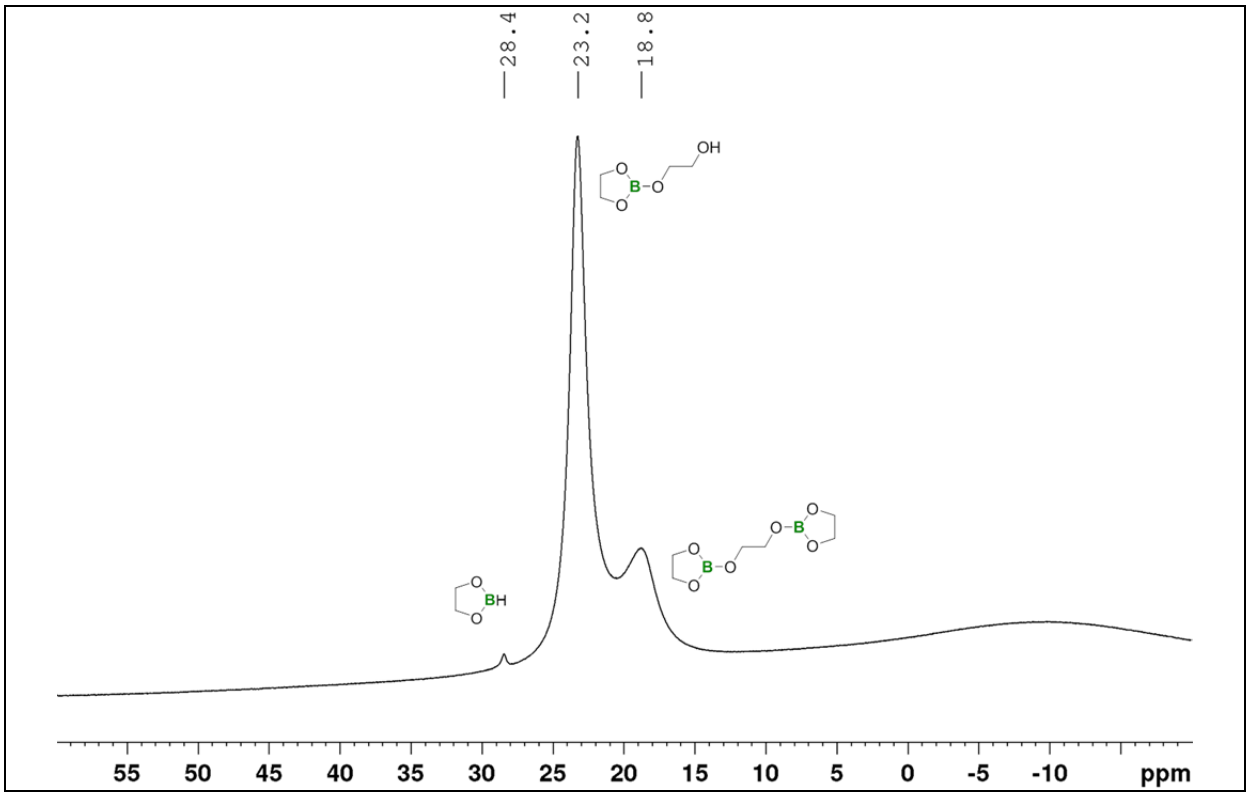

Figure 22. Reaction of 1.0 equiv BH_3•THF with 1.5 equivalents of ethylene glycol.

The $^{11}B\{^1H\}$ NMR spectra showed the formation of the mono-substituted HBeg (28.4 ppm), the di-substituted egB–OCH_2CH_2OH (23.2 ppm) and the desired product B_2eg_3 (18.8 ppm). The compounds in this mixture could not be separated, but the literature described the disproportion of HBeg[182] and egB–OCH_2CH_2OH[179,181] to B_2eg_3 (Scheme 47). Therefore, the solvent was removed under reduced pressure and the residue was heated to 100 °C to complete the disproportion to B_2eg_3 and yield pure compound **111**. Interestingly, once B_2eg_3 was isolated, it was observed that compound **111** was not soluble in C_6H_6, CH_2Cl_2, $CHCl_3$ and MeCN, and the solubility in THF was strongly decreased. This observation was also described in the literature.[181]

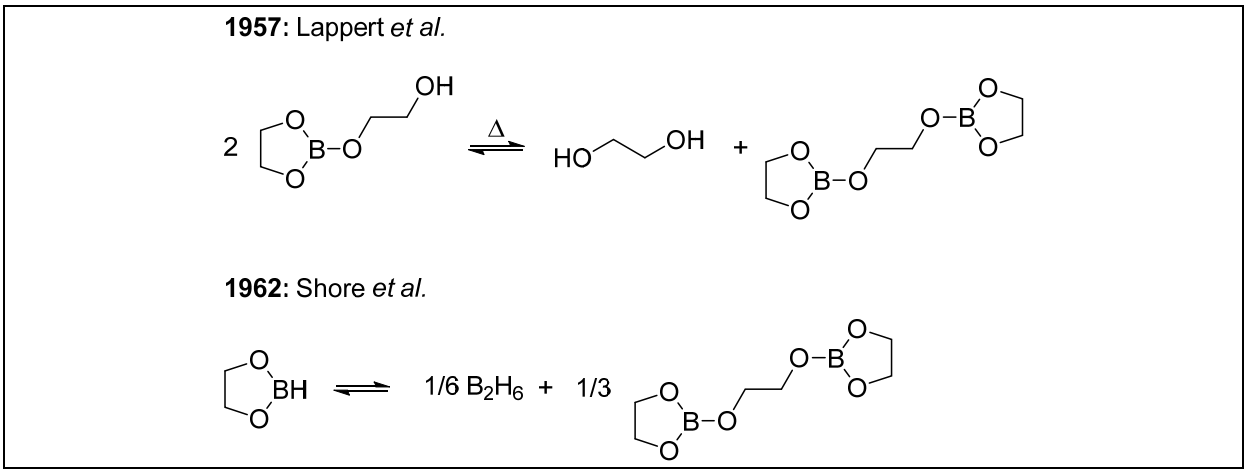

*Scheme 47. Disproportion of HBeg or egB–OCH_2CH_2OH to B_2eg_3 **111** reported by Lappert et al. and Shore et al.*

Due to the poor solubility of compound **111**, the characterization was accomplished *via* solid-state NMR spectroscopy, high resolution mass spectrometry and elemental analysis.

The ^{11}B RSHE/MAS (rotor synchronized Hahn echo) NMR spectrum shows a signal with an isotropic shift at 18.9 ppm with the typical line shape (MAS second-order quadrupole powder pattern) for a trigonal planar sp^2-B atom (Figure 23) and matches the $^{11}B\{^1H\}$ NMR signal in solution (18.8 ppm), *vide supra*. The ^{13}C CP/MAS spectrum shows three signals (61.7, 63.1 and 64.3 ppm) for the carbon atoms of the ethylene glycol bridge and the chelated diolate (Figure 24).

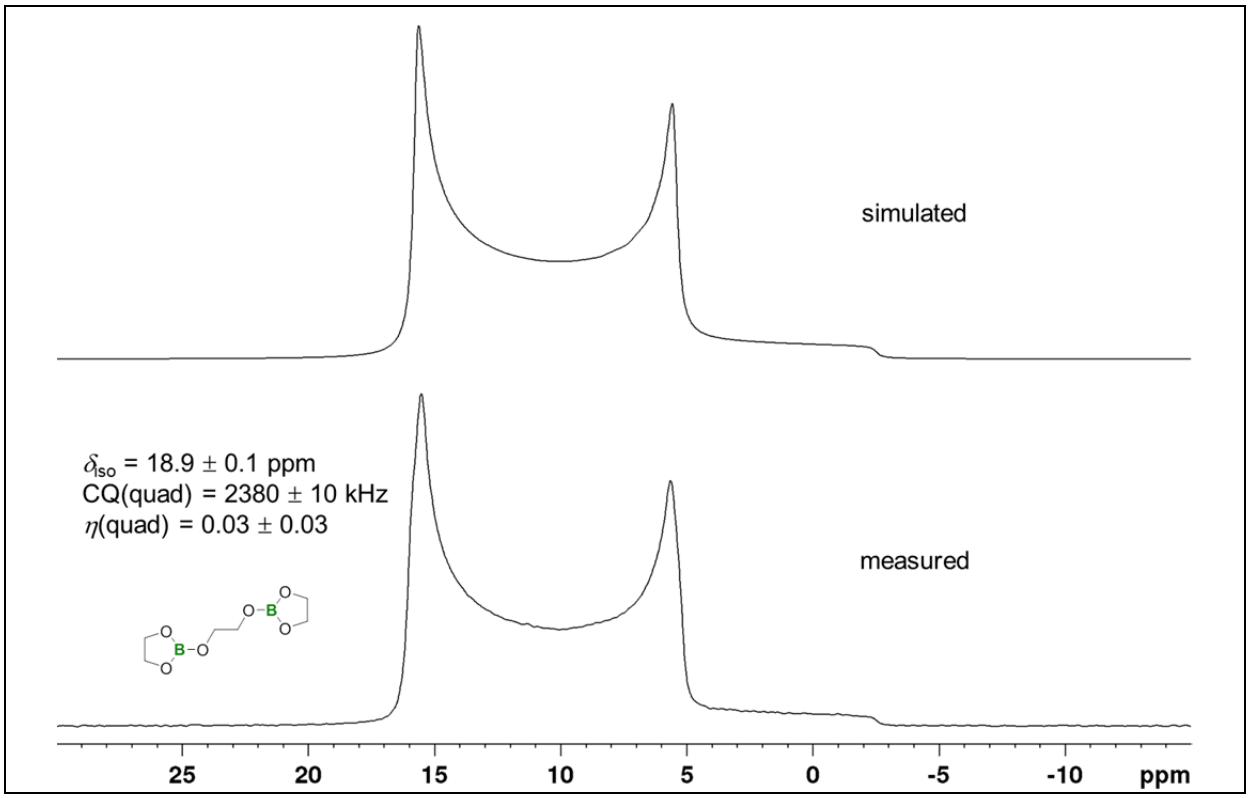

Figure 23. ^{11}*B RSHE/MAS NMR spectrum of compound* ***111*** *(128 MHz, 22 °C,* ν *rot = 15000* Hz).

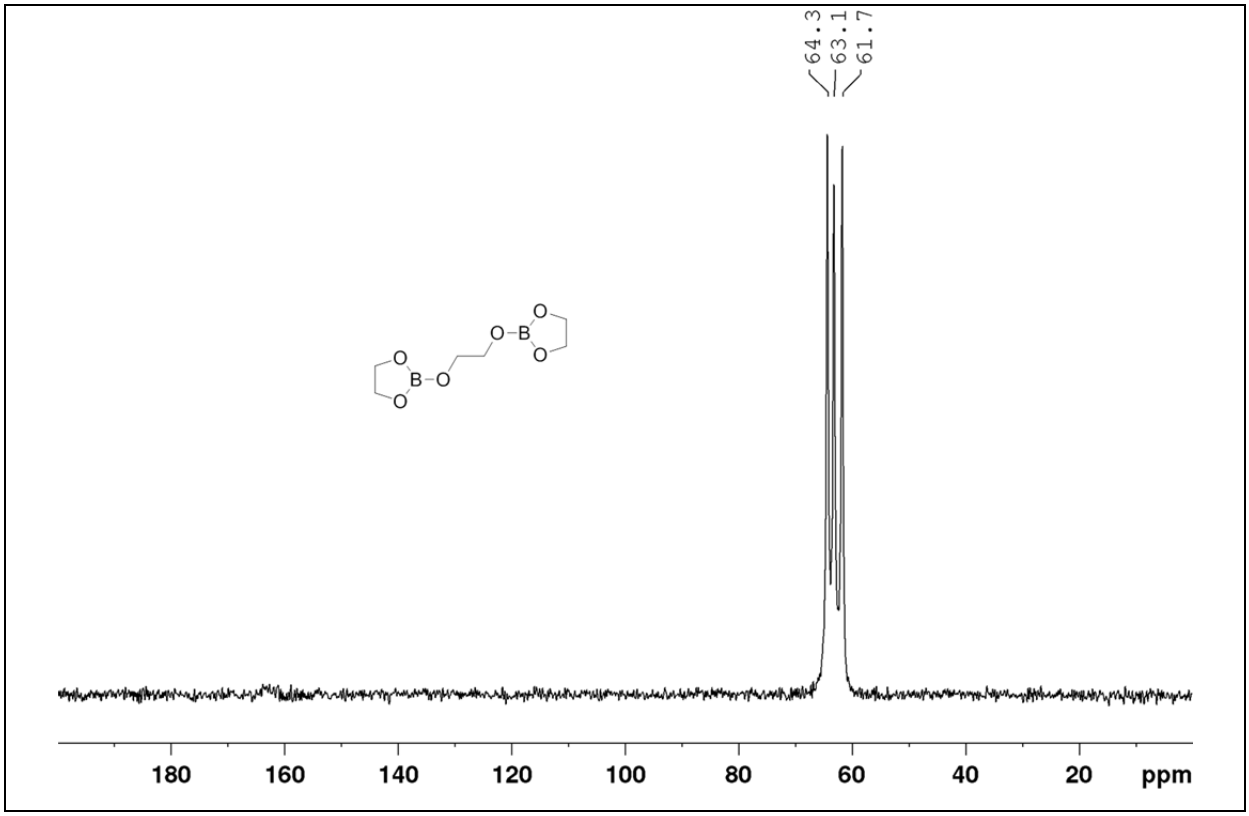

Figure 24. ^{13}*C CP/MAS NMR spectrum of compound* ***111*** *(101 MHz, 22 °C,* ν *rot = 10000 Hz).*

2.2.3 Reaction of B_2eg_2 with NHCs of different steric demand

To investigate the reactivity and the potential of B_2eg_2 **110** for B–B bond and C–N bond activation, *via* mono/bis-adduct formation or ring-expansion reaction (RER), compound **110** was reacted with NHCs of different steric demand (Scheme 48).

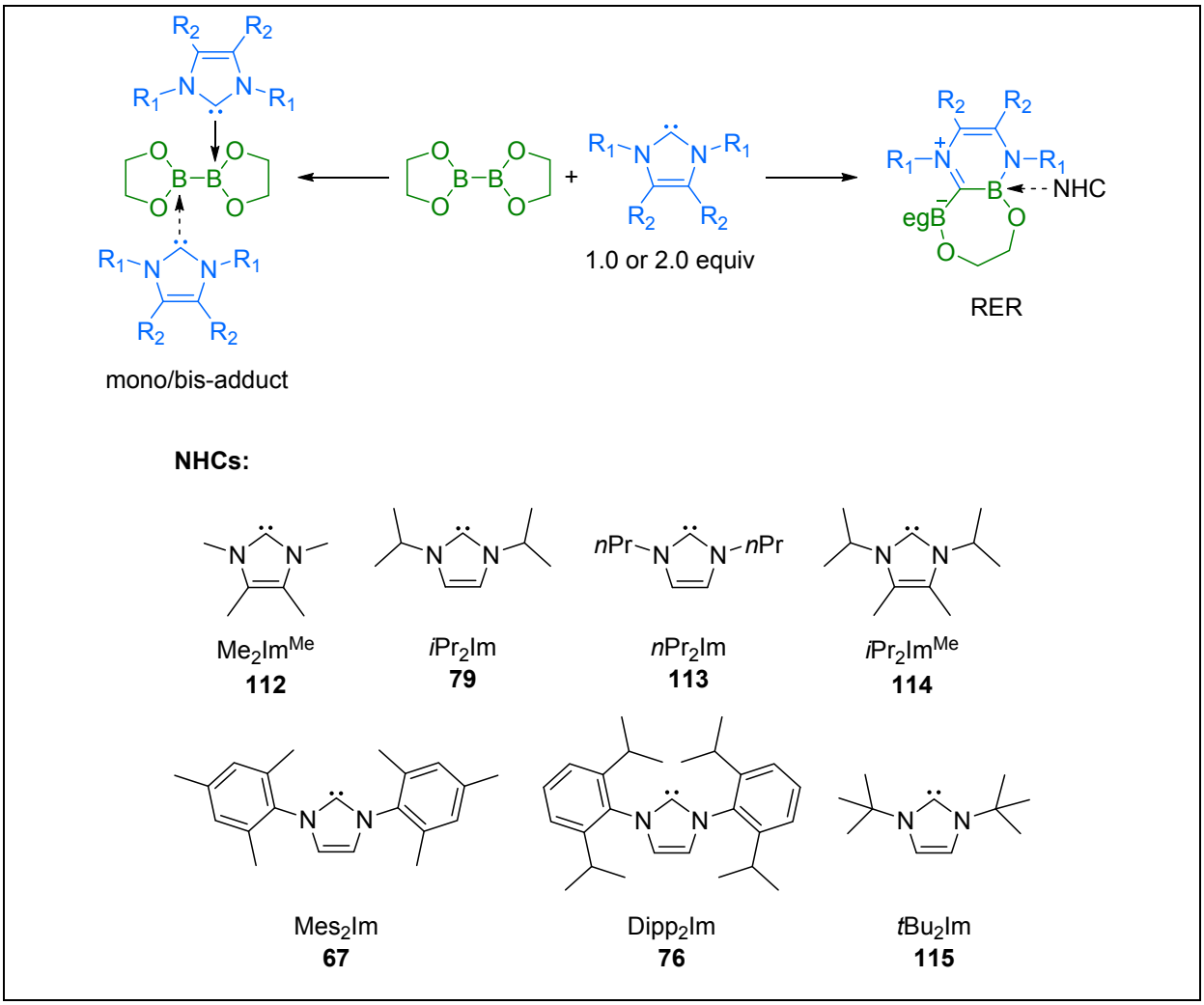

Scheme 48. Reactivity of B_2eg_2 with NHCs of different steric demand.

These reactions and the resulting observations are described in detail in the following paragraphs.

2.2.3.1 Reactions of B_2eg_2 with the NHCs *t*Bu_2Im and $Dipp_2$Im

The reactions of B_2eg_2 **110** with the bulky NHCs *t*Bu_2Im and $Dipp_2$Im were carried out at room temperature and were monitored by *in situ* $^{11}B\{^1H\}$ and ^1H NMR spectroscopy (Scheme 49).

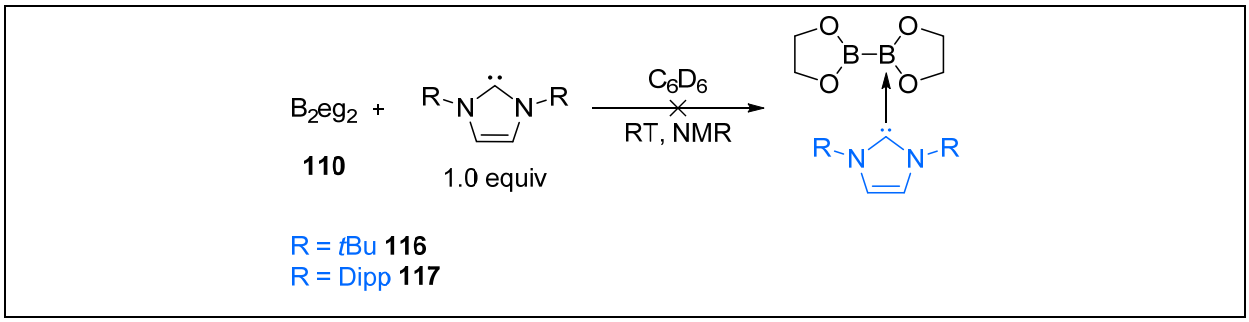

*Scheme 49. Reaction of B_2eg_2 **110** with tBu_2Im **115** and $Dipp_2Im$ **76** monitored by in situ NMR spectroscopy.*

The *in situ* $^{11}B\{^1H\}$ and ^1H NMR spectra of the reaction of compound **110** with the sterically demanding NHC *t*Bu_2Im do not show any significant shift indicative of adduct formation (Figure 25 and Figure 26). Although, a very small, broad peak may be apperent at ca. 34 ppm in the $^{11}B\{^1H\}$NMR spectrum and three very small peaks at 1.46, 2.93 amd 3.64 ppm are apperent in the ^1H NMR spectrum, which could not be assigned.

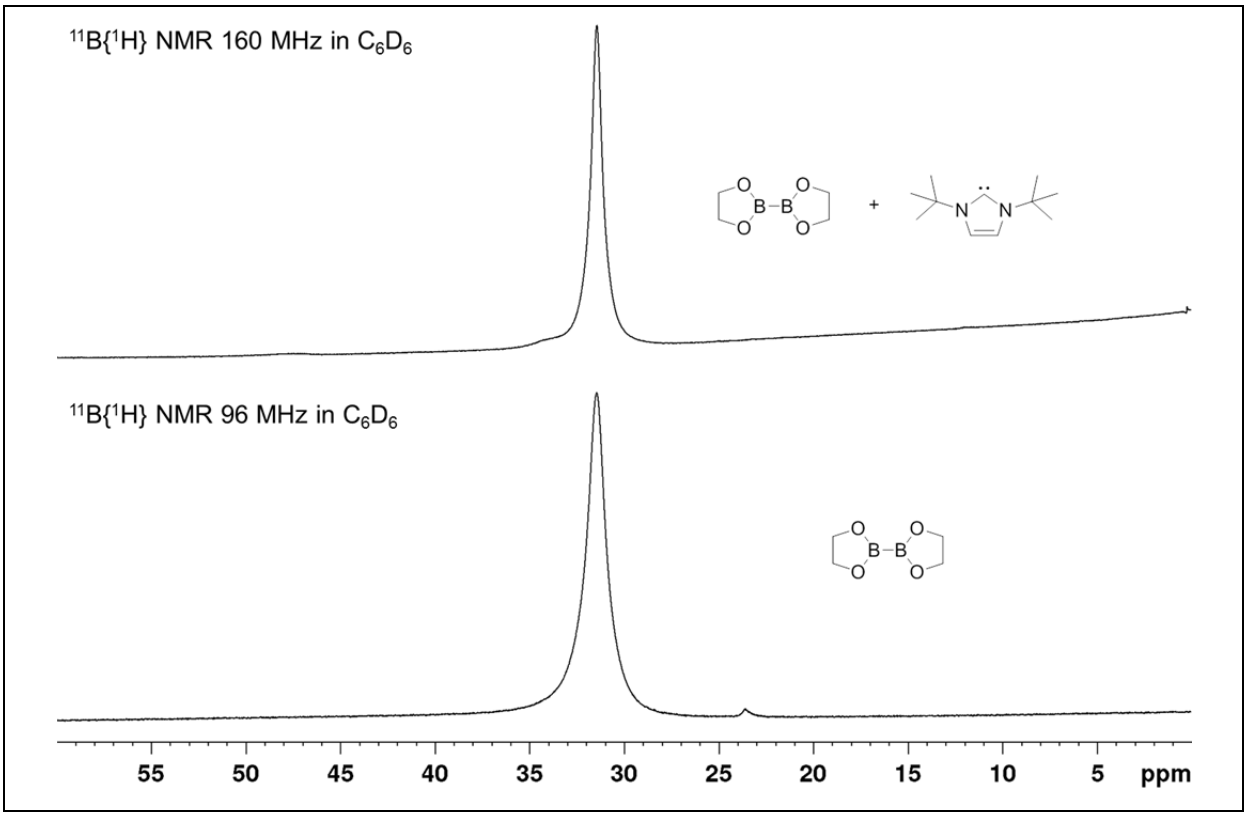

*Figure 25. In situ $^{11}B\{^1H\}$ NMR spectrum of the reaction of B_2eg_2 **110** with tBu_2Im (top) in C_6D_6 (160 MHz, 25 °C).*

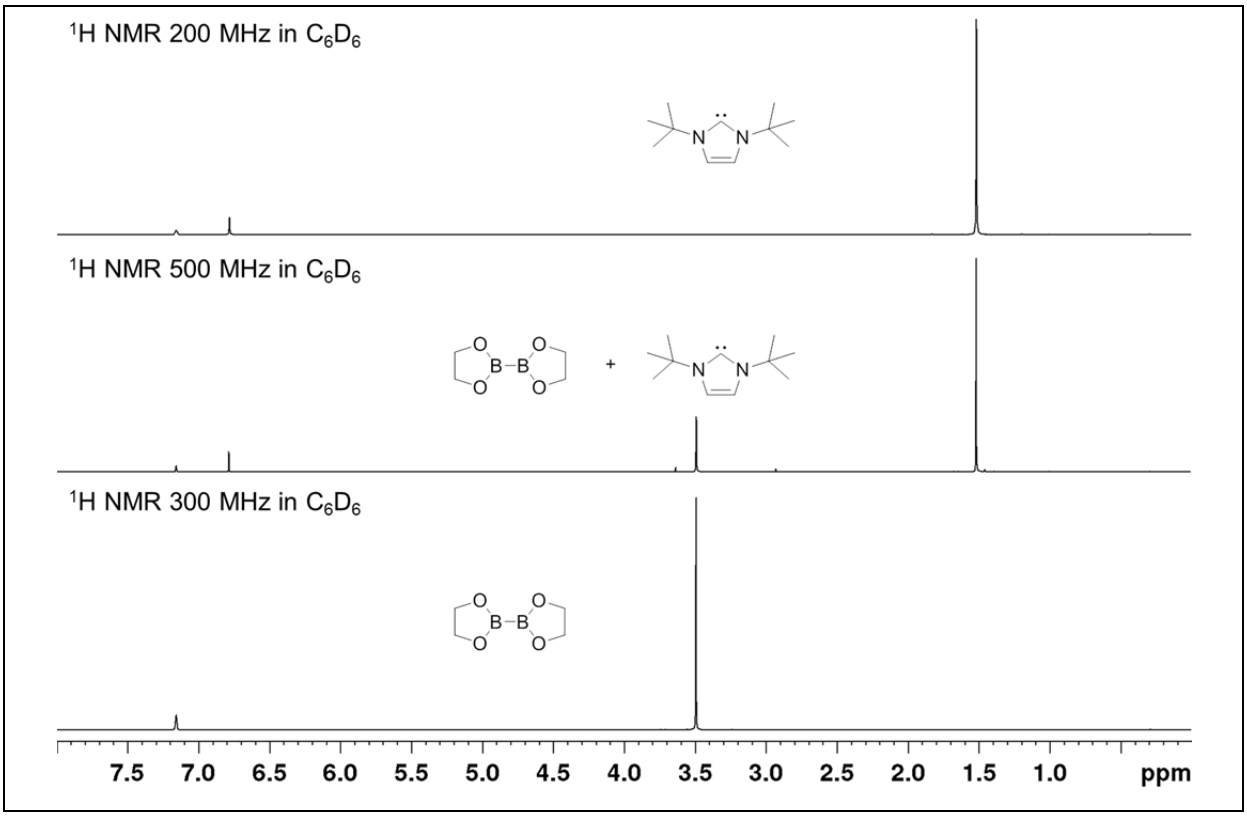

*Figure 26. In situ ^1H NMR spectrum of the reaction of B_2eg_2 **110** with tBu_2Im (middle) in C_6D_6 (500 MHz, 25 °C).*

In contrast, the reaction of B_2eg_2 with the bulky NHC $Dipp_2Im$ showed a very weak dynamic interaction of the carbene and the diboron(4) compound. As a result, a small up-field shift (by 3.10 ppm), and a broadening of the signal was observed in the $^{11}B\{^1H\}$ NMR spectrum (Figure 27). In addition, in the ^1H NMR spectrum, slight shifts compared to the pure starting materials were observed. Interestingly, the NHC backbone protons (C*H*C*H*) were down-field shifted by 0.09 ppm, the protons of the backbone of B_2eg_2 (CH_2) and the NHC isopropyl protons (C*H*CH_3) were up-field shifted by 0.06 ppm, one set of the NHC methyl-protons (CHCH_3) was down-field shifted by 0.17 ppm and the other set of methyl-protons (CHCH_3) was up-field shifted by 0.03 ppm (Figure 28).

Nevertheless, for both reactions, neither evidence for an adduct formation (e.g. ^{11}B NMR: sp^2-B ≥ 20 ppm, sp^3-B ≤ 20 ppm) was found or it could not be isolated, respectively, nor was any other reactivity observed. This might be explained by the high steric demand of these NHCs.

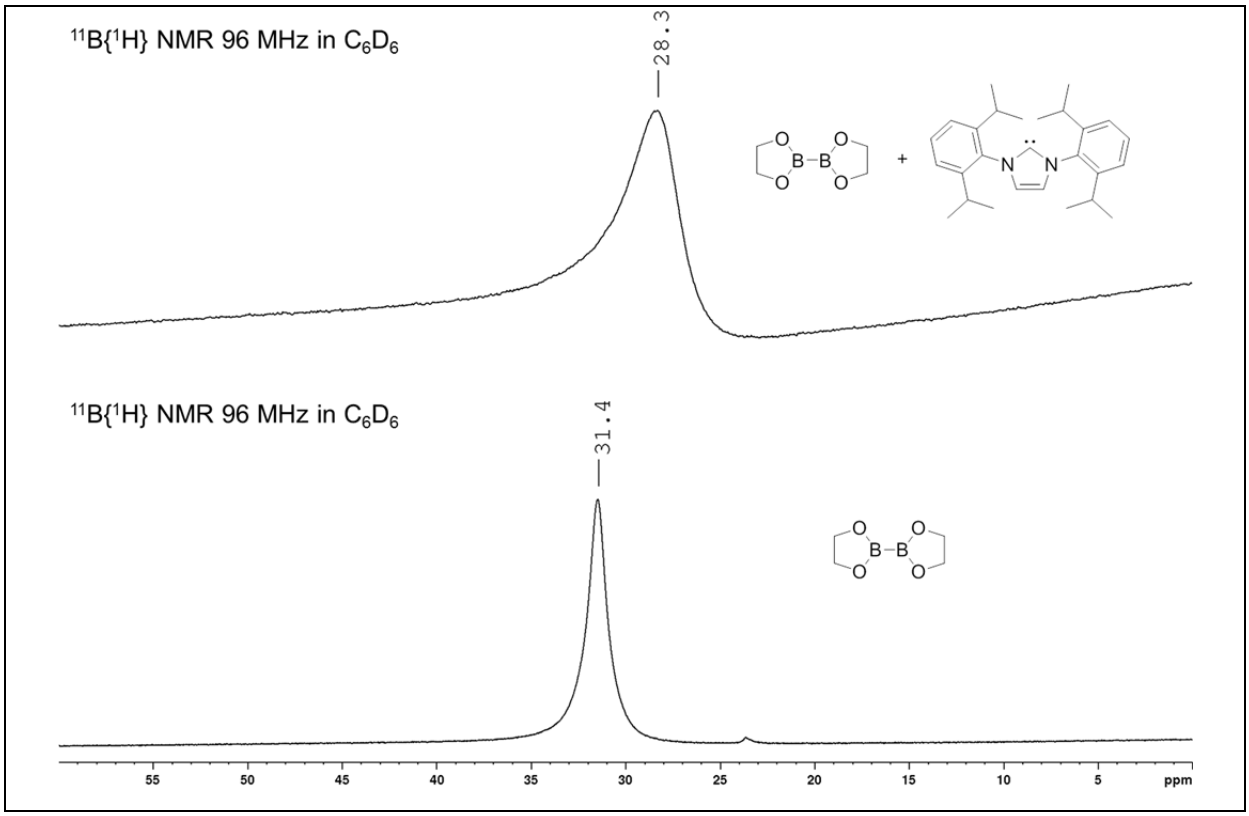

Figure 27. In situ $^{11}B\{^1H\}$ NMR spectrum of the reaction of B_2eg_2 ***110*** *with $Dipp_2Im$ (top) in C_6D_6 (96 MHz, 25 °C).*

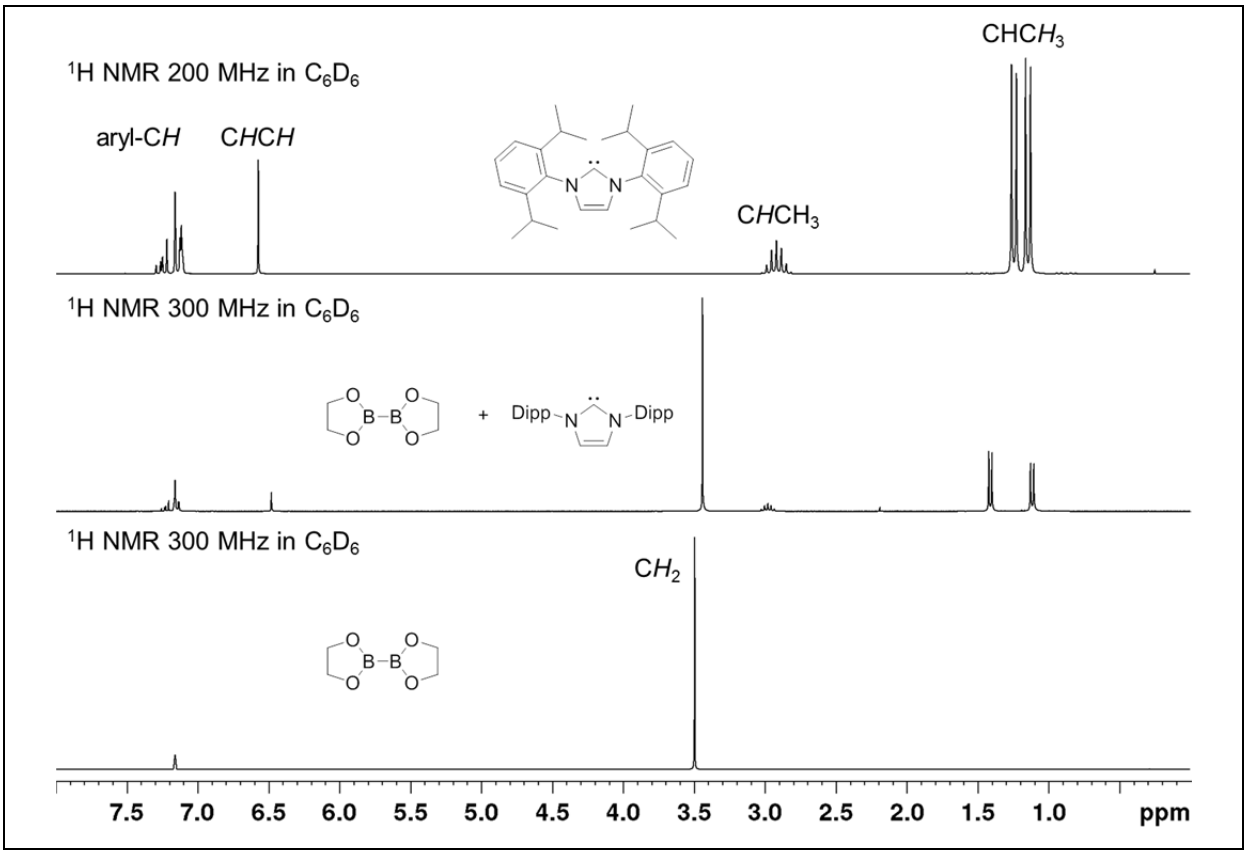

*Figure 28. In situ ^{1}H NMR spectrum of the reaction of B_2eg_2 **110** with $Dipp_2Im$ (middle) in C_6D_6 (300 MHz, 25 °C).*

2.2.3.2 Reaction of B_2eg_2 with the NHC Mes_2Im

The reaction of B_2eg_2 **110** with the sterically demanding NHC Mes_2Im **67** was carried out at room temperature (Scheme 50) and gave the mono-NHC adduct B_2eg_2•Mes_2Im **118** as a colorless solid in good yield (71%), and was characterized *via* solution and solid-state NMR spectroscopy, high resolution mass spectrometry as well as by single-crystal X-ray diffraction.

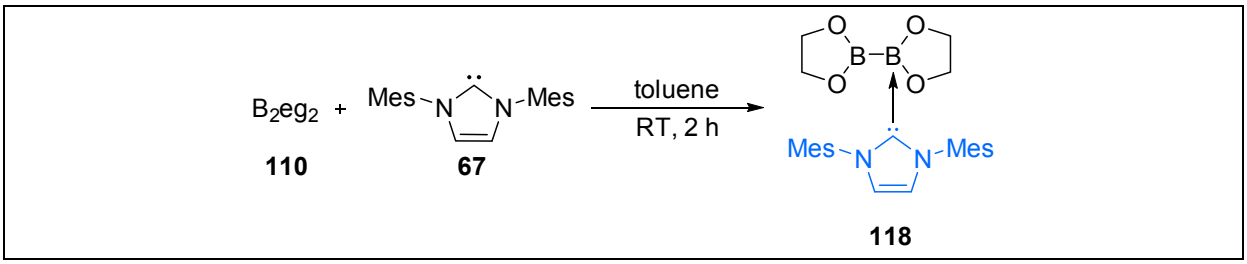

*Scheme 50. Synthesis of the mono NHC adduct B_2eg_2•Mes_2Im **118**.*

In the solid-state ^{11}B RSHE/MAS NMR spectrum, two signals with isotropic shifts of 3.90 ppm for the sp^3-B atom and 35.1 ppm for the sp^2-B atom were observed as expected for a mono-adduct (Figure 29; for more detailed spectra, see appendix A3)

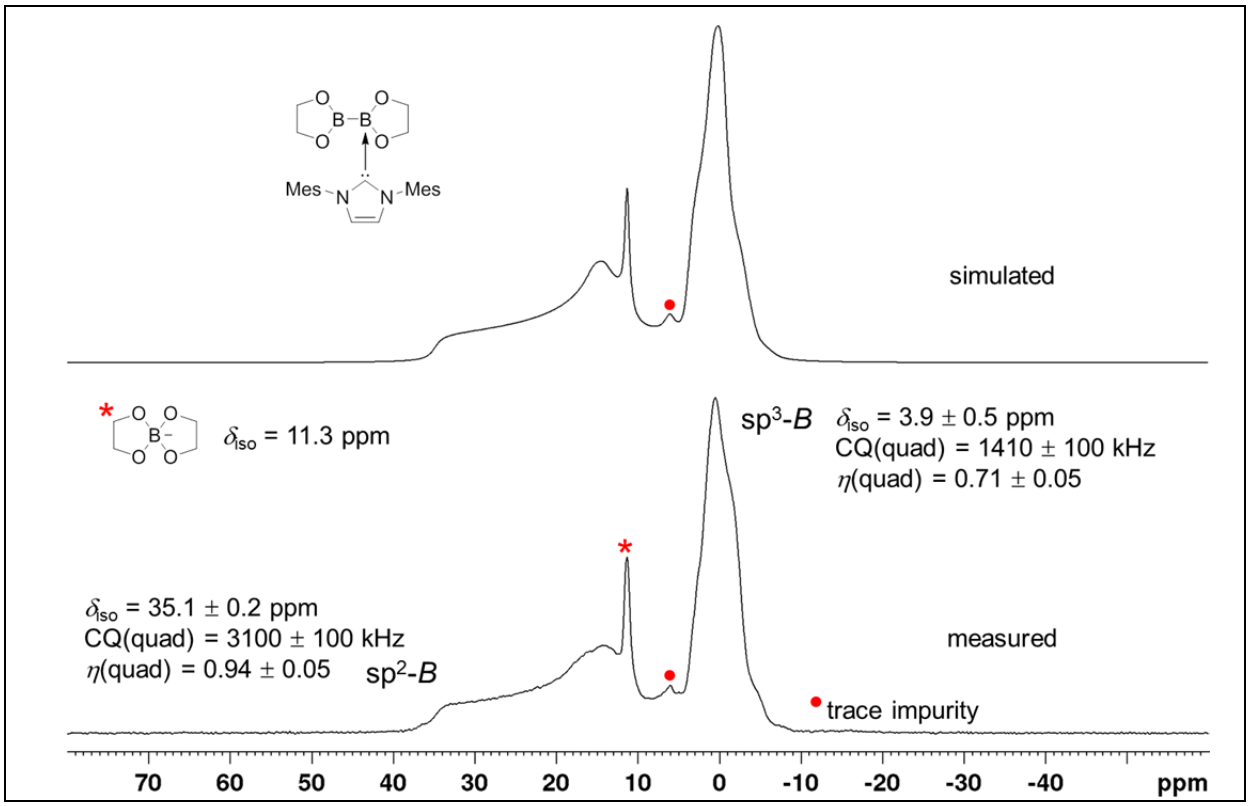

*Figure 29. ^{11}B RSHE/MAS NMR spectrum of B_2eg_2•Mes_2Im **118** (128 MHz, 22 °C, ν rot = 15000* Hz).

Furthermore, an impurity with an isotropic shift at 11.3 ppm was detected and identified as the spiro-borate anion $[Beg_2]^-$, which is certainly not surprising as the formation of spiro-borate anions are well known side products using alkoxy (di)boranes in syntheses (*vide supra*).[111,147,170,172,176,177]

While the ^{11}B RSHE/MAS NMR spectrum shows the characteristic line shape for an sp^2-sp3 diboron(4) adduct with two isotropic shifts, in the ^{11}B{^{1}H} NMR spectrum in solution, however, only one broad signal at 22.6 ppm was observed (Figure 30). This observation can be explained by the fast dynamic exchange of the NHC between the two boron atoms of B_2eg_2 **110**. The dynamic process is also reflected in the solution ^{1}H NMR spectrum in which only one signal at 3.44 ppm (shifted 0.06 ppm up-field compared to the ^{1}H signal of B_2eg_2) is observed for the backbone of B_2eg_2 (Figure 31), whereas two signals were expected for the unsymmetrical mono-NHC adduct B_2eg_2•Mes_2Im **118**. To investigate the dynamics, a low temperature NMR experiment was performed but, unfortunately, failed due to the poor solubility of compound **118** at lower temperatures (up to -40 °C).

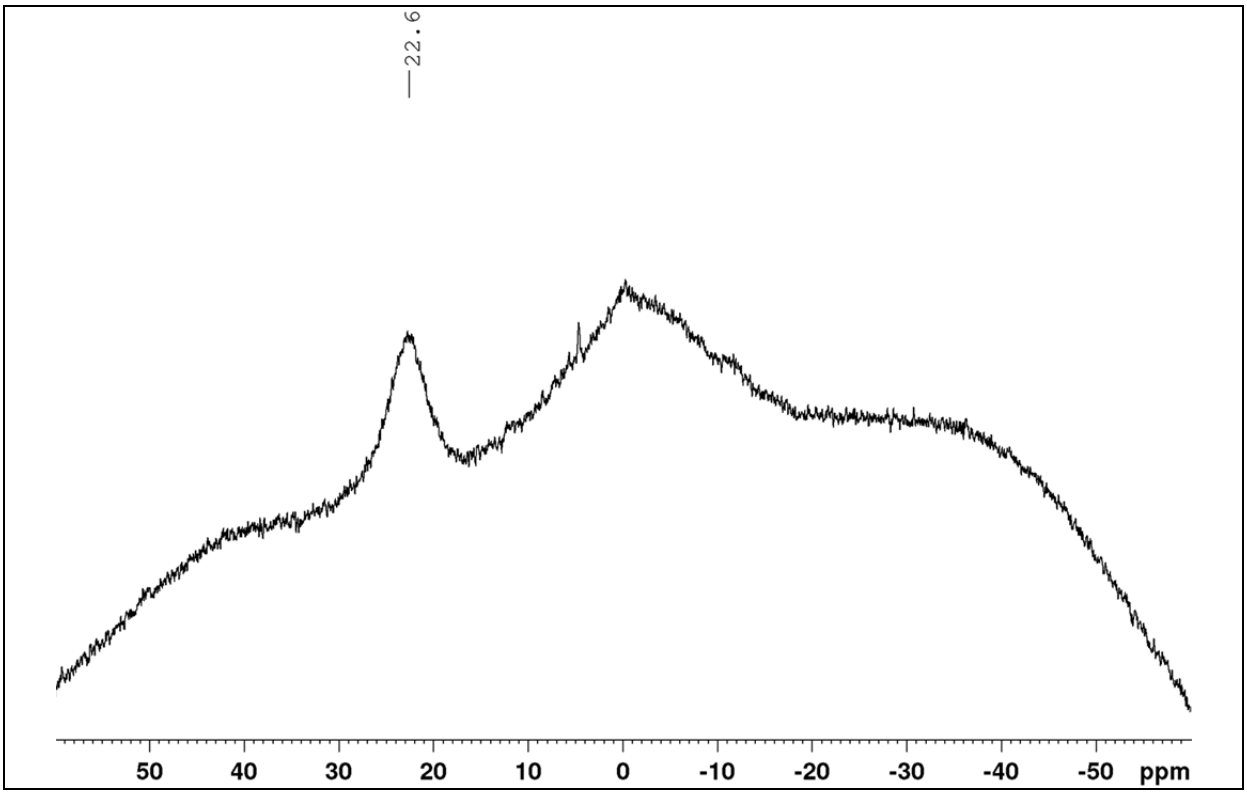

Figure 30. $^{11}B\{^{1}H\}$ *NMR spectrum of* B_2eg_2•Mes_2Im ***118*** *in* C_6D_6 *(96 MHz, 25 °C).*

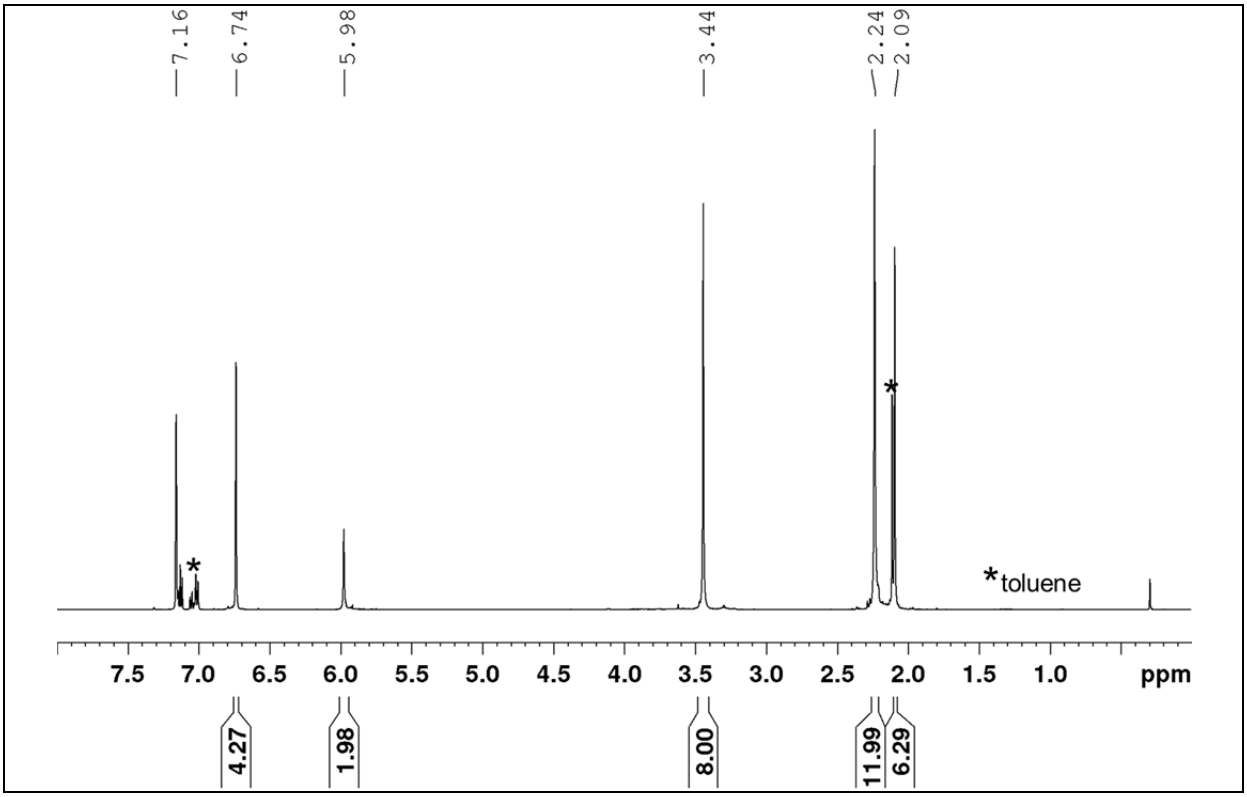

Figure 31. ^{1}H *NMR spectrum of* B_2eg_2•Mes_2Im ***118*** *in* C_6D_6 *(300 MHz, 25 °C).*

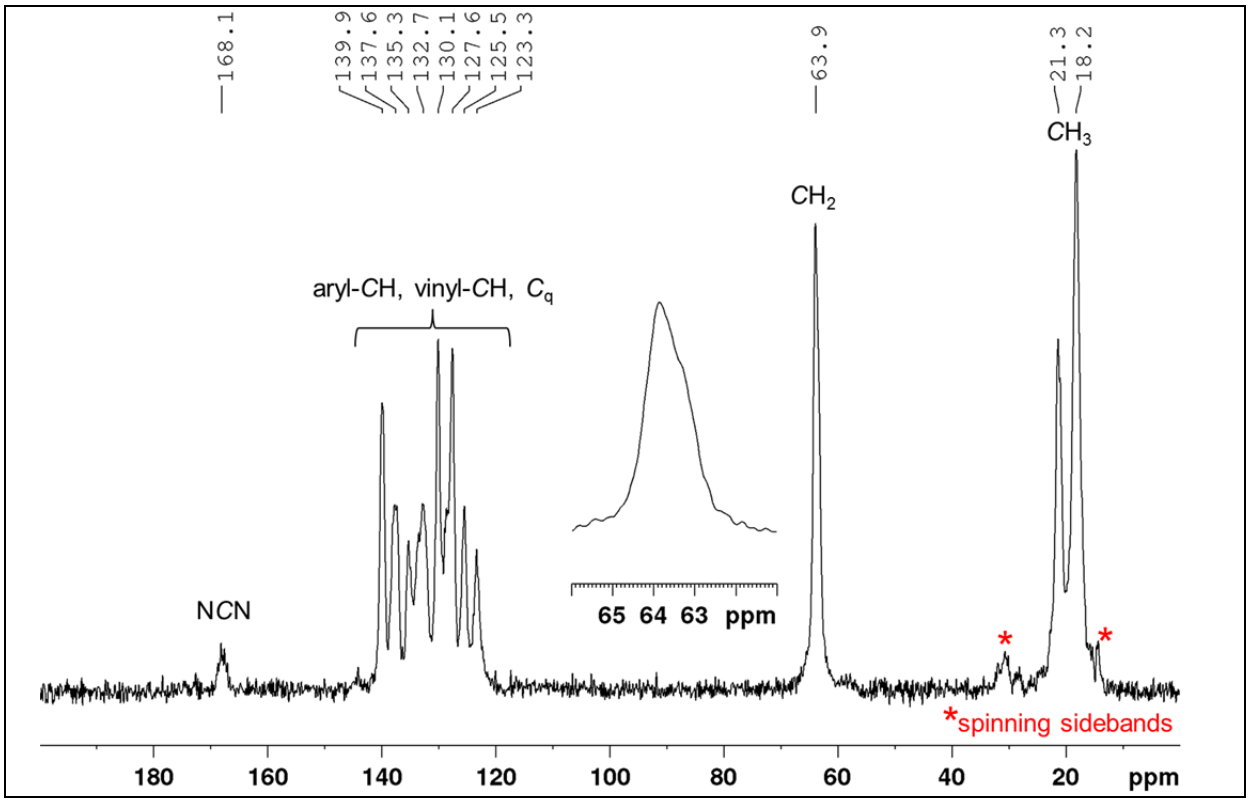

*Figure 32. ^{13}C CP/MAS NMR spectrum of B_2eg_2•Mes_2Im **112** (101 MHz, 22 °C, ν rot = 11000 Hz).*

However, the solid state ^{13}C CP/MAS NMR spectrum shows the characteristic peak for the C_{NHC}–B bond of the mono-NHC adduct at 168.1 ppm. For the backbone of the Beg-moieties, one broad signal was observed at 63.9 ppm, and a small shoulder on this peak indicates that two different Beg-moieties are present in the solid state (Figure 32). This is also supported by the ^{15}N CP/MAS NMR spectrum (Figure 33) showing two signals (-185.9 and -189.9 ppm) for the two N-atoms of the NHC.

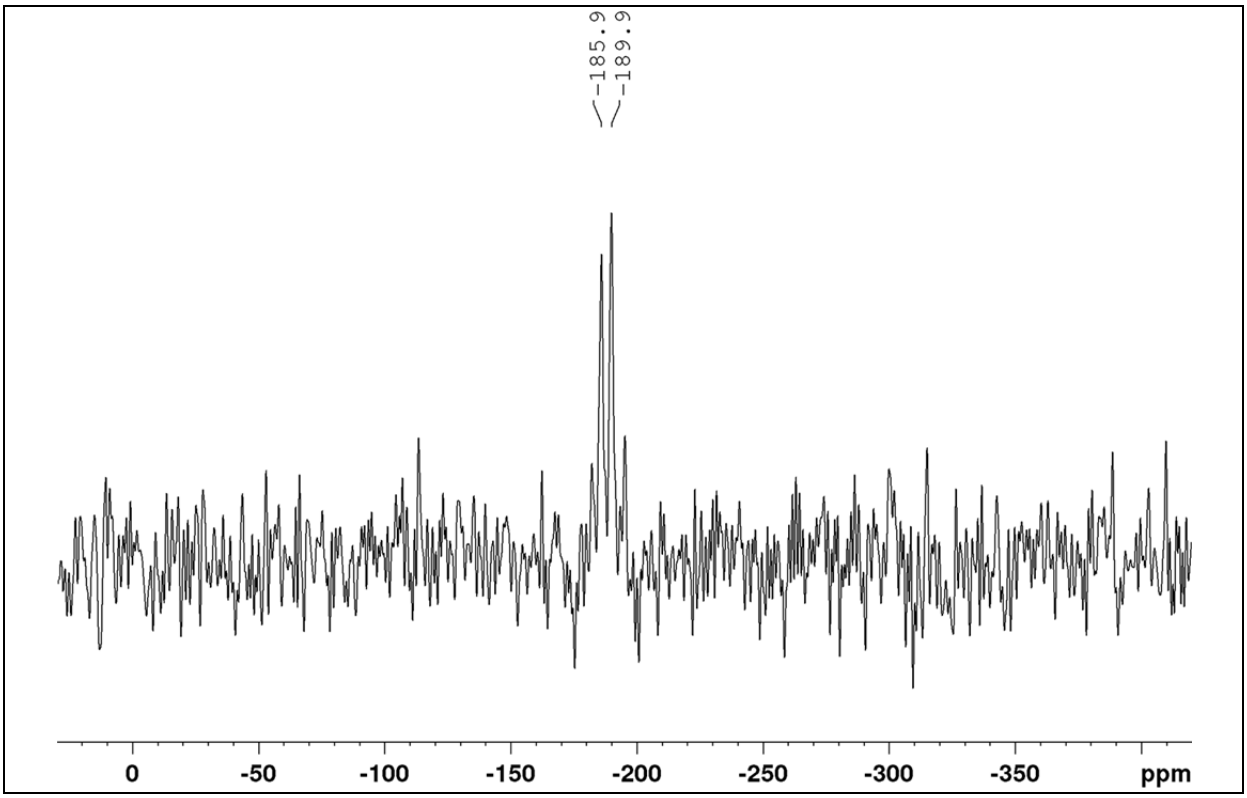

*Figure 33. ^{15}N CP/MAS NMR spectrum of B_2eg_2•Mes_2Im **118** (41 MHz, 22 °C, ν rot = 7000 Hz).*

Furthermore, the counter-ion to the spiro-borate anion $[Beg_2]^-$ was identified (*via* HRMS) as the protonated NHC $[Mes_2Im\text{-}H]^+$. Nevertheless, the corresponding carbon resonances in the ^{13}C CP/MAS NMR spectrum are overlapping with the signals of the mono-NHC adduct **118**. However, the very small impurity, the spiro-borate NHC salt $[Beg_2][Mes_2Im\text{-}H]$ and compound **118** could not be separated due to the similar solubility in organic solvents.

The mono-NHC adduct B_2eg_2•Mes_2Im **118** is stable at room temperature. Even at elevated temperature (60 °C), the reaction of B_2eg_2 with two equivalents of Mes_2Im does not show further rearrangement to a ring-expanded product (Figure 34 andFigure 35).

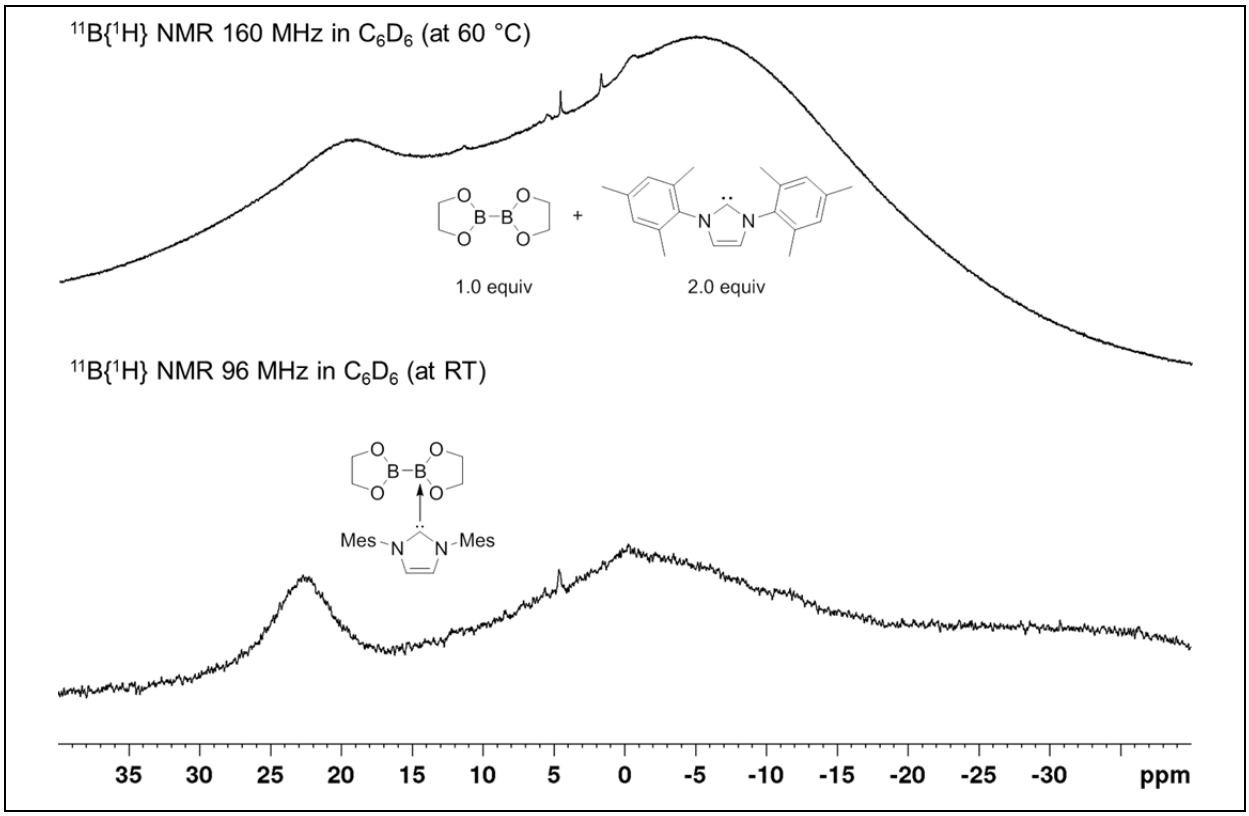

*Figure 34. In situ $^{11}B\{^1H\}$ NMR spectrum of the reaction of B_2eg_2 **110** with 2.0 equivalents Mes_2Im (top) in C_6D_6 (160 MHz, 60 °C).*

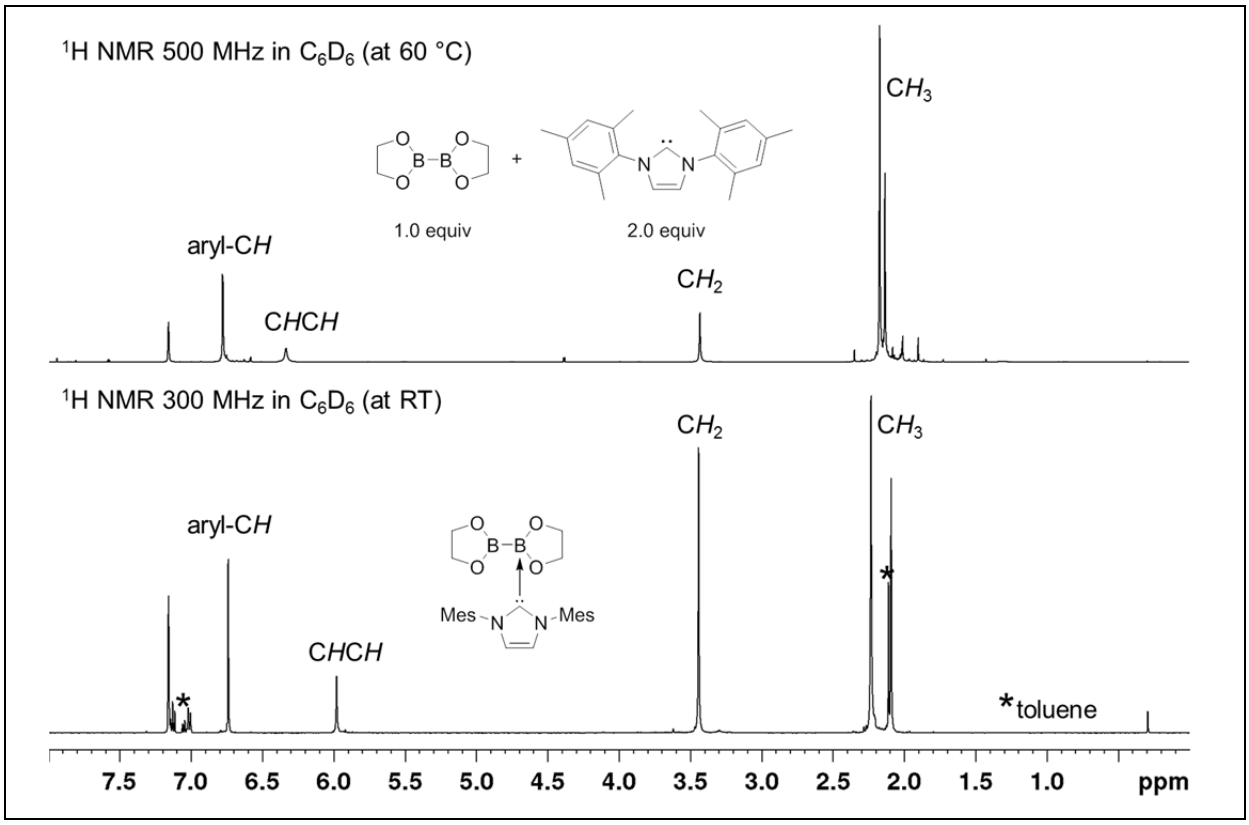

*Figure 35. In situ ^1H NMR spectrum of the reaction of B_2eg_2 **110** with 2.0 equivalents Mes_2Im (top) in C_6D_6 (500 MHz, 60 °C).*

Single-crystal X-ray diffraction studies of compound **118** confirmed the structure of the mono-NHC diboron adduct (Figure 36). The molecular structure of B_2eg_2•Mes_2Im **118** is similar to those known of the diboron adducts B_2pin_2•Cy_2Im, B_2cat_2•Me_2Im^{Me} and B_2cat_2•$Dipp_2SIm$, B_2pin_2•*i*Pr_2Im.[111,147,170] The boron atom B1 is essentially planar, while B2 is tetrahedral. The B–B distance (B1–B2 1.737(7) Å) is slightly longer than that found in B_2eg_2 (B1–B2 1.704(2) Å).[111] The B2–C1 distance (1.680 (2) Å) is similar to that found in B_2pin_2•Cy_2Im (B2–C1 1.673(2) Å),[147] slightly shorter than that in B_2pin_2•*i*Pr_2Im (1.693(3) Å)[111] and slightly longer than that in B_2cat_2•Me_2Im^{Me} (1.647(2) Å)[170] and B_2cat_2•$Dipp_2SIm$ (1.645(2) Å).[111]

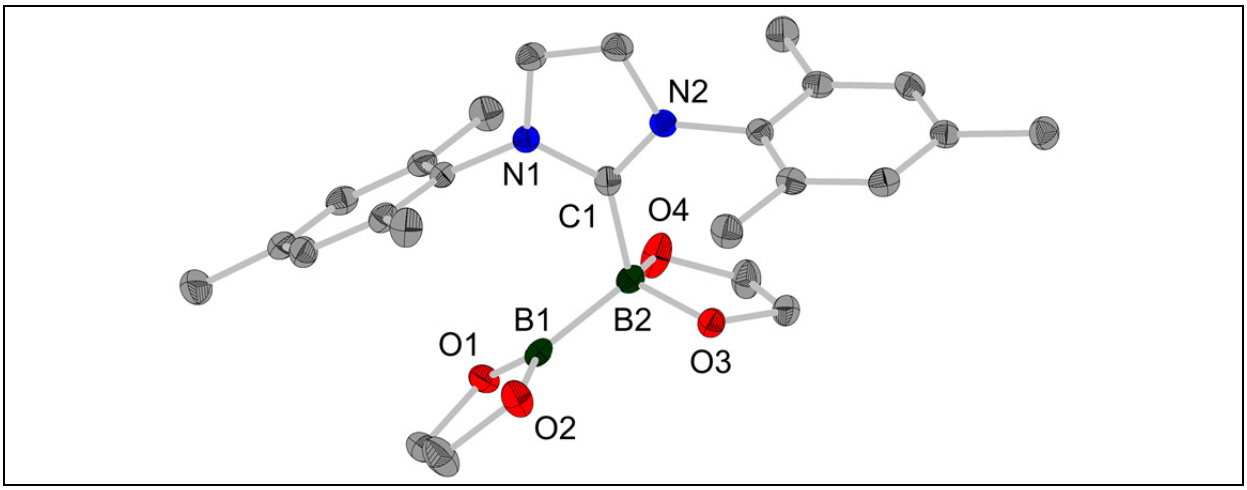

*Figure 36. Molecular structure of B_2eg_2•Mes_2Im **118** with thermal ellipsoids drawn at the 50% probability level; hydrogen atoms are for clarity. Selected bond distances (Å) and angles (°) for **118**: B1–B2 1.737(3), B2–C1 1.680 (2), B1–O1 1.379(2), B1–O2 1.380(2), B2–O3 1.477(2), B1-O4 1.485(2); C1-B2-B1 110.39(12), C1-B2-O3 110.87(12), C1-B2-O4 106.14(12).*

2.2.3.3 Reactions of B_2eg_2 with the NHC *i*Pr_2Im^{Me}

The reaction of B_2eg_2 **110** with the sterically demanding NHC *i*Pr_2Im^{Me} (also sterically demanding in the backbone) was carried out at room temperature and gave the mono-NHC adduct B_2eg_2•*i*Pr_2Im^{Me} **119** as a colorless solid in moderate yield (41%), which was characterized *via* solution NMR (Scheme 51).

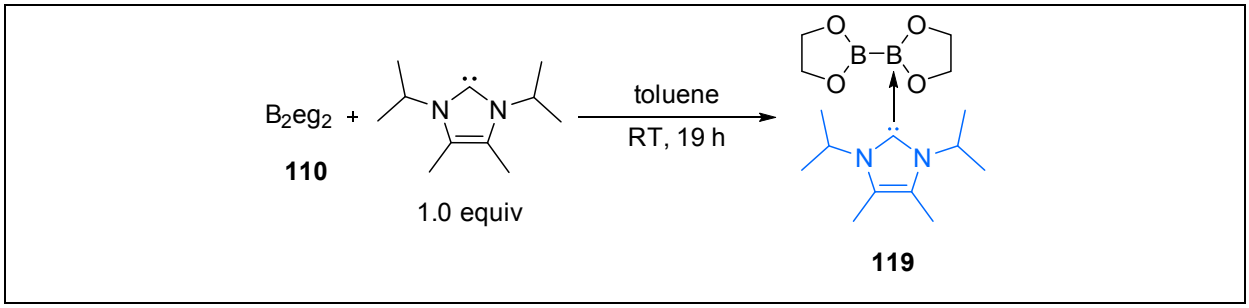

*Scheme 51. Reaction of B_2eg_2 **110** with iPr_2Im^{Me} monitored by in situ NMR spectroscopy.*

In the $^{11}B\{^1H\}$ NMR spectrum, one broad signal at 23.8 ppm and two signals for trace impurities were observed (Figure 37). The sharp peak at 12.2 ppm indicating a sp^3-B atom was identified as the spiro-borate anion $[Beg_2]^-$ (supported by HRMS); the very sharp peak at 5.19 ppm could not be identified. Furthermore, high resolution mass spectrometry provided evidence for the formation of the borenium cation species, $[(iPr_2Im^{Me})Beg]^+$. However, the trace impurities and compound **119** could not be separated.

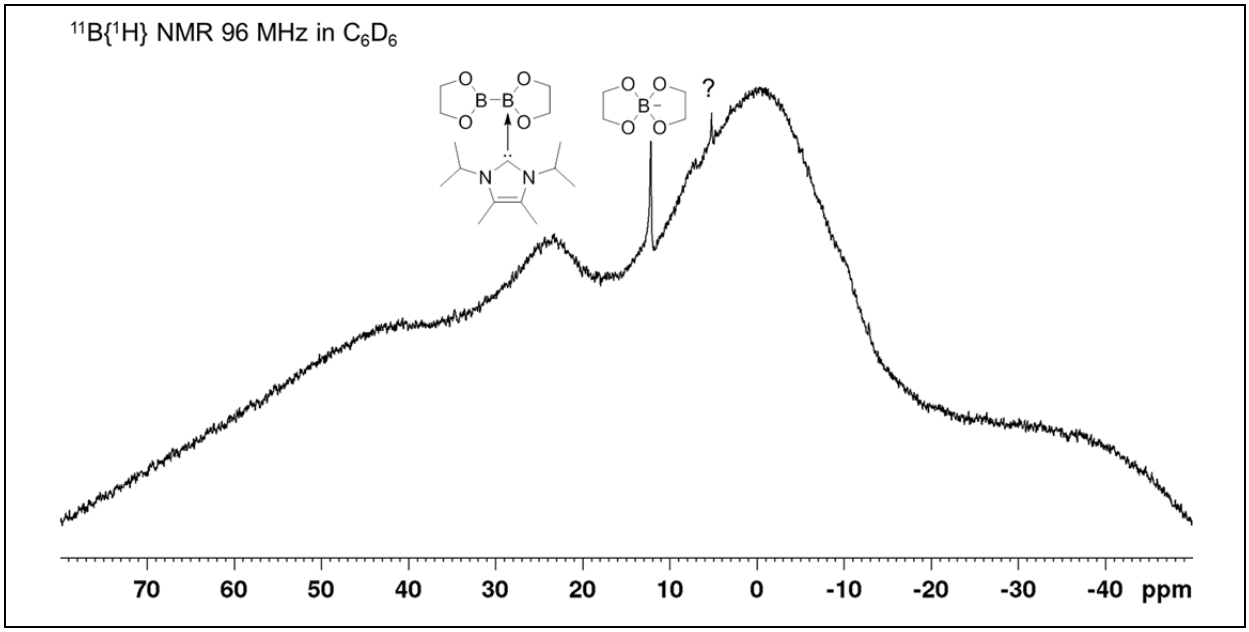

*Figure 37. $^{11}B\{^1H\}$ NMR spectrum of B_2eg_2•iPr_2Im^{Me} **119** in C_6D_6 (96 MHz, 25 °C).*

The $^{11}B\{^1H\}$ NMR signal at 23.7 ppm is quite similar compared to the (dynamic) signal of the mono-NHC adduct B_2eg_2•Mes_2Im **118** (*vide supra*) and can also be explained by a dynamic exchange of the NHC between the two boron atoms of B_2eg_2. This dynamic process might be not as fast as for compound **118**, due to the sterically more demanding NHC iPr_2Im^{Me}. This observation is also reflected in the solution ^1H NMR spectrum, in which the signal at 3.84 ppm for the backbone of the Beg moieties in B_2eg_2 is broadened and about 0.34 ppm down-field shifted compared to the ^1H NMR signal of B_2eg_2. In addition, the resonances for the protons of the NHC isopropyl protons (C*H*CH_3) at 6.39 ppm were broadened and down-field shifted by 2.44 ppm. Both the NHC backbone methyl-protons (CH_3) at 1.60 ppm were up-field shifted by 0.13 ppm, and the *iso*propyl-methyl-protons (CHCH_3) at 1.26 ppm were up-field shifted by 0.24 ppm (Figure 38). Compared to compound **118**, the ^1H NMR signals of mono-NHC adduct B_2eg_2•iPr_2Im^{Me} are significantly shifted. This fact might be evidence for a slower dynamic exchange of the NHC between the two boron atoms of B_2eg_2.

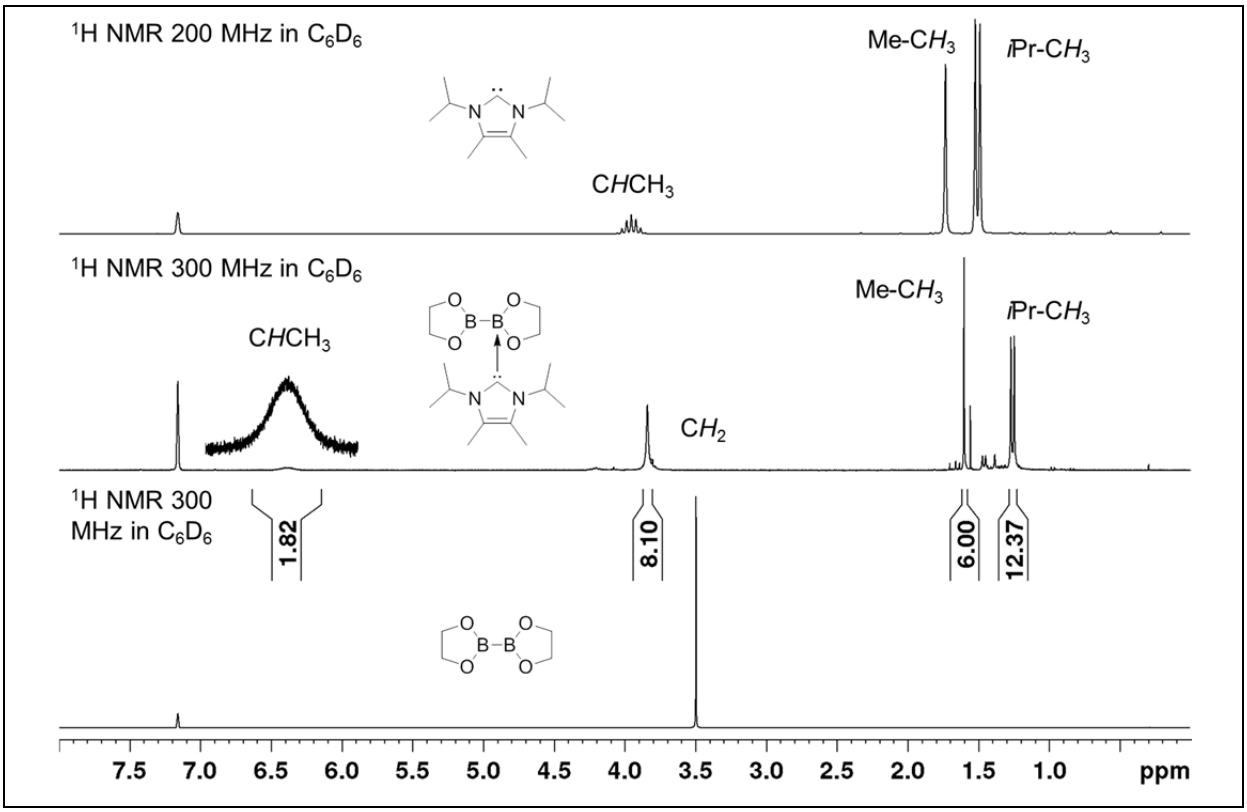

Figure 38. ^1H NMR spectrum of B_2eg_2•iPr_2Im^{Me} ***119*** *in C_6D_6 (300 MHz, 25 °C).*

All attempts to grow crystals suitable for single-crystal X-ray diffraction unfortunately failed. However, an *in situ* NMR experiment with two equivalents of iPr_2Im^{Me} was

carried out, to investigate the observed dynamics (*vide supra*), bis-adduct formation and the possible potential of the NHC for B–B bond activation.

In the *in situ* $^{11}B\{^1H\}$ NMR spectrum at -40 °C, two signals were observed. One peak at 3.79 ppm (sp^3-B atom) and one very broad at ~38.0 ppm (sp^2-B atom) indicate the formation of both the mono- and bis-NHC adduct (Figure 39). Thus, at -40 °C the sp^3-B atom signals for the bis-NHC adduct might overlap with the sp^3-B atom signal of the mono-NHC adduct. However, the ^1H NMR spectrum at -40 °C (Figure 40) showed free carbene as the main component, with additional signals indicating and supporting the formation of both the mono-NHC adduct and the bis-NHC adduct. The ^1H NMR signals marked in blue and red are the corresponding C*H*CH_3/CHC*H*$_3$ protons of the mono- and bis-NHC adducts (assigned *via* $^1H,^1H$ COSY NMR). Compared to the spectrum of the mono-NHC adduct (Figure 38), and taking the temperature gradient into account, the blue marked signals might belong to the mono-NHC adduct and the red marked signals to the bis-NHC adduct, but an accurate assignment was not possible, due to the overlap of the signals and the dynamic exchange between the NHC(s) and B_2eg_2.

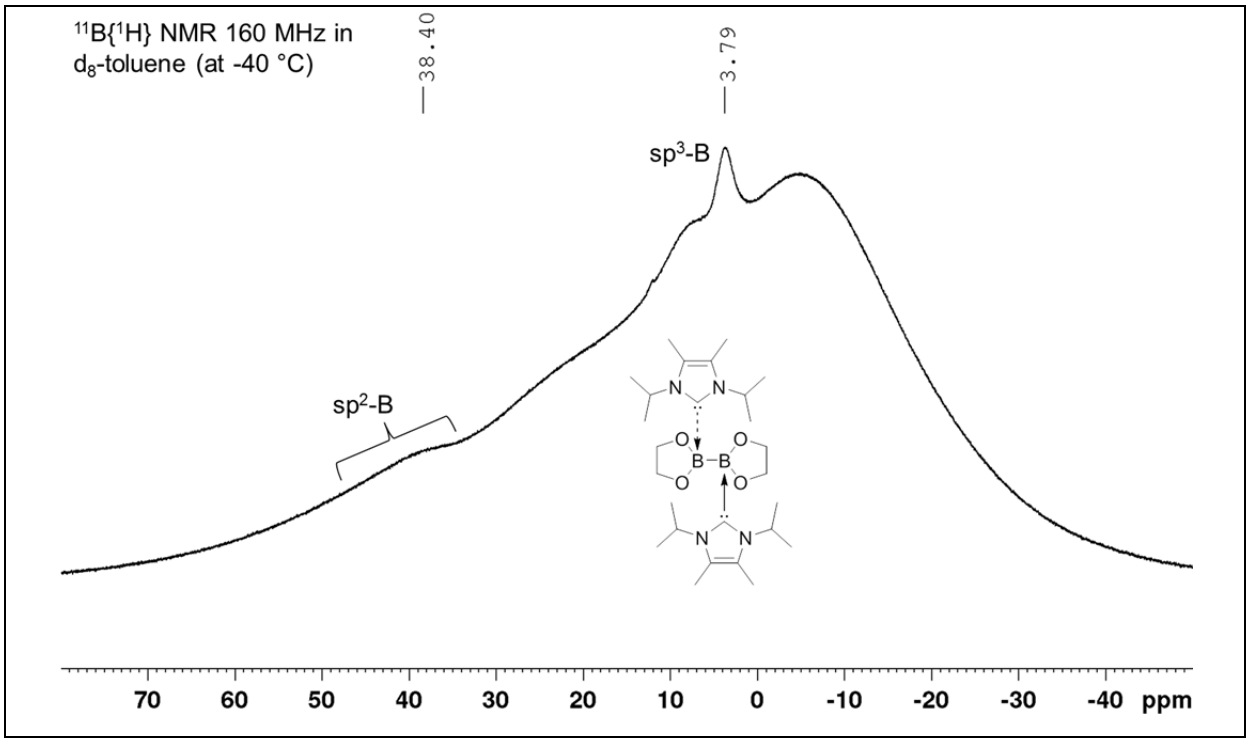

*Figure 39. In situ $^{11}B\{^1H\}$ NMR spectrum of the reaction of B_2eg_2 **110** with two equivalents of iPr_2Im^{Me} in d_8-toluene (160 MHz, -40 °C).*

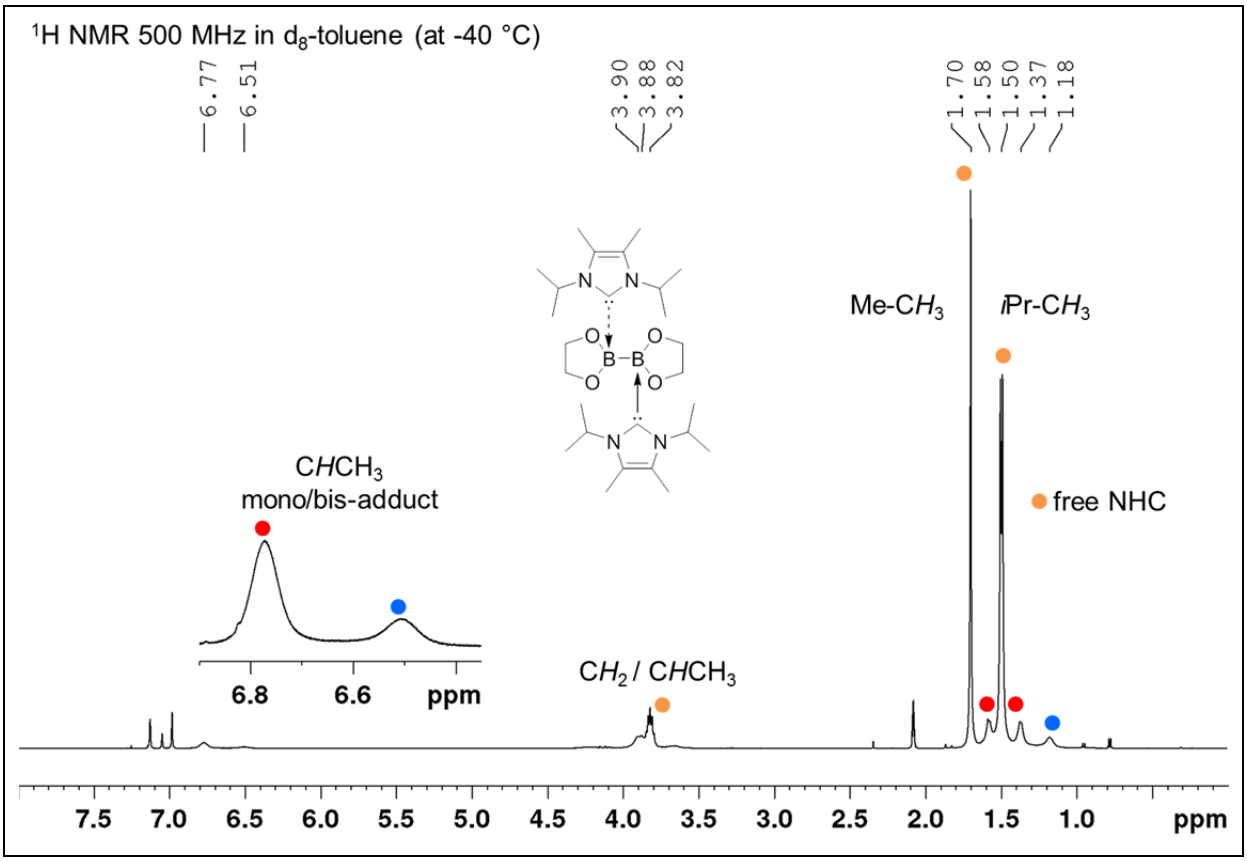

*Figure 40. In situ ^{1}H NMR spectrum of the reaction of B_2eg_2 **110** with two equivalents of iPr_2Im^{Me} in d_8-toluene (500 MHz, -40 °C); signals marked in **blue** and **red** are the corresponding $CHCH_3$ protons of the mono- and bis-NHC adducts (assigned via ^{1}H,^{1}H COSY), but it is not clear which is which.*

In the *in situ* ^{11}B{^{1}H} NMR spectrum at -20 °C, only the mono-NHC adduct formation is clearly observed, and the signal for the sp^3-B atom was assigned at 3.79 ppm and the sp^2-B atom at 37.5 ppm (Figure 41). The corresponding ^{1}H NMR spectrum (Figure 42) shows the NHC *iso*propyl protons (C*H*CH$_3$) at 6.50 and 6.70 ppm (down-field shifted by ~2.70 ppm compared to the free carbene) and a broad signal at 3.85 ppm (down-field shifted by 0.35 ppm) for the backbone of B_2eg_2. Again, the proton signals are overlapping and starting to merge and the increasing dynamics is broadening the resonances. This observation might be explained by the great steric demand of the NHC iPr_2Im^{Me}. Thus, at lower temperatures, the bis-NHC adduct is quite stable, but with increasing temperature, the second NHC is dissociating due to the steric effects which is reflected in the observed dynamic process. This dissociative process in solution was also observed and reported in the literature for the bis-NHC adducts B_2neop_2•$(Me_2Im^{Me})_2$, B_2neop_2•$(iPr_2Im^{Me})_2$ and B_2neop_2•(Me*i*PrIm)$_2$.[183]

However, there is no evidence for a ring-expansion reaction at temperatures of -40 °C to -20 °C.

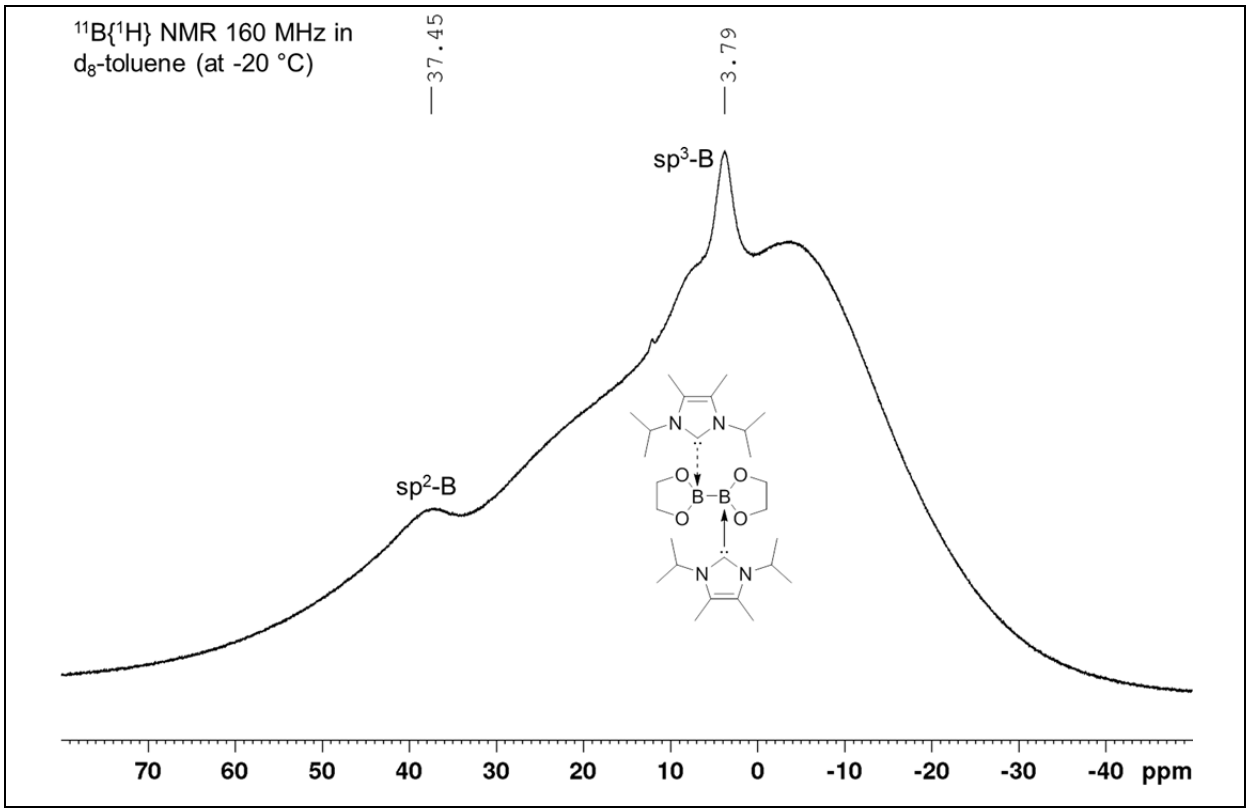

*Figure 41. In situ $^{11}B\{^1H\}$ NMR spectrum of the reaction of B_2eg_2 **110** with two equivalents of iPr_2Im^{Me} in d_8-toluene (160 MHz, -20 °C).*

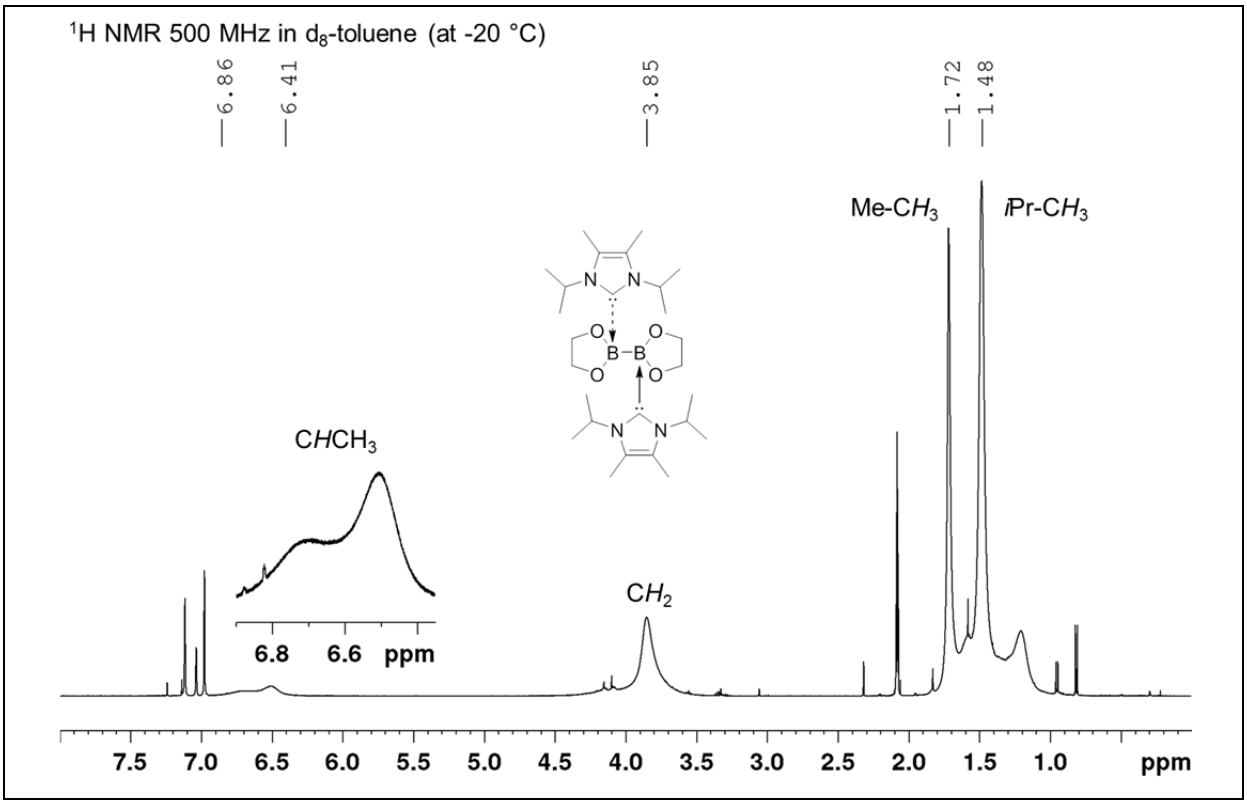

*Figure 42. In situ ^{1}H NMR spectrum of the reaction of B_2eg_2 **110** with two equivalents of iPr_2Im^{Me} in d_8-toluene (500 MHz, -20 °C).*

In the $^{11}B\{^1H\}$ NMR spectrum at 0 °C, the signals for the sp^3-B atoms are slightly down-field shifted (4.50 ppm) and broadened, due to the temperature gradient and the increasing dynamic process (Figure 43). This is also reflected in the ^{1}H NMR spectrum which shows significant broadening of all proton signals (Figure 44). Furthermore, in the $^{11}B\{^1H\}$ NMR spectrum, a peak arose at 12.0 ppm, which was assigned as the spiro-borate anion $[Beg_2]^-$; this observation is consistent with the reaction of B_2eg_2 **110** with one equivalents of the NHC iPr_2Im^{Me} (*vide supra*).

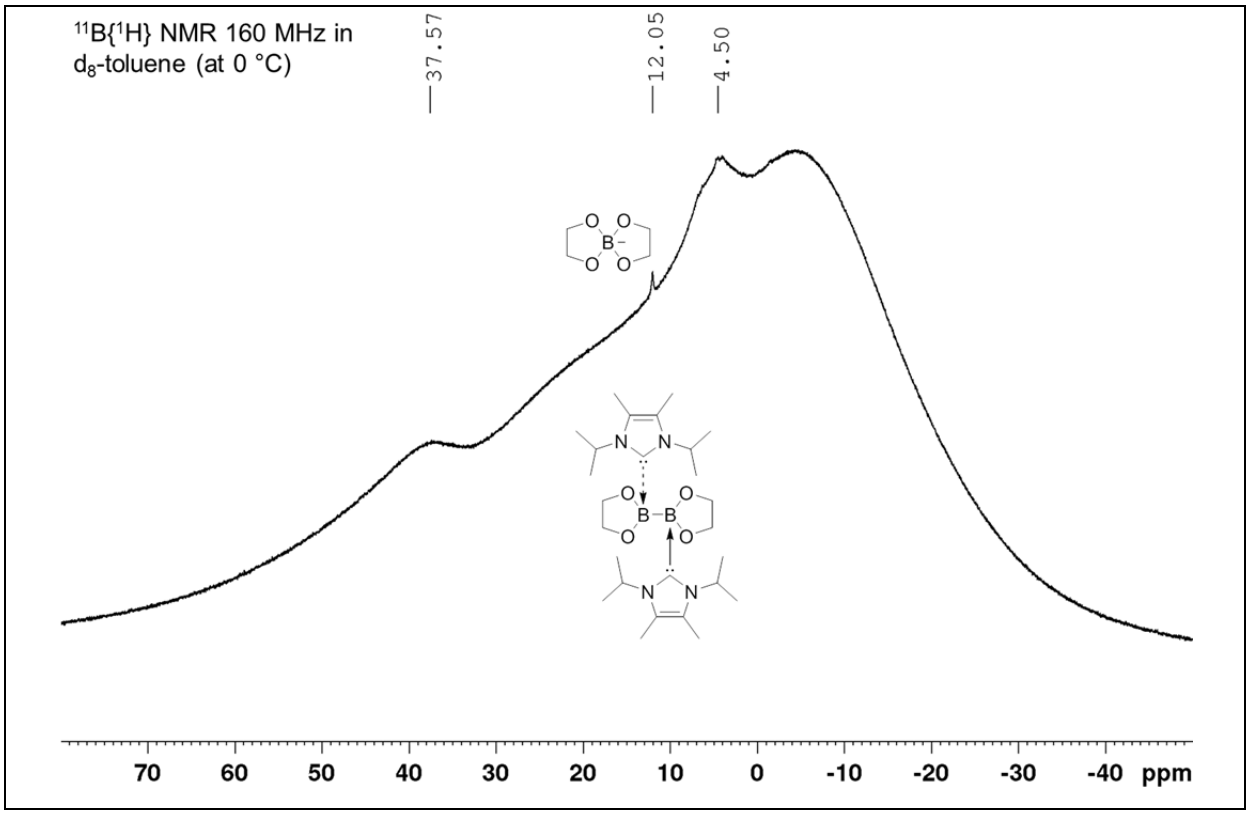

*Figure 43. In situ $^{11}B\{^{1}H\}$ NMR spectrum of the reaction of B_2eg_2 **110** with two equivalents of iPr_2Im^{Me} in d_8-toluene (160 MHz, 0 °C).*

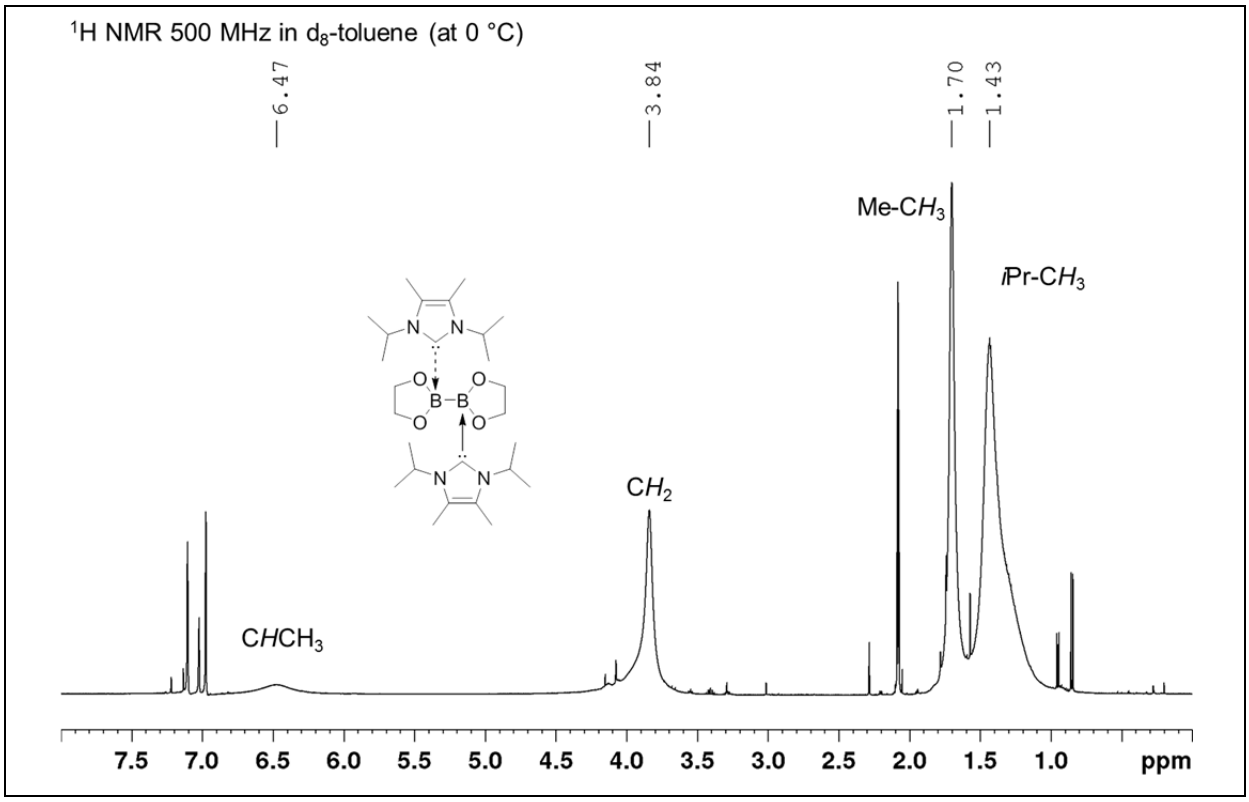

*Figure 44. In situ ^{1}H NMR spectrum of the reaction of B_2eg_2 **110** with two equivalents of iPr_2Im^{Me} in d_8-toluene (500 MHz, 0 °C).*

The $^{11}B\{^1H\}$ NMR spectrum at 10 °C shows that the system is near the coalescence temperature (Figure 45).

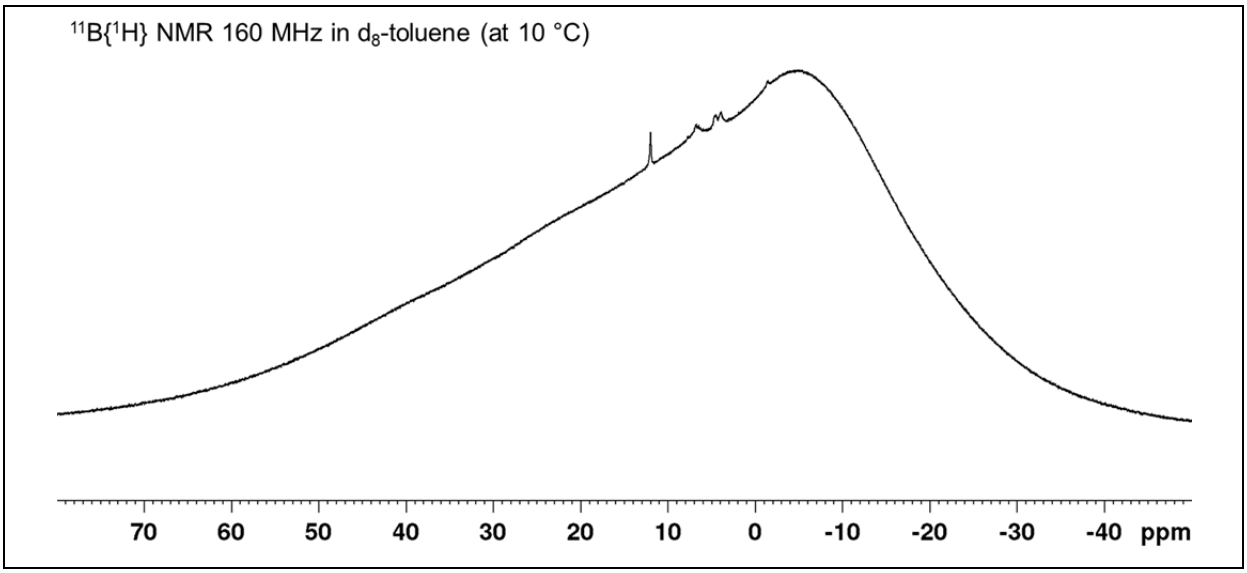

*Figure 45. In situ $^{11}B\{^1H\}$ NMR spectrum of the reaction of B_2eg_2 **110** with two equivalents of iPr_2Im^{Me} in d_8-toluene (160 MHz, 10 °C).*

At room temperature, the $^{11}B\{^1H\}$ NMR spectrum shows a broad signal at 20.2 ppm and new signals which could not be assigned are arising at ~6.00 ppm (Figure 46). The ^1H NMR spectrum also reflects the dynamics (Figure 47). The C*H*CH_3 proton signals are very broad (~5.60 – 6.90 ppm) and are barely visible above the noise of the baseline. While the signals for all methyl protons are broadening and tailing, the signal for the ethylene glycol backbone remains quite sharp and shifted down-field by 0.33 ppm compared to these of free B_2eg_2.

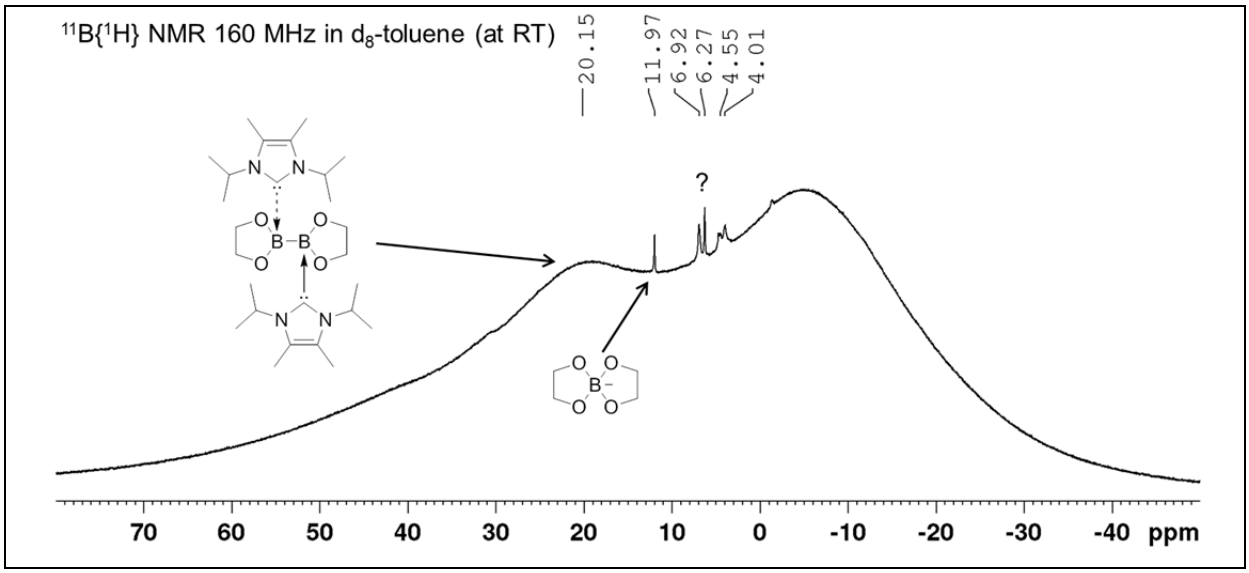

*Figure 46. In situ $^{11}B\{^1H\}$ NMR spectrum of the reaction of B_2eg_2 **110** with two equivalents of iPr_2Im^{Me} in d_8-toluene (160 MHz, 25 °C).*

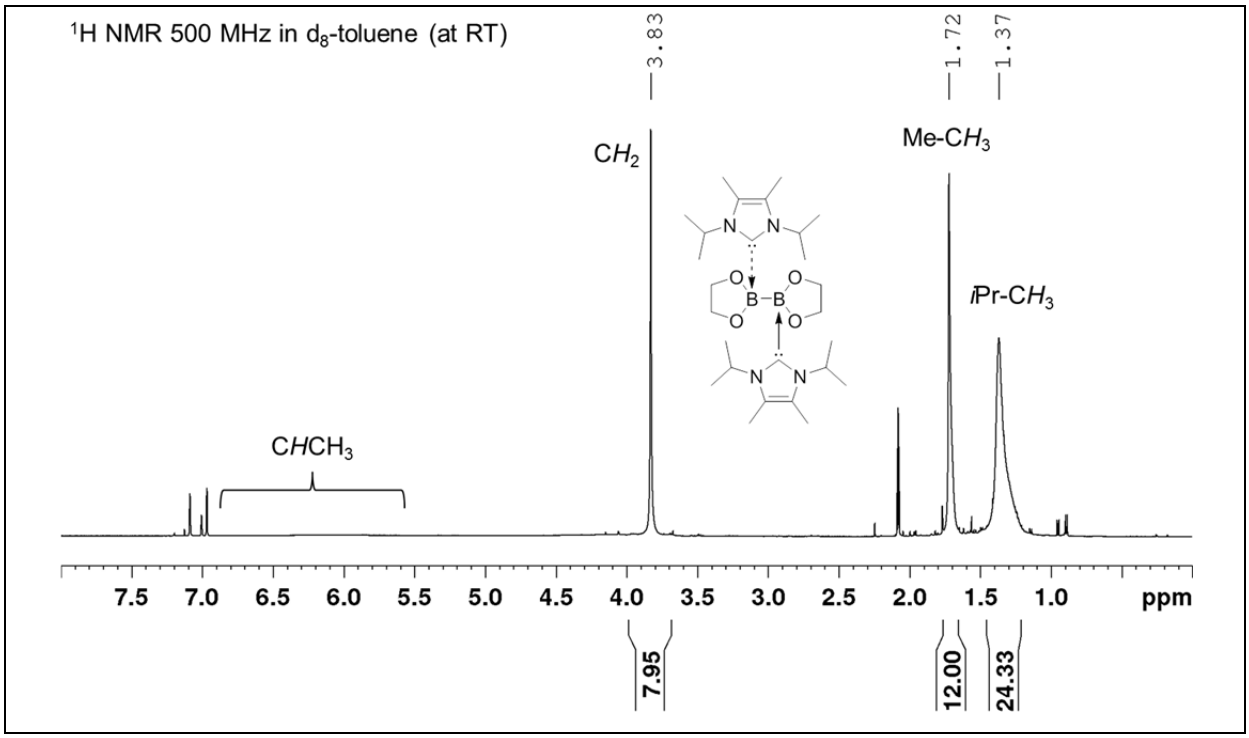

*Figure 47. In situ ^1H NMR spectrum of the reaction of B_2eg_2 **110** with two equivalents of iPr_2Im^{Me} in d_8-toluene (500 MHz, 25 °C).*

A separate NMR experiment at room temperature showed that the bis-NHC adduct is not stable. Both the $^{11}B\{^1H\}$ NMR and ^1H NMR spectra provided evidence for the formation of different compounds, which could not be identified or isolated, respectively (Figure 48 and Figure 49).

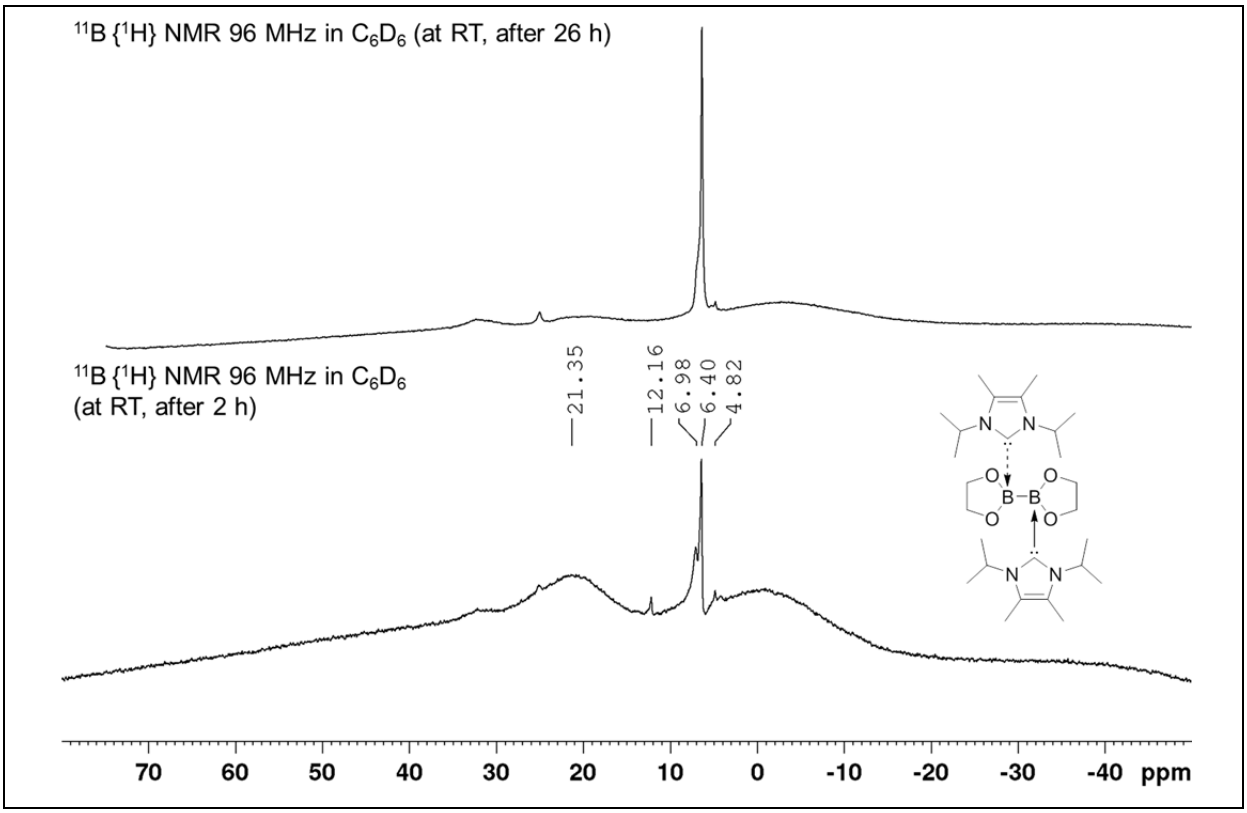

*Figure 48. In situ $^{11}B\{^{1}H\}$ NMR spectrum of the reaction of B_2eg_2 **110** with two equivalents of iPr_2Im^{Me} in C_6D_6 (96 MHz, 25 °C) after 2 h and 26 h.*

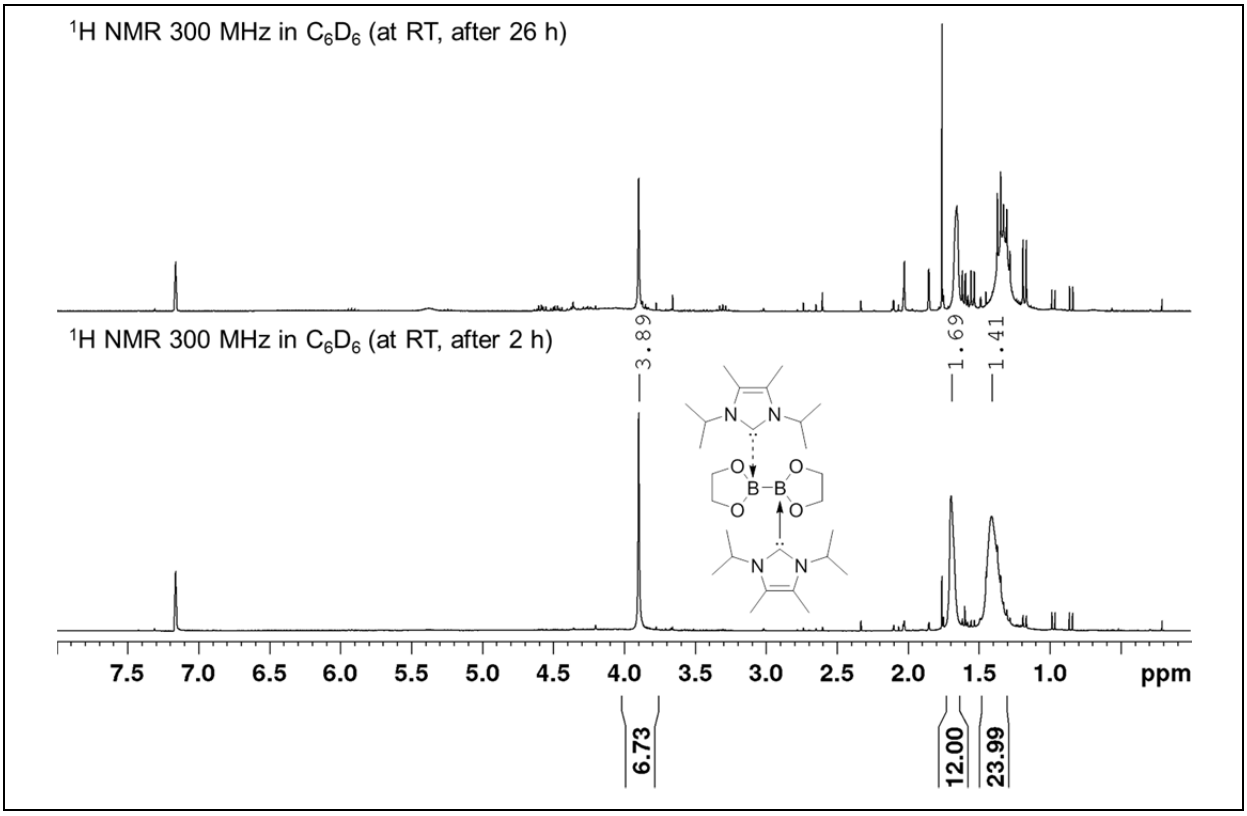

*Figure 49. In situ ^{1}H NMR spectrum of the reaction of B_2eg_2 **110** with two equivalents of iPr_2Im^{Me} in C_6D_6 (300 MHz, 25 °C) after 2 h and 26 h.*

2.2.3.4 Reaction of B_2eg_2 with the NHC *i*Pr_2Im

The reaction of B_2eg_2 **110** with the NHC *i*Pr_2Im in the stoichiometry 1:2 at room temperature resulted in an orange-colored solution. The *in situ* $^{11}B\{^1H\}$ and ^1H NMR spectra did not show the peak pattern expected either for an adduct or a ring-expanded product. However, low temperature *in situ* NMR experiments (-40 °C) provided evidence for the formation of a ring-expanded product and its decomposition above a temperature of -10 °C. As a result, the stoichiometric reaction was repeated at a lower temperature (-30 °C), and the compound RER-B_2eg_2•(*i*Pr_2Im)$_2$ **120** was isolated in good yield (62%) by crystallization at this temperature (Scheme 52).

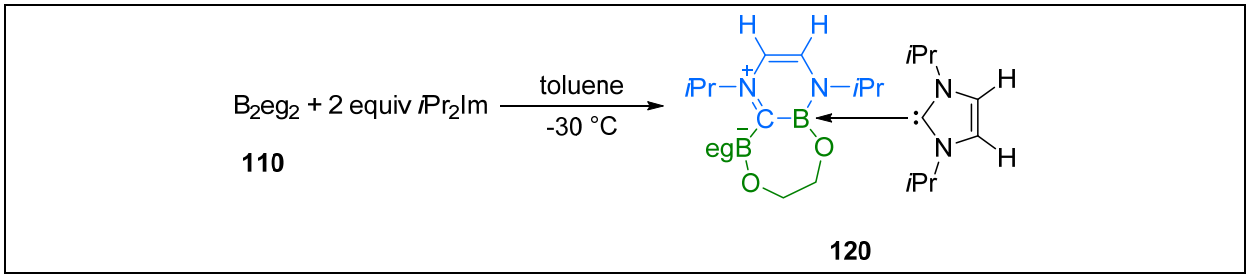

*Scheme 52. Synthesis of the ring-expanded product RER-B_2eg_2•(*i*Pr_2Im)$_2$ **120**.*

Re-dissolving isolated compound **120** at room temperature showed decomposition as well; therefore, RER-B_2eg_2•(*i*Pr_2Im)$_2$ **120** was stored at -30 °C. The molecular structure of **120** was confirmed by single-crystal X-ray diffraction (Figure 52) and full characterization was completed *via* NMR spectroscopy, high resolution mass spectrometry and elemental analysis. The solid-state ^{11}B RSHE/MAS NMR spectrum (Figure 50) revealed two signals for the sp^3-B atoms with isotropic shifts of 7.00 ppm and -1.10 ppm, which matched the signals ^{11}B NMR spectrum in solution (Figure 51; for more detailed spectra, see appendix A4)

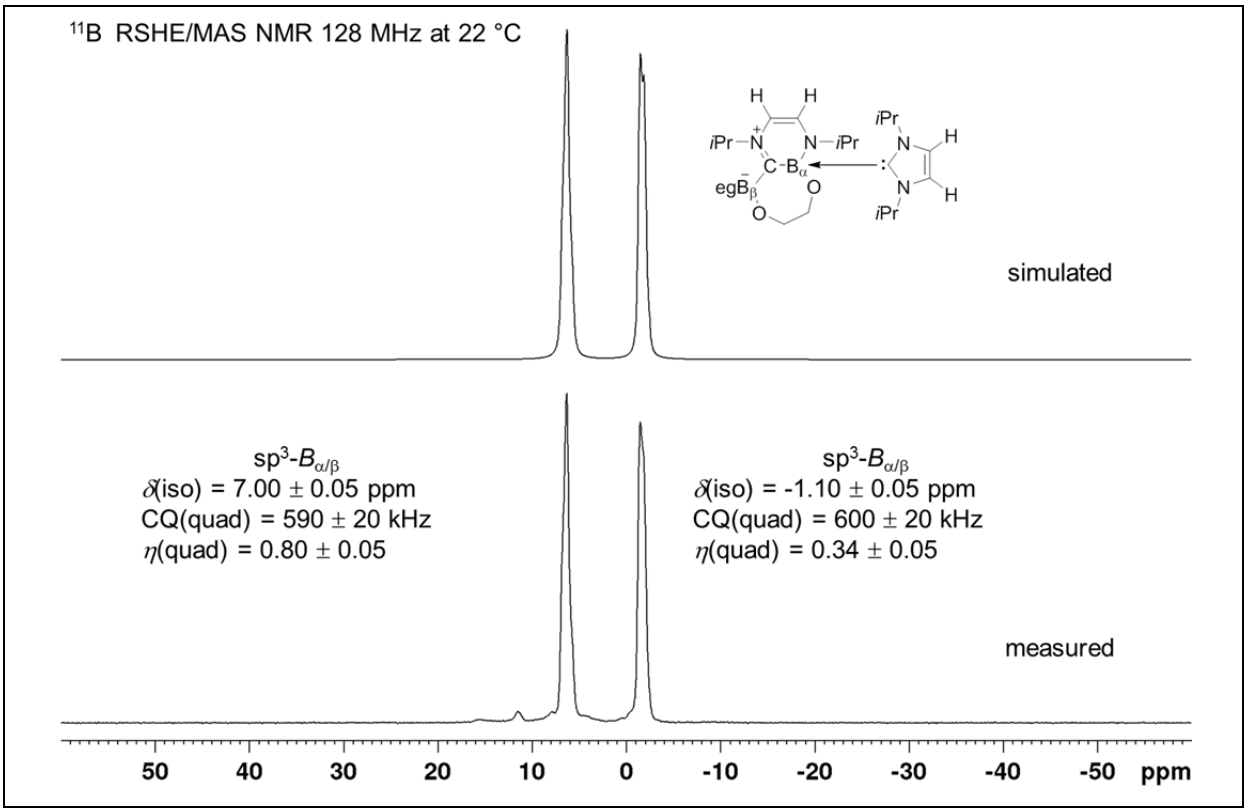

*Figure 50. ^{11}B RSHE/MAS NMR spectrum of RER-B$_2$eg$_2$•(iPr$_2$Im)$_2$ **120** (128 MHz, 22 °C, ν rot = 15000 Hz).*

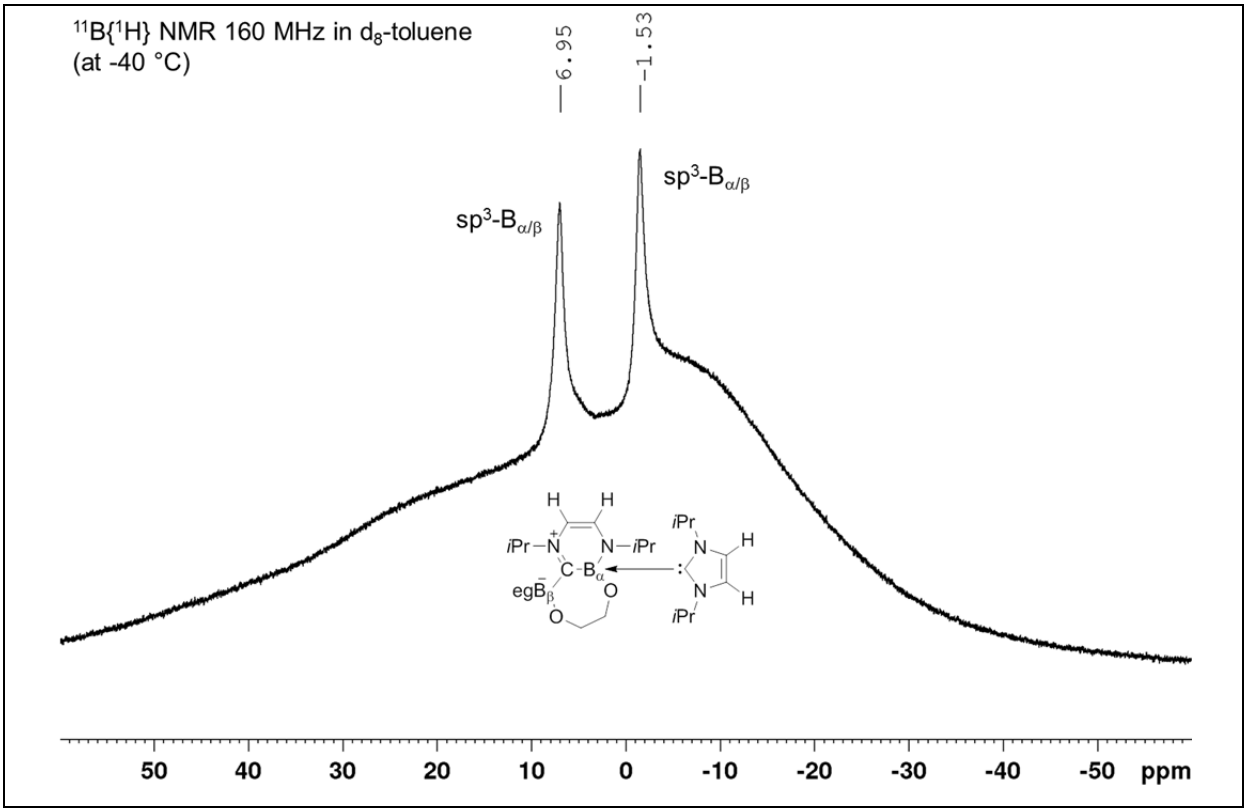

*Figure 51. ^{11}B{^{1}H} NMR spectrum of RER-B$_2$eg$_2$•(iPr$_2$Im)$_2$ **120** in d$_8$-toluene (160 MHz, -40 °C).*

The structure of **120** is similar to that observed for the ring-expansion reaction of B_2neop_2 with nPr$_2$Im (RER-B_2neop_2•(nPr$_2$Im)$_2$).[170] One boron atom inserts into the C-N bond of the NHC and the second boron atom remains bonded to the former carbene-carbon atom; however, the eg-moiety of the *endo*-cyclic boron atom opens and binds to the *exo*-cyclic boron atom. As a result, the second NHC binds to the *endo*-cyclic boron atom.[170]

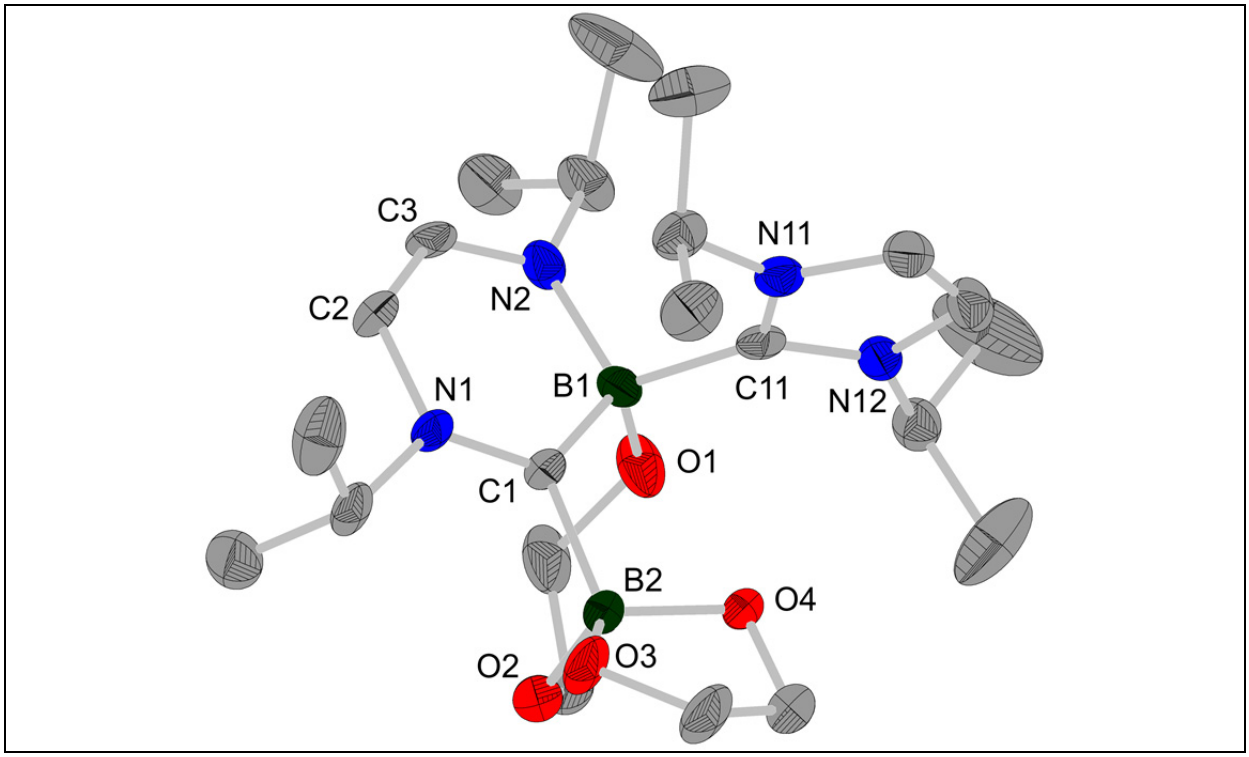

*Figure 52. Molecular structure of the major product RER-B_2eg_2•(iPr_2Im)$_2$ **120** with thermal ellipsoids drawn at the 50% probability level; hydrogen atoms are omitted for clarity. Selected bond distances (Å) and angles (°) for **120**: B1–C1 1.625(5), C1–N1 1.319(4), N1–C2 1.409(4), C2–C3 1.350(4), C3–N2 1.335(4), N2–B1 1.535(4), C1–B2 1.636(5), B1–O1 1.456(4), B2–O2 1.468(5), B2–O3 1.483(5), B2–O4 1.470(5), B1–C11 1.648(4); C1-B1-N2 110.5(3), B1-N2-C3 121.1(3), N2-C3-C2 124.6(3), C3-C2-N1 120.9(3), C2-N1-C1 122.8(3), N1-C1-B1 119.8(3), B1-C1-B2 115.6(3).*

An isomer of compound **120** was detected by single-crystal picking, which was identified as the minor species **120'** (Figure 53). Compound **120'** has a structure which is similar to that of the ring-expanded product from the reaction of B_2cat_2 with nPr$_2$Im, namely RER-B_2cat_2•(nPr$_2$Im)$_2$.[170] Presumably, **120'** is a precursor to **120**.

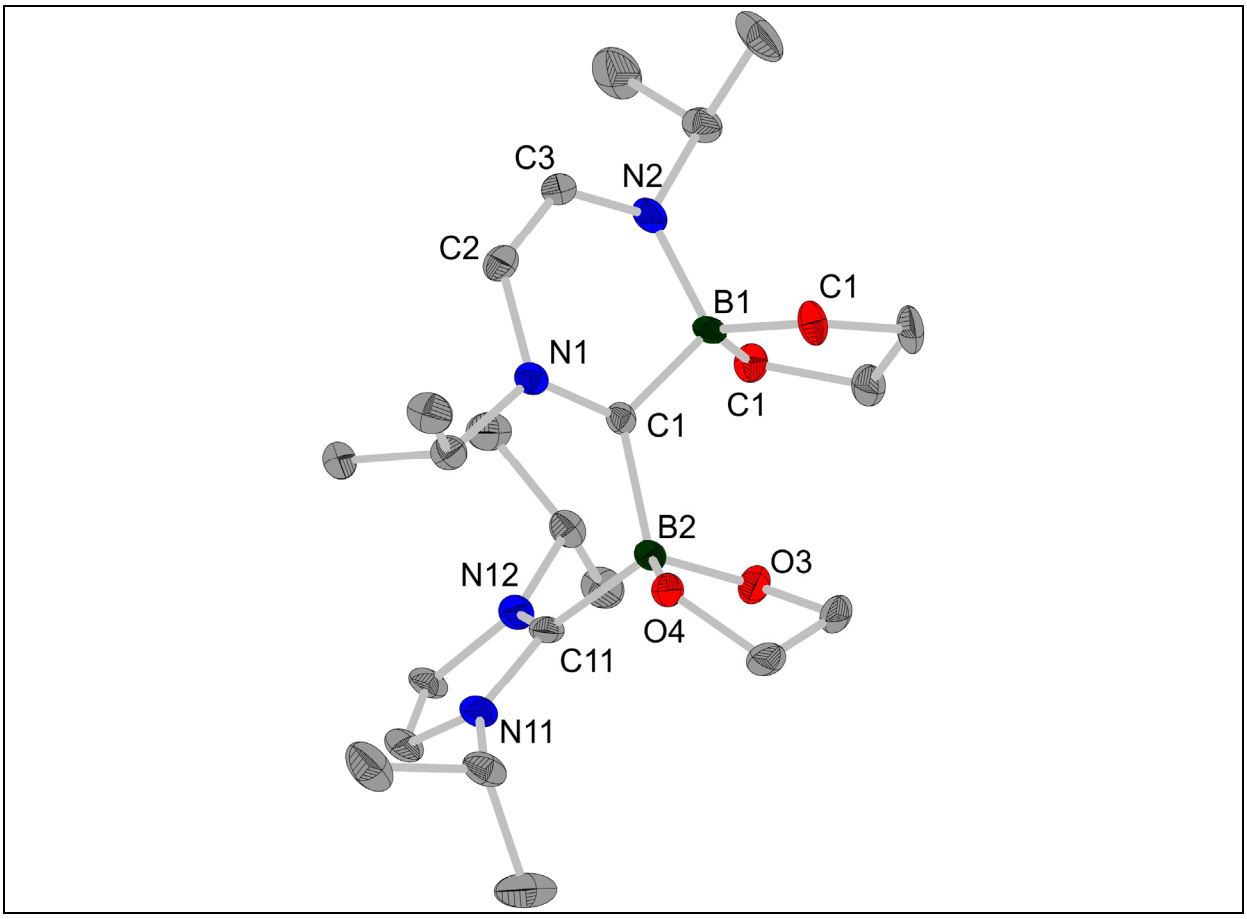

Figure 53. Molecular structure of the minor product RER-B_2eg_2•$(iPr_2Im)_2$ ***120'*** *with thermal ellipsoids drawn at the 50% probability level; hydrogen atoms are omitted for clarity. Compound* ***120'*** *crystallises with two molecules in the asymmetric unit. Selected bond distances (Å) and angles (°) for* ***120'^{a}****: $B1^a$–$C1^a$ 1.648(4), $C1^a$–$N1^a$ 1.321(3), $N1^a$–$C2^a$ 1.405(2), $C2^a$–$C3^a$ 1.344(4), $C3^a$–$N2^a$ 1.342(4), $N2^a$–$B1^a$ 1.543(3), $C1^a$–$B2^a$ 1.652(3), $B1^a$–$O1^a$ 1.472(3), $B1^a$–$O2^a$ 1.479(2), $B2^a$–$O3^a$ 1.465(3), $B2^a$–$O4^a$ 1.474(3), $B1^a$–$C11^a$ 1.680(3); $C1^a$-$B1^a$-$N2^a$ 108.7(2), $B1^a$-$N2^a$-$C3^a$ 121.33(17), $N2^a$-$C3^a$-$C2^a$ 123.6(2), $C3^a$-$C2^a$-$N1^a$ 121.30(18), $C2^a$-$N1^a$-$C1^a$ 123.43(17), $N1^a$-$C1^a$-$B1^a$ 118.79(18), $B1^a$-$C1^a$-$B2^a$ 120.59(16). Selected bond distances (Å) and angles (°) for* ***120'^{b}****: $B1^b$–$C1^b$ 1.653(4), $C1^b$–$N1^b$ 1.319(3), $N1^b$–$C2^b$ 1.408(2), $C2^b$–$C3^b$ 1.348(4), $C3^b$–$N2^b$ 1.338(4), $N2^b$–$B1^b$ 1.548(3), $C1^b$–$B2^b$ 1.654(3), $B1^b$–$O1^b$ 1.491(3), $B1^b$–$O2^b$ 1.478(3), $B2^b$–$O3^b$ 1.459(4), $B2^b$–$O4^b$ 1.488(3), $B1^b$–$C11^b$ 1.682(3); $C1^b$-$B1^b$-$N2^b$ 108.28(17), $B1^b$-$N2^b$-$C3^b$ 121.22(17), $N2^b$-$C3^b$-$C2^b$ 124.5(2), $C3^b$-$C2^b$-$N1^b$ 120.57(19), $C2^b$-$N1^b$-$C1^b$ 123.46(17), $N1^b$-$C1^b$-$B1^b$ 119.35(19), $B1^b$-$C1^b$-$B2^b$ 120.72(17).*

All attempts to isolate adducts or ring-expansion products of the reaction of B_2eg_2 **110** with the congener NHC nPr$_2$Im unfortunately failed.

2.2.3.5 Reactions of B_2eg_2 with the NHCs Me_2Im^{Me}

Reacting B_2eg_2 **110** with Me_2Im^{Me} also resulted in a ring-expanded product (Scheme 53).

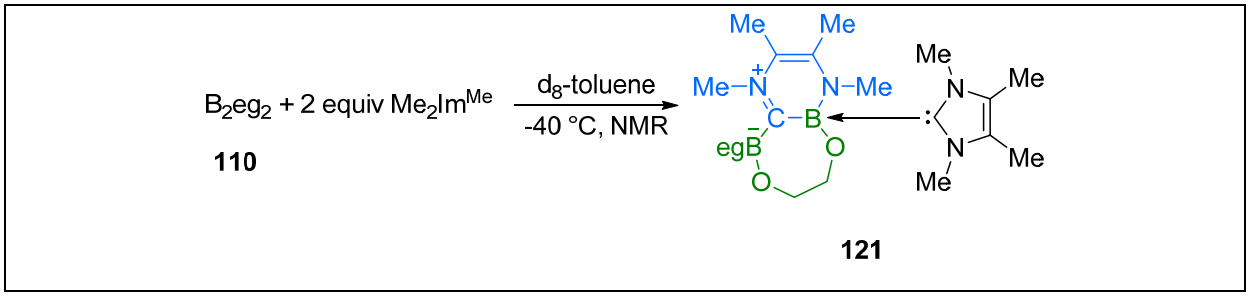

*Scheme 53. Synthesis of the ring-expanded product RER-B_2eg_2•$(Me_2Im^{Me})_2$ **121** monitored by in situ NMR spectroscopy.*

However, due to the high reactivity of the small NHC and the Lewis-acidity of B_2eg_2, RER-B_2eg_2•$(Me_2Im^{Me})_2$ **121** could not be isolated, so the reaction was monitored by low temperature *in situ* NMR spectroscopy (-40 °C). A $^{11}B\{^1H\}$ signal at 4.12 ppm showed the formation of the bis-NHC adduct. After warming the sample to room temperature for one minute, further $^{11}B\{^1H\}$ NMR signals arising at 6.19 ppm and -0.89 ppm were observed (Figure 54), which are quite similar to those of **120** indicating the formation of the ring-expanded product **121**. The ^1H NMR spectrum also provides evidence for the RER occurring (Figure 55). Interestingly, similar spectra were obtained for the reaction of B_2eg_2 **110** with one equivalent of the NHC Me_2Im^{Me}.

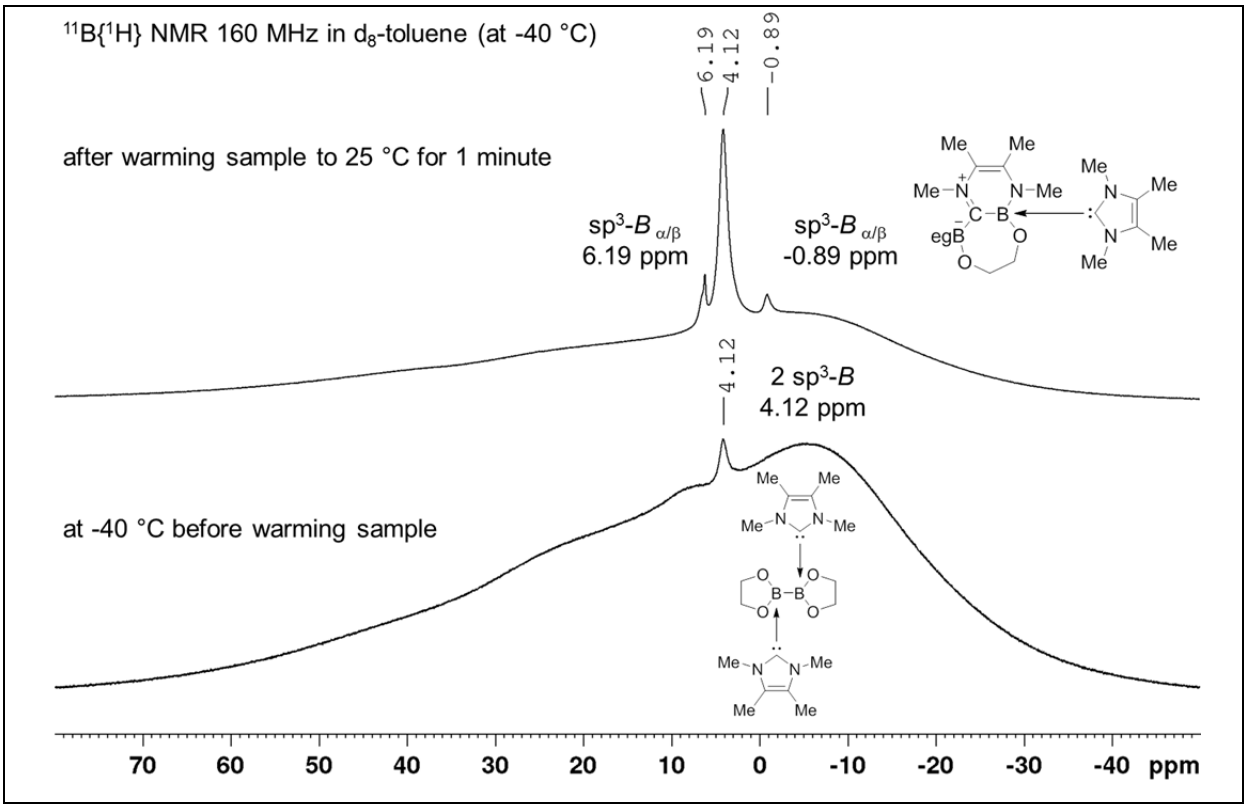

Figure 54. $^{11}B\{^1H\}$ *NMR spectrum of RER-B₂eg₂•(Me₂Im^Me)₂* ***121*** *in d₈-toluene (160 MHz, -40 °C).*

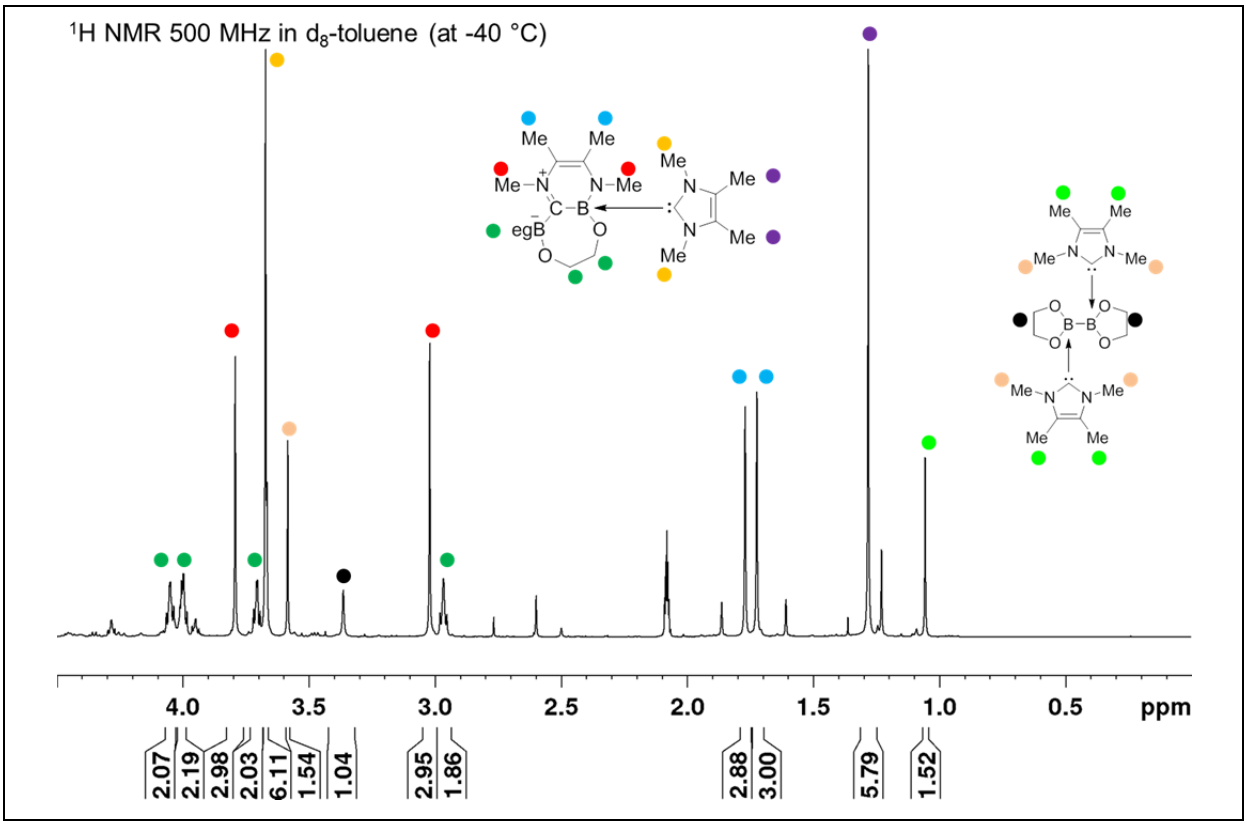

Figure 55. ^1H *NMR spectrum of RER-B₂eg₂•(Me₂Im^Me)₂* ***121*** *in d₈-toluene (160 MHz, -40 °C).*

2.2.4 Decomposition of the ring-expanded-products

The reactions of two equivalents of the NHCs iPr_2Im^{Me}, nPr_2Im, iPr_2Im or Me_2Im^{Me}, respectively, with B_2eg_2 **110** (Scheme 54) resulted in decomposition at room temperature and a similar pattern in the $^{11}B\{^1H\}$ NMR spectra was observed (Figure 56).

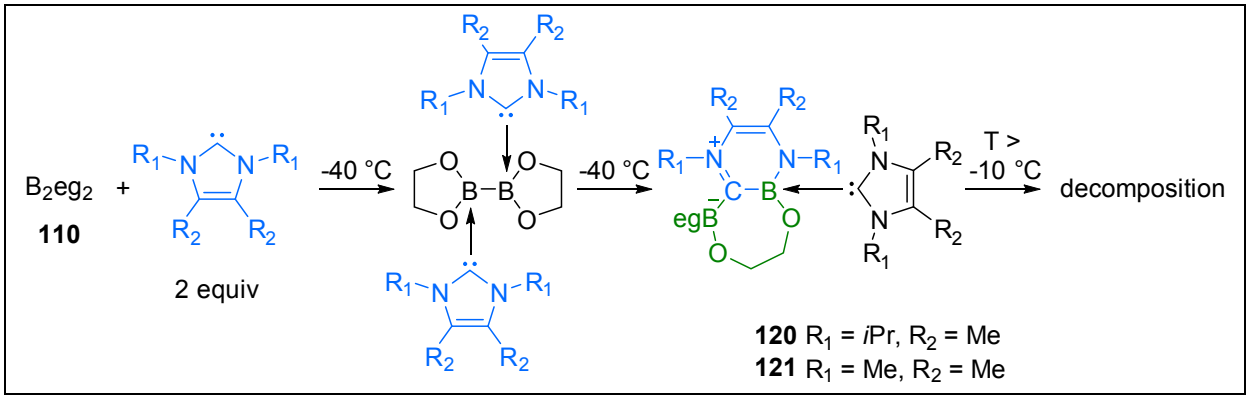

*Scheme 54. Reaction of B_2eg_2 **110** with two equivalents of NHC.*

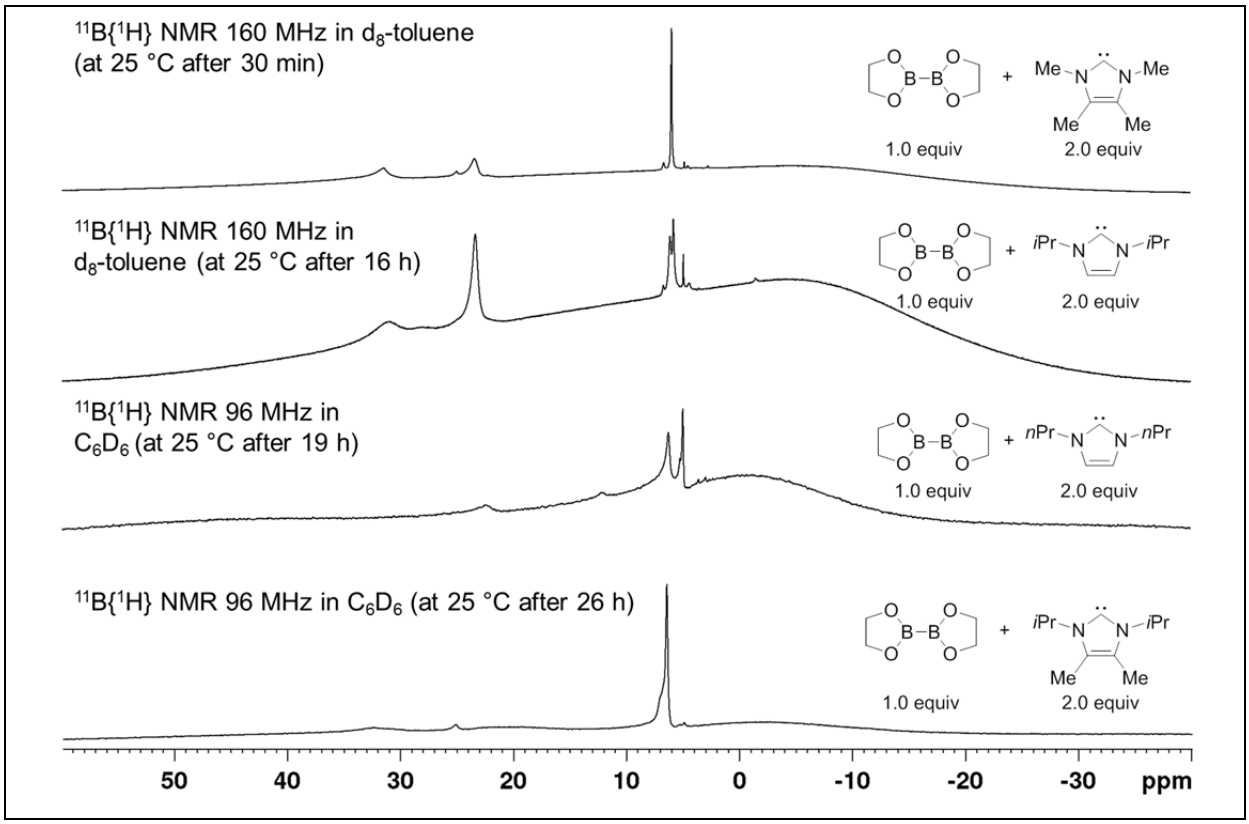

*Figure 56. $^{11}B\{^1H\}$ NMR spectra of the reaction of B_2eg_2 **110** with two equivalents of various NHCs and the resulting decomposition at RT (160 MHz, 96 MHz, 25 °C).*

2.2.4.1 The bis-NHC adduct B_2eg_3•(*i*Pr_2Im)$_2$

Although we tried to characterize as many of these decomposition products as possible, we could not identify or isolate all of them. As described for the reaction of NHC *i*Pr_2Im and B_2cat_2,[111] scrambling of the diboron substituent was expected here. In fact, the bis-NHC adduct B_2eg_3•(*i*Pr_2Im)$_2$ **122** could be isolated from the reaction of B_2eg_2 **110** with two equivalents of the NHC *i*Pr_2Im by single-crystal picking, and its structure was confirmed by single-crystal X-ray diffraction (Figure 57).

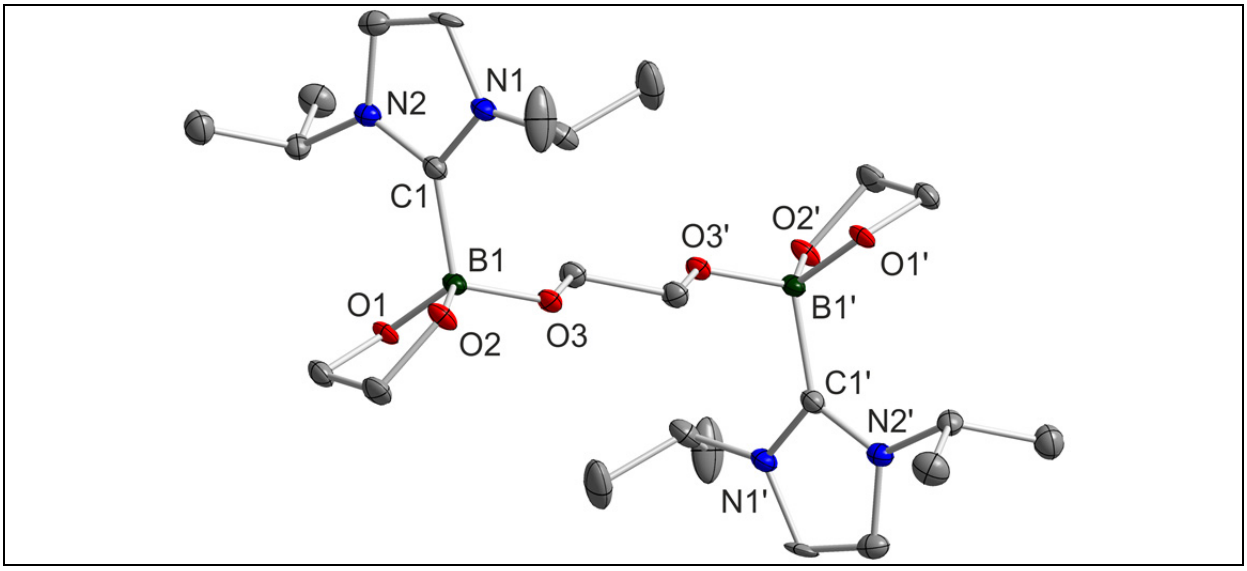

*Figure 57. Molecular structure of B_2eg_3•(*i*Pr_2Im)$_2$ **122** with thermal ellipsoids drawn at the 50% probability level; hydrogen atoms are omitted for clarity. Compound **122** crystallizes with two half molecules in the asymmetric unit, with each full molecule lying on an inversion centre. Selected bond distances (Å) and angles (°) for **122**: C1–B1 1.684(6), B1–O1 1.463(4), B1–O2 1.461(5), B1–O3 1.457(5); C1-B1-O1 112.3(3), C1-B1-O2 105.9(3), C1-B1-O3 108.5(3).*

2.2.4.2 Reactions of B_2eg_3 with the NHCs *i*Pr_2Im and Me_2Im^{Me}

To establish further the nature of the bis-NHC adduct B_2eg_3•(*i*Pr_2Im)$_2$ **122** and to characterize this compound, tris(ethylene glycolato)diboron (B_2eg_3) was reacted with the NHC *i*Pr_2Im at room temperature and with the NHC Me_2Im^{Me} at 65 °C (Scheme 55). The colorless solids were collected by filtration of the resulting suspensions and were assumed to be the corresponding bis-NHC adducts of **111**.

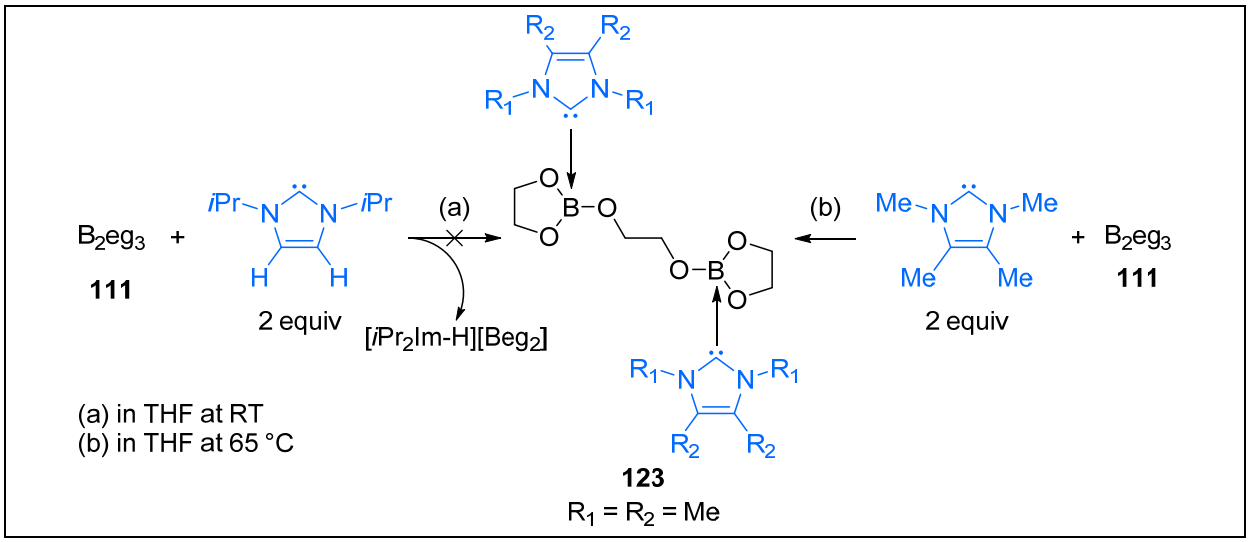

*Scheme 55. Reaction of B_2eg_3 **111** with Me_2Im^{Me} or iPr_2Im.*

Due to its very poor solubility in almost all suitable solvents such as C_6D_6 and d_8-toluene, solid-state NMR spectra of the isolated solids were recorded, but the formation of the bis-NHC adduct B_2eg_3•(iPr$_2$Im)$_2$ **122** was not observed. Instead, the ^{11}B RSHE/MAS NMR spectrum of the product from the reaction of compound **111** with iPr$_2$Im (Figure 58) reveals two signals, one peak (MAS second-order quadrupole powder pattern) for unreacted B_2eg_3 (δ_{iso} = 18.9 ppm) and a second, sharp peak with an isotropic shift of 11.3 ppm, indicating an sp^3-B atom, which was identified as the spiro-borate anion $[Beg_2]^-$. The ^{13}C CP/MAS and ^{15}N CP/MAS NMR spectra (Figure 59 and Figure 60) also showed no evidence for adduct formation, whereas signals for the protonated NHC $[i\text{Pr}_2\text{Im-H}]^+$ were observed and high resolution mass spectrometry confirmed these observations. Moreover, the HRMS showed evidence for the formation of a boronium cation species, $[(i\text{Pr}_2\text{Im})_2\text{Beg}]^+$ and a borenium cation species, $[(i\text{Pr}_2\text{Im})\text{Beg}]^+$ (for HRMS spectra, see appendix B1)

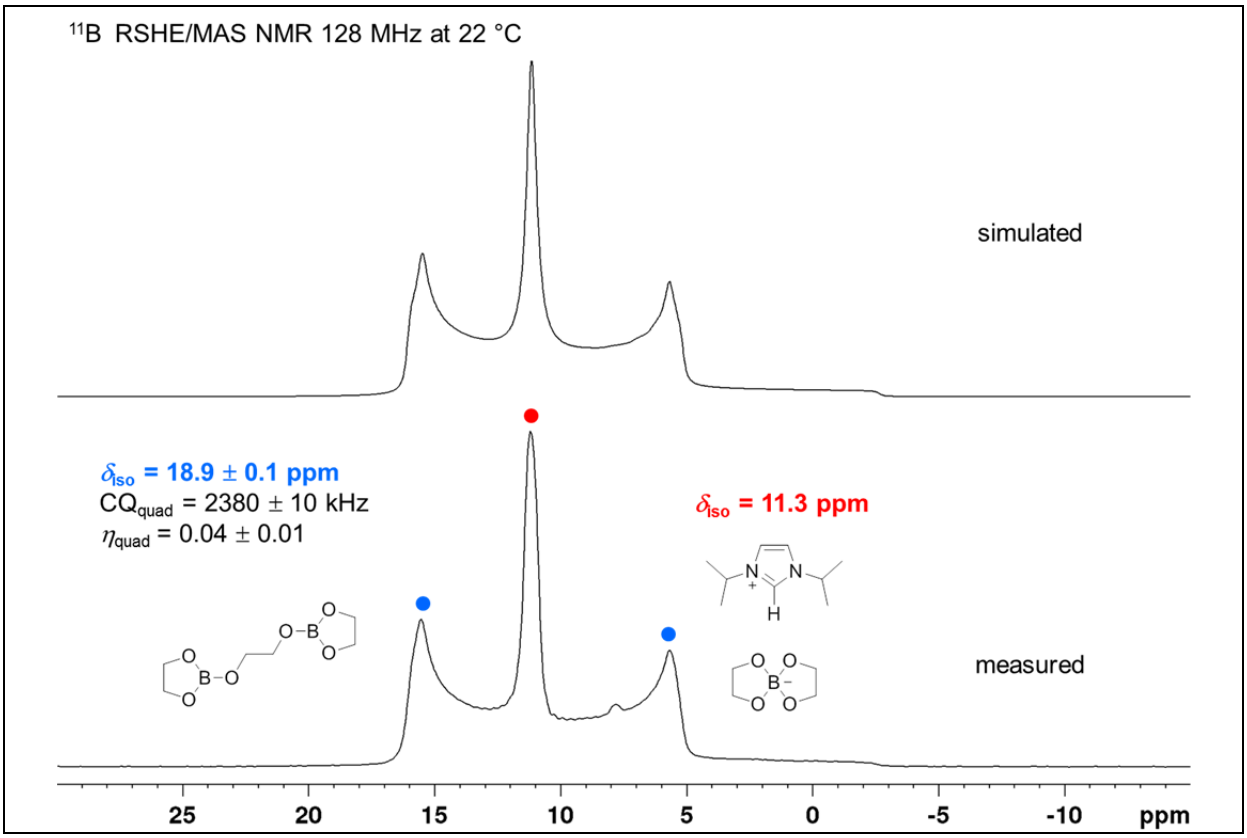

Figure 58. ^{11}*B RSHE/MAS NMR spectrum corresponding to the reaction of* B_2eg_3 *with two equivalents of* iPr_2Im*; (**red**: spiro-borate* $[Beg_2][iPr_2Im\text{-}H]$*; **blue** (one signal):* B_2eg_3 ***111**); (128 MHz, 22 °C,* ν *rot = 15000 Hz).*

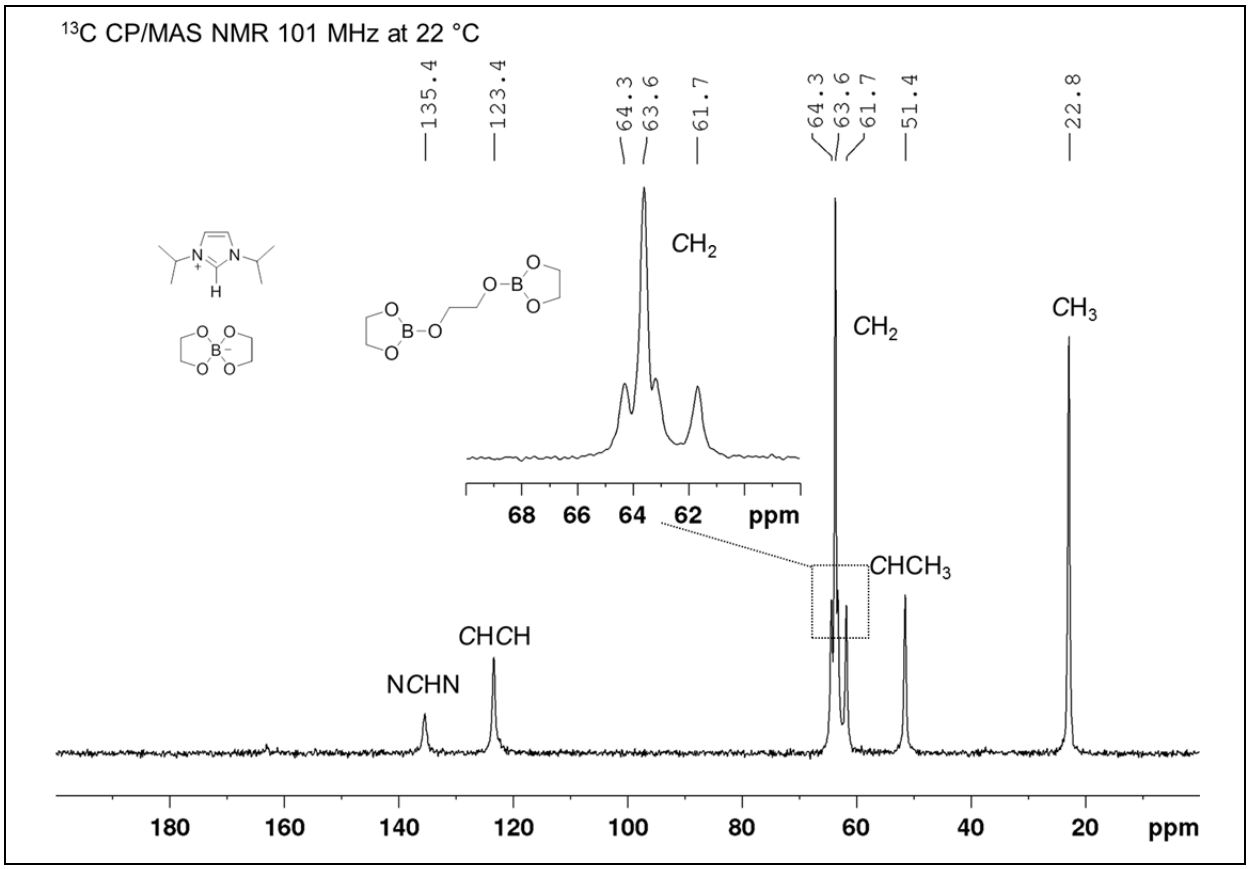

*Figure 59. ^{13}C CP/MAS NMR spectrum corresponding to the reaction of B_2eg_3 **111** with two equivalents of iPr_2Im (101 MHz, 22 °C, ν rot = 10000 Hz).*

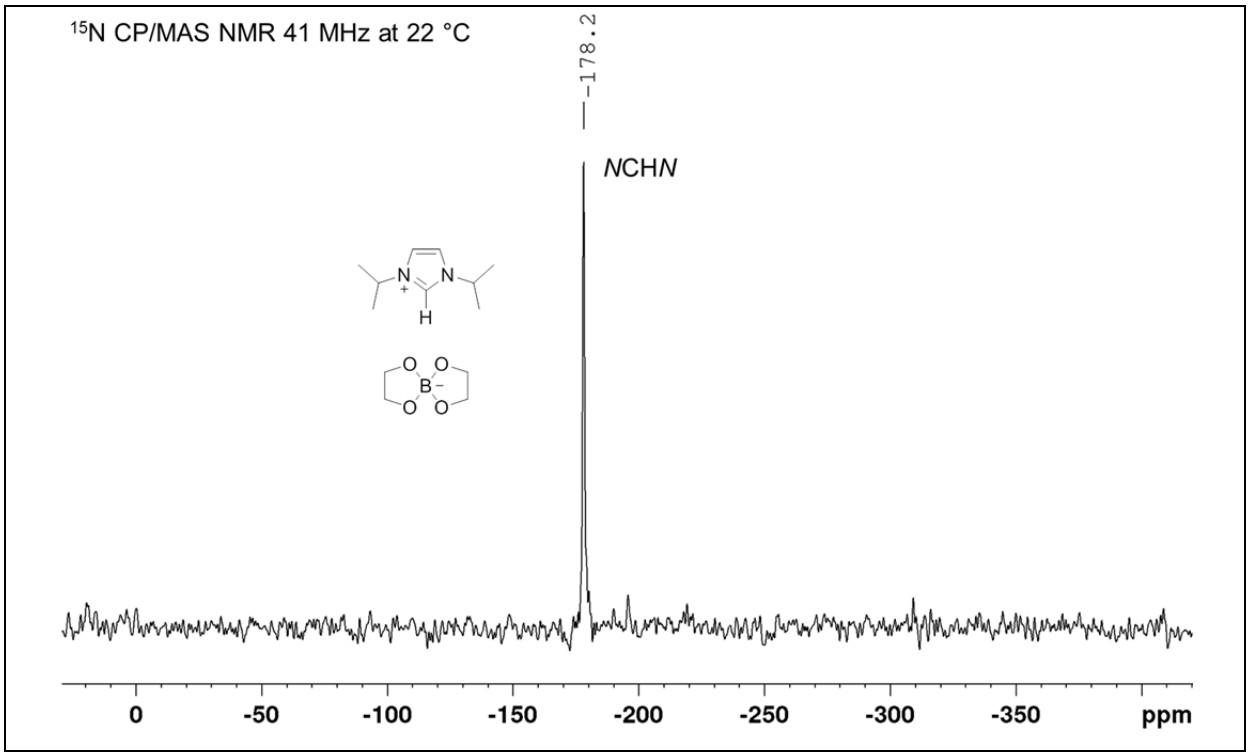

*Figure 60. ^{15}N CP/MAS NMR spectrum corresponding to the reaction of B_2eg_3 **111** with two equivalents of iPr_2Im (41 MHz, 22 °C, ν rot = 8000 Hz).*

The reaction of compound **111** with Me_2Im^{Me} was carried out at 65 °C (Scheme 55). After work-up, a colorless solid was obtained which was investigated *via* solid-state NMR spectroscopy. The ^{11}B RSHE/MAS NMR spectrum (Figure 61) displays two sharp signals for sp^3-B atoms, with isotropic shifts of 11.1 ppm and 5.86 ppm.

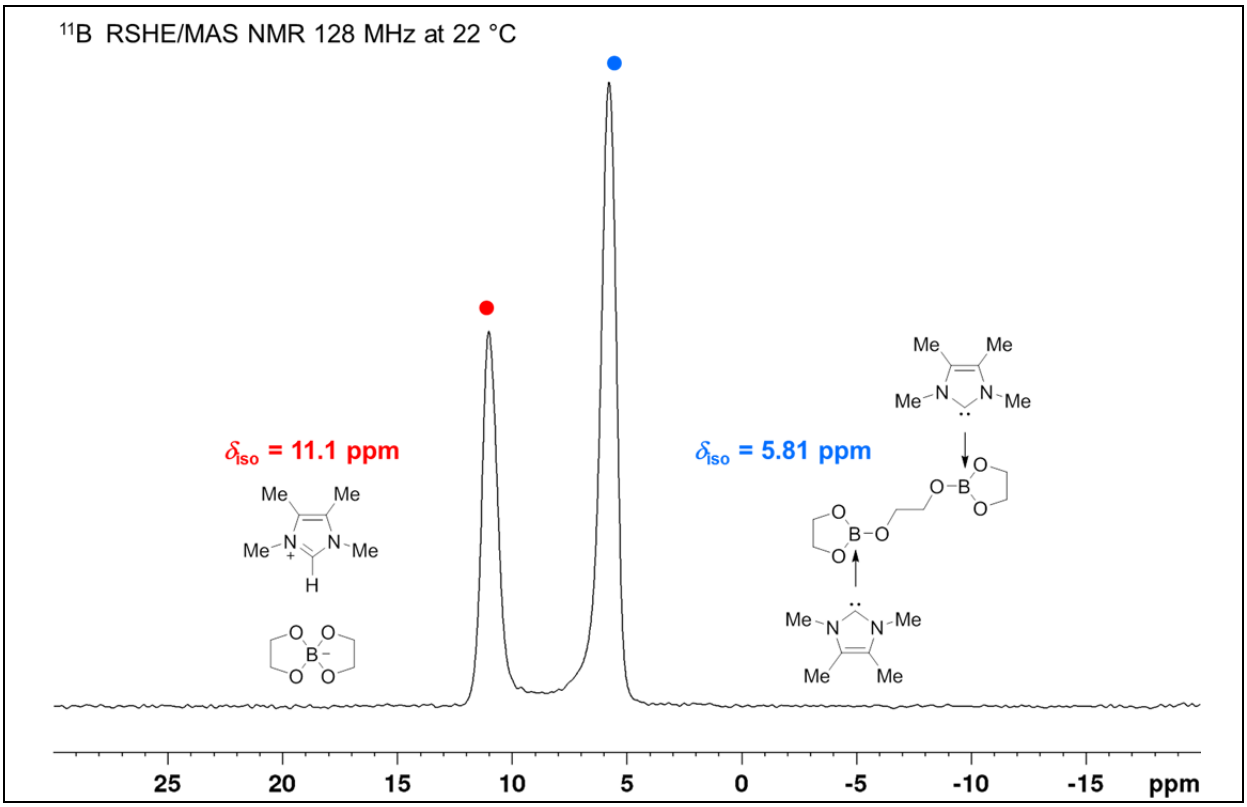

*Figure 61. ^{11}B RSHE/MAS NMR spectrum corresponding to the reaction of B_2eg_3 **111** with Me_2Im^{Me} (**red**: spiro-borate $[Beg_2][Me_2Im^{Me}\text{-}H]$; **blue**: $B_2eg_3\bullet(Me_2Im^{Me})_2$ **123**); (128 MHz, 22 °C, ν rot = 15000 Hz).*

Furthermore, the ^{13}C CP/MAS and ^{15}N CP/MAS NMR spectra (Figure 62 and Figure 63) reveal evidence for the formation of two compounds, which were identified as the bis-NHC adduct $B_2eg_3\bullet(Me_2Im^{Me})_2$ **123** and the spiro-borate $[Beg_2]^-$ anion along with the corresponding imidazolium salt (protonated NHC) $[Me_2Im^{Me}\text{-}H]^+$ as the counter-ion. High resolution mass spectrometry again provided evidence for the formation of a boronium cation species, $[(Me_2Im^{Me})_2Beg]^+$ and a borenium cation species, $[(Me_2Im^{Me})Beg]^+$. However, due to the very similar solubility of these compounds in organic solvents, we could not separate the bis-NHC adduct **123** from the spiro-borate $[NHC\text{-}H]^+$ salt (for HRMS spectra, see appendix B2).

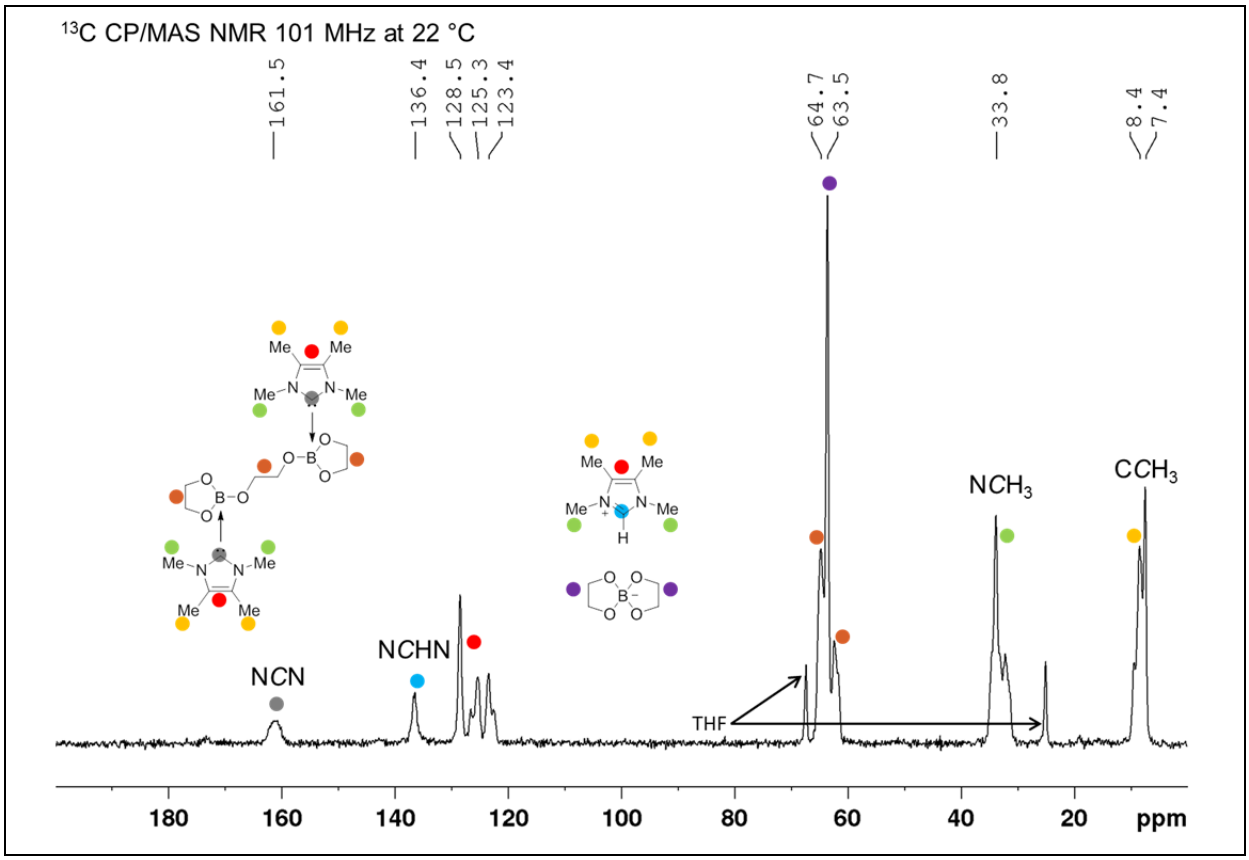

*Figure 62. ^{13}C CP/MAS NMR spectrum corresponding to the reaction of B_2eg_3 **111** with two equivalents of Me_2Im^{Me} (101 MHz, 22 °C, ν rot = 11000 Hz).*

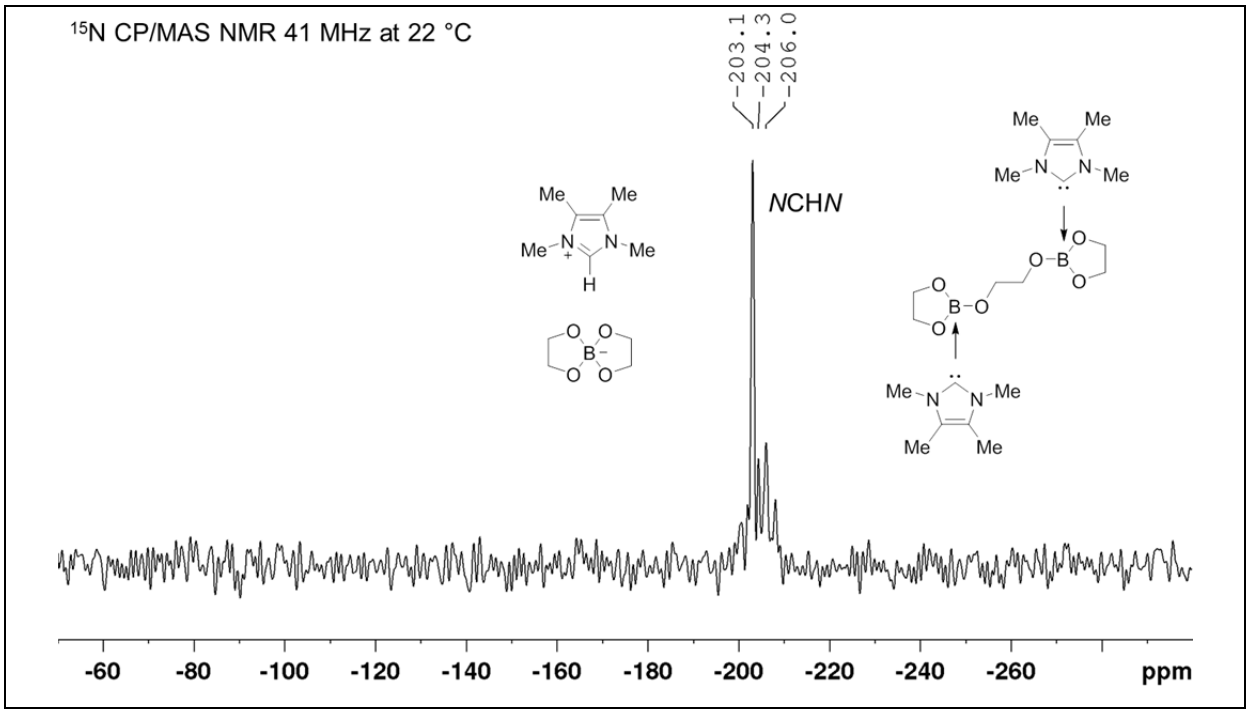

*Figure 63. ^{15}N CP/MAS NMR spectrum corresponding to the reaction of B_2eg_3 **111** with two equivalents of Me_2Im^{Me} (41 MHz, 22 °C, ν rot = 8000 Hz).*

2.2.5 Conclusion (NHC adducts and RERs of B_2eg_2)

The reactions of B_2eg_2 **110** with sterically more or less demanding NHCs resulted in the formation of mono- and bis-NHC adducts. Moreover, B–B bond activation and ring-expansion reactions of the NHCs were observed at lower temperatures (-40 °C to -30 °C) for the NHCs with less steric demand, such as Me_2Im^{Me} or iPr_2Im. While only a weak interaction of the bulky NHC $Dipp_2Im$ with **110** was observed, no significant indication was found for any reactivity of the bulky NHC tBu_2Im with B_2eg_2. In general, very high reactivity was observed for the smaller NHCs, which decreased with increasing steric demand of the NHC. Thus, dynamic processes were also observed for the NHCs Mes_2Im and iPr_2Im^{Me}, in which the NHC(s) are exchanging between the boron atoms of B_2eg_2 **110**.

2.3 Reactions of B_2eg_2 with phosphines of different steric demand

In 1997, Marder, Norman and co-workers[135] reported the isolation and characterization of mono- and bis-phosphine adducts of the thiolate derivative ($B_2(1,2\text{-}S_2C_6H_4)_2$) of B_2cat_2. Furthermore, in 1999, Orpen and Norman *et al.*[184] reported the observation of mono- and bis-phosphine adducts of B_2cat_2 with PMe_3, while they were investigating phosphine exchange reactions involving *cis*-$[Pt(PPh_3)_2(Bcat)_2]$ and the oxidative addition of $1,2\text{-}B_2Cl_2(NMe_2)_2$ to platinum(0). However, Marder and co-workers have tried several times to observe phosphine adducts of B_2cat_2 and PMe_3 but were not able to observe any evidence for such adducts.

Moreover, in 2010, Fernández *et al.*[118] reported a metal-free catalytic borylation reaction of α,β-unsaturated substrates, and proposed a mechanism for B–B bond activation and borylation *via* the formation of a phosphine adduct of B_2pin_2 in the presence of alkoxide. They also claimed that NMR experiments showed significant peaks and shifts to supported the formation of a phosphine-adduct under these conditions. Later, they claimed that phosphine adduct formation of B_2pin_2 is not involved in the borylation process.[153]

However, these observations, and the possibility of sp^2-sp^3 adduct formation of diboron(4) compounds with Lewis-basic phosphines, warrants a better understanding of the reactivity of phosphines with diboron(4) reagents. This is because both

phosphines and diboron(4) compounds are used as reactants in transition metal-catalyzed borylation reactions. The formation of an adduct as an intermediate might affect the borylation process and would require a new perspective on the reaction mechanism.

Therefore, in this study, the reaction of the potentially more Lewis-acidic (compared to B_2pin_2) diboron(4) compound B_2eg_2 **110** with commonly used and commercially available phosphines of different steric demand and basicity, was investigated (Scheme 56, Table 18). The reactions were monitored by *in situ* ^{1}H, ^{11}B{^{1}H} and ^{31}P{^{1}H} NMR spectroscopy (see appendix A5 and A6 for selected spectra).

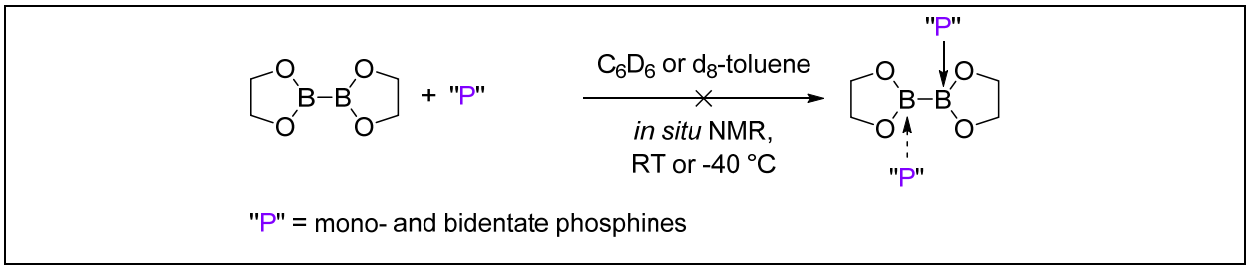

Scheme 56. Reaction of B_2eg_2 with 1.0 equivalents of phosphines of different steric demand.

Table 18. Selected phosphines for the reaction with B_2eg_2 at various temperatures.

entry	phosphine	pk$_a$	temp. [°C]	adduct formation observed?
1	PCy_3	9.70[83]	25 or -40	✘
2	$P(nBu)_3$	8.43[83]	25 or -40	✘
3	dppe	3.86[85]	25	✘
4	dppp	2.91[85]	25	✘
5	PPh_3	2.73[83]	25	✘
6	$P(OMe)_3$	0.83[84]	25	✘
7	H_2PPh	-2.00[82]	25 or 70	✘
8	xantphos	n.a.	25	✘

However, no significant NMR shifts indicating adduct formation were observed for any phosphine examined, either at room temperature or at lower temperature (-40 °C). For the sterically less demanding phosphine H_2PPh, even after heating to 70 °C and storing it for one month in the reaction vessel, no evidence for adduct formation was observed. However, an increase of the signal of an unknown impurity (egB–O–Beg?) was observed in the NMR spectra (Figure 64 to Figure 66).

Nevertheless, no evidence for adduct formation of the phosphines used with the Lewis-acidic diboron(4) compound B_2eg_2 **110** was found. Thus, the previously reported[118,184] observations cannot yet be confirmed.

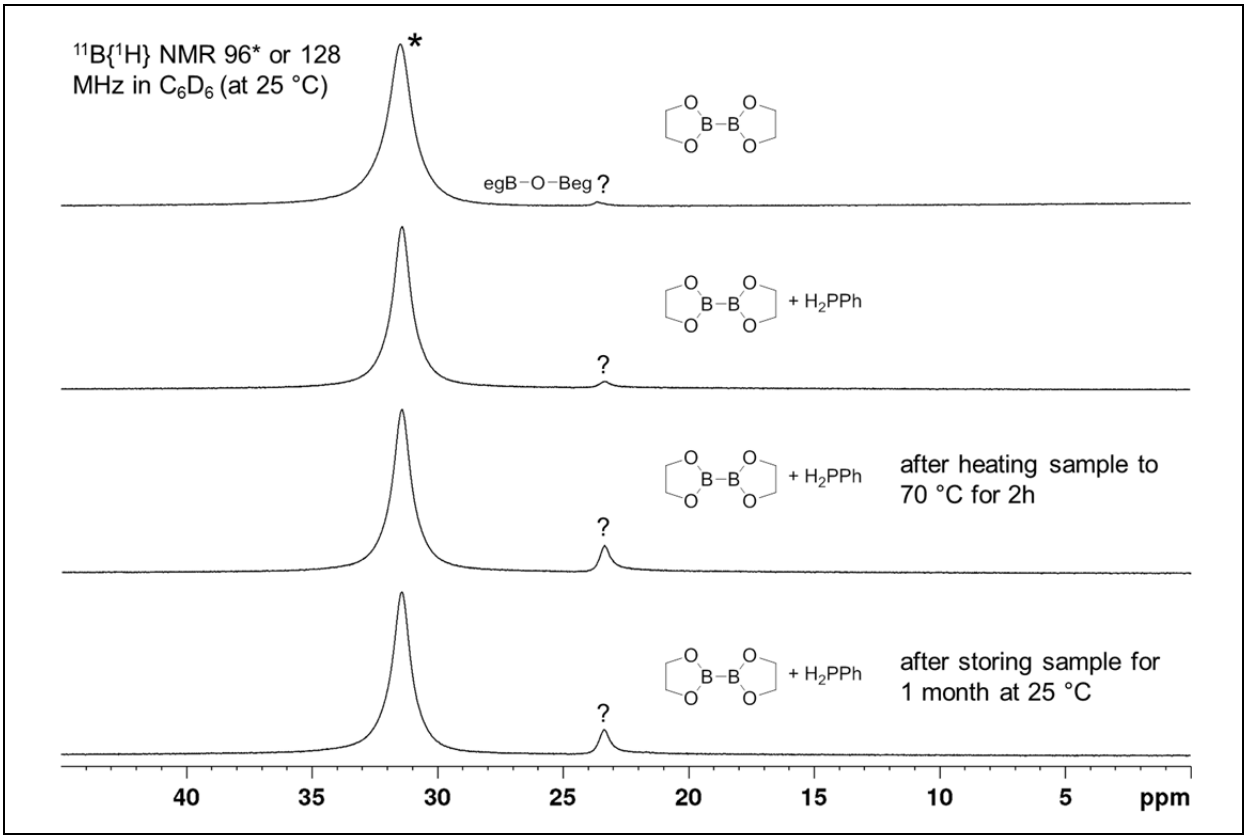

*Figure 64. In situ $^{11}B\{^1H\}$ NMR spectrum of the reaction of B_2eg_2 **110** with H_2PPh (2nd from the top) in C_6D_6 (128 MHz, 25 °C).*

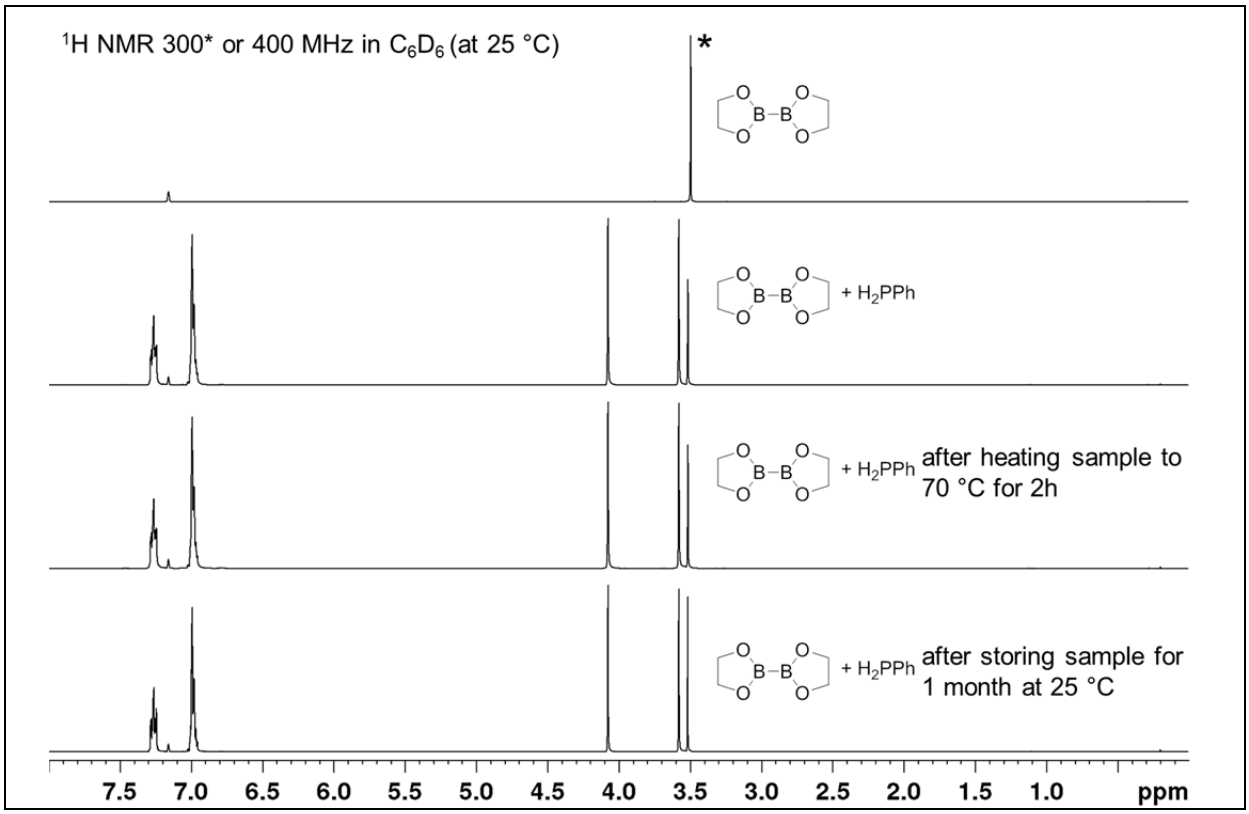

*Figure 65 In situ ^{1}H NMR spectrum of the reaction of B_2eg_2 **110** with H_2PPh (2nd from the top) in C_6D_6 (400 MHz, 25 °C).*

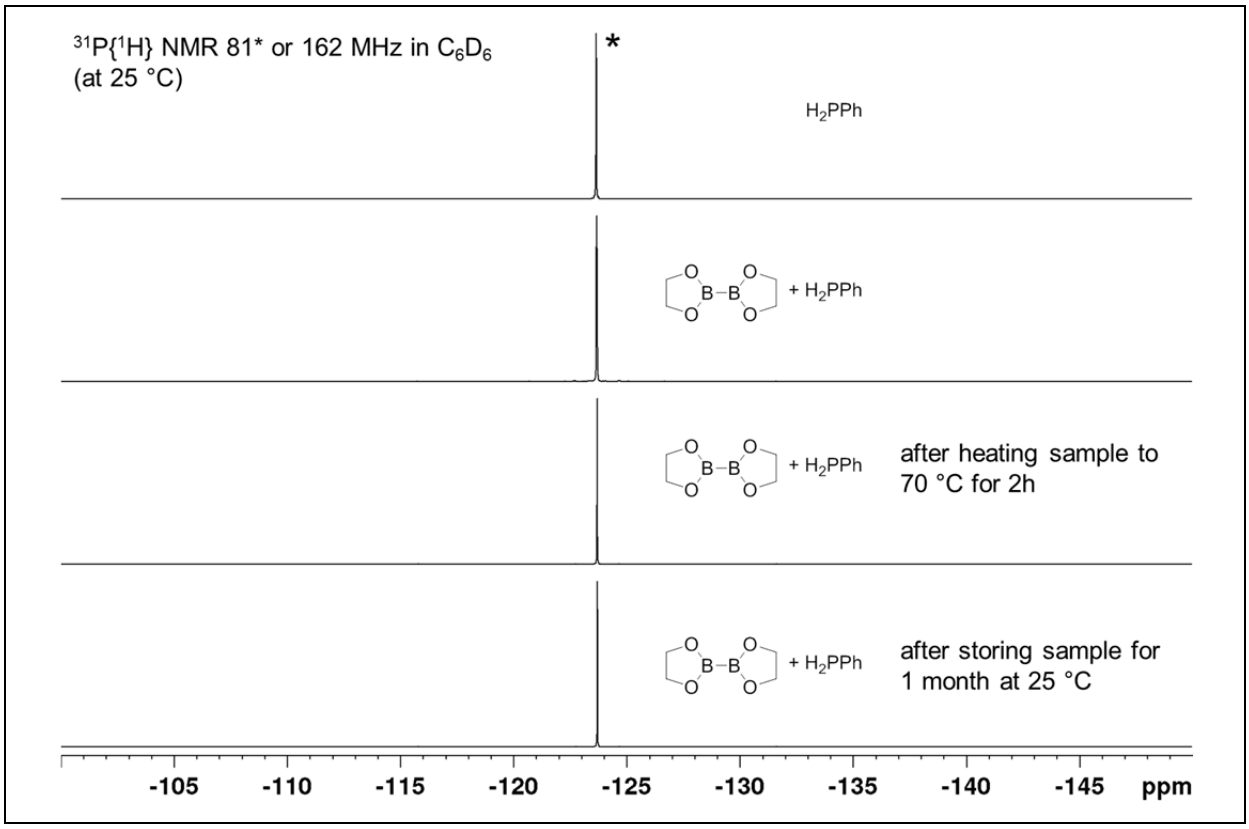

*Figure 66. In situ $^{31}P\{^{1}H\}$ NMR spectrum of the reaction of B_2eg_2 **110** with H_2PPh (2nd from the top) in C_6D_6 (162 MHz, 25 °C).*

2.4 Reactions of $B_2(OMe)_4$ with NHCs of different steric demand

To extend the investigations on the role of the diboron(4) compound, $B_2(OMe)_4$ with a more flexible structure compared to B_2pin_2, B_2cat_2, B_2neop_2 and B_2eg_2, (which have a ridgid backbone) was reacted with NHCs of different steric demand (Scheme 57). The reactions were monitored by *in situ* ^1H and $^{11}B\{^1H\}$ NMR spectroscopy.

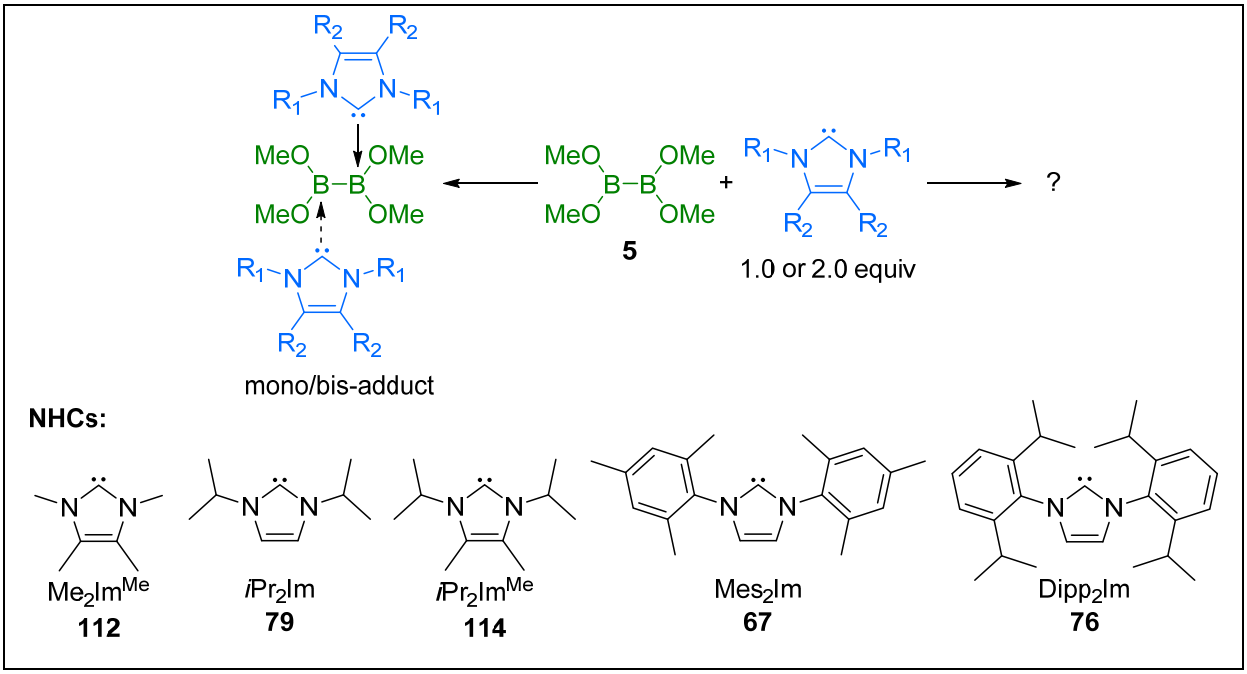

Scheme 57. Reactivity of $B_2(OMe)_4$ with NHCs of different steric demand.

2.4.1 Reactions of $B_2(OMe)_4$ with the NHC Me_2Im^{Me}

The reaction of $B_2(OMe)_4$ **5** with one equivalent of the NHC Me_2Im^{Me} showed, in the *in situ* $^{11}B\{^1H\}$ NMR spectrum, the signals typical for an sp^2-B atom and an sp^3-B atom indicating, the formation of a mono-NHC adduct (Figure 67). Furthermore, the *in situ* ^1H NMR spectrum supports this observation and shows significant shifts compared to those of the free reactants as well as a broadening of the proton signals (Figure 68). When reacting the diboron(4) compound with two equivalents of NHC, a very similar signal pattern in the *in situ* $^{11}B\{^1H\}$ NMR spectrum is observed. While for a bis-NHC adduct, one signal for two sp^3-B atoms was expected, only the signals for a mono-NHC adduct were observed. This fact might be explained by a dynamic process (dissociative and associative exchange of the NHCs) which also was present for B_2eg_2 and the recently reported[170,183] bis-NHC adducts of B_2cat_2 and B_2neop_2.

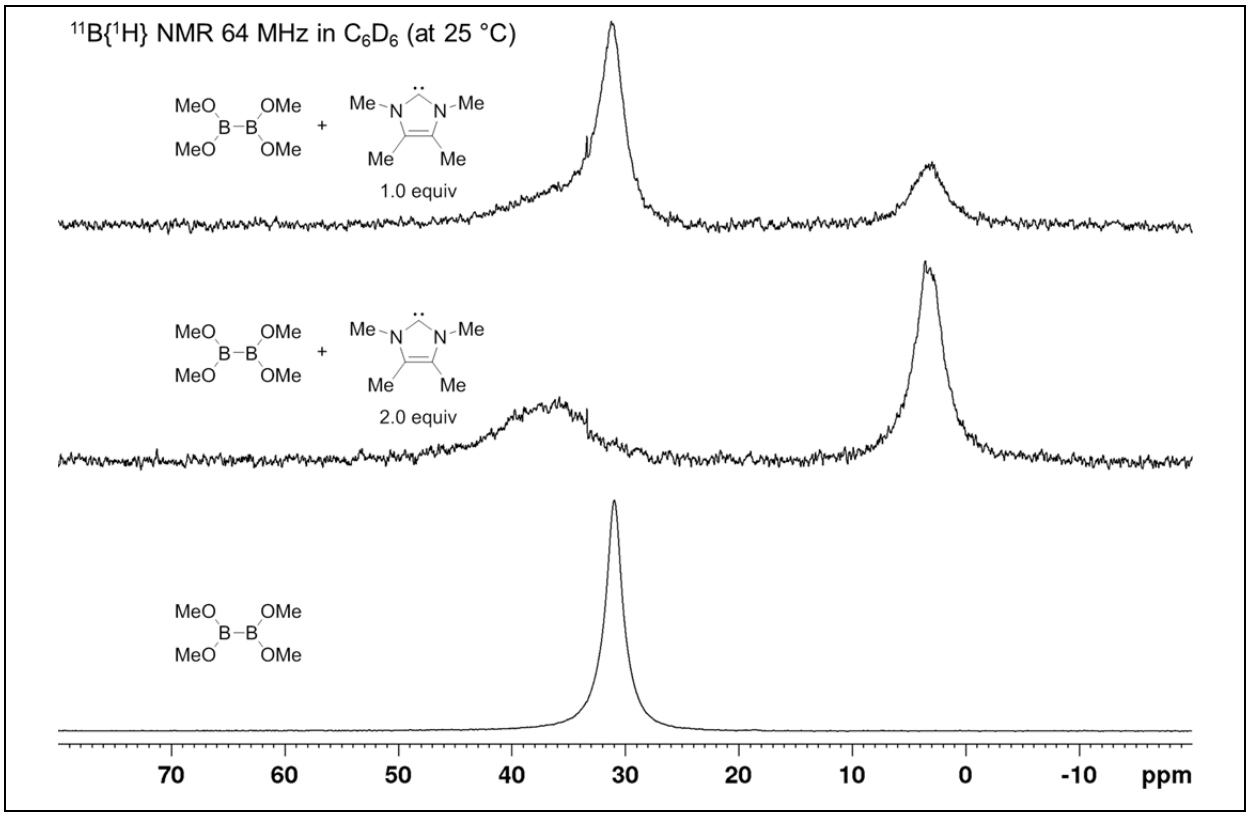

*Figure 67. In situ $^{11}B\{^1H\}$ NMR spectrum of the reaction of $B_2(OMe)_4$ **5** with Me_2Im^{Me} in C_6D_6 (64 MHz, 25 °C).*

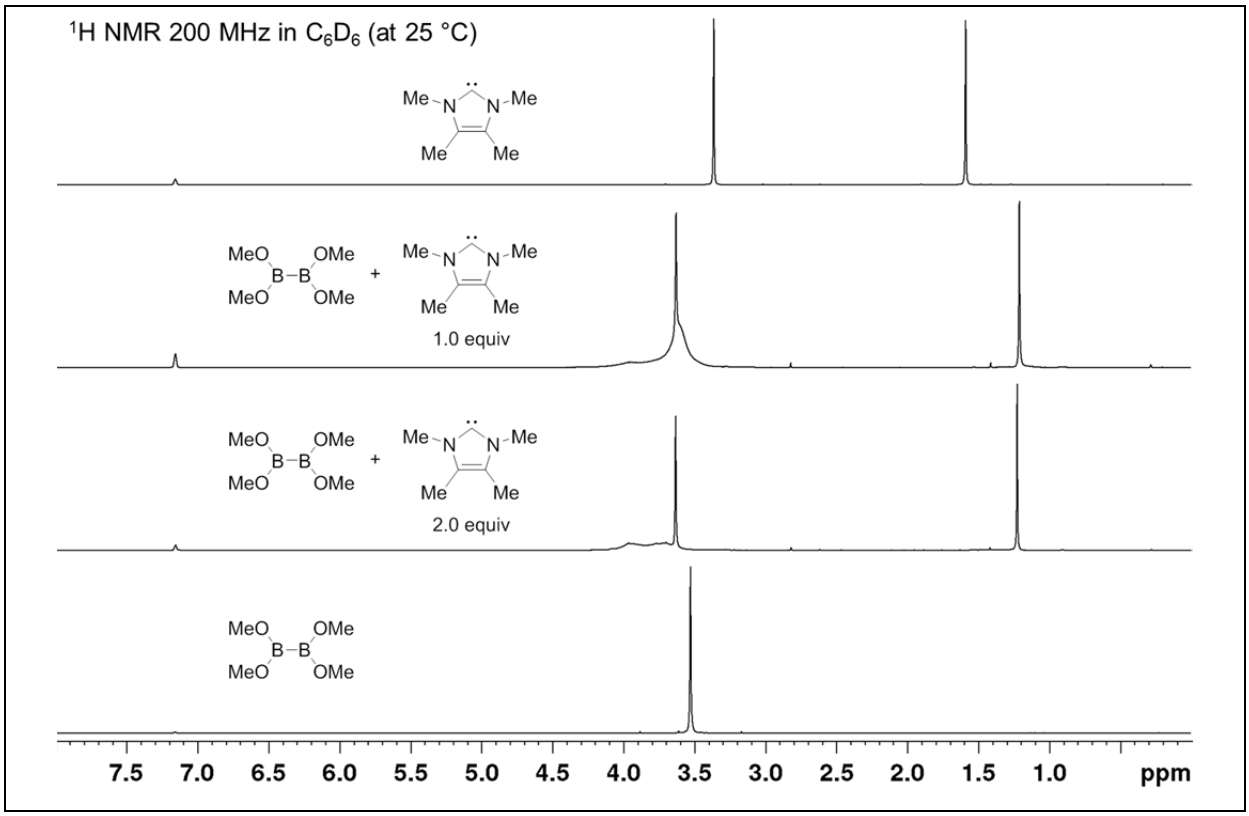

*Figure 68. In situ ^1H NMR spectrum of the reaction of $B_2(OMe)_4$ **5** with Me_2Im^{Me} in C_6D_6 (200 MHz, 25 °C).*

2.4.2 Reactions of $B_2(OMe)_4$ with the NHCs *i*Pr_2Im and *i*Pr_2Im^{Me}

Reacting $B_2(OMe)_4$ **5** with the NHCs *i*Pr_2Im and *i*Pr_2Im^{Me} resulted in similar observations compared to the NHC Me_2Im^{Me}, and the *in situ* $^{11}B\{^1H\}$ and ^1H NMR spectra showed evidence (significant shifts and broadening of the ^1H signals) for both mono- and bis-NHC adduct formation (Figure 69 to Figure 72).

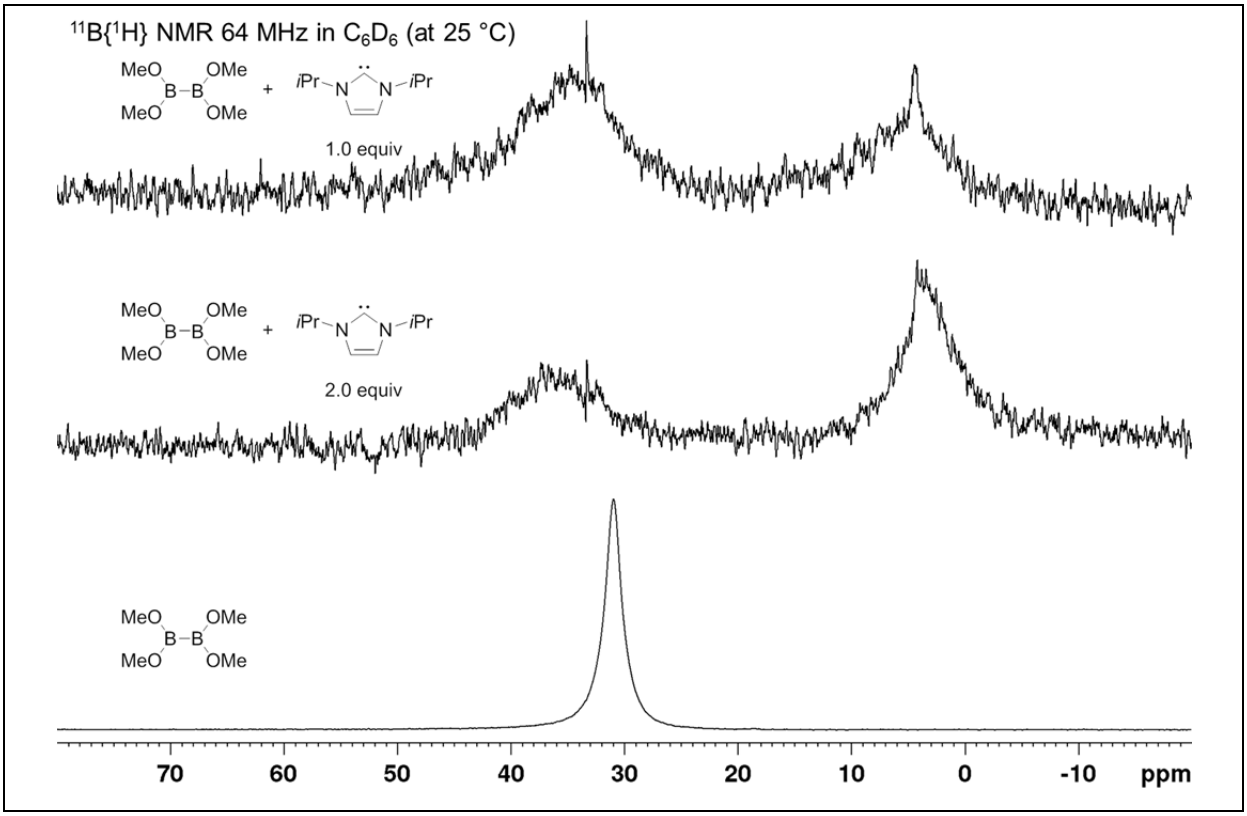

*Figure 69. In situ $^{11}B\{^1H\}$ NMR spectrum of the reaction of $B_2(OMe)_4$ **5** with iPr_2Im in C_6D_6 (64 MHz, 25 °C).*

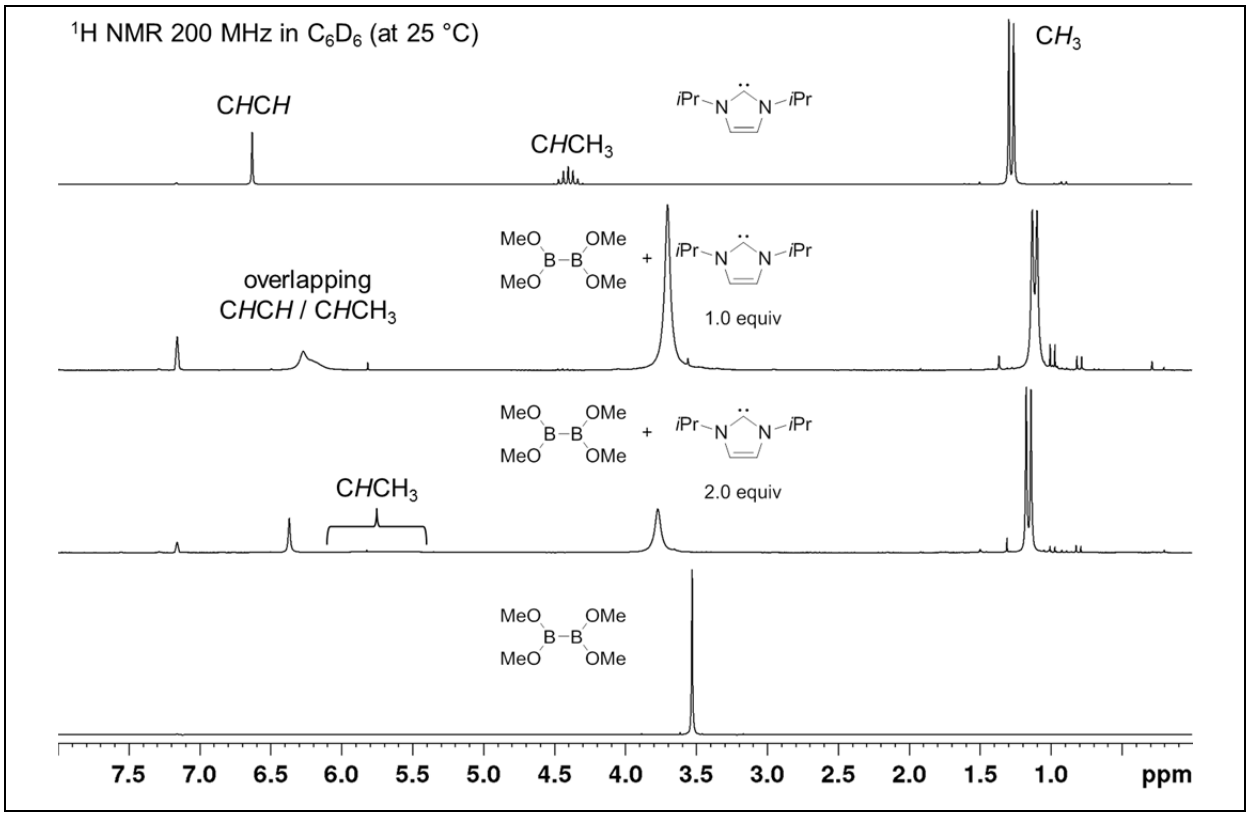

*Figure 70. In situ ^{1}H NMR spectrum of the reaction of $B_2(OMe)_4$ **5** with iPr_2Im in C_6D_6 (200 MHz, 25 °C).*

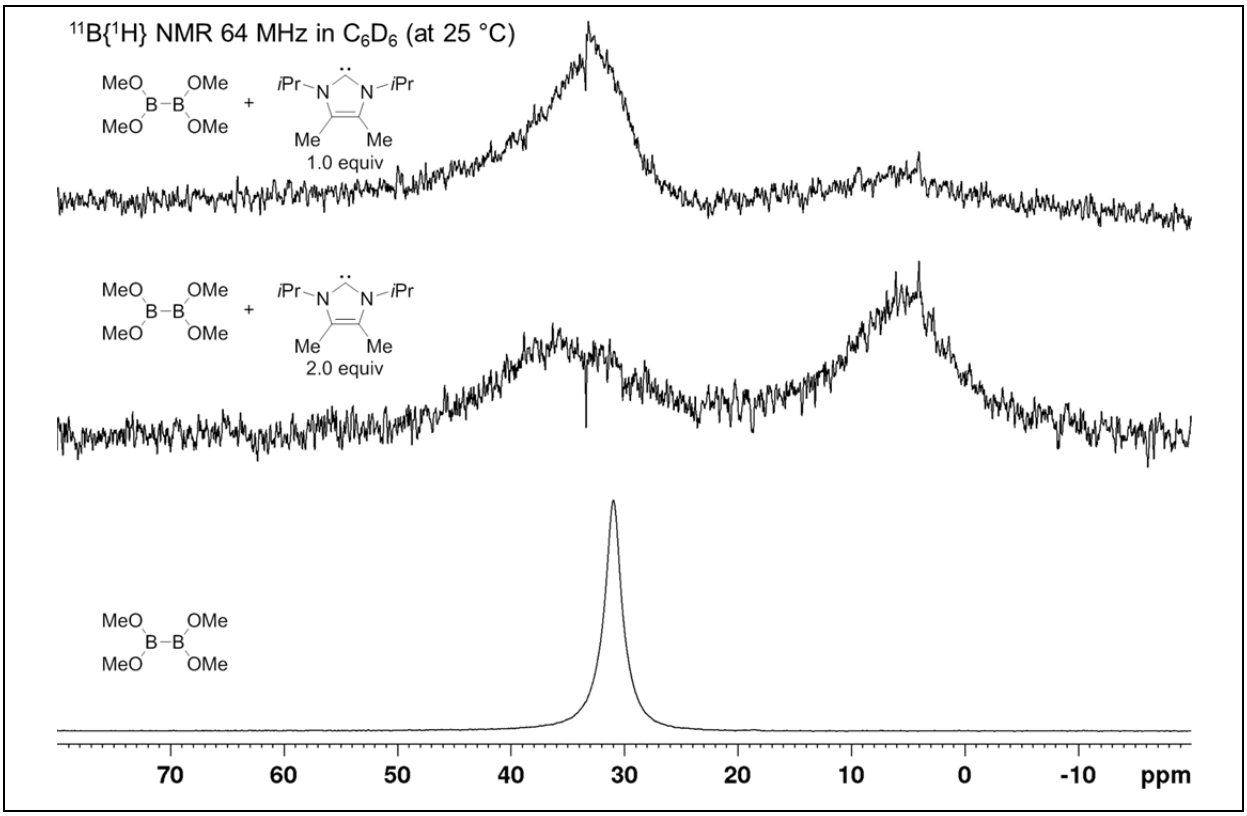

*Figure 71. In situ $^{11}B\{^{1}H\}$ NMR spectrum of the reaction of $B_2(OMe)_4$ **5** with iPr_2Im^{Me} in C_6D_6 (64 MHz, 25 °C).*

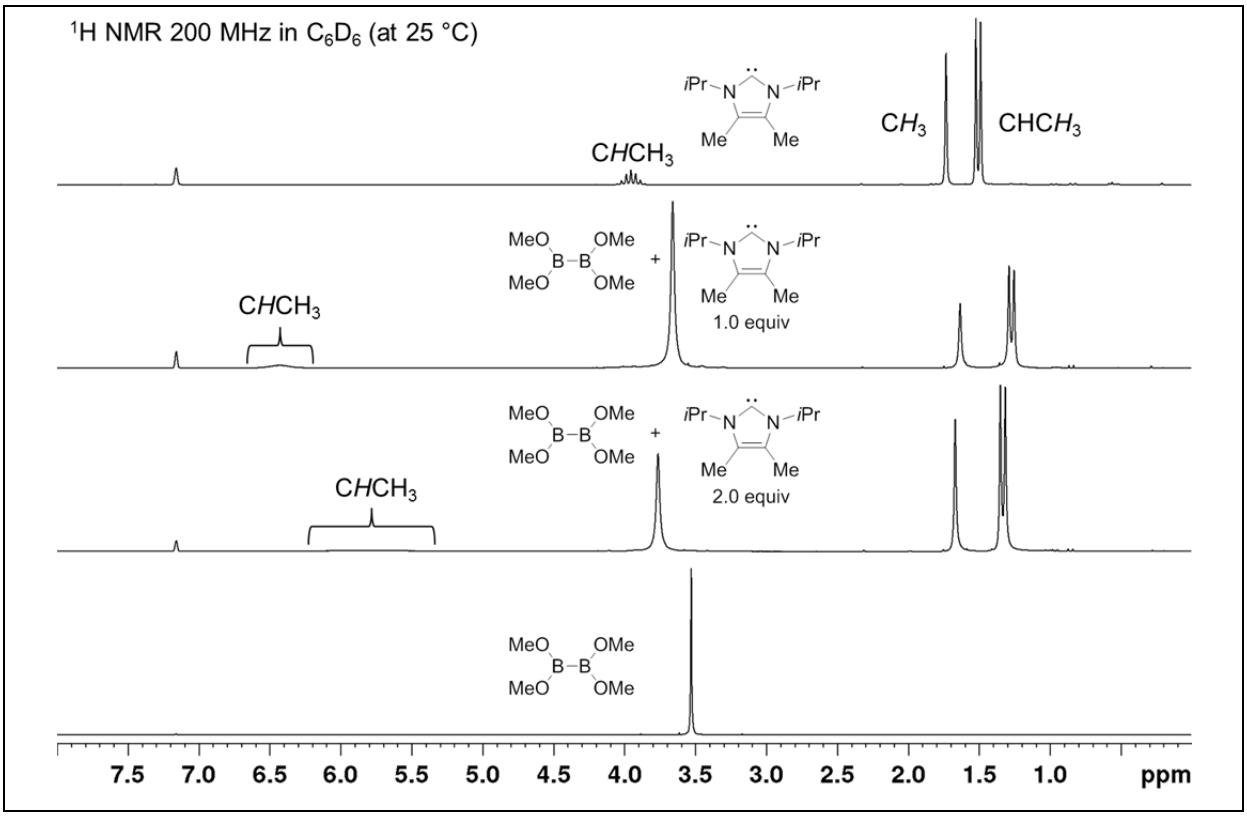

*Figure 72. In situ ^{1}H NMR spectrum of the reaction of $B_2(OMe)_4$ **5** with iPr_2Im^{Me} in C_6D_6 (200 MHz, 25 °C).*

The low temperature (-70 °C) *in situ* NMR spectra (Figure 73 and Figure 74) reinforced the formation of the bis-NHC adducts at this temperature, while at room temperature a dynamic process was observed.

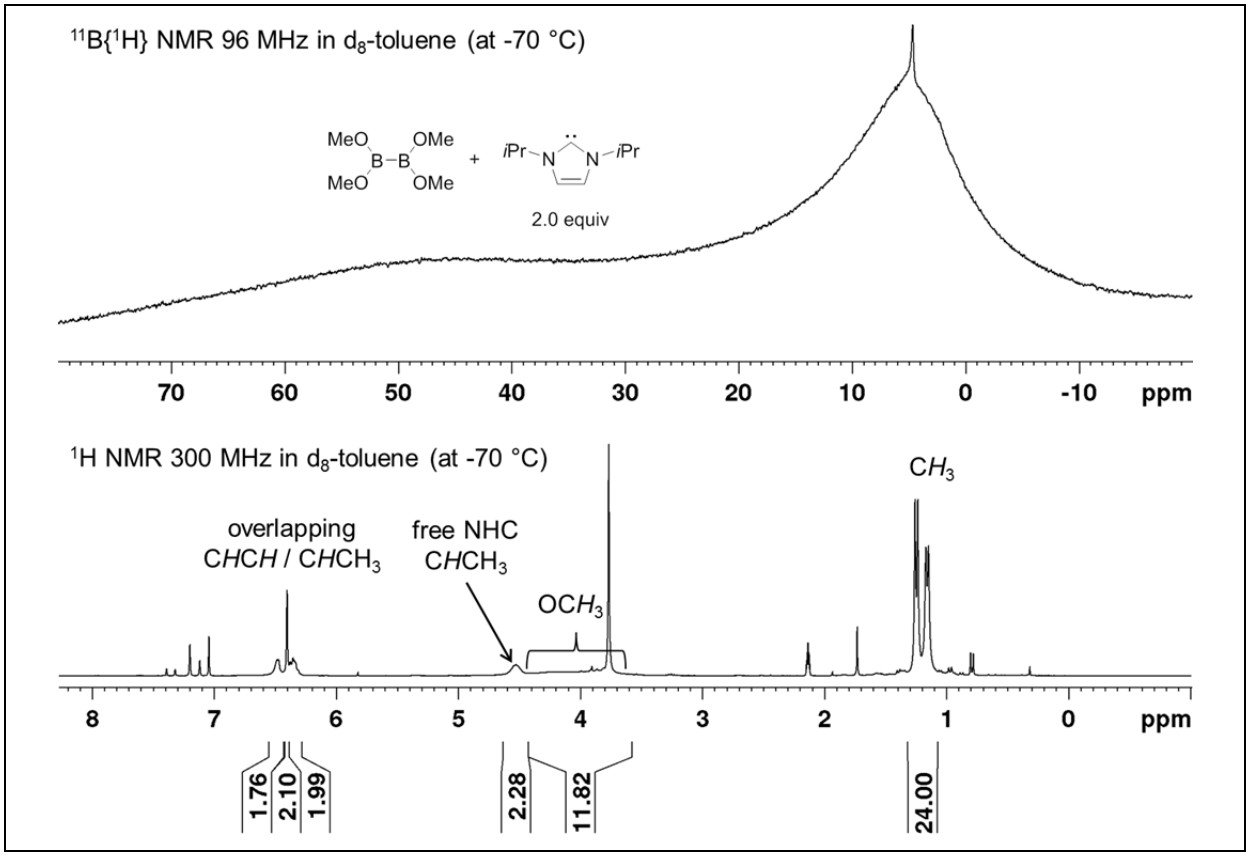

*Figure 73. In situ $^{11}B\{^1H\}$ NMR (top) and ^1H NMR (bottom) spectra of the reaction of $B_2(OMe)_4$ **5** with iPr_2Im in C_6D_6 (64 MHz and 200 MHz, -70 °C).*

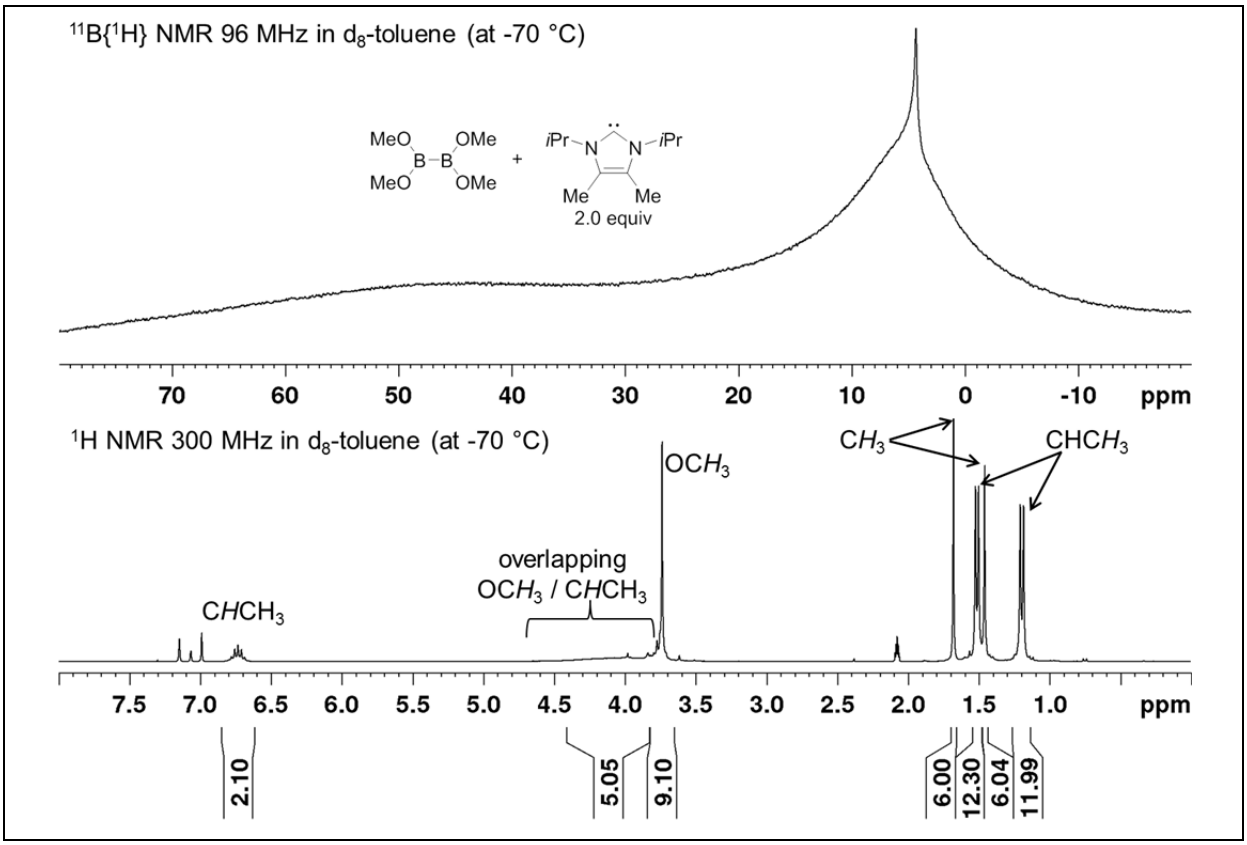

*Figure 74. In situ $^{11}B\{^1H\}$ NMR (top) and ^1H NMR (bottom) spectra of the reaction of $B_2(OMe)_4$ **5** with iPr_2Im^{Me} in C_6D_6 (64 MHz and 200 MHz, -70 °C).*

2.4.3 Reactions of $B_2(OMe)_4$ with the NHC Mes_2Im

Increasing the steric demand of the NHC caused an increase of the dynamic exchange of the NHCs between the two boron atoms of $B_2(OMe)_4$ **5**, which is very well reflected in the $^{11}B\{^1H\}$ NMR spectrum of the reaction of compound **5** with Mes_2Im (Figure 75). The observed boron signal at 26.3 ppm (one equivalent of NHC) is shifted up-field compared to that of the free diboron(4) compound. Increasing the concentration of the carbene (two equivalents) resulted in a further up-field shift to 23.3 ppm and a second peak arising at 10.7 ppm, indicating the formation of a bis-NHC adduct. This is reinforced and reflected in the ^1H NMR spectra (Figure 76) which show significant shifts of the NHC backbone as well as a broadening of the methoxy-group signals. Furthermore, the low temperature (-70 °C) *in situ* $^{11}B\{^1H\}$ NMR spectrum (Figure 77) shows two peaks at 3.61 and 2.17 ppm, in the expected region for sp^3-B atoms and the two signals might be explained by the steric demand of the NHC Mes_2Im and the resulting hindered rotation at -70 °C. The corresponding ^1H NMR spectrum at -70 °C (Figure 77) also shows two signals for the $B(OMe)_2$ moieties presumably due to the hindered rotation at this temperature.

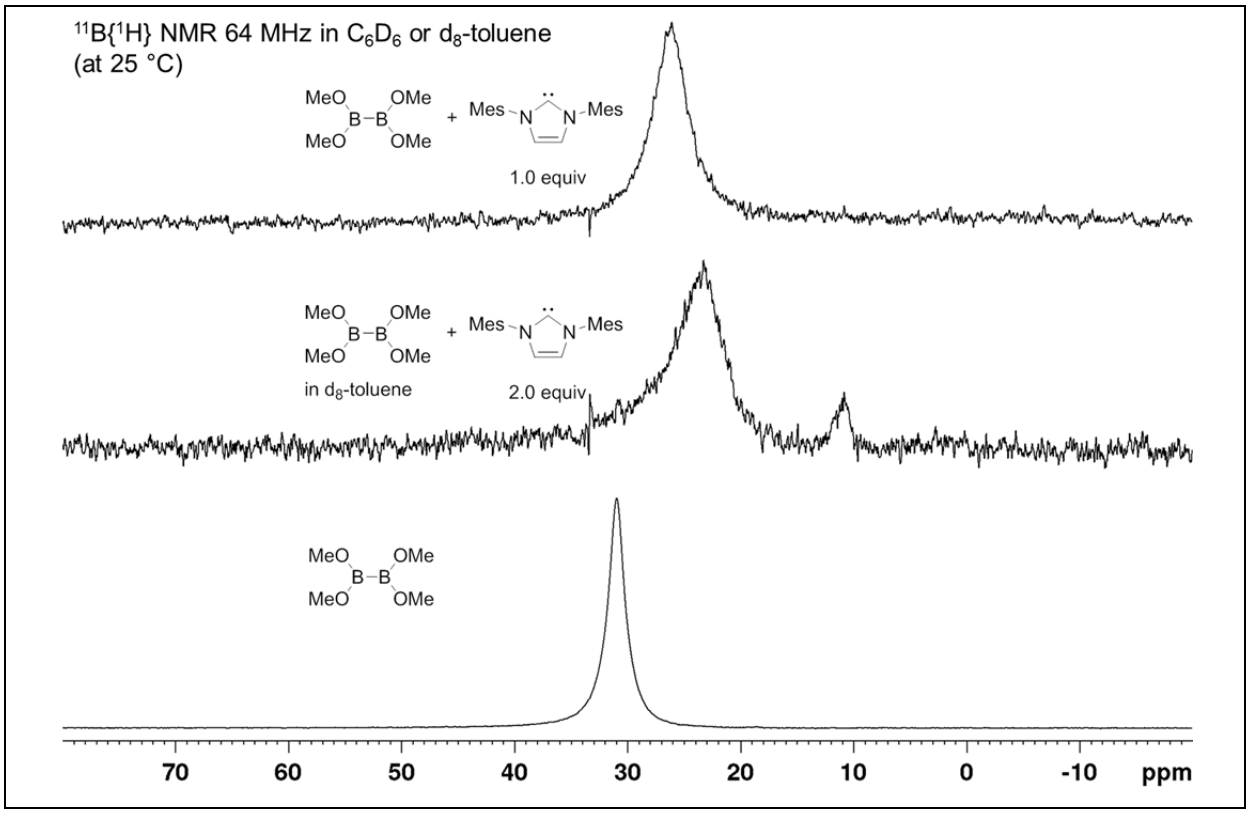

*Figure 75. In situ $^{11}B\{^1H\}$ NMR spectra of the reaction of $B_2(OMe)_4$ **5** with Mes_2Im in C_6D_6 (64 MHz, 25 °C).*

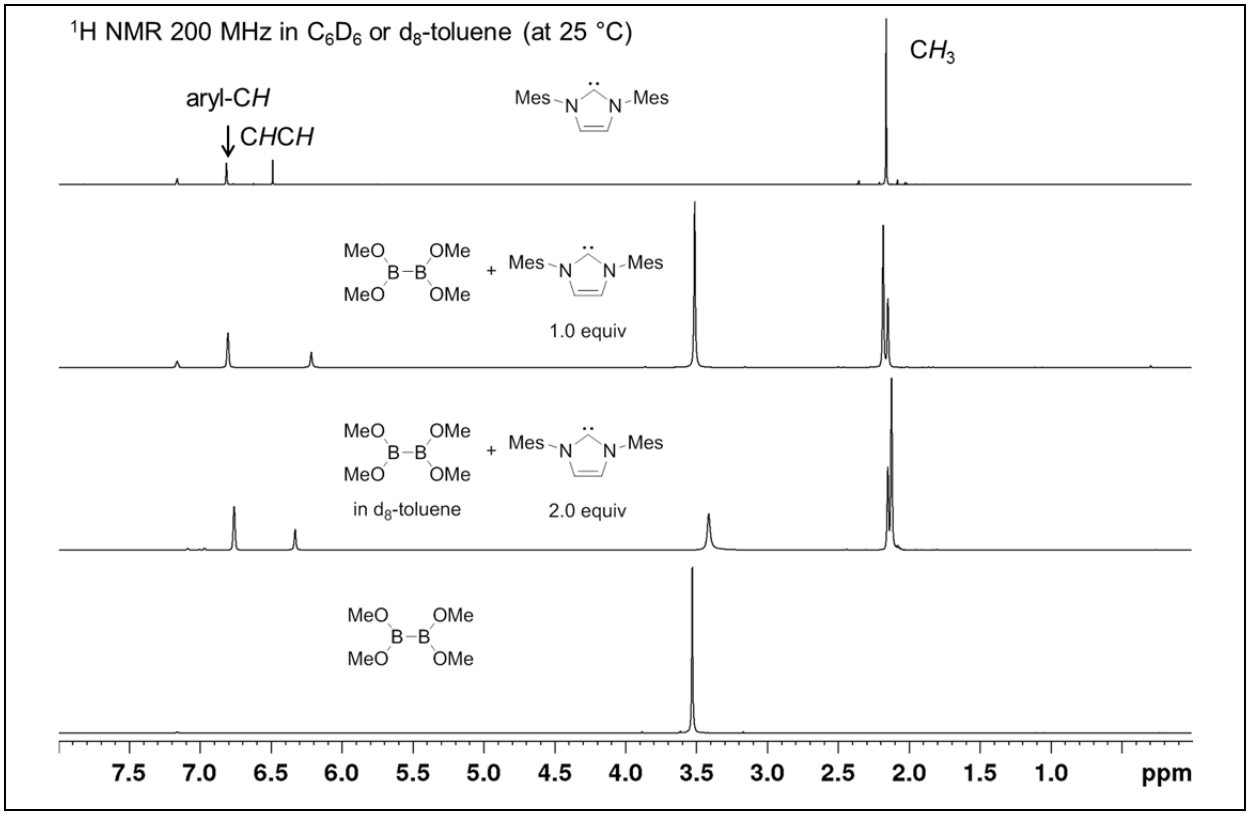

*Figure 76. In situ ^1H NMR spectra of the reaction of $B_2(OMe)_4$ **5** with Mes_2Im in C_6D_6 or d_8-toluene (200 MHz, 25 °C).*

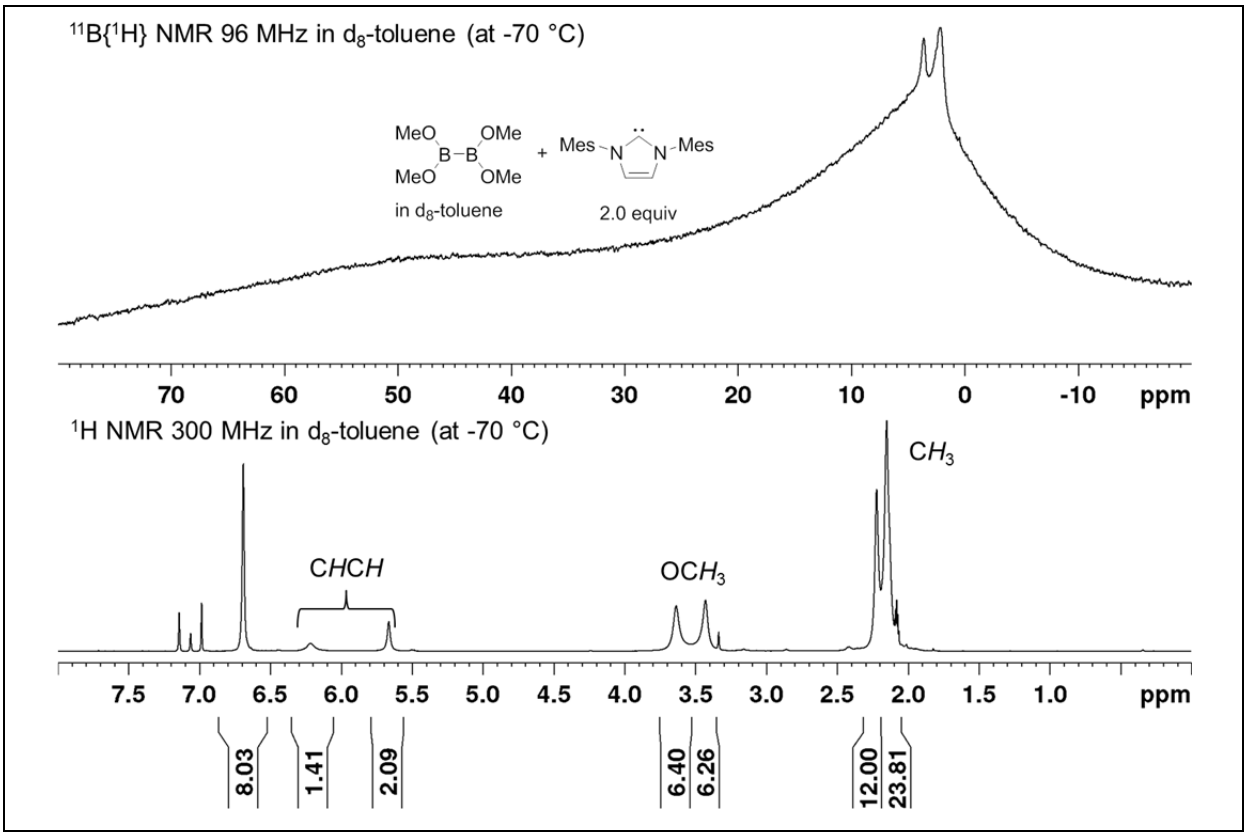

*Figure 77. In situ $^{11}B\{^1H\}$ NMR (top) and ^1H NMR (bottom) spectra of the reaction of $B_2(OMe)_4$ **5** with Mes_2Im in C_6D_6 (64 MHz and 200 MHz, -70 °C).*

Nevertheless, it is still possible that at -70 °C it is still a mixture of both a mono-NHC and a bis-NHC adduct.

2.4.4 Reactions of $B_2(OMe)_4$ with the NHC $Dipp_2Im$

No evidence for any interaction of $Dipp_2Im$ with the diboron(4) compound was observed in the *in situ* $^{11}B\{^1H\}$ and ^1H NMR spectra (Figure 78).

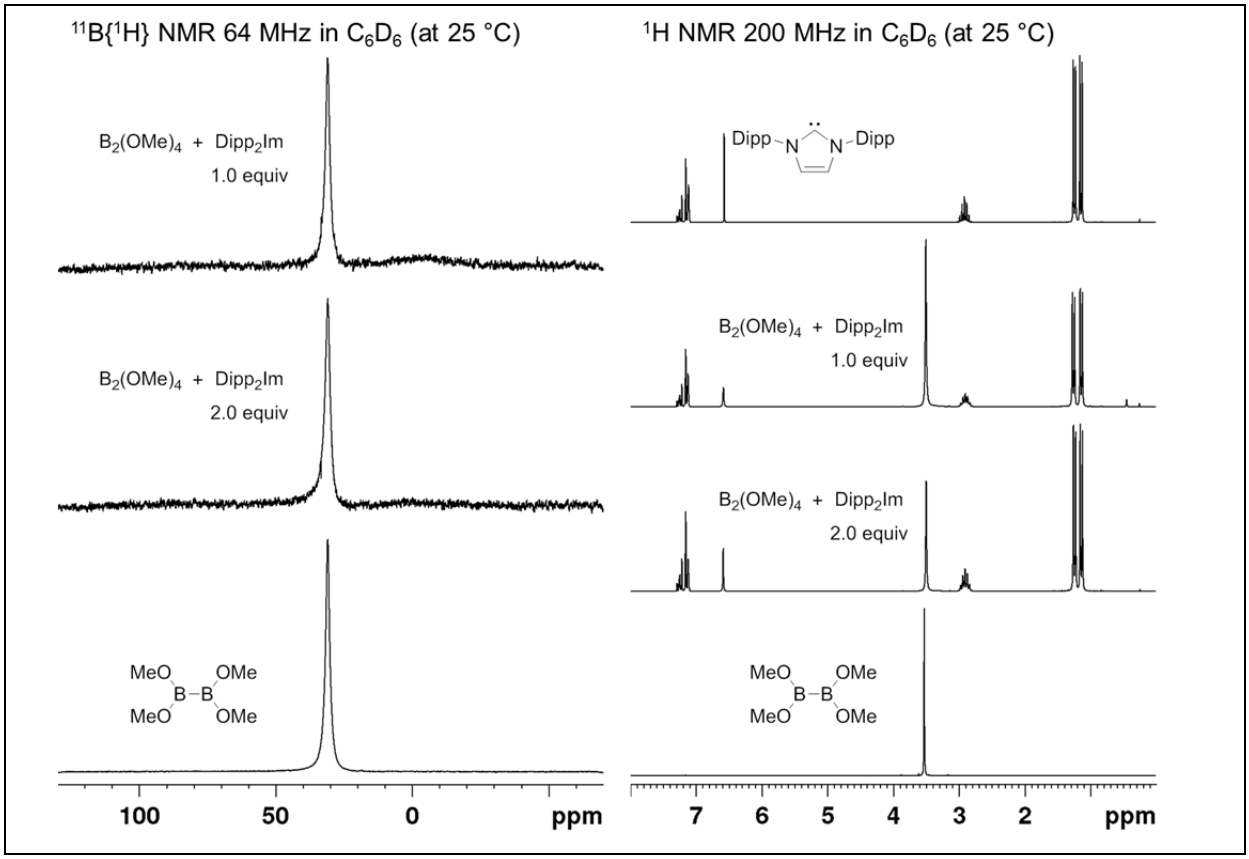

*Figure 78. In situ $^{11}B\{^1H\}$ NMR (right) and ^1H NMR (left) spectra of the reaction of $B_2(OMe)_4$ **5** with $Dipp_2Im$ in C_6D_6 (64 MHz and 200 MHz, 25 °C).*

Interestingly, single-crystals suitable for X-ray diffraction were obtained by single-crystal picking from the NMR sample of the reaction of $B_2(OMe)_4$ with $Dipp_2Im$ after storing it for two days at room temperature (standard NMR tube with rubber cap). The molecular structure of this compound (**124**) is shown in Figure 79, but the mechanism for the formation of compound **124** cannot be explained yet. It is likely, a result of trace H_2O being present.

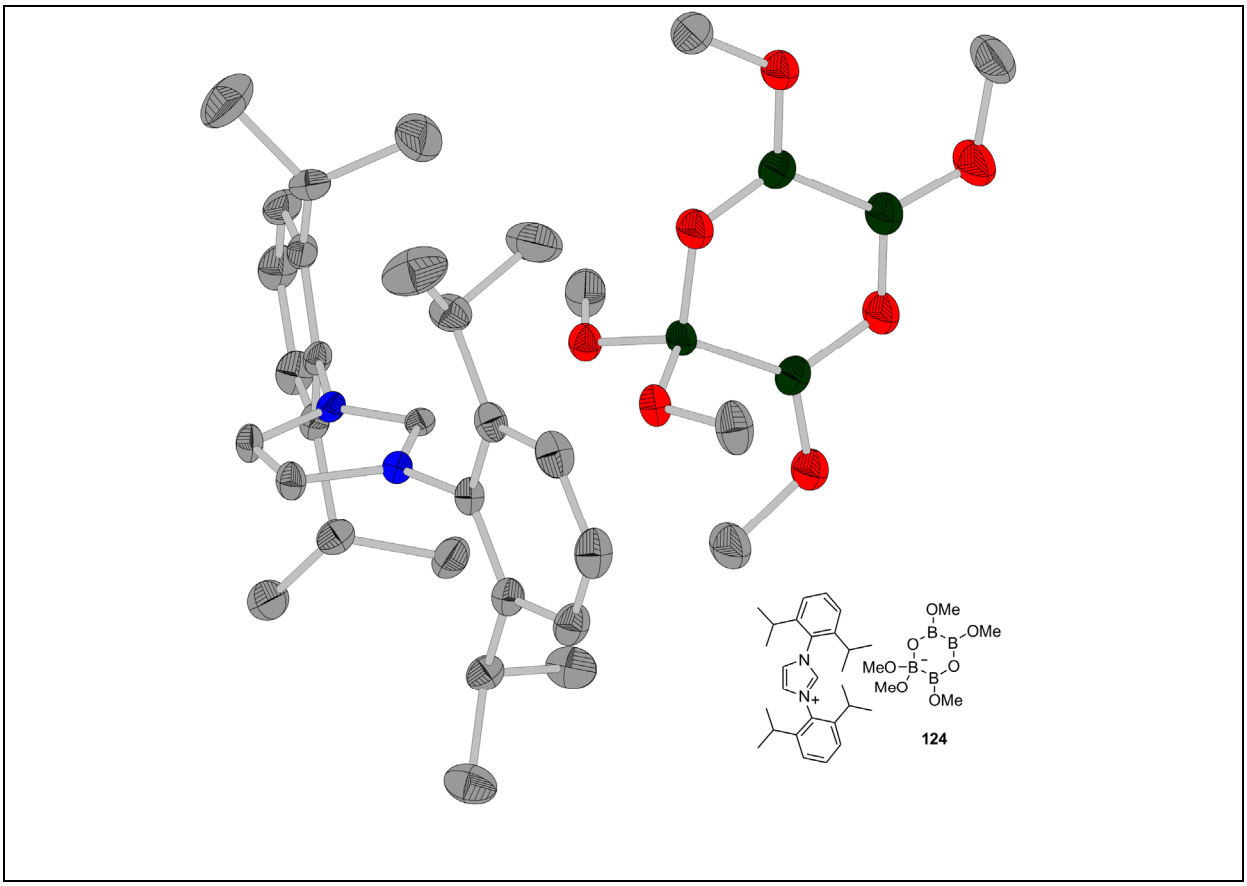

*Figure 79. Molecular structure of compound **124** which was obtained by single-crystal picking of the reaction of $B_2(OMe)_4$ with $Dipp_2Im$.*

2.4.5 Conclusion (NHC adducts of $B_2(OMe)_4$)

In conclusion, the reactions of the diboron(4) compound $B_2(OMe)_4$ **5** with NHCs of different steric demand resulted in the expected formation of mono- or bis-NHC adducts. Compound **5** is more flexible compared to other diboron(4) compounds (e.g. B_2eg_2, B_2pin_2) and the *in situ* NMR spectra showed evidence for bis-adduct formation as well. While dependent on the steric demand of the NHC a similar reactivity as for B_2eg_2 and a dynamic exchange of the NHCs was observed, no evidence for a ring-expansion reaction was found for any NHC. The isolation of single-crystals of compound **124**, probably a result of partial hydrolosis of the diboron(4) compound **5**, was an interesting observation, while for the reaction of $B_2(OMe)_4$ with the NHC $Dipp_2Im$, no evidence for any reactivity was found in the *in situ* NMR spectra.

CHAPTER THREE

-

Summary / Zusammenfassung

“I learned from Linus Pauling it's not a disgrace in science to publish something that's wrong. What's bad is to publish something that's not very interesting.”

Prof. William Lipscomb (1919-2011)

CHAPTER THREE
-
Summary / Zusammenfassung

1 Summary

The purpose of the present work was, in the first part, to investigate the potential of iron-based metal complexes in catalytic borylation reactions with alkyl halides as substrates and B_2pin_2 as the borylation reagent. Moreover, extended studies of the recently reported,[48] copper mediated borylation reactions of aryl halides were performed, including the screening of substrates and alkoxy bases as well as ligand-screening. Investigations were undertaken on the role of Cu-nanoparticles, which might be involved in this catalytic reaction. Furthermore, Cu-phosphine complexes were synthesized as precursors, but attempts to isolate Cu-boryl species which are intermediates in the proposed catalytic cycle[48] were unsuccessful, although ^{11}B NMR evidence for a Cu-boryl complex was obtained.

In the second part of this work, the alternative, Lewis-acidic diboron(4) compound bis(ethylene glycolato)diboron (B_2eg_2) was synthesized to compare its reactivity with the reactivity of other diboron(4) compounds (e.g. B_2neop_2, B_2cat_2, B_2pin_2 and $B_2(NMe_2)_4$). Therefore, reactions of B_2eg_2 with different Lewis-bases, such as NHCs and phosphines, were performed to investigate the possible formation of sp^2-sp^3 or sp^3-sp^3 adducts and ring-expansion reactions (RERs).

The aim was to obtain a better general insight into the reactivity of diboron(4) compounds with Lewis-bases because they are both used as reactants in transition metal-catalyzed and metal-free borylation reactions. Understanding the B–B bond activation process promoted by Lewis-bases provides a new perspective on the reaction pathways available for various borylation reactions.

1.1 CHAPTER ONE: Catalysis

1.1.1 Iron-catalyzed borylation reactions

Fe-catalyzed borylation reactions, using the diboron(4) compound B_2pin_2 and 1-bromohexane as a primary alkyl halide substrate and bromocyclohexane as a secondary alkyl halide substrate, were carried out and resulted in poor to moderate yields of boronate esters.

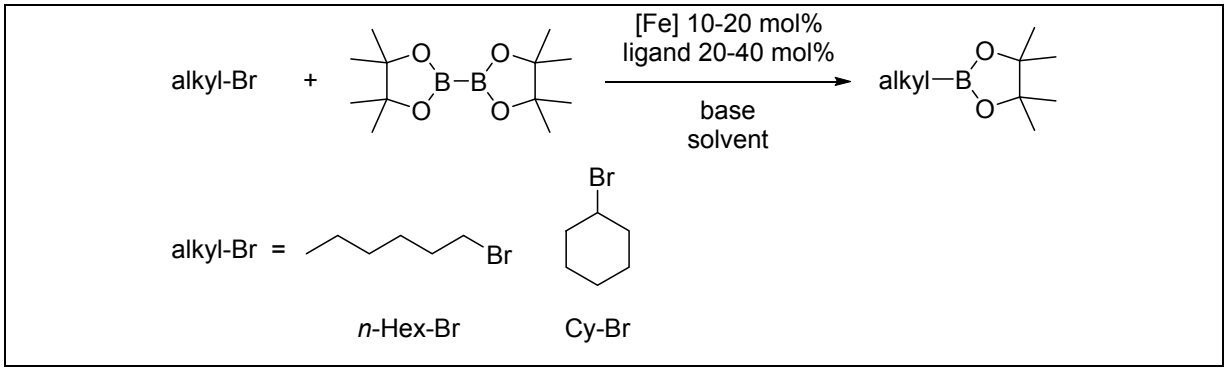

For the substrate 1-bromohexane, the best yield of 27% was obtained using $FeCl_3$ (20 mol%) as pre-catalyst, TEEDA (20 mol%) as ligand, LiO*t*Bu as base and THF as solvent with a reaction time of 24 h at 50 °C. Non-polar solvents such as toluene were not suitable for the reaction due to the very poor solubility of the reactants. For the substrate bromocyclohexane, the best yield of 76% was obtained using $FeCl_3$ (20 mol%) as pre-catalyst, TMEDA (40 mol%) as ligand, KOMe as base and slightly polar solvents such as MTBE or Et_2O with a reaction time of 96 h at 45 °C. Preliminary mechanistic studies showed the possible involvement of a radical process. Furthermore, the reactions with a radical initiator or a radical scavenger as addditives decreased the yield or shut down the reaction, respectively. Thus, a radical pathway in this borylation might be possible, but the mechanism of this catalysis is still not clear. However, at this stage, the performance of these Fe-catalyzed borylation reactions does not compete with other catalysts such as copper-, nickel- or zinc-based systems, and the use of highly reactive activating agents such as Grignard or *t*BuLi, as reported by Cook *et al.*[64] or Bedford *et al.*[65] is undesirable.

1.1.2 Copper-catalyzed borylation reactions

Cu-catalyzed borylation reactions of aryl halides with B_2pin_2 as diboron(4) compound were carried out.

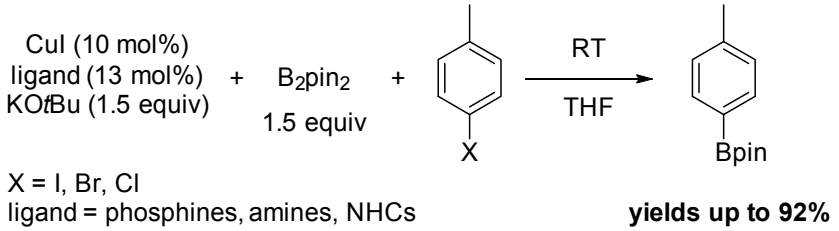

While the borylation reactions of 4-iodotoluene and 4-bromotoluene gave moderate to very good yields up to 92%, the substrate 4-chlorotoluene could not be borylated. The steric demand of the phosphine ligands used and their basicity played a key role in the performance of the reactions. The best results were obtained with the monodentate phosphines PCy_3 and $P(nBu)_3$. Using chelating phosphine ligands resulted in moderate yields and, in this case, a combination of electronic and steric (bite angle) effects might affect the performance. The best results using bidentate phosphines were obtained with dppe, dppbz and xantphos.

The screening of different alkoxy bases showed the importance of the solubility of the base itself or of the presumably formed base adduct of the diboron(4) compound B_2pin_2. $tBuO^-$ and MeO^- as base additives showed good to very good conversions of up to 100% of the starting material, whereas using LiOMe resulted in poor (12%) conversion due to its poor solubility. Carbonate bases resulted in trace conversions.

Furthermore, while screening other substrates, a side reaction for aryl halides containing a nitro-group, was identified as an elegant route for reductive (B_2pin_2 as reductant) N=N bond coupling to give azoxy-arenes and azo-arenes.

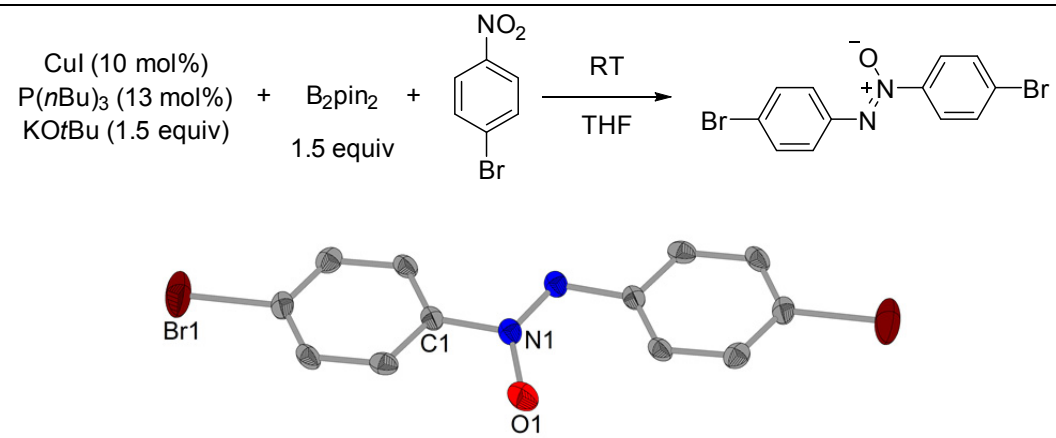

Investigations on Cu-nanoparticles and their impact on the catalysis did not provide any evidence for significant activity in the catalytic borylation of aryl halides under the specific conditions employed.

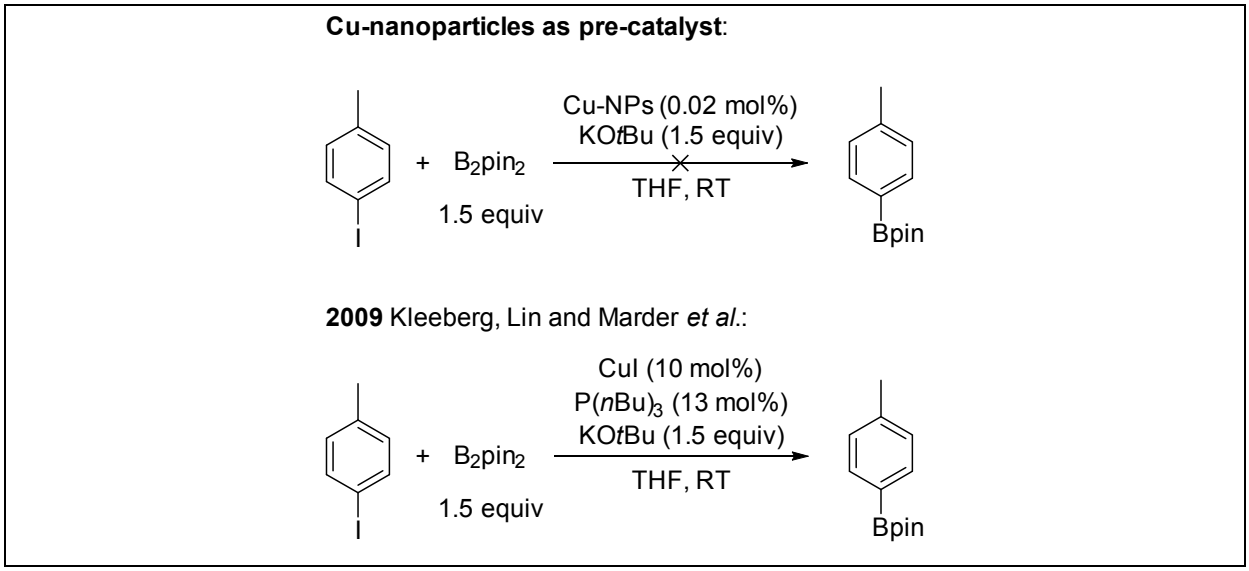

All attempts to isolate phosphine-Cu-boryl complexes, unfortunately, failed due to their very high reactivity, but spectroscopic evidence for a Cu-boryl species, observed in an *in situ* $^{11}B\{^1H\}$ NMR experiment from the reaction of $[(PCy_3)Cu(\mu\text{-}I_2)Cu(PCy_3)]$ with the anionic adduct $[K(18\text{-crown-}6)][(B_2pin_2)OMe]$, was a promising result.

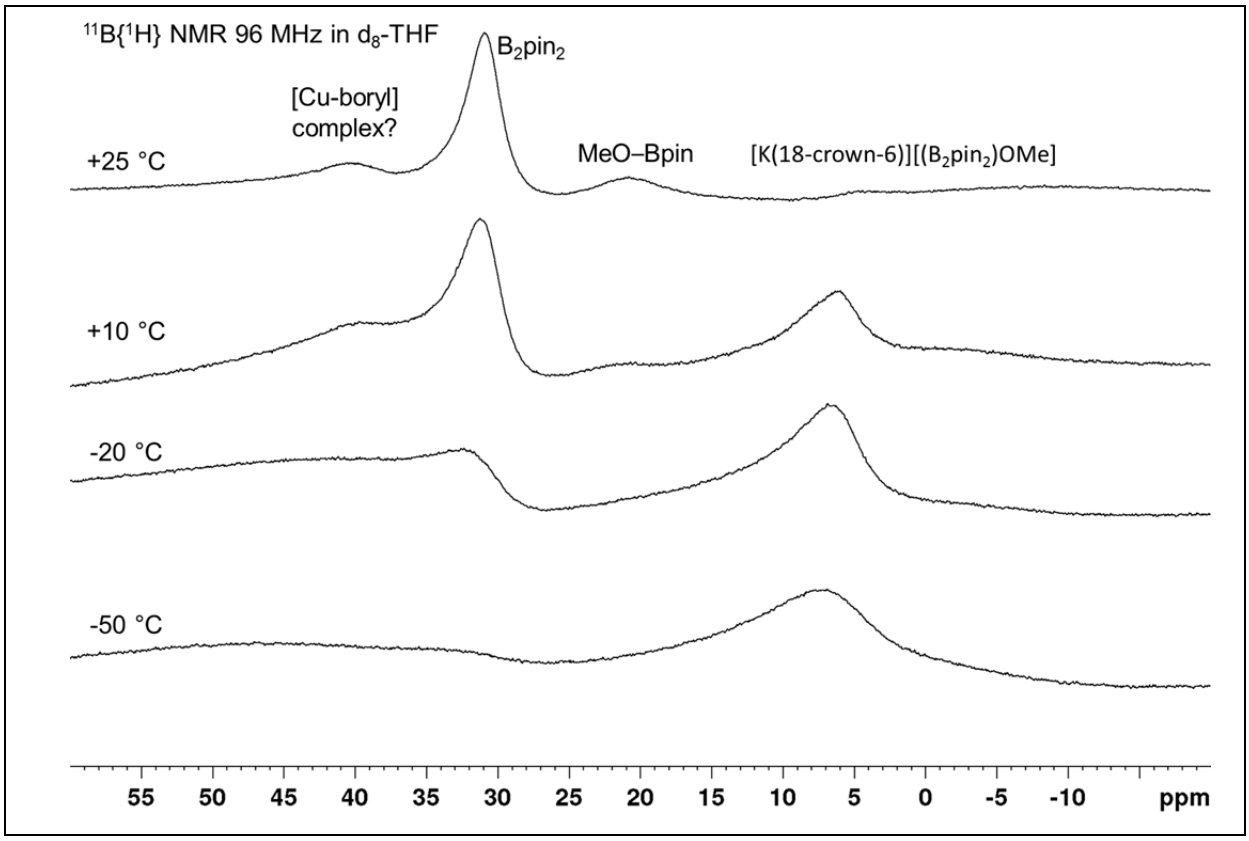

1.2 CHAPTER TWO: Reactivity of Bis(ethylene glycolato)diboron B_2eg_2

The reactions of B_2eg_2 with NHCs of different steric demand resulted in the formation of the corresponding mono- and bis-NHC adducts, as well as B–B and C–N bond activation at lower temperatures (-40 °C to -30 °C) than previously found for other diboron(4) reagents.

While for sterically less demanding NHCs (e.g. Me_2Im^{Me} or iPr_2Im), ring-expansion reactions were observed, for sterically more demanding NHCs (e.g. Mes_2Im or iPr_2Im^{Me}), only the mono- or bis-NHC adducts were formed, and for very bulky NHCs, only a weak interaction (for $Dipp_2Im$) or no significant evidence for any reactivity (for tBu_2Im) was observed.

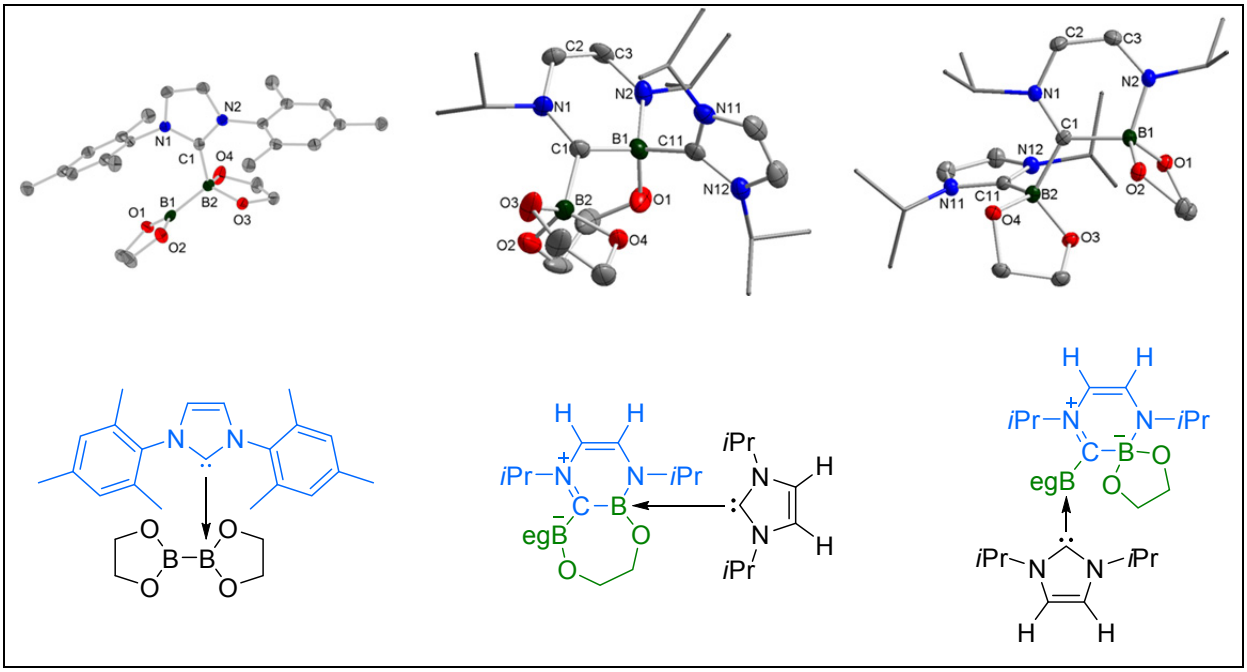

Thus, in general, smaller NHCs showed very high reactivity, which decreased with increasing steric demand of the NHC. However, in solution, dissociative dynamic processes were observed for the NHCs examined, in which the NHCs exchange between the two boron atoms of B_2eg_2.

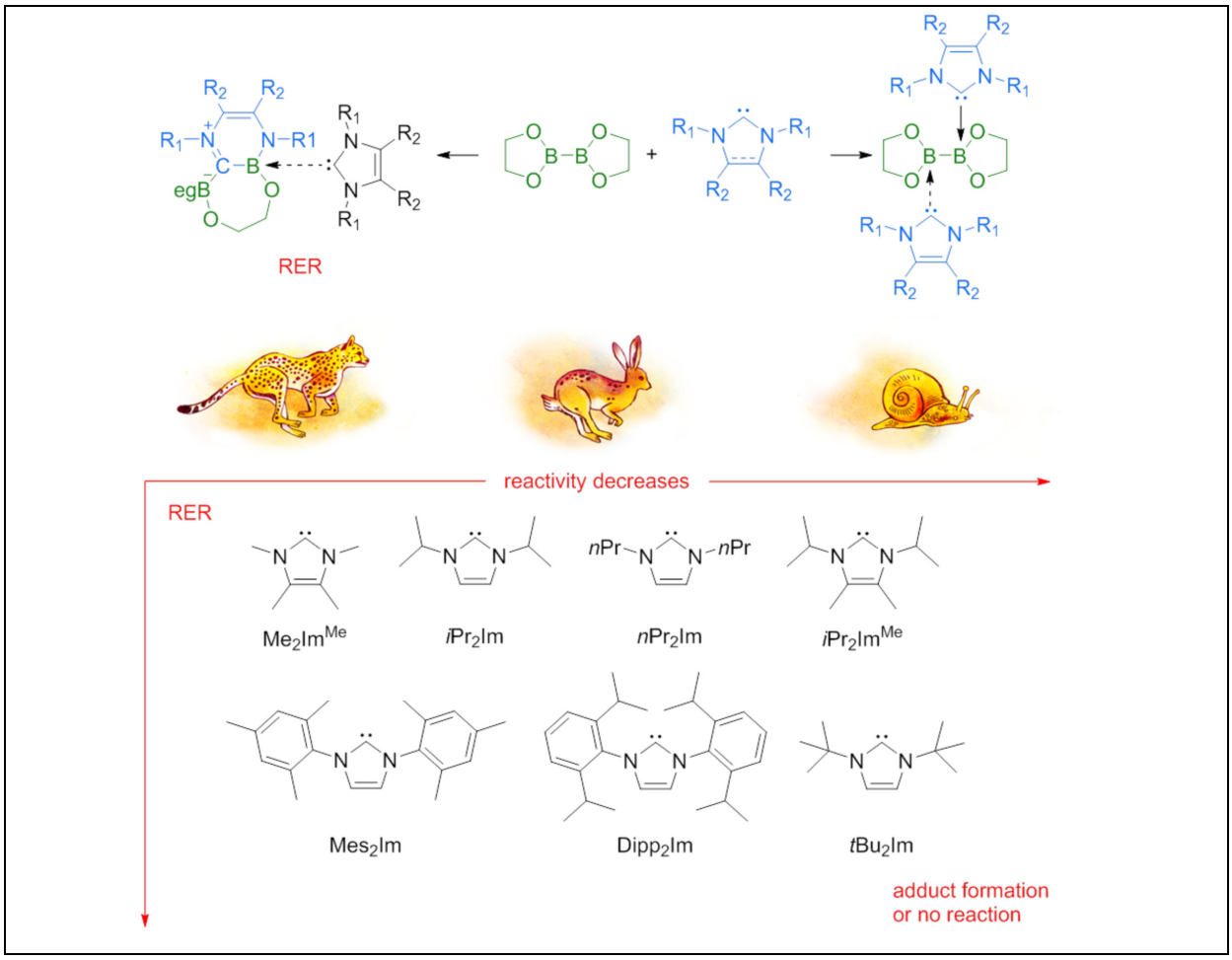

Moreover, the bis-NHC adduct B_2eg_3•(iPr$_2$Im)$_2$ was obtained as side product when reacting B_2eg_2 with the NHC iPr$_2$Im. A further detailed investigation of the reaction of the B_2eg_3 with the NHCs iPr$_2$Im and Me$_2$Im^{Me} resulted in the observation (HRMS) of a boronium $[L_2B(OR)_2]^+$ and a borenium $[LB(OR)_2]^+$ cation. Thus, the activation of bis-borates with NHCs and Lewis bases in general, might be a facile and simple route to access boron cations.

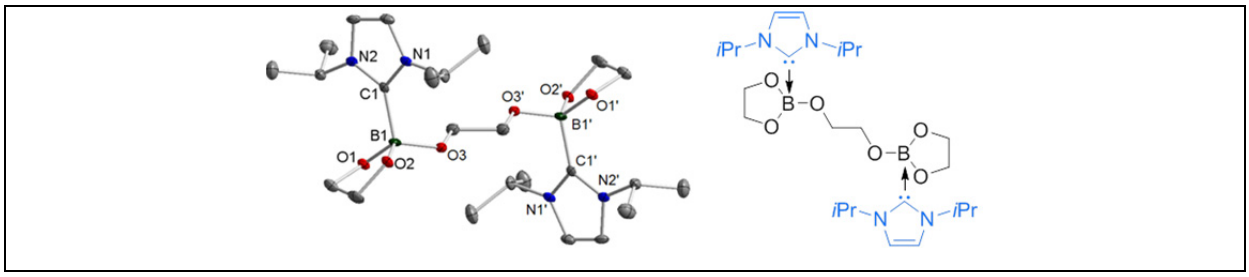

In situ NMR studies of the reactions of phosphines with B_2eg_2 did not support the previously reported[118,184] observations of phosphine adducts of diboron(4) compounds. No evidence for adduct formation was observed.

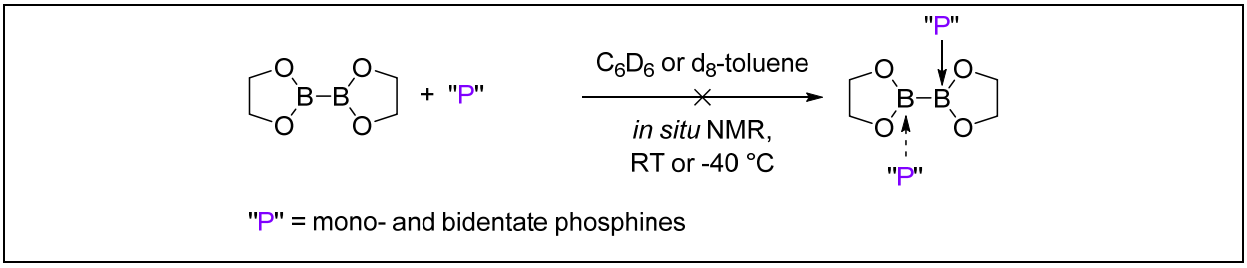

In addition, reactions of the diboron(4) compound $B_2(OMe)_4$ with NHCs of different steric demand were carried out for comparison, and were monitored by NMR spectroscopy.

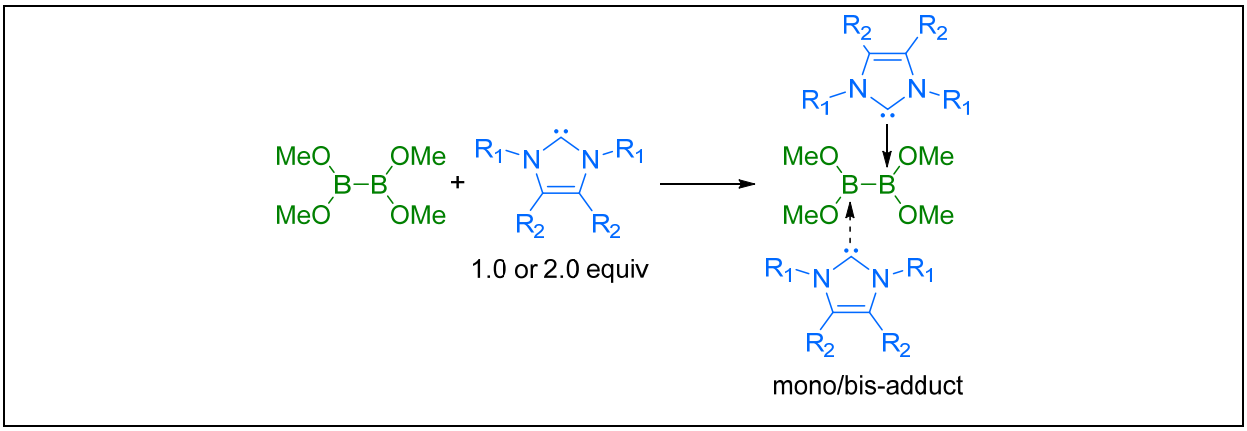

The resulting spectra showed evidence for the expected formation of mono- or bis-NHC adducts. Due to the higher flexibility of $B_2(OMe)_4$ compared to other diboron(4) compounds (e.g. B_2eg_2, B_2neop_2, B_2cat_2 and B_2pin_2) the *in situ* NMR spectra showed evidence for bis-adduct formation as well. While dependent on the steric demand of the NHC, a reactivity quite similar to that of B_2eg_2, and a dynamic exchange of the NHCs was observed, no evidence for a ring-expansion reaction was found for any NHC.

1.3 Conclusion

Organoboronate esters, especially arylboronates, are extremely useful reagents in organic synthesis, for example in Suzuki-Miyaura and other cross-coupling reactions. The boronate moiety can also be converted into virtually any functional group. Thus, the challenge is to develop new ways to prepare boronate esters.

Understanding B–B bond activation processes promoted by Lewis-bases provides a new perspective on the reaction pathways available for metal-catalyzed or metal-free borylation reactions.

2 Zusammenfassung

Im ersten Teil der vorliegenden Arbeit wurde das Potential eisenkatalysierter Borylierungsreaktionen von Alkylhalogeniden (Substrate) mit B_2pin_2 als Borylierungsreagenz untersucht. Weiterhin wurden detaillierte und intensive Untersuchungen zur literaturbekannten[48] kupferkatalysierten Borylierung von Arylhalogeniden durchgeführt, einschließlich eines Screenings von unterschiedlich funktionalisierten Substraten und diversen Alkoxybasen. Es wurde ebenfalls ein sehr umfangreiches Ligandenscreening durchgeführt. Des Weiteren wurden die mögliche Entstehung und der mögliche Einfluss von Kupfernanopartikeln auf die Borylierungsreaktion untersucht.

Um Intermediate der kupferkatalysierten Borylierung zu untersuchen wurden Kupferphosphankomplexe als Vorläufermoleküle für die Synthese von Kupferborylkomplexen hergestellt. Aufgrund der sehr hohen Reaktivität gelang es jedoch nicht, die entsprechenden Kupferborylkomplexe zu isolieren und zu charakterisieren. Es gelang allerdings in einem *in situ* $^{11}B\{^1H\}$-NMR-Experiment, ein $^{11}B\{^1H\}$-Signal zu detektieren, welches in dem zu erwartendem Bereich für einen Kupferborylkomplex lag und einen ersten Hinweis für die Bildung eines solchen Kupferborylkomplexes lieferte.

Im zweiten Teil der vorliegenden Arbeit wurde das alternative, lewissaure Diboran(4)-Derivat Bis(ethylenglykol)diboran (B_2eg_2) synthetisiert, um dessen Reaktivität mit der Reaktivität von anderen Diboran(4)-Verbindungen (z.B. B_2neop_2, B_2cat_2, B_2pin_2 und $B_2(NMe_2)_4$) zu vergleichen. Hierfür wurden Reaktionen von B_2eg_2 mit unterschiedlichen Lewisbasen wie NHCs und Phosphanliganden durchgeführt und die mögliche Bildung von sp^2-sp^3 oder sp^3-sp^3 hybridisierten mono- bzw. bis-Addukten sowie mögliche NHC-Ringerweiterungsreaktionen untersucht.

Im Allgemeinen wurde im zweiten Teil der Arbeit versucht ein besseres Verständnis über die Reaktivität von Diboran(4)-Verbindungen mit Lewisbasen zu erlangen, da beide als Reaktanten in übergangsmetallkatalysierten und metallfreien Borylierungsreaktionen verwendet werden. Dies macht es zwingend erforderlich die B–B-Bindungsaktivierung durch Lewisbasen zu verstehen, da hierdurch eine komplett neue Perspektive auf mögliche Reaktionspfade vieler Borylierungsreaktionen eröffnet wird.

2.1 CHAPTER ONE: Katalyse

2.1.1 Fe-katalysierte Borylierungsreaktionen

Es wurden Fe-katalysierte Borylierungsreaktionen mit B_2pin_2 als Borylierungsreagenz durchgeführt. Als Alkylhalogenid-Substrate wurden 1-Bromhexan (primäres Substrat) und Bromcyclohexan (sekundäres Substrat) verwendet und die entsprechenden Borsäureester als Produkte wurden in schlechten bis moderaten Ausbeuten erhalten.

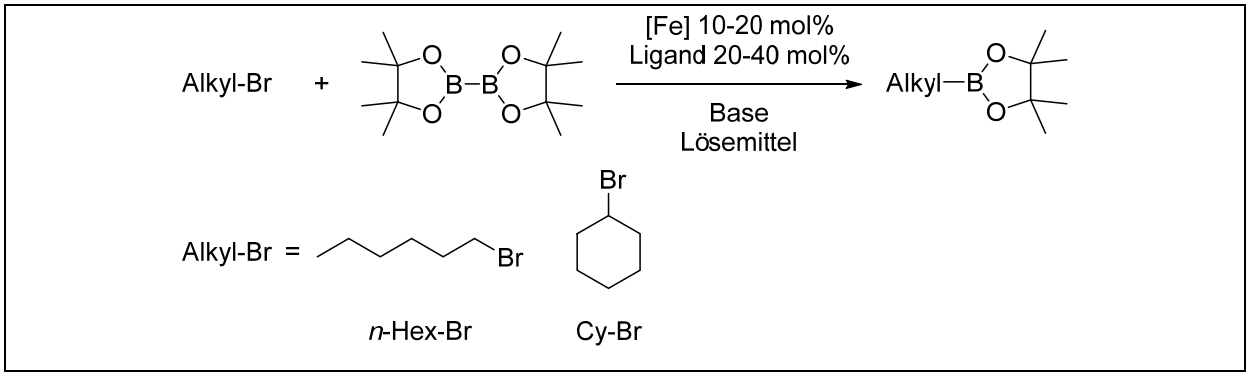

Die beste Ausbeute für das primäre Substrat 1-Bromhexan betrug 27% und wurde unter folgenden Reaktionsbedingungen erzielt: $FeCl_3$ (20 mol%) als Präkatalysator, TEEDA (20 mol%) als Ligand, LiO*t*Bu als Base und THF als Lösemittel, 24 h Reaktionsdauer bei 50 °C. Aufgrund der schlechten Löslichkeit der Reaktanten in nicht polaren Lösemitteln (z.B. Toluol) waren letztere für die Reaktion nicht geeignet.

Die beste Ausbeute für das sekundäre Substrat Bromcyclohexan betrug 76% und wurde unter folgenden Reaktionsbedingungen erzielt: $FeCl_3$ (20 mol%) als Präkatalysator, TMEDA (40 mol%) als Ligand, KOMe als Base, leicht polare Lösemittel wie Et_2O oder MTBE und 96 h Reaktionsdauer bei 45 °C.

Erste mechanistische Untersuchungen ergaben die mögliche Beteiligung von Radikalen im Borylierungsprozess. Weiterhin wurden Reaktionen mit einem Radikalstarter und Reaktionen mit einem Abfangreagenz durchgeführt, welche beide zu einer schlechteren Ausbeute oder keiner Umsetzung führten. Daher kann ein Radikalmechanismus nicht ausgeschlossen werden. Der genaue Mechanismus der eisenkatalysierten Borylierung ist allerdings weiterhin unklar.

Des Weiteren kann die eisenkatalysierte Borylierung in diesem Stadium nicht mit anderen Katalysatoren auf Kupfer-, Nickel- oder Zink-Basis konkurrieren. Eine Aktivierung durch hochreaktive Reagenzien (z.B. Grignard-Verbindungen oder

*t*BuLi), wie kürzlich von Cook *et al.*[64] und Bedford *et al.*[65] veröffentlicht, ist nicht wünschenswert.

2.1.2 Cu-katalysierte Borylierungsreaktionen

Es wurden Cu-katalysierte Borylierungsreaktionen von Arylhalogeniden mit B_2pin_2 als Borylierungsreagenz durchgeführt.

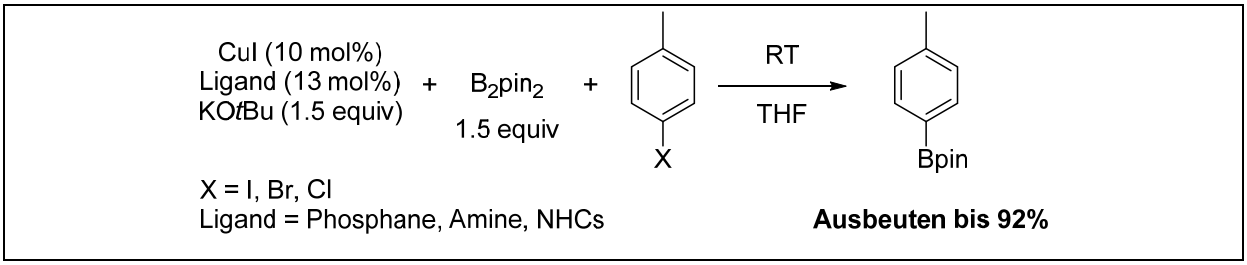

Die Borylierungsreaktionen von 4-Iodtoluol und 4-Bromtoluol erzielten moderate bis sehr gute Ausbeuten von 92%. Jedoch konnte 4-Chlortoluol unter den angewendeten Reaktionsbedingungen nicht boryliert werden.

Der sterische Anspruch der angewandten Phosphanliganden, sowie deren unterschiedliche Basizität hatten unterschiedliche Auswirkung auf die Ausbeute. Die besten Ausbeuten konnten mit den Phosphanliganden PCy_3 und $P(nBu)_3$ erlangt werden. Die Verwendung von chelatisierenden Phosphanliganden resultierte in moderaten Ausbeuten, wobei die besten Ergebnisse mit den Chelatliganden dppe, dppbz und xantphos erzielt wurden.

Das Screening der Alkoxybasen zeigte, wie sich die Löslichkeit der Base auf die Umsetzung des Substrates auswirkte. Die Verwendung von $tBuO^-$ und MeO^- Basen ergab gute bis sehr gute Umsetzungen bis zu 100%. Hingegen konnte mit der Base LiOMe nur ein schlechter Umsatz von 12% erzielt werden, was auf die schlechte Löslichkeit der Base zurückzuführen ist. Bei Verwendung von CO_3^{2-} Basen konnte kein Umsatz des Substrates erzielt werden.

Weiterhin wurde eine Nebenreaktion aufgeklärt, durch die es nicht möglich war, Nitro-substituierte Arylhalogenide Cu-katalysiert zu borylieren. Gegenüber Nitrosubstituenten fungiert B_2pin_2 als Reduktant und reduziert die Nitrogruppe des Substrates, sodass dann eine N=N Kupplungsreaktion zu Azoxyarenen stattfindet.

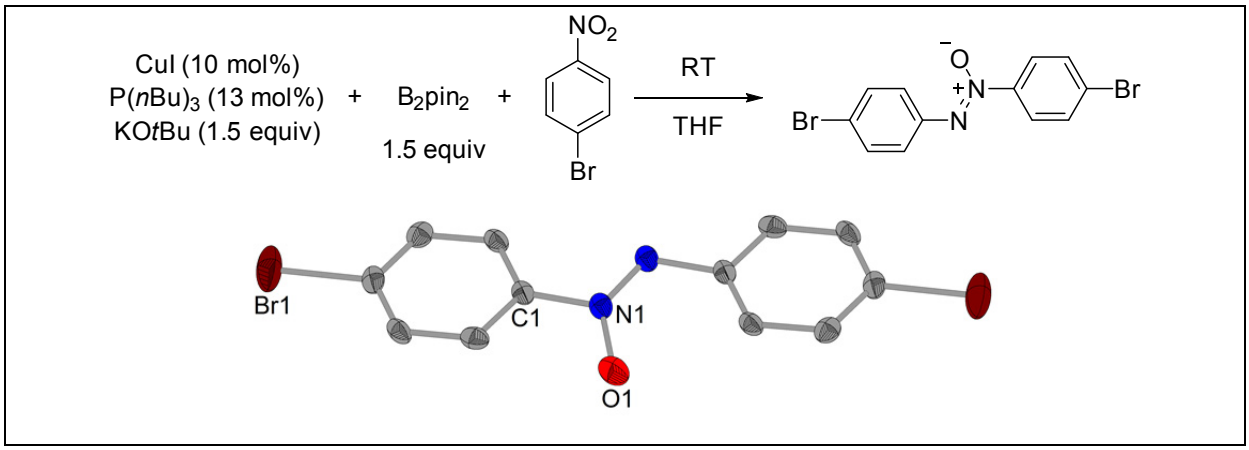

Untersuchungen von Cu-Nanopartikeln und deren Einfluss auf die Cu-katalysierte Borylierungsreaktion resultierte in keiner Umsetzung des Substrates zum entsprechenden Organoboronsäureester unter den angewandten Standardbedingungen.

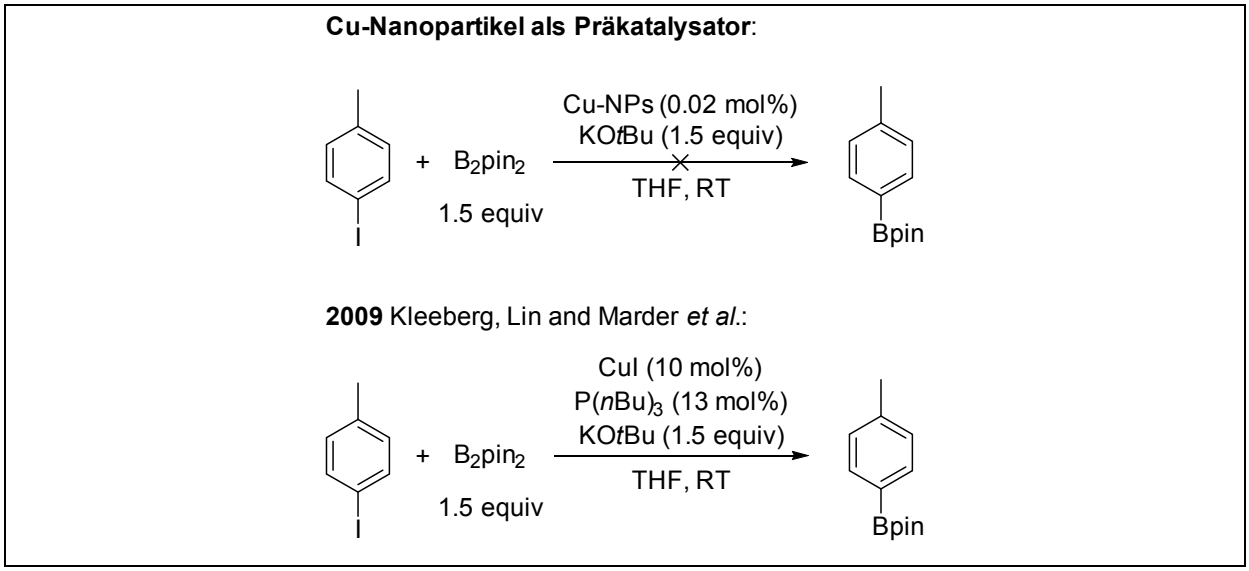

Aufgrund der sehr hohen Reaktivität scheiterten alle Versuche, Kupferborykomplexe zu isolieren und zu charakterisieren, jedoch konnte bei der Reaktion des Kupferphosphankomplexes $[(PCy_3)Cu(\mu\text{-}I_2)Cu(PCy_3)]$ mit dem anionischen Addukt $[K(18\text{-Krone-}6)][(B_2pin_2)OMe]$ per *in situ* $^{11}B\{^1H\}$-NMR-Experiment die Bildung einer Kupferborylspezies beobachtet werden.

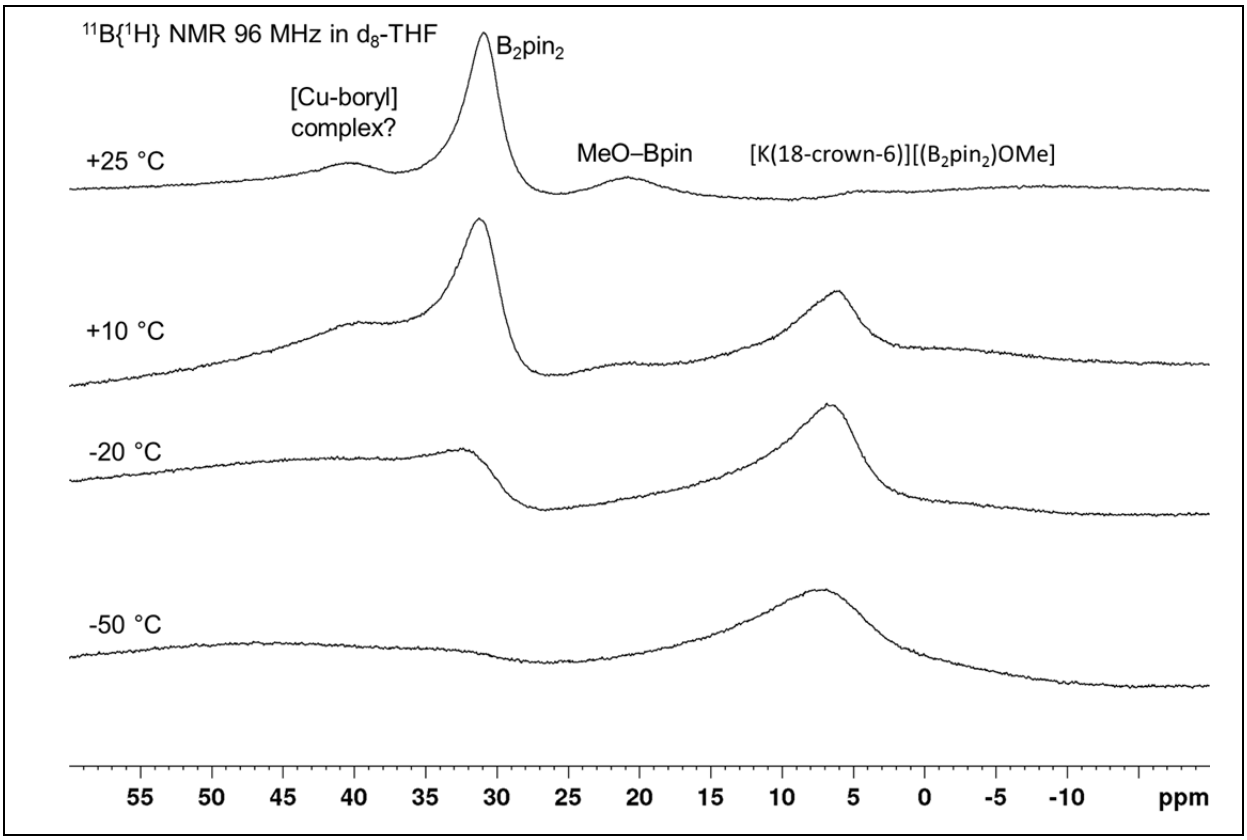
$^{11}B\{^1H\}$ NMR 96 MHz in d_8-THF
B_2pin_2
[Cu-boryl]
complex?
MeO–Bpin
[K(18-crown-6)][(B_2pin_2)OMe]
+25 °C
+10 °C
-20 °C
-50 °C
55 50 45 40 35 30 25 20 15 10 5 0 -5 -10 ppm

2.2 CHAPTER TWO: Reaktivität von Bis(ethylenglykol)diboran B_2eg_2

Die durchgeführten Reaktionen von B_2eg_2 mit NHCs unterschiedlichen sterischen Anspruchs führten zur Bildung der entsprechenden mono- und bis-NHC Addukte sowie zur B–B- und C–N-Bindungsaktivierung bei niedrigeren Temperaturen (-40 °C bis -30 °C), als für andere Diboran(4)-Verbindungen beobachtet wurde.

Für NHCs mit geringem sterischen Anspruch (z.B. Me_2Im^{Me} oder iPr_2Im) wurden NHC-Ringöffnungsreaktionen beobachtet, für NHCs mit sterisch größerem Anspruch (z.B. Mes_2Im oder iPr_2Im^{Me}) allerdings die korrespondierenden mono- und bis-NHC-Addukte. Für sehr sperrige NHCs wurden nur schwache Wechselwirkungen (für $Dipp_2Im$) mit B_2eg_2 oder keine signifikante Reaktivität (für tBu_2Im) beobachtet.

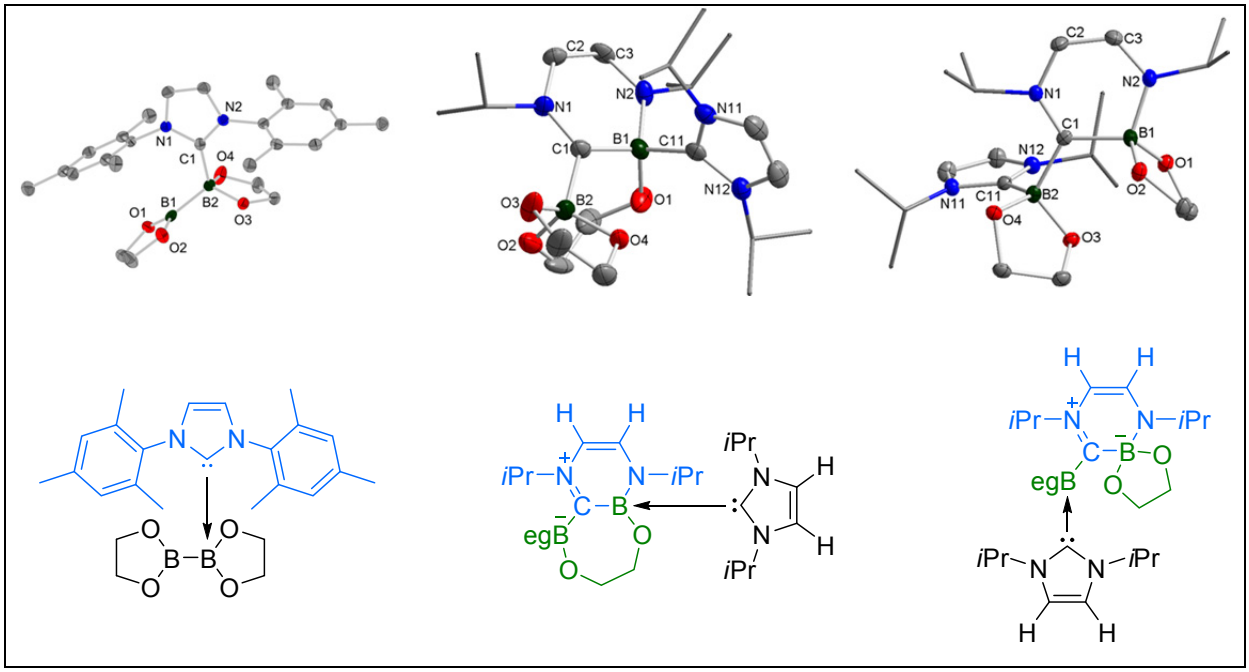

Im Allgemeinen zeigten kleinere NHCs eine sehr hohe Reaktivität, welche mit zunehmender Sterik der NHCs geringer wurde. Darüber hinaus wurden in Lösung dissoziative, dynamische Prozesse beobachtet, da es zum Austausch der NHCs zwischen den beiden Boratomen von B_2eg_2 kam.

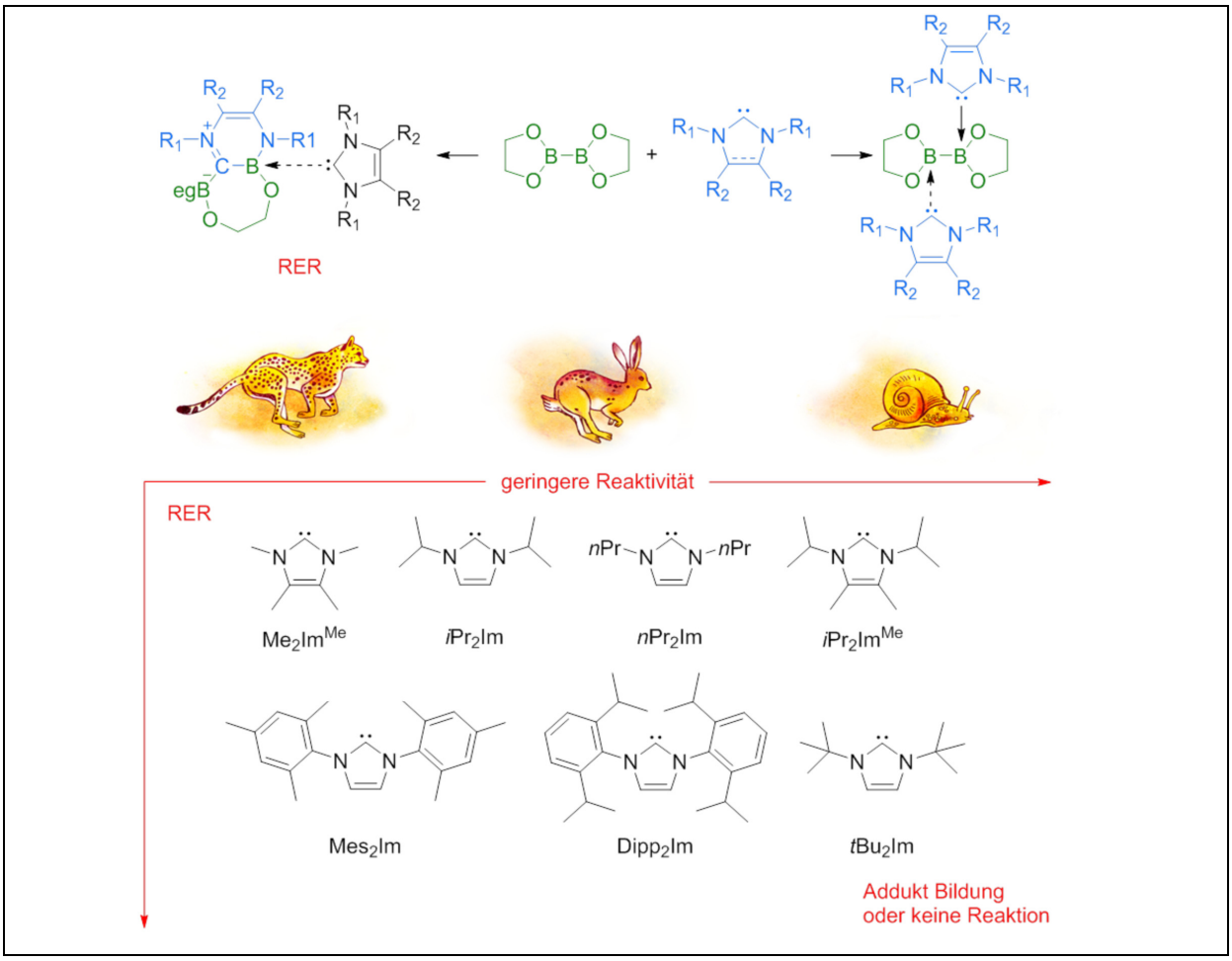

Darüber hinaus konnte das bis-NHC-Addukt B_2eg_3•(iPr$_2$Im)$_2$ als Nebenprodukt aus der Reaktion von B_2eg_2 mit dem NHC iPr$_2$Im erhalten werden. Weitere detaillierte Untersuchungen der Reaktion von B_2eg_3 mit den NHCs iPr$_2$Im und Me$_2$Im^{Me} führten zu der Beobachtung von Boronium- $[L_2B(OR)_2]^+$ und Borenium- $[LB(OR)_2]^+$ Kationen. Im Allgemeinen stellt dieses Resultat eine potenzielle Synthese von Borkationen durch Aktivierung von Bisboraten duch NHCs bzw. Lewisbasen dar.

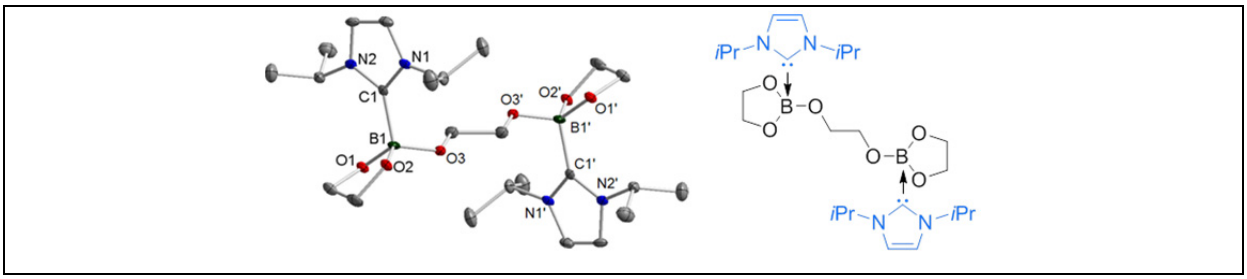

In situ NMR-Experimente der Reaktionen von Phosphanen mit B_2eg_2 konnten keinen Beiweis für die Bildung von Phosphanaddukten mit B_2eg_2 liefern und somit auch nicht früher beobachtete und veröffentlichte Ergebnisse[118,184] unterstützen bzw. bestätigen.

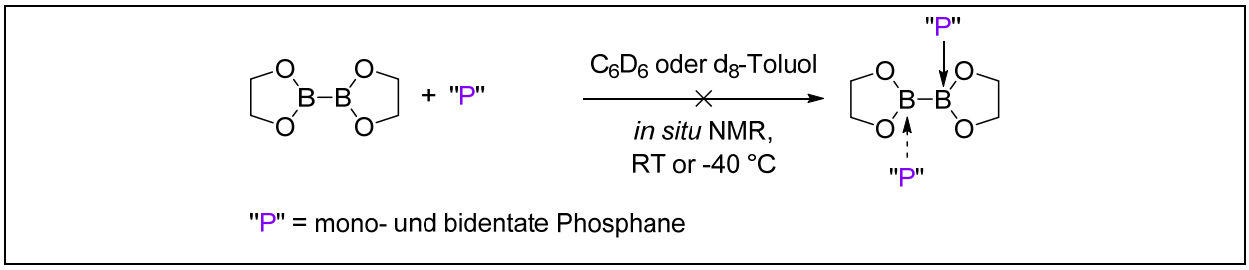

Weiterhin wurden Reaktionen der Diboran(4)-Verbindung $B_2(OMe)_4$ mit NHCs unterschiedlichen sterischen Anspruchs durchgeführt und mit *in situ* NMR-Spektroskopie verfolgt.

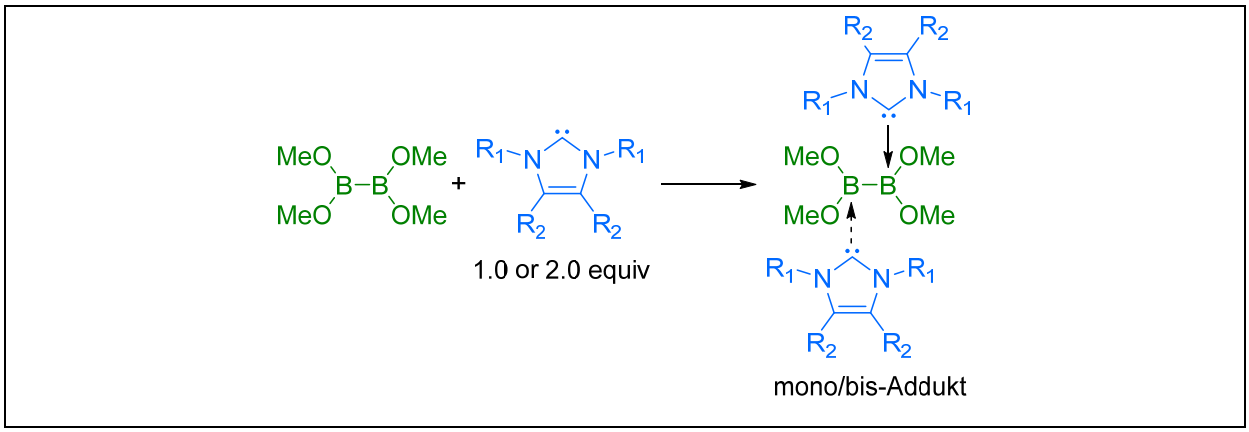

Die resultierenden Spektren zeigten die Bildung der korrespondierenden mono- und bis-NHC-Addukte. Durch die flexiblere Struktur von $B_2(OMe)_4$ im Vergleich zu anderen Diboran(4)-Verbindungen (z.B. B_2eg_2, B_2neop_2, B_2cat_2 und B_2pin_2) konnten in den *in situ* NMR-Spektren Signale für bis-NHC-Addukte beobachtet werden. In Abhängigkeit des sterischen Anspruchs des NHCs wurde eine ähnliche Reaktivität wie für B_2eg_2 beobachtet, jedoch keine Ringöffnungs-Reaktionen.

2.3 Fazit

Organoboronsäureester stellen eine wichtige Substanzklasse für die organische Synthese wie z.B. für Suziki-Miyaura Kreuzkupplungsreaktionen dar, da die Boronsäureester prinzipiell in jede andere funktionelle Gruppe überführt werden

können. Deshalb ist es von großer Bedeutung neue Synthesewege zu Organoboronsäureestern zu entwickeln.

Es ist wichtig, ein besseres Verständnis der B–B-Bindungsaktivierung von Diboran(4)-Verbindungen durch Lewisbasen zu erlangen. Hierdurch wird eine komplett neue Perspektive auf die Reaktionswege metallkatalysierter oder metallfreier Borylierungsreaktionen eröffnet.

CHAPTER FOUR

-

Experimental

“My information on that conference is second-hand, but the key conversation at the conference was quoted as follows: • Malta group: “We haven’t been able to stabilize the diborane-acetylene product. How do you people do it?” • Niagara Falls group: “We couldn’t. Our stuff wasn’t stable either.” • Malta group: “Good grief! Why didn’t you tell us?” • Niagara Falls group: “You never asked.” Instances like this, of course, account for the credibility gap that sometimes exists between chemists and chemical engineers.”

Andrew Dequasie, The Green Flame

CHAPTER FOUR
-
Experimental

1 General considerations

1.1 Experiment preparation

Unless otherwise noted, all manipulations were performed using standard Schlenk or glovebox techniques under dry argon (99.999%, Linde). An Innovative Technology Inc. glovebox was used under argon (99.999% Linde). HPLC grade solvents (Sigma Aldrich) were supplied argon-saturated and dried using an Innovative Technology Inc. Pure-Solv 400 Solvent Purification System, and further deoxygenated by using the freeze-pump-thaw method. C_6D_6, CD_2Cl_2, $CDCl_3$, and d_8-toluene were purchased from Euriso-Top GmbH or Sigma Aldrich. C_6D_6 and was dried and distilled over potassium; d_8-toluene was dried and distilled over sodium, and $CDCl_3$ and CD_2Cl_2 were dried and distilled over CaH_2. Ethylene glycol was dried and distilled over anhydrous $MgSO_4$. All other reagents were purchased from Alfa Aesar, ABCR, Acros or Sigma Aldrich, and were checked for purity by GC-MS and/or ^{1}H NMR spectroscopy and used as received. Commercially available 99.99% (trace metals basis) $FeCl_2$ and $FeCl_3$, 95% KOMe (Sigma Aldrich), 99% (trace metals basis) Cs_2CO_3 and 99.9% (trace metals basis) LiO*t*Bu (Alfa Aesar) were stored under argon and used as received. KO*t*Bu (Sigma Aldrich) was dried and sublimed under vacuum and then stored under argon prior to use. B_2pin_2 and $B_2(NMe_2)_4$ were kindly donated by AllylChem Co. Ltd. (Dalian, China). Diverse *N*-heterocyclic carbenes were synthesized according the literature[185-189] and kindly provided by the group of Prof. Dr. Udo Radius. $B_2(OMe)_4$ was synthesized according the literature[19] and kindly provided by the group of Prof. Dr. Holger Braunschweig.

1.2 Microwave reactions

Microwave reactions were performed in septum-containing, crimp-capped, sealed vials in a Biotage® Initiator$^+$ reactor. The wattage was automatically adjusted to maintain the desired temperature for the desired period of time.

1.3 Thin Layer Chromatography (TLC)

Commercially available, precoated TLC plates (Polygram© Sil G/UV_{254}) were purchased from Machery-Nagel.

1.4 Column chromatography

Column chromatography was carried out in air using silica gel (Kieselgel 60, 0.063-0.200 mm) obtained from Merck. Flash chromatography was performed with a Biotage® Isolera Four system equipped with HP-Sil or KP-Sil cartridges and a diode array UV-vis detector. Seperation occured by running a solvent gradient in automatic mode. The solvent was removed on a rotary evaporator under vacuum at a maximum temperature of 40 °C.

1.5 Nuclear Magnetic Resonance spectroscopy (NMR)

All NMR spectra were recorded at 298 K or at 233 K for the low temperature experiments and at 295 K for solid state NMR, using Bruker Avance 200 (^{1}H: 199.92 MHz; ^{11}B{^{1}H}: 64.14 MHz; ^{31}P{^{1}H}: 80.93 MHz), Bruker DRX-300 (^{1}H: 300.18 MHz; ^{11}B{^{1}H}: 96.31 MHz; ^{13}C{^{1}H}: 75.48 MHz; ^{31}P{^{1}H}: 121.51 MHz); Bruker Avance DPX-400 (^{1}H: 400.39 MHz; ^{11}B{^{1}H}: 128.46 MHz) and Bruker Avance 500 (^{1}H: 500.13 MHz; ^{11}B{^{1}H}: 160.46 MHz; ^{13}C{^{1}H}: 125.75 MHz; ^{15}N: 50.69 MHz; ^{31}P{^{1}H}: 202.45 MHz) spectrometers. ^{1}H NMR chemical shifts were referenced *via* residual proton resonances of the corresponding deuterated solvent ($CDCl_3$: 7.26 ppm; CD_2Cl_2: 5.32 ppm; C_6D_6: 7.16 ppm and d_8-toluene: 2.08 ppm) whereas ^{13}C NMR spectra are reported relative to TMS using the carbon signals of the deuterated solvent ($CDCl_3$: 77.16 ppm; CD_2Cl_2: 53.84 ppm; C_6D_6: 128.06 ppm and d_8-toluene: 20.43 ppm). ^{11}B NMR chemical shifts are reported relative to BF_3•Et_2O as external standard and ^{15}N NMR chemical shifts were obtained by ^{15}N,^{1}H correlation experiments, and referenced to nitromethane.

The solid-state magic-angle spinning (MAS) NMR spectra were recorded using a Bruker DSX-400 solid state spectrometer (^{11}B: 128.38 MHz; ^{13}C: 100.61 MHz; ^{15}N: 40.56 MHz; ZrO_2 rotor 4 mm OD). . The ^{11}B solid-state spectra were simulated with the software package SOLA.[190]

1.6 High-Resolution Mass Spectrometry (HRMS)

The high resolution mass analyses were measured on a Thermo Scientific Exactive Plus mass spectrometer, equipped with an Orbitrap Mass Analyzer. Measurements were accomplished using an ASAP/APCI source with a corona needle and carrier-gas (N_2) temperature of 400 °C and 350 °C or 250 °C, respectively.

1.7 Gas Chromatography (GC-MS)

GC-MS analyses were performed using an Agilent 7890A gas chromatograph (column: HP-5MS, 30 m, Ø 0.25 mm, film 0.25 µm; injector: 250 °C; oven: 40 °C (2 min), 40 °C to 250 °C (20 °C min^{-1}), 280 °C (5 min); carrier gas: He (1.6 mL min^{-1})) equipped with an Agilent 5975C inert mass selective detector (MSD) operating in EI mode and an Agilent 7693A automatic liquid handling system (ALS) functioning as autosampler/injector; or a Varian (Bruker) gas chromatograph GC450 (column: DB-5MS, 30 m, Ø 0.25 mm, film 0.25 µm; injector: 220 °C; oven: 40 °C (2 min), 40 °C to 280 °C (20 °C min^{-1}); carrier gas: He (1.0 mL min^{-1})) equipped with a Varian (Bruker) 320 SQ-MS, single quad mass spectrometer operating in EI mode.

1.8 Elemental analysis (CHN)

Elemental analysis were performed in the microanalytical laboratory of the Institute of Inorganic Chemistry (University of Würzburg) with an Elementar vario micro cube.

1.9 Quantitation and determination of the response factors

Gas chromatography in combination with a mass spectrometer is a very useful tool for quantitation and enables both high reaction throughput and *in situ* evaluation. This method requires the determination of the compound-specific response factors (RF) against an internal standard. The real ratios of compounds of an analyte can be different from their raw relative peak integrations, because of the different chemical nature of the specific compounds and their resulting ionization. This means a prepared mixture with compound A and B with the ratio 1:1 can show an integration

area ratio of 1:5, for example. The relative ratios depend on the (unknown) concentration of the compounds in the reaction mixture, whereas the concentration of the internal standard has to be known and constant. This enables the calibration for a specific range of concentrations. The concentration of the reaction mixtures to be analyzed has to be in the range of the concentration of the calibration run, otherwise the error would increase if the concentration is out of range (too high or too low).

The quantitation was performed using the internal standard method, and the compounds of interest were calibrated against biphenyl or *n*-dodecane as inert internal standard. Examples for a calibration run, with three different concentrations for the compounds of interest, against a constant concentration of internal standard are shown in Figure 80 to Figure 82. For the calibration, five samples of each stock solution were measured.

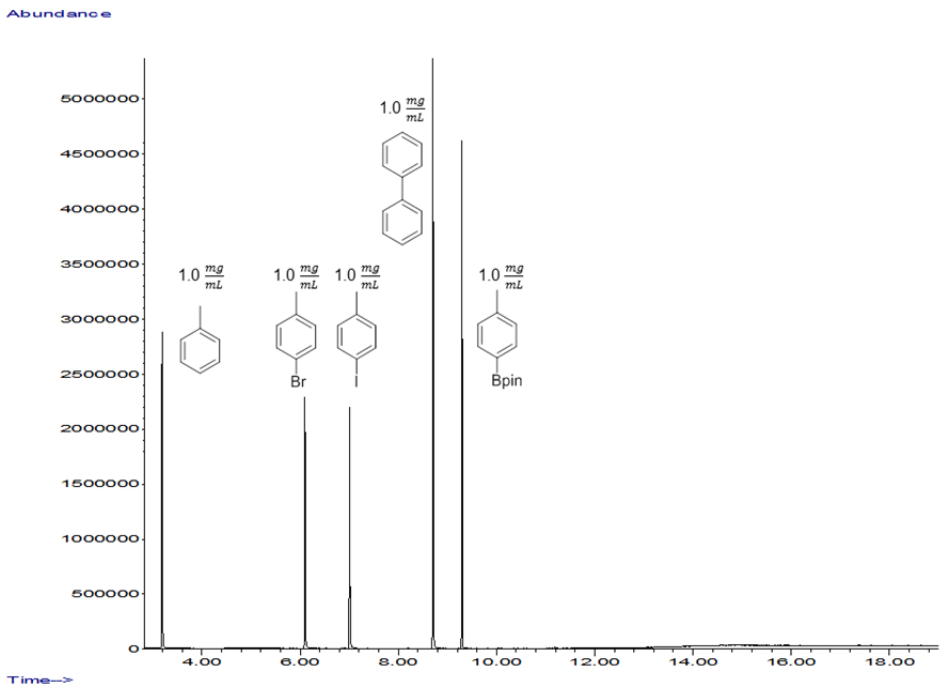

Figure 80. Total ion chromatogram of a stock solution (1.0 $\frac{mg}{mL}$) of toluene, 4-bromotoluene, 4-iodo-toluene, 4-(4,4,5,5-tetramethyl-1,3,2-dioxaborolan-2-yl)-toluene and biphenyl (1.0 $\frac{mg}{mL}$) as internal standard.

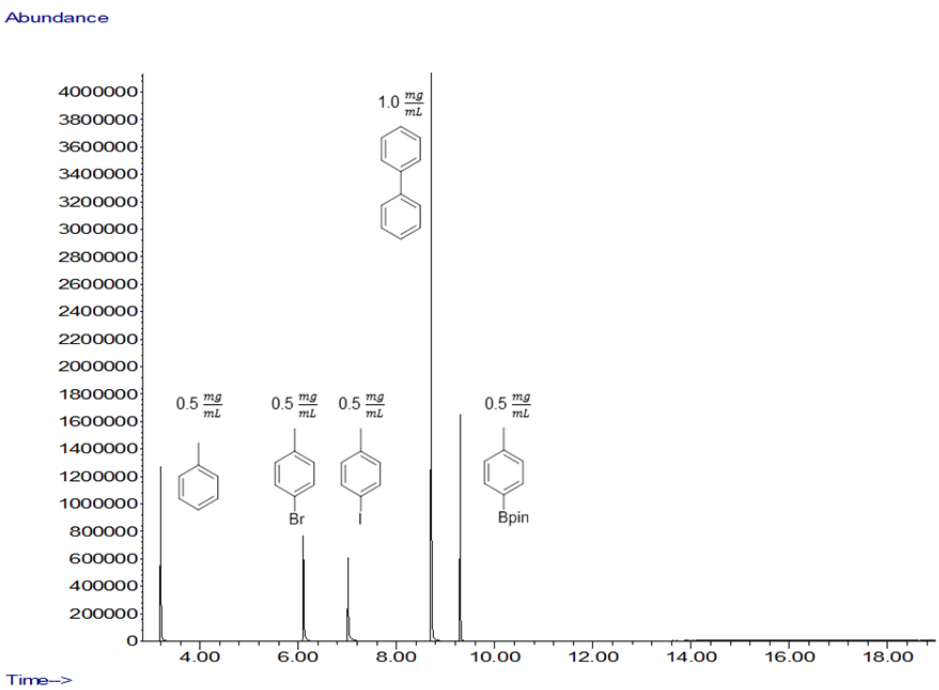

Figure 81. Total ion chromatogram of a stock solution (0.5 $\frac{mg}{mL}$) of toluene, 4-bromotoluene, 4-iodo-toluene, 4-(4,4,5,5-tetramethyl-1,3,2-dioxaborolan-2-yl)-toluene and biphenyl (0.5 $\frac{mg}{mL}$) as internal standard.

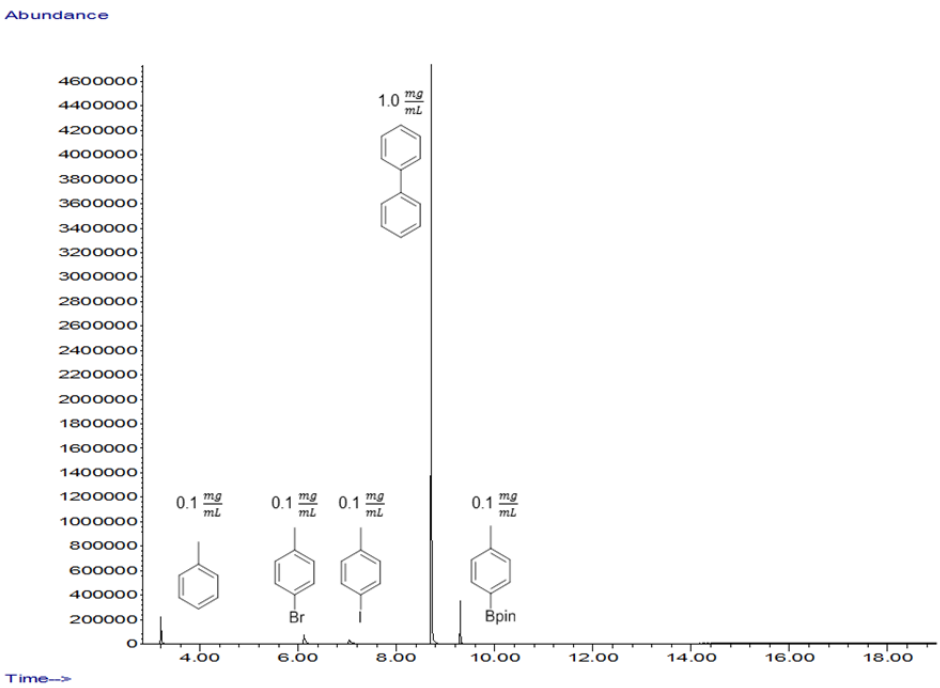

Figure 82. Total ion chromatogram of a stock solution (0.1 $\frac{mg}{mL}$) of toluene, 4-bromotoluene, 4-iodo-toluene, 4-(4,4,5,5-tetramethyl-1,3,2-dioxaborolan-2-yl)-toluene and biphenyl (1.0 $\frac{mg}{mL}$) as internal standard.

The compound-specific response factors (RF), were calculated according to Equation 1 for each stock solution concentration (0.1 $\frac{mg}{mL}$, 0.5 $\frac{mg}{mL}$, 1.0 $\frac{mg}{mL}$) of the calibration runs. The amount of a specific compound of an analyte was calculated according to Equation 2, with the average value of the compound-specific response factor. Examples of calculated response factors of a calibration run are shown in Table 19 to Table 22. The calibration always was carried out directly before a batch of samples was measured.

Equation 1. Calculation of the response factor of a specific compound.

$$RF_{\text{specific compound}} = \frac{\text{area}_{\text{internal standard}} \times \text{amount}_{\text{specific compound}}}{\text{amount}_{\text{internal standard}} \times \text{area}_{\text{specific compound}}}$$

Equation 2. Calculation of the amount of a specific compound in an analyte.

$$\text{amount}_{\text{specific compound}} = \frac{\text{amount}_{\text{internal standard}} \times \text{area}_{\text{specific compound}} \times RF_{\text{specific compound}}}{\text{area}_{\text{internal standard}}}$$

Table 19. Response factor for toluene against biphenyl as internal standard.

RF (toluene)			
	stock solution concentration [mg/mL]		
measurement no.	**0.1**	**0.5**	**1.0**
1	1.8014	1.7494	1.7179
2	1.8542	1.7586	1.6985
3	1.8606	1.7783	1.6809
4	1.8350	1.7704	1.6812
5	1.8880	1.7692	1.6751
total average RF			**1.7679**

Table 20. Response factor for 4-bromotoluene against biphenyl as internal standard.

RF (4-bromotoluene)			
	stock solution concentration [mg/mL]		
measurement no.	**0.1**	**0.5**	**1.0**
1	2.4840	2.2670	2.1302
2	2.5751	2.2746	2.1494
3	2.5346	2.2769	2.1483
4	2.5808	2.2832	2.1327
5	2.5502	2.2582	2.1602
total average RF			**2.1442**

Table 21. Response factor for 4-iodotoluene against biphenyl as internal standard.

RF (4-iodotoluene)			
	stock solution calibration [mg/mL]		
measurement no.	**0.1**	**0.5**	**1.0**
1	3.3605	2.6281	2.2861
2	3.3410	2.6389	2.3010
3	3.7152	2.6602	2.3030
4	3.4506	2.7116	2.2916
5	3.4079	2.6810	2.3014
total average RF			**2.2966**

Table 22. Response factor for tolyl-Bpin against biphenyl as internal standard.

RF (tolyl-Bpin)			
	stock solution concentration [mg/mL]		
measurement no.	**0.1**	**0.5**	**1.0**
1	1.4120	1.3907	1.2177
2	1.4273	1.3878	1.2374
3	1.5033	1.3750	1.2544
4	1.5100	1.3977	1.2626
5	1.5582	1.3965	1.2718
total average RF			**1.2488**

2 Experimental considerations

2.1 Synthesis of primary and secondary alkyl boronates

2.1.1 Synthesis of 2-hexyl-4,4,5,5-tetramethyl-1,3,2-dioxaborolane

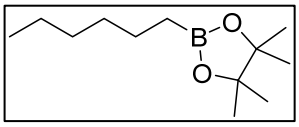

According to the literature,[191,192] 1-bromohexane (**69**, 990 µL, 7.05 mmol, 1.5 equiv) was dissolved in THF (10 mL), and the resulting solution was added dropwise to Mg (217 mg, 8.93 mmol, 1.9 equiv) and then stirred and heated under reflux for 1 h. The solution was filtered and transferred to a dropping funnel *via* cannula and then added dropwise, at RT within 5 min, to HBpin (**23**, 683 µL, 4.70 mmol, 1.0 equiv) in THF (2 mL). The reaction mixture was stirred for 1 h at RT. For work up, the mixture was cooled to 0 °C (ice bath) and acidified with 3M HCl (3 mL), then stirred for 10 min at 0 °C and a further 30 min at RT (CAUTION: HYDROGEN EVOLUTION!). After extraction with Et_2O (3 x 15 mL), the combined organic layers were washed with brine (30 mL) and dried over anhydrous $MgSO_4$. The solvent was removed under reduced pressure (10^{-3} mbar) and the crude product was purified by column chromatography (hexane/ethyl acetate 9:1) to give a colorless oil.

Isolated yield: 652 mg (3.07 mmol, 65%, lit.:[192] 90%)

^{1}H NMR (500 MHz, 25 °C, $CDCl_3$): δ = 0.76 (t, J = 7 Hz, 2H), 0.87 (t, J = 8 Hz, 3H), 1.24 (s, 12H), 1.25-1.33 (m, 6H), 1.36-1.46 (m, 2H) ppm.
^{11}B{^{1}H} NMR (160 MHz, 25 °C, $CDCl_3$): δ = 34.2 ppm.
GC-MS: [t = 8.237 min] m/z 197 (M^+-CH_3).

The spectroscopic data for **76** match those reported in the literature.[192]

2.1.2 Synthesis of 2-cyclohexyl-4,4,5,5-tetramethyl-1,3,2-dioxaborolane

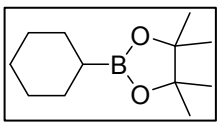

The reaction was performed in an argon-filled glovebox. $FeCl_3$ (3.21 g, 20.0 mmol, 20 mol%) was dissolved in MTBE (300 mL) and TMEDA (**70**, 6.00 mL, 40.0 mmol, 40 mol%) was added dropwise. After 5 min, in the following sequence, KOMe (10.5 g, 150 mmol, 1.5 equiv), B_2pin_2

(**7**, 38.2 g, 150 mmol, 1.5 equiv) and the substrate, bromocyclohexane, (**66**, 12.3 mL, 100 mmol, 1.0 equiv) were added (between the addition of each component was a period of 5 min). The resulting suspension was stirred for 96 h at RT. For work up, the reaction mixture was diluted with brine (400 mL) and extracted with Et_2O (5 × 100 mL). The combined organic layers were washed with brine (200 mL) and dried over anhydrous $MgSO_4$. The solvent was removed under vacuum (10^{-3} mbar) and the crude product was purified by flash chromatography (HP-Sil cartridge, pentane/Et_2O 98:2) to give a colorless oil.

Isolated yield: 5.88 g (28.0 mmol, 28%)

^{1}H NMR (500 MHz, 25 °C, $CDCl_3$): δ = 0.94-1.02 (m, 1H), 1.23 (s, 12H), 1.24-1.39 (m, 6H), 1.57-1.69 (m, 4H) ppm.
^{11}B{^{1}H} NMR (160 MHz, 25 °C, $CDCl_3$): δ = 34.1 ppm.
GC-MS: [t = 3.754 min] m/z 210 (M^+), 195 (M^+-CH_3).

The spectroscopic data for **68** match those reported in the literature.[192]

2.2 Iron-catalyzed borylation of 1-bromohexane and bromo-cylclohexane

2.2.1 General procedure for the iron-catalyzed borylation of 1-bromohexane

In an argon-filled glovebox, the desired amount of $FeCl_3$ (10-20 mol%), Li*t*OBu (2 equiv), B_2pin_2 (**7**, 1.5 equiv) and ligand (20 mol%) were added to a Schlenk tube and dissolved in THF (1 mL). Then the substrate 1-bromohexane (**69**, 70.2 µL, 0.5 mmol, 1.0 equiv) was added and the suspension was stirred and heated for the scheduled time. For work up (performed outside the glovebox), the reaction mixture was diluted with ethyl acetate (5 mL) and filtered through a plug (Ø 20 × 30 mm) of silica gel (silica size 0.063–0.200 mm) into a 28 mL screw cap vial (Wheaton) and *n*-dodecane was added as an internal standard. The product yields were determined by GC-MS.

2.2.2 General procedure for the iron-catalyzed borylation of bromocyclohexane

Under an argon atmosphere, in a glovebox, the desired amount of iron source (10-20 mol%) was added to a Schlenk tube and dissolved in the desired solvent (2-5 mL). After 5 min, in the following sequence, ligand (20-40 mol%), base (2 equiv), B_2pin_2 (**7**, 1.5 equiv) and the substrate bromocyclohexane (**66**, 61.6 µL, 0.5 mmol, 1.0 equiv) were added (between the addition of each component was a period of 5 min). The resulting suspension was stirred and heated for the scheduled time. For work up (performed outside the glovebox), the reaction mixture was diluted with ethyl acetate (5 mL) and filtered through a plug (Ø 20 × 30 mm) of silica gel (silica size 0.063–0.200 mm) into a 28 mL screw cap vial (Wheaton) and *n*-dodecane was added as an internal standard. The product yields were determined by GC-MS.

2.3 Synthesis of 4-(4,4,5,5-tetramethyl-1,3,2-dioxaborolan-2-yl)-toluene

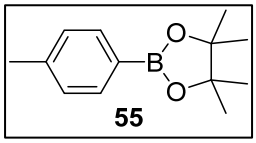

55

According to the literature,[48] in an argon-filled glovebox, a microwave vial was charged with CuI (87.6 mg, 0.46 mmol, 10 mol%) and dissolved in THF (15 mL). Then the ligand P(*n*Bu)$_3$ (149 µL, 0.60 mmol, 13 mol%), KO*t*Bu (1.03 g, 9.20 mmol, 2.0 equiv), B_2pin_2 (2.34 g, 9.20 mmol, 2.0 equiv) and the substrate 4-iodotoluene (1.00 g, 4.60 mmol, 1.0 equiv) were added. The reaction mixture was heated in a microwave reactor and stirred for 30 min at 60 °C. Then the precipitates were removed by filtration and washed with hexane (5 mL). The solvent of the filtrate was removed under reduced pressure to give a crude yellow oil. Further purification was performed by flash chromatography (KP-Sil cartridge, hexane 100%) to give a colorless solid.

Due to the polarity of the compound, the resulting interaction with the silica gel and the non-polar eluant (hexane), it was accepted to sacrifice the yield, concerning the importance of purity over quantity, for further determination of the response factor by GC-MS.

Isolated yield: 350 mg (1.61 mmol, 35%, lit.:[48] 92%)

^{1}H NMR (300 MHz, 25 °C, C_6D_6): δ = 1.13 (s, 12H), 2.06 (m, 3H), 7.05 (m, 2H), 8.12 (m, 2H) ppm.

^{13}C{^{1}H} NMR (75 MHz, 25 °C, C_6D_6): δ = 21.6, 25.0, 83.6, 128.9, 135.6, 141.5 ppm. The carbon attached to the boron was not observed due to quadrupolar broadening.

^{11}B{^{1}H} NMR (96 MHz, 25 °C, C_6D_6): δ = 31.2 ppm.

The spectroscopic data for **55** match those reported in the literature.[48]

2.4 Synthesis of 4,4'-dibromoazoxybenzene

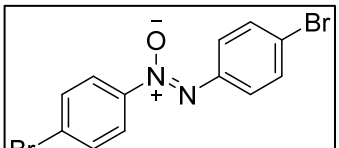

100

In an argon-filled glovebox, a Schlenk flask was charged with CuI (213 mg, 1.12 mmol, 0.1 equiv) and THF (80 mL). Then the ligand xantphos (845 mg, 1.46 mmol, 0.13 equiv), the base KO*t*Bu (1.89 g, 16.8 mmol, 1.5 equiv), B_2pin_2 (5.69 g, 22.4 mmol, 2.0 equiv) and 1-bromo-4-nitrobenzene (2.27 g, 11.2 mmol, 1.0 equiv) were added. The resulting suspension turned dark violet in color and was stirred for 48 h at room temperature. For the work up (performed outside the glovebox), the mixture was concentrated under vacuum (357 mbar, 40 °C), filtered through a plug (Ø 40 × 60 mm) of silica gel and washed with ethyl acetate (3 × 10 mL). The filtrate was concentrated under vacuum (240 mbar, 40 °C) and the resulting residue was recrystallized from refluxing EtOH. The resulting precipitate was collected by filtration and washed with EtOH (2 × 50 mL); the mother liquor from the recrystallization was concentrated under vacuum (10^{-2} mbar) and the resulting precipitate was also collected by filtration and washed with EtOH (2 × 50 mL). The two crude products were combined and further purified by flash column chromatography (KP-Sil cartridge, hexane/CH_2Cl_2 9:1 → 1:1) to give a yellow crystalline solid, which was suitable for X-ray diffraction.

Isolated yield: 857 mg (2.41 mmol, 43%)

^{1}H NMR (200 MHz, 25 °C, C_6D_6): δ = 7.05 (m, 2H), 7.25 (m, 2H), 7.79 (m, 2H), 7.95 (m, 2H) ppm.
HRMS-ASAP (m/z): $[M + H]^+$ calcd for $C_{12}H_9{}^{79}Br_2N_2O$, 354.9076; found, 354.9056.

The spectroscopic data for **100** match those reported in the literature.[193]

2.5 Copper-catalyzed borylation of *p*-tolylhalides

2.5.1 General procedure for the copper-catalyzed borylation of 4-iodotoluene, 4-bromotoluene and 4-chlorotoluene with copper(I)iodide as copper source.

In an argon-filled glovebox, a 28 mL screw cap vial (Wheaton) was charged with the desired amount of CuI (10 mol%, 46.0 µmol) which was then dissolved in THF (1 mL). Then, in sequence, the ligand (13 mol%, 60.0 µmol) and THF (1 mL), KO*t*Bu (1 mL of stock solution, 689 µmol/mL in THF, 1.5 equiv) and B_2pin_2 (**7**, 1 mL of stock solution, 689 µmol/mL in THF, 1.5 equiv) were added (between the addition of each component was a period of 5 min stirring). Finally, the substrate (459 µmol, 1.0 equiv) was added and the suspension was stirred for 19 h at RT. For work up (performed outside the glovebox), the reaction mixture was diluted with Et_2O (5 mL) and filtered through a plug (Ø 20 × 30 mm) of celite into a 28 mL screw cap vial (Wheaton) and *n*-dodecane or biphenyl was added as internal standard. The product yields were determined by GC-MS.

2.5.2 General procedure for the copper-catalyzed borylation of 4-iodotoluene with copper-nanoparticles as copper source.

The Cu-nanoparticles were generated according to a procedure in the literature.[95]
In an argon-filled glovebox, a 28 mL screw cap vial (Wheaton) or a 5 mL microwave vial (reactions under microwave irradiation and/or at elevated temperatures), was charged with the desired amount of Cu-NPs (0.02 mol%, 1 mL of 0.10 mM Cu-NPs solution in DMF). Then KO*t*Bu (689 µmol, 1.5 equiv), B_2pin_2 (**7**, 689 µmol, 1.5 equiv), 4-iodotoluene (459 µmol, 1.0 equiv) and DMF (4 mL) were added and the suspension was stirred for 19 h at the desired temperature or 45 min in case of microwave irradiation. For work up (performed outside the glovebox), the reaction mixture was diluted with Et_2O (5 mL) and filtered through a plug (Ø 20 × 30 mm) of celite into a 28 mL screw cap vial (Wheaton) and *n*-dodecane was added as internal standard. The product yields were determined by GC-MS.

2.6 Phosphine ligand synthesis: 1,2-bis(diphenylphosphino)-benzene

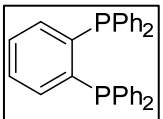

83

Under an argon atmosphere, potassium (3.53 g, 90.0 mmol, 4.5 equiv) was added to a round bottom flask (250 mL) and layered with THF (75 mL). Then chlorodiphenylphosphine (8.00 mL, 45.0 mmol, 2.25 equiv) was added and the reaction mixture was stirred under reflux until the potassium was completely dissolved and the mixture became red in color. To the refluxing mixture, 1,2-difluorobenzene (2.00 mL, 20.0 mmol, 1.0 equiv) was added dropwise followed by toluene (65 mL) and the mixture was stirred under reflux for 24 h. After cooling to room temperature, all volatiles were removed under reduced pressure and the residue was re-dissolved in toluene. Then, activated charcoal (5 g) was added and the mixture and was stirred for 5 min before hot filtration through a celite pad. After washing with EtOH, the solvent was removed under vacuum (10^{-3} mbar) to give a colorless crystalline solid.

Isolated yield: 3.10 g (6.95 mmol, 35%, lit.:[194] 75%)

^{1}H NMR (500 MHz, 25 °C, $CDCl_3$): δ = 7.03 – 7.08 (m, 2H), 7.14 – 7.28 (m, 22H) ppm.
^{13}C{^{1}H} NMR (125 MHz, 25 °C, $CDCl_3$): δ = 128.4 (m), 128.5 (s), 129.2 (s), 134.0 (m), 134.2 (m), 137.2 (m), 143.8 (m) ppm.
^{31}P{^{1}H} NMR (202 MHz, 25 °C, $CDCl_3$): δ = -13.9 ppm.
HRMS-ASAP (m/z): $[M + H]^+$ calcd for $C_{30}H_{25}P_2$, 447.1426; found, 447.1415.

The spectroscopic data for **83** match those reported in the literature.[195]

2.7 Synthesis of copper complexes

2.7.1 Synthesis of copper(I)-*tert*-butoxide $[(CH_3)_3COCu]_4$

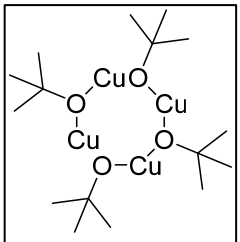

105

In an argon-filled glovebox, a Schlenk tube (desirable for sublimation) was charged with KO*t*Bu (1.00 g, 8.90 mmol, 1.0 equiv) and CuI (1.70 g, 8.90 mmol, 1.0 equiv). On a Schlenk vacuum line, it was cooled to -78 °C and THF (25 mL) was added very slowly. Then the cooling was removed and the reaction mixture was stirred for 19.5 h and allowed to reach room temperature. The solvent was removed under reduced pressure and a cold-finger was attached under an argon stream. Sublimation for 5 h (160 °C, 1.0×10^{-3} mbar) gave a yellow crystalline solid.

Isolated yield: 753 mg (5.51 mmol, 62%, lit.:[101] 80%)

^{1}H NMR (500 MHz, 25 °C, $CDCl_3$): δ = 1.31 (s, 9H) ppm.
HRMS-ASAP (m/z): $[M + H]^+$ (tetramer) calcd for $C_{16}H_{37}O_4{}^{63}Cu_4$, 544.9870; found, 544.9869.

The spectroscopic data for **105** match those reported in the literature.[101]

2.7.2 Synthesis of copper-xantphos-iodo complex

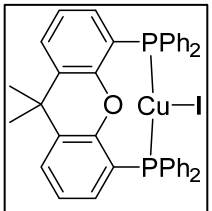

106a

Using standard Schlenk techniques, CuI (100 mg, 0.53 mmol, 1.0 equiv) and xantphos (365 mg, 0.63 mmol, 1.2 equiv) were added to a Schlenk tube, which was then evacuated three times and refilled with argon. Then, MeCN (5 mL) was added and the resulting suspension was stirred for 2.5 h at 50 °C and overnight at RT. The precipitate was collected by filtration, washed with MeCN (10 mL) and dried under high vacuum (10^{-5} mbar) to give a colorless solid.

Isolated yield: 350 mg (0.46 mmol, 88%, lit.:[102] 98%)

^{1}H NMR (300 MHz, 25 °C, CD_2Cl_2): δ = 1.66 (s, 6H), 6.56 – 6.64 (m, 2H), 7.12 (t, *J* = 8 Hz, 2H), 7.21 – 7.29 (m, 8H), 7.30 – 7.47 (m, 12H), 7.58 (d, *J* = 8 Hz, 2H) ppm.

$^{13}C\{^1H\}$ NMR (75 MHz, 25 °C, CD_2Cl_2): δ = 28.6, 36.1, 125.1, 127.4, 128.9 (m), 130.3, 131.6, 132.1, 133.7, 137.3 (m) ppm.
$^{31}P\{^1H\}$ NMR (121 MHz, 25 °C, CD_2Cl_2): δ = -17.9 (br) ppm.

The spectroscopic data for **106a** match those reported in the literature.[102]

2.7.3 Synthesis of copper-xantphos-chloro complex

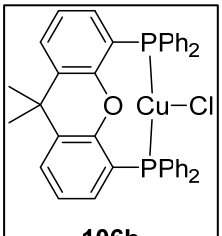

106b

In a glovebox CuCl (52.0 mg, 0.53 mmol, 1.0 equiv) and Xantphos (365 mg, 0.63 mmol, 1.2 equiv) were added to a Schlenk tube. Then MeCN (5 mL) was added and the resulting suspension was stirred for 2.5 h at 50 °C. The precipitate was collected by filtration, washed with MeCN (10 mL) and dried under high vacuum (10^{-5} mbar) to give a colorless solid.

Isolated yield: 227 mg (0.35 mmol, 65%, lit.[103]: 87%)

^1H NMR (200 MHz, 25 °C, CD_2Cl_2): δ = 1.66 (s, 6H), 6.54 – 6.66 (m, 2H), 7.13 (t, 2H, J = 7.7 Hz), 7.18 – 7.35 (m, 12H), 7.35 – 7.49 (m, 8H), 7.54 – 7.61 (m, 2H) ppm.
$^{31}P\{^1H\}$ NMR (81 MHz, 25 °C, CD_2Cl_2): δ = -18.3 (br) ppm.
HRMS-ASAP (m/z): $[M]^+$ calcd for $C_{39}H_{32}{}^{63}CuOP_2{}^{35}Cl$, 676.0907; found, 676.0899.

The spectroscopic data for **106b** match those reported in the literature.[103]

2.7.4 Synthesis of $[(PCy_3)_2CuBr]$

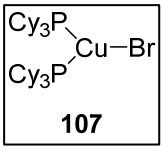

107

According to the literature,[106,107] a Schlenk tube was charged with $CuBr_2$ (335 mg, 1.50 mmol, 1.0 equiv) and PCy_3 (1.30 g, 4.65 mmol, 3.1 equiv). Then EtOH (20 mL) was added and the resulting mixture was stirred for 2 h at 80 °C and overnight at room temperature. EtOH (10 mL) was added for dilution and the mixture was heated for 1 h to 80 °C, then slowly cooled to room temperature by keeping the vessel in the oil bath. The resulting precipitate was collected by filtration, washed with EtOH (3 × 5 mL) and dried under reduced pressure (10^{-3} mbar) to give a colorless solid.

Isolated yield: 580 mg (0.82 mmol, 55%, lit.[106,107]: n.a.)

For X-ray diffraction: A concentrated solution in EtOH was heated to 80 °C and then slowly cooled to room temperature to obtain single-crystals suitable for X-ray diffraction.

^{1}H NMR (200 MHz, 25 °C, C_6D_6): δ = 1.03 – 1.41 (m, 18H), 1.44 – 1.87 (m, 30H), 1.89 – 2.16 (m, 18H) ppm.

^{31}P{^{1}H} NMR (81 MHz, 25 °C, C_6D_6): δ = 11.3 ppm.

HRMS-ASAP (m/z): $[M - Br]^+$ calcd for $C_{36}H_{66}{}^{63}CuP_2$, 623.3930; found, 623.3923.

EIMS (m/z): $[M - PCy_3]^+$ calcd for $C_{18}H_{33}BrCuP$, 422.01; found, 422.00.

The spectroscopic data for **107** are similar to those reported for the ^{31}P CP/MAS NMR in the literature.[107]

2.7.5 Synthesis of [(dppbz)CuCl]

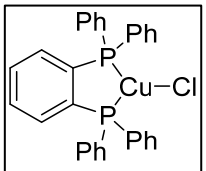

108

According to the literature,[104,105,108] CuCl (52.0 mg, 0.52 mmol, 1.0 equiv), dppbz (232 mg, 0.52 mmol, 1.0 equiv) and MeCN (10 mL) were added to a Schlenk tube, and the resulting mixture was stirred for 2 h at 50 °C. The resulting bright green precipitate was collected, washed with EtOH (2 × 5 mL) and MeCN (2 × 5 mL), and then dried under reduced pressure (10^{-3} mbar) to give a bright green solid.

Isolated yield: 212 mg (0.39 mmol, 75%, lit.[105]: 16% (dimer))

^{1}H NMR (400 MHz, 25 °C, CD_2Cl_2): δ = 6.93 – 7.01 (m, 4H), 7.03 – 7.15 (m, 8H), 7.17 – 7.24 (m, 2H), 7.24 – 7.39 (m 10H) ppm.

^{31}P{^{1}H} NMR (162 MHz, 25 °C, CD_2Cl_2): δ = -18.4 ppm.

HRMS-ASAP (m/z): $[M]^+$ (monomer) calcd for $C_{30}H_{24}{}^{63}CuP_2{}^{35}Cl$, 544.0332; found, 544.0329.

The spectroscopic data for **108** are similar to those reported for the dinuclear complex in the literature.[103]

2.7.6 Synthesis of [$PCy_3Cu(\mu\text{-}I_2)CuPCy_3$]

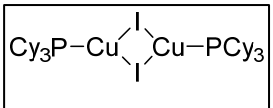

109

According to the literature,[106,107] CuI (95.0 mg, 0.50 mmol, 1.0 equiv), PCy_3 (154 mg, 0.55 mmol, 1.1 equiv) and EtOH (10 mL) were added to a Schlenk tube, and the resulting mixture was stirred for 1 h at 70 °C and then stored at 5 °C for crystallization over the weekend. The resulting precipitate was collected by filtration, washed with EtOH (2 × 5 mL) and dried under reduced pressure (10^{-3} mbar) to give a colorless solid.

Isolated yield: 201 mg (0.43 mmol, 85%, lit.[106,107]: n.a.)

^{1}H NMR (300 MHz, 25 °C, C_6D_6): δ = 1.10 – 1.35 (m, 18H), 1.52 – 1.82 (m, 30H), 1.93 – 2.20 (m, 18H) ppm.
^{31}P{^{1}H} NMR (121 MHz, 25 °C, C_6D_6): δ = 10.1 ppm.
HRMS-LIFDI (m/z): $[M]^+$ (dimer) calcd for $C_{36}H_{66}{}^{63}Cu_2P_2{}^{127}I_2$, 940.1316; found, 940.1301

The spectroscopic data for **109** are similar to those reported for the ^{31}P CP/MAS NMR in the literature.[107]

2.8 Synthesis of diboron compounds

2.8.1 Preparation of HCl•Et_2O

Under argon atmosphere, an oven dried Schlenk flask was charged with Et_2O (500 mL) and cooled to 0 °C. Then a HCl gas cylinder was connected to the Schlenk flask with a gas inlet tube and the HCl gas was passed through the Et_2O for 20 min, until a strong bubbling was observed. The HCl in Et_2O was allowed to warm to RT (NOTE: PRESSURE EQUALIZING!) and then cooled back to 0°°C. The gas passing procedure was repeated one more time to get a 5M to 6M HCl•Et_2O. The exact concentration was determined prior to use by titration.

2.8.2 Synthesis of bis(ethylene glycolato)diboron, B_2eg_2[22]

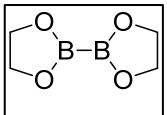

110

$B_2(NMe_2)_4$ (27.9 g, 141 mmol, 1.0 equiv) was charged into a round bottom flask and dissolved in CH_2Cl_2 (300 mL), and ethylene glycol (18.4 g, 296 mmol, 2.1 equiv) was added and the mixture was cooled to -78 °C. Then, precooled (-78 °C) HCl•Et_2O (5 M, 123 mL, 615 mmol, 4.35 equiv) in a dropping funnel, was added dropwise within 1 h. The reaction mixture was stirred for 2 h at -78 °C and the ammonium salts started to precipitate. For completion, the reaction mixture was slowly warmed to room temperature and stirred overnight. Then volatile components were removed *in vacuo* and to the resulting solid, toluene (100 mL) was added with stirring for 10 min. Then, the solvent was transferred and filtered by cannula into a separate Schlenk flask. This step was repeated four times for completion of the extraction. The solvent was removed under reduced pressure to give the crude product (10.7 g). Further purification was performed by sublimation under vacuum (ca. 10^{-2}–10^{-3} mbar, 80 °C) to give colorless crystals which were also suitable for X-ray diffraction.

Isolated yield: 9.44 g (67 mmol, 48%, lit.[22]: 65-75%)

^{1}H NMR (300 MHz, 25 °C, C_6D_6): δ = 3.50 (s, 8H, C*H*$_2$).
^{11}B{^{1}H} NMR (96 MHz, 25 °C, C_6D_6): δ = 31.5.
^{13}C{^{1}H} NMR (75 MHz, 25 °C, C_6D_6): δ = 65.3.
HRMS-ASAP (m/z): $[M+H]^+$ calcd for $C_4H_9{}^{10}B^{11}BO_4$, 142.0718; found, 142.0713.
GC-MS [t = 4.421 min] m/z 141 (M^+).

2.8.3 Synthesis of tris(ethylene glycolato)diboron (B_2eg_3)[179-182]

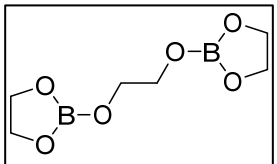

111

A Schlenk tube was charged with $NaBH_4$ (5.00 g, 132 mmol, 1.0 equiv), evacuated (10^{-2} mbar) and refilled with argon three times. After dissolving in THF (200 mL), TMSCl (16.6 mL, 132 mmol, 1.0 equiv) was added dropwise and the resulting mixture was stirred overnight at room temperature. The precipitated salts were removed by filtration through celite and washed twice with THF (10 mL). The filtrate, containing the BH_3●THF adduct, was cooled to -78 °C and ethylene glycol (12.3 g, 198 mmol, 1.5 equiv) in THF (10 mL) was added dropwise within 30 min to control hydrogen evolution. For completion, the reaction mixture was stirred overnight and was allowed to warm to room temperature. The solvent and all volatiles were removed under reduced pressure (10^{-3} mbar) and, finally, heating to 100 °C gave a colorless solid.

Isolated yield: 4.66 g (23.1 mmol, 35% over 2 steps, lit.[179]: 99%)

Anal. Calcd for $C_6H_{12}B_2O_6$: C, 35.72; H, 5.99. Found: C, 35.55; H, 5.95.

^{11}B RSHE/MAS NMR (128 MHz, 22 °C): δ_{iso} = 18.9 ± 0.1, CQ_{quad} = 2380 ± 10 kHz, η_{quad} = 0.03 ± 0.03.

^{13}C CP/MAS NMR (101 MHz, 22 °C): δ = 61.7, 63.1, 64.3.

HRMS-ASAP (m/z): $[M+H]^+$ calcd for $C_6H_{13}{}^{10}B^{11}BO_6$, 202.0929; found, 202.0927.

No NMR spectroscopic data are available for **111** in the literature.[179]

2.9 Reactions of NHCs or phosphines with alkoxy diboron compounds

2.9.1 General procedure for the reactions of NHCs with B_2eg_2 (*in situ* NMR experiments)

In an argon-filled glovebox, B_2eg_2 (10 mg, 71.0 µmol, 1.0 equiv) and the desired NHC (71.0 µmol, 1.0 equiv or 142 µmol, 2.0 equiv) were added to an NMR tube. Outside the glovebox, on a Schlenk line, deuterated solvent (0.60 mL) was added. If the NHC was a liquid, first the B_2eg_2 was dissolved in the deuterated solvent, then the NHC was added by microliter syringe.

2.9.2 Synthesis of mono-NHC adduct B_2eg_2•Mes_2Im

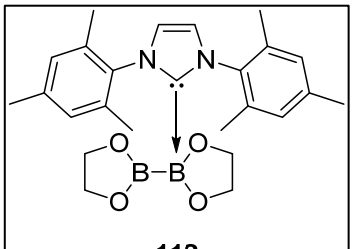

118

In an argon-filled glovebox, B_2eg_2 (100 mg, 706 µmol, 1.0 equiv) and Mes_2Im (215 mg, 706 µmol, 1.0 equiv) were added to a Schlenk tube. Outside the glovebox, at a Schlenk line, toluene (20 mL) was added and the suspension was stirred for 2 h at room temperature, then heated to 80 °C and the precipitated residue was removed by hot filtration. The filtrate was layered with hexane (100 mL) and stored at -40 °C over the weekend. The resulting precipitate was collected *via* filtration and washed with toluene (5 mL). The mother liquor was layered with *n*-hexane (60 mL) and stored at -40 °C overnight. The obtained precipitate was collected *via* filtration and washed with toluene (5 mL). Both precipitates were combined and dried under high vacuum (10^{-6} mbar) to give a slightly yellow solid.

For X-ray diffraction: Single-crystals suitable for X-ray diffraction were obtained by slow evaporation of the solvent of a saturated solution (NMR sample) of B_2eg_2•Mes_2Im in C_6D_6.

Isolated Yield: 224 mg (0.50 mmol, 71%)

^{1}H NMR (500 MHz, 25 °C, C_6D_6): δ = 2.09 (s, 6H, Mes-C*H*$_3$), 2.24 (s, 12H, Mes-C*H*$_3$), 3.44 (s, 8H, C*H*$_2$), 5.98 (s, 2H, C*H*C*H*), 6.74 (s, 4H, Mes-C*H*).

^{11}B{^{1}H} NMR (96 MHz, 25 °C, C_6D_6): δ = 22.6 (s_{br}).

^{13}C{^{1}H} NMR (125 MHz, 25 °C, C_6D_6): δ = 18.0 (*C*H$_3$), 21.0 (*C*H$_3$), 64.5 (*C*H$_2$), 121.4 (*C*H*C*H), 128.9 (*C*H), 135.3 (C_q), 136.0 (C_q), 138.6 (C_q), 173.7 (N*C*N, assigned *via* ^{13}C,^{1}H HMBC)

^{15}N,^{1}H HMBC NMR (51 MHz, 25 °C, C_6D_6): δ = -194.4.

^{11}B RSHE/MAS NMR (128 MHz, 22 °C): δ_{iso} = 3.90 ± 0.5 (sp^3-B), CQ$_{quad}$ = 1410 ± 100 kHz, η_{quad} = 0.71 ± 0.05; δ_{iso} = 35.1 ± 0.2 (sp^2-B), CQ$_{quad}$ = 3100 ± 100 kHz, η_{quad} = 0.94 ± 0.05.

^{13}C CP/MAS NMR (101 MHz, 22 °C): δ = 18.2 (*C*H$_3$), 21.3 (*C*H$_3$), 63.9 (*C*H$_2$), 123.3, 125.5, 127.6, 130.1, 132.7, 135.3, 137.6, 139.9, 168.1 (N*C*N).

^{15}N CP/MAS NMR (41 MHz, 22 °C): δ = -189.9, -185.9.

HRMS-ASAP (m/z): [M+H]$^+$ calcd for $C_{25}H_{33}{}^{10}B^{11}BN_2O_4$, 446.2657; found, 446.2656.

2.9.3 Synthesis of RER-B$_2$eg$_2$•(*i*Pr$_2$Im)$_2$

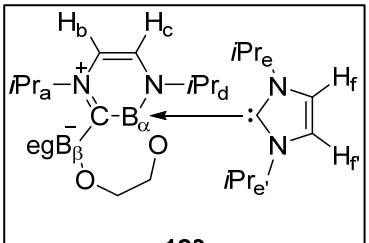

120

A Schlenk tube was charged with bis(ethylene glycolato)diboron(4) (B$_2$eg$_2$, 300 mg, 2.12 mmol, 1.0 equiv) then toluene (10 mL) was added and the mixture was stirred until dissolution of B$_2$eg$_2$ was complete. Then, *i*Pr$_2$Im (646 µL, 4.24 mmol, 2.0 equiv) was added and the mixture was stirred at RT for 5 minutes and then stored in a freezer at -30 °C for crystallisation (2 weeks). The obtained crystalline solid was suitable for X-ray diffraction. The solid was collected *via* filtration at -30 °C and washed with cold hexane (5 mL, -30 °C); then dried under high vacuum (10^{-5} mbar) to give a yellow solid. Single-crystals for X-ray diffraction of **120'** were obtained from the cold (-30 °C) mother liquor by single-crystal picking. At room temperature, compound **120** decomposes in solution.

Isolated Yield: 589 mg (1.32 mmol, 62%)

Elemental analysis calcd (%) for $C_{22}H_{40}B_2N_4O_4$: C, 59.22; H, 9.04; N, 12.56. Found: C, 59.53; H, 8.92; N, 12.09.

^{1}H NMR (500 MHz, -40 °C, d$_8$-toluene): δ = 0.77 (d, $^3J_{HH}$ = 7 Hz, 3H, *i*Pr$_d$-C*H*$_3$), 0.97 (d, $^3J_{HH}$ = 7 Hz, 3H, *i*Pr$_{e,e'}$-C*H*$_3$), 1.13 (d, $^3J_{HH}$ = 7 Hz, 3H, *i*Pr$_{e,e'}$-C*H*$_3$), 1.24 (d, $^3J_{HH}$ = 7 Hz, 3H, *i*Pr$_d$-C*H*$_3$), 1.26 (d, $^3J_{HH}$ = 7 Hz, 3H, *i*Pr$_{e,e'}$-C*H*$_3$), 1.32 (d, $^3J_{HH}$ = 7 Hz, 3H, *i*Pr$_a$-C*H*$_3$), 1.39 (d, $^3J_{HH}$ = 7 Hz, 3H, *i*Pr$_a$-C*H*$_3$), 1.61 (d, $^3J_{HH}$ = 7 Hz, 3H, *i*Pr$_{e,e'}$-C*H*$_3$), 3.02

(m, 1H, CH_2), 3.36 (m, 1H, iPr$_d$-CH), 3.45 (m, 1H, CH_2), 3.69 (m, 1H, iPr$_{e,e'}$-CH), 3.83-3.94 (m, 3H, CH_2), 3.97 (m, 1H, CH_2), 4.26 (m, 1H, CH_2), 4.45 (m, 1H, CH_2), 5.29 (d, $^3J_{HH}$ = 6 Hz, 1H, CH_b), 6.23 (d, $^3J_{HH}$ = 6 Hz, 1H, CH_c), 6.31 (m, 1H, iPr$_a$-CH), 6.51 (s, 1H, C$H_{f,f'}$), 6.57 (s, 1H, C$H_{f,f'}$), 6.92 (m, 1H, iPr$_{e,e'}$-CH).

^{11}B{^{1}H} NMR (160 MHz, -40 °C, d$_8$-toluene): δ = -1.53 (s, sp^3-$B_{\alpha/\beta}$), 6.95 (s, sp^3-$B_{\alpha/\beta}$).

^{13}C{^{1}H} NMR (125 MHz, -40 °C, d$_8$-toluene): δ = 20.9 (iPr$_a$-CH$_3$), 22.0 (iPr$_a$-CH$_3$), 22.1 (iPr$_{e,e'}$-CH$_3$), 22.2 (iPr$_d$-CH$_3$), 22.3 (iPr$_{e,e'}$-CH$_3$), 24.1 (iPr$_{e,e'}$-CH$_3$), 24.3 (iPr$_{e,e'}$-CH$_3$), 24.5 (iPr$_d$-CH$_3$), 47.0 (iPr$_d$-CH), 48.2 (iPr$_{e,e'}$-CH), 48.5 (iPr$_{e,e'}$-CH), 57.7 (iPr$_a$-CH), 64.3 (CH$_2$), 64.6 (CH$_2$), 66.0 (CH$_2$), 67.9 (CH$_2$), 95.5 (CH$_b$), 115.7 (CH$_{f,f'}$), 116.8 (CH$_{f,f'}$), 129.8 (CH$_c$), 162.7 (NCN), 208.8 (B$_2$$C$=N, assigned *via* ^{13}C,^{1}H HMBC).

^{15}N,^{1}H HMBC NMR (51 MHz, -40 °C, d$_8$-toluene): δ = -268.6 (N_d)-184.7 ($N_{e,e'}$),-184.1 ($N_{e,e'}$), -156.5 (N_a).

^{11}B RSHE/MAS NMR (128 MHz, 22 °C): δ_{iso} = -1.10 ± 0.05 (sp^3-$B_{\alpha/\beta}$), CQ$_{quad}$ = 600 ± 20 kHz, η_{quad} = 0.34 ± 0.05; δ_{iso} = 7.00 ± 0.05 (sp^3-$B_{\alpha/\beta}$), CQ$_{quad}$ = 590 ± 20 kHz, η_{quad} = 0.80 ± 0.05.

^{13}C CP/MAS NMR (101 MHz, 22 °C): δ = 21.9 (iPr-CH$_3$), 23.5 (iPr-CH$_3$), 25.6 (iPr-CH$_3$), 26.3 (iPr-CH$_3$), 46.2 (iPr$_d$-CH), 48.5 (iPr$_{e,e'}$-CH), 48.9 (iPr$_{e,e'}$-CH), 57.5 (iPr$_a$-CH), 63.9 (CH$_2$), 64.6 (CH$_2$), 66.6 (CH$_2$), 67.9 (CH$_2$), 96.6 (CH$_b$), 117.0 (CH$_{f,f'}$), 119.5 (CH$_{f,f'}$), 129.7 (CH$_c$), 162.5 (NCN), 207.1 (B$_2$$C$=N).

^{15}N CP/MAS NMR (41 MHz, 22 °C): δ = -263.2 (br, N_d), -180.4 ($N_{e,e'}$), -177.0 ($N_{e,e'}$), -149.7 (N_a).

HRMS-ASAP (m/z): [M]$^-$ calcd for $C_{22}H_{40}{}^{10}B^{11}BN_4O_4$, 445.3266; found, 445.3281.

2.9.4 Synthesis of RER-B$_2$eg$_2$•(Me$_2$Im^{Me})$_2$

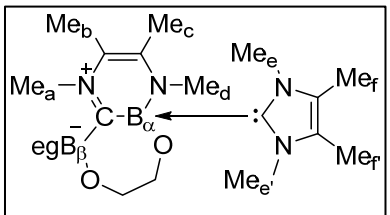

121

In an argon-filled glovebox, B$_2$eg$_2$ (10.0 mg, 71.0 µmol, 1.0 equiv) and Me$_2$Im^{Me} (17.6 mg, 142 µmol, 2.0 equiv) were added to a J-Young tap-equipped NMR tube. At a Schlenk line, precooled (-40 °C), d$_8$-toluene (0.60 mL) was added and the sample was kept at -40 °C until the NMR measurements were completed. Due to solubility issues, the sample was warmed and shaken for one min after the first ^{1}H and ^{11}B{^{1}H} spectra were measured. The solubility of the NHC was much better than that of B$_2$eg$_2$. After the low temperature experiment, a control measurement at room temperature revealed

decomposition, which was also observed for compound **120**. Compound **121** could not be isolated, due to its very high reactivity.

^{1}H NMR (500 MHz, -40 °C, d_8-toluene): δ = 1.28 (s, 6H, $Me_{f,f'}$-CH_3), 1.72 (s, 3H, $Me_{b,c}$-CH_3), 1.77 (s, 3H, $Me_{b,c}$-CH_3), 2.97 (s, 2H, CH_2), 3.02 (s, 3H, $Me_{a,d}$-CH_3), 3.67 (s, 6H, $Me_{e,e'}$-CH_3), 3.71 (m, 2H, CH_2), 3.79 (s, 3H, $Me_{a,d}$-CH_3), 4.00 (m, 2H, CH_2), 4.05 (m, 2H, CH_2).

^{11}B{^{1}H} NMR (160 MHz, -40 °C, d_8-toluene): δ = -0.89 (s, sp^3-$B_{\alpha/\beta}$), 6.19 (s, sp^3-$B_{\alpha/\beta}$).

2.9.5 Synthesis of bis-NHC adduct B_2eg_3•(*i*Pr_2Im)$_2$

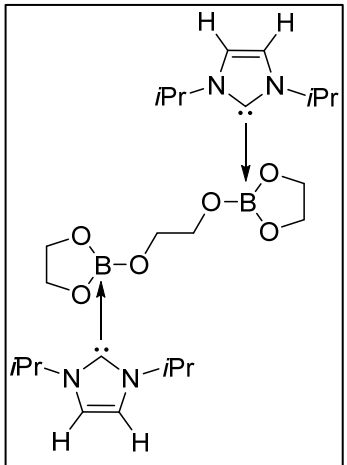

122

A Schlenk tube was charged with B_2eg_3 (100 mg, 496 µmol, 1.0 equiv) and *i*Pr_2Im (153 µL, 992 µmol, 2.0 equiv), then THF (20 mL) was added. The resulting suspension was stirred for 3 h at room temperature and the precipitate obtained was collected *via* filtration, washed with THF (2 × 10 mL) and dried under vacuum (10^{-3} mbar) to give a white solid (96 mg). Due to incomplete reaction and decomposition to the spiro-borate NHC salt [Beg_2][*i*Pr_2Im-H], pure compound **122** could not be isolated.

For X-ray diffraction: Single-crystals of **122** were obtained by single-crystal picking from the mother liquor (-30 °C) of worked-up compound **120**.

2.9.6 Synthesis of bis-NHC adduct B_2eg_3•(Me_2Im^{Me})$_2$

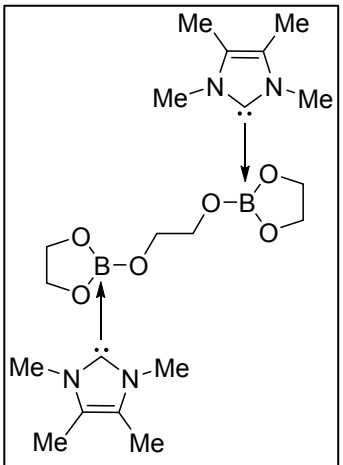

123

A Schlenk tube was charged with B_2eg_3 (100 mg, 496 µmol, 1.0 equiv) and Me_2Im^{Me} (123 mg, 992 µmol, 2.0 equiv), then THF (20 mL) was added. The resulting suspension was stirred for 3 h at 65 °C. Then, the precipitate was collected *via* filtration, washed with THF (2 × 10 mL) and dried under vacuum (10^{-3} mbar) to give a colourless solid (101 mg). The bis-NHC adduct B_2eg_3•(Me_2Im^{Me})$_2$ could not be separated from the decomposition product [Beg_2][Me_2Im^{Me}-H]. The approximate ratio of bis-NHC adduct to the spiro-borate NHC salt was 1:1.

^{11}B RSHE/MAS NMR (128 MHz, 22 °C): δ_{iso} = 5.81.

^{13}C CP/MAS NMR (101 MHz, 22 °C): δ = 6.80-10.2 (*C*H$_3$), 30.3-35.4 (*C*H$_3$), 60.9-66.1 (*C*H$_2$), 121.6-129.5 (vinyl-*C*$_q$), 161.5 (N*C*N).

^{15}N CP/MAS NMR (41 MHz, 22 °C): δ = -206.0, -204.3.

HRMS-ASAP (m/z): [M+H]$^+$ calcd for $C_{20}H_{37}{}^{10}B^{11}BN_4O_6$, 450.2930; found, 450.2922.

2.9.7 General procedure for the reactions of phosphines with B_2eg_2 (*in situ* NMR experiments)

In an argon-filled glovebox, B_2eg_2 (10 mg, 71.0 µmol, 1.0 equiv) and the desired phosphine (71.0 µmol, 1.0 equiv) were added to an NMR tube. Outside the glovebox, on a Schlenk line, C_6D_6 (0.60 mL) was added. If the phosphine was a liquid, first the B_2eg_2 was dissolved in C_6D_6, then the phosphine was added by microliter syringe.

2.9.8 General procedure for the reactions of NHCs with $B_2(OMe)_4$ (*in situ* NMR experiments)

In an argon-filled glovebox, the desired NHC (69.0 µmol, 1.0 equiv or 138 µmol, 2.0 equiv) was added to an NMR tube. Outside the glovebox, on a Schlenk line, the NHC was dissolved in deuterated solvent (0.60 mL), then $B_2(OMe)_4$ (10.0 mg, 69.0 µmol, 1.0 equiv) was weight and added by microliter syringe. If the NHC was also a liquid, first the $B_2(OMe)_4$ was dissolved in the deuterated solvent, then the NHC was added by microliter syringe.

3 X-ray crystallography

3.1 Structure determinations

Crystals were immersed in a film of perfluoropolyether oil on a glass fibre and transferred to the cold nitrogen gas stream of the diffractometer.[196] The data were either collected either on a Bruker X8 Apex-2 instrument with a CCD area detector using mirror-monochromated MoK_{α} radiation and equipped with low-temperature devices. Data were typically collected at 100 K. The images were processed and, if necessary, corrected for Lorentz and polarisation effects and absorption as implemented in the manufacturers software packages. The structures were solved employing the SHELXS, SHELXT or SIR-92 programmes and refined anisotropically for all non-hydrogen atoms by full-matrix least squares on all F^2 data using SHELXL software.[197-199] Difference Fourier syntheses revealed the positions of all other non-hydrogen atoms and they were refined anisotropically. Hydrogen atoms were included in calculated positions and refined employing riding models; methyl groups were treated as rigid bodies and were allowed to rotate about the $E\text{-}CH_3$ bond. Extinction corrections were applied as required. During refinement and analysis of the crystallographic data the software packages SHELXTL, WinGX, PLATON, Mercury and Diamond were used.[198,200-203]

3.2 Crystallographic data collection parameters

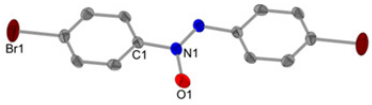

100

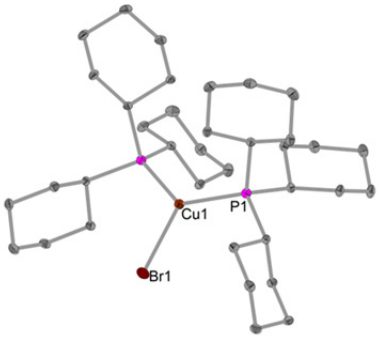

107

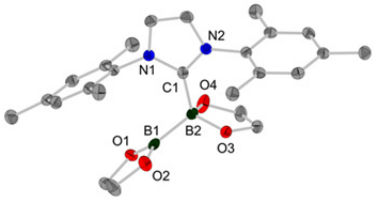

118

Crystallographic data collection parameters for compounds **100**, **107**, **118**

	compound **100**	compound **107**	compound **118**
Chemical Formula	$C_{12}H_8N_2O_1Br_2$	$C_{36}H_{66}BrCuP_2$	$C_{25}H_{32}B_2N_2O_4$
Formula mass ($g \cdot mol^{-1}$)	356.02	704.27	446.14
Temp. (K)	100(2)	100(2)	100(2)
μ (mm^{-1}), Radiation	6.871, MoK_α	1.886, MoK_α	0.084, MoK_α
Crystal system	monoclinic	monoclinic	monoclinic
Space group (no.)	$P2_1/c$	$C2/c$	$P2_1/c$
Z	2	2	4
a (Å)	3.8991(9)	16.8320(8)	8.3809(3)
b (Å)	5.9987(14)	9.0659(4)	18.6842(6)
c (Å)	25.156(6)	24.2850(14)	15.0663(5)
α (°)	90°	90°	90
β (°)	90.420(8)°	109.6792(13)°	99.245(2)
γ (°)	90°	90°	90
Volume ($Å^3$)	588.4(2)	3489.4(3)	2328.59(14)
ρ_{calcd} ($g \cdot cm^{-3}$)	2.009	1.341	1.273
GooF on F^2	1.033	1.051	1.022
R_{int}	0.0816	0.0275	0.0367
R_1 [$I > 2\sigma(I)$]	0.0515	0.0234	0.0422
wR_2 (all data)	0.1207	0.0590	0.1103
Largest peak/hole ($e \cdot Å^{-3}$)	1.250/-1.300	0.530/-0.230	0.386/-0.251
CCDC no.	see also CCDC no. 1319622[204]	see also CCDC no. 175635[107]	1529575

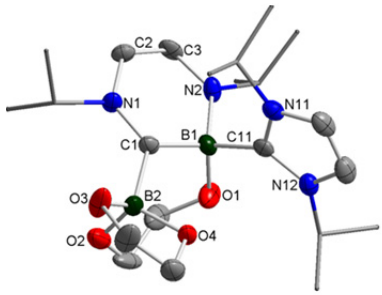

120

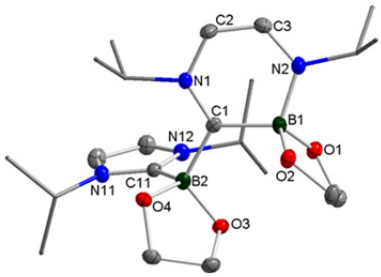

120‘

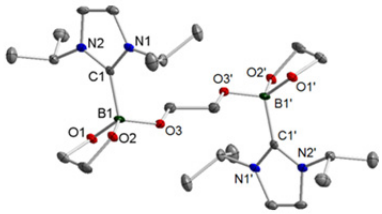

122

Crystallographic data collection parameters for compounds **120**, **120’**, **122**

	compound **120**	compound **120’**	compound **122**
Chemical Formula	$C_{22}H_{40}B_2N_4O_4$	$C_{44}H_{80}B_4N_8O_8$•3(C_7H_8)	$C_{24}H_{44}B_2N_4O_6$•2(C_6H_6)
Formula mass (g·mol^{-1})	446.20	1168.80	662.46
Temp. (K)	100(2)	100(2)	100(2)
μ (mm^{-1}), Radiation	0.080, MoK$_\alpha$	0.075, MoK$_\alpha$	0.079, MoK$_\alpha$
Crystal system	monoclinic	triclinic	triclinic
Space group (no.)	$P2_1/c$	$P\bar{1}$	$P\bar{1}$
Z	4	2	2
a (Å)	9.9858(3)	14.7679(15)	7.5233(13)
b (Å)	15.1342(19)	14.7780(15)	12.070(2)
c (Å)	16.5840(2)	17.5940(18)	21.443(4)
α (°)	90	81.875(3)	94.556(5)
β (°)	91.132(4)	81.666(3)	92.752(5)
γ (°)	90	62.615(2)	106.214(5)
Volume (Å^3)	2505.8(6)	3359.5(6)	1858.7(5)
ρ_{calcd} (g·cm^{-3})	1.183	1.155	1.184
GooF on F^2	1.018	1.021	1.097
R_{int}	0.0849	0.0358	0.0517
R_1 [$I > 2\sigma(I)$]	0.0757	0.0380	0.0696
wR_2 (all data)	0.1541	0.0887	0.1513
Largest peak/hole (e·Å^{-3})	0.241/-0.247	0.299/-0.205	0.266/-0.337
CCDC no.	1529582	1529574	1529577

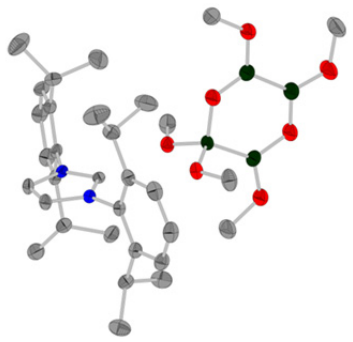

124

Crystallographic data collection parameters for compounds **124**

	compound **124**
Chemical Formula	$C_{32}H_{52}B_4N_2O_7$
Formula mass ($g \cdot mol^{-1}$)	619.99
Temp. (K)	100(2)
μ (mm^{-1}), Radiation	0.078, MoK_α
Crystal system	orthorhombic
Space group (no.)	P_{nma}
Z	4
a (Å)	20.5133(15)
b (Å)	14.9398(12)
c (Å)	11.6151(9)
α (°)	90°
β (°)	90°
γ (°)	90°
Volume ($Å^3$)	3559.6(5)
ρ_{calcd} ($g \cdot cm^{-3}$)	1.157
GooF on F^2	1.070
R_{int}	0.0508
R_1 [$I > 2\sigma(I)$]	0.0519
wR_2 (all data)	0.1412
Largest peak/hole ($e \cdot Å^{-3}$)	0.561/-0.220
CCDC no.	not published

REFERENCES

[1] A. Stock, A. Brandt, H. Fischer, *Chem. Ber.* **1925**, *58*, 643-657.

[2] H. I. Schlesinger, H. C. Brown, B. Abraham, A. C. Bond, N. Davidson, A. E. Finholt, J. R. Gilbreath, H. Hoekstra, L. Horvitz, E. K. Hyde, J. J. Katz, J. Knight, R. A. Lad, D. L. Mayfield, L. Rapp, D. M. Ritter, A. M. Schwartz, I. Sheft, L. D. Tuck, A. O. Walker, *J. Am. Chem. Soc.* **1953**, *75*, 186-190.

[3] M. F. Lappert, *Chem. Rev.* **1956**, *56*, 959-1064.

[4] W. Gerrard, *The Organic Chemistry of Boron*, Academic Press, New York, **1961**.

[5] H. C. Brown, *Boranes in Organic Chemistry*, Cornell University Press, Ithaca, London, **1972**.

[6] H. Steinberg, A. L. McCloskey, *Progress in Boron Chemistry, Vol. 1*, Pergamon Press, Oxford, **1964**.

[7] R. J. Brotherton, H. Steinberg, *Progress in Boron Chemistry, Vol. 2*, Pergamon Press, Oxford, **1970**.

[8] R. J. Brotherton, H. Steinberg, *Progress in Boron Chemistry, Vol. 3*, Pergamon Press, Oxford, **1970**.

[9] E. C. Neeve, S. J. Geier, I. A. I. Mkhalid, S. A. Westcott, T. B. Marder, *Chem. Rev.* **2016**, *116*, 9091-9161.

[10] T. D. Coyle, J. J. Ritter, in *Advances in Organometallic Chemistry (Eds. F. G. A. Stone, R. West), Vol. 10*, Academic Press, New York, London, **1972**, pp. 237-272.

[11] M. Kameda, J. A. Driscoll, G. Kodama, *Inorg. Chem.* **1990**, *29*, 3791-3795.

[12] R. W. Parry, *Phosphorus, Sulfur, Silicon Relat. Elem.* **1994**, *87*, 177-191.

[13] K. Schluter, A. Berndt, *Angew. Chem. Int. Ed.* **1980**, *19*, 57-58.

[14] W. Biffar, H. Nöth, H. Pommerening, *Angew. Chem. Int. Ed.* **1980**, *19*, 56-57.

[15] H. Nöth, *Z. Naturforsch., B: Chem. Sci.* **1984**, *39*, 1463-1466.

[16] A. Moezzi, M. M. Olmstead, R. A. Bartlett, P. P. Power, *Organometallics* **1992**, *11*, 2383-2388.

[17] A. Moezzi, M. M. Olmstead, P. P. Power, *J. Am. Chem. Soc.* **1992**, *114*, 2715-2717.

[18] R. J. Brotherton, A. L. McCloskey, L. L. Petterson, H. Steinberg, *J. Am. Chem. Soc.* **1960**, *82*, 6242-6245.

[19] R. J. Brotherton, A. L. McCloskey, J. L. Boone, H. M. Manasevit, *J. Am. Chem. Soc.* **1960**, *82*, 6245-6248.

[20] R. J. Brotherton, W. G. Woods, US3009941, **1961**.

[21] T. Ishiyama, M. Murata, T. Ahiko, N. Miyaura, *Org. Synth.* **2004**, *10*, 115.

[22] C. N. Welch, S. G. Shore, *Inorg. Chem.* **1968**, *7*, 225-230.

[23] F. J. Lawlor, N. C. Norman, N. L. Pickett, E. G. Robins, P. Nguyen, G. Lesley, T. B. Marder, J. A. Ashmore, J. C. Green, *Inorg. Chem.* **1998**, *37*, 5282-5288.

[24] W. Clegg, M. R. J. Elsegood, F. J. Lawlor, N. C. Norman, N. L. Pickett, E. G. Robins, A. J. Scott, P. Nguyen, N. J. Taylor, T. B. Marder, *Inorg. Chem.* **1998**, *37*, 5289-5293.

[25] S. Shimada, A. S. Batsanov, J. A. K. Howard, T. B. Marder, *Angew. Chem. Int. Ed.* **2001**, *40*, 2168-2171.

[26] H. Braunschweig, F. Guethlein, *Angew. Chem. Int. Ed.* **2011**, *50*, 12613-12616.

[27] H. Braunschweig, F. Guethlein, EP2554547A1, **2013**.

[28] T. Ishiyama, N. Matsuda, N. Miyaura, A. Suzuki, *J. Am. Chem. Soc.* **1993**, *115*, 11018-11019.

[29] X. Y. Liu, *Synlett* **2003**, 2442-2443.

[30] T. B. Marder, N. C. Norman, *Top. Catal.* **1998**, *5*, 63-73.

[31] T. Ishiyama, M. Murata, N. Miyaura, *J. Org. Chem.* **1995**, *60*, 7508-7510.

[32] P. Nguyen, H. P. Blom, S. A. Westcott, N. J. Taylor, T. B. Marder, *J. Am. Chem. Soc.* **1993**, *115*, 9329-9330.

[33] C. N. Iverson, M. R. Smith, *J. Am. Chem. Soc.* **1999**, *121*, 7696-7697.

[34] J. Y. Cho, M. K. Tse, D. Holmes, R. E. Maleczka, M. R. Smith, *Science* **2002**, *295*, 305-308.

[35] T. Ishiyama, J. Takagi, K. Ishida, N. Miyaura, N. R. Anastasi, J. F. Hartwig, *J. Am. Chem. Soc.* **2002**, *124*, 390-391.

[36] T. M. Boller, J. M. Murphy, M. Hapke, T. Ishiyama, N. Miyaura, J. F. Hartwig, *J. Am. Chem. Soc.* **2005**, *127*, 14263-14278.

[37] H. Tamura, H. Yamazaki, H. Sato, S. Sakaki, *J. Am. Chem. Soc.* **2003**, *125*, 16114-16126.

[38] T. Ishiyama, N. Miyaura, *J. Organomet. Chem.* **2003**, *680*, 3-11.

[39] I. A. I. Mkhalid, J. H. Barnard, T. B. Marder, J. M. Murphy, J. F. Hartwig, *Chem. Rev.* **2010**, *110*, 890-931.

[40] C. Seechurn, V. Sivakumar, D. Satoskar, T. J. Colacot, *Organometallics* **2014**, *33*, 3514-3522.

[41] H. Y. Chen, J. F. Hartwig, *Angew. Chem. Int. Ed.* **1999**, *38*, 3391-3393.

[42] M. Murata, S. Watanabe, Y. Masuda, *J. Org. Chem.* **1997**, *62*, 6458-6459.

[43] M. Murata, T. Oyama, S. Watanabe, Y. Masuda, *J. Org. Chem.* **2000**, *65*, 164-168.

[44] K. C. Lam, T. B. Marder, Z. Lin, *Organometallics* **2010**, *29*, 1849-1857.

[45] T. Ishiyama, K. Ishida, N. Miyaura, *Tetrahedron* **2001**, *57*, 9813-9816.

[46] A. Furstner, G. Seidel, *Org. Lett.* **2002**, *4*, 541-543.

[47] W. Zhu, D. W. Ma, *Org. Lett.* **2006**, *8*, 261-263.

[48] C. Kleeberg, L. Dang, Z. Lin, T. B. Marder, *Angew. Chem. Int. Ed.* **2009**, *48*, 5350-5354.

[49] A. Bonet, C. Pubill-Ulldemolins, C. Bo, H. Gulyás, E. Fernández, *Angew. Chem. Int. Ed.* **2011**, *50*, 7158-7161.

[50] H. Gulyás, A. Bonet, C. Pubill-Ulldemolins, C. Sole, J. Cid, E. Fernández, *Pure Appl. Chem.* **2012**, *84*, 2219-2231.

[51] G. Yan, M. H. Yang, J. Yu, *Lett. Org. Chem.* **2012**, *9*, 71-75.

[52] J. Ratniyom, N. Dechnarong, S. Yotphan, S. Kiatisevi, *Eur. J. Org. Chem.* **2014**, *2014*, 1381-1385.

[53] H. Ito, K. Kubota, *Org. Lett.* **2012**, *14*, 890-893.

[54] J. H. Kim, Y. K. Chung, *RSC Adv.* **2014**, *4*, 39755-39758.

[55] A. S. Dudnik, G. C. Fu, *J. Am. Chem. Soc.* **2012**, *134*, 10693-10697.

[56] M. S. Cheung, F. K. Sheong, T. B. Marder, Z. Y. Lin, *Chem. Eur. J.* **2015**, *21*, 7480-7488.

[57] J. Yi, J.-H. Liu, J. Liang, J.-J. Dai, C.-T. Yang, Y. Fu, L. Liu, *Adv. Synth. Catal.* **2012**, *354*, 1685-1691.

[58] H. Xu, C. Zhao, Q. Qian, W. Deng, H. Gong, *Chem. Sci.* **2013**, *4*, 4022-4029.

[59] A. Joshi-Pangu, X. Ma, M. Diane, S. Iqbal, R. J. Kribs, R. Huang, C.-Y. Wang, M. R. Biscoe, *J. Org. Chem.* **2012**, *77*, 6629-6633.

[60] Y. Nagashima, R. Takita, K. Yoshida, K. Hirano, M. Uchiyama, *J. Am. Chem. Soc.* **2013**, *135*, 18730-18733.

[61] S. K. Bose, K. Fucke, L. Liu, P. G. Steel, T. B. Marder, *Angew. Chem. Int. Ed.* **2014**, *53*, 1799-1803.

[62] S. K. Bose, T. B. Marder, *Org. Lett.* **2014**, *16*, 4562-4565.

[63] S. K. Bose, A. Deißenberger, A. Eichhorn, P. G. Steel, Z. Lin, T. B. Marder, *Angew. Chem. Int. Ed.* **2015**, *54*, 11843-11847.

[64] T. C. Atack, R. M. Lecker, S. P. Cook, *J. Am. Chem. Soc.* **2014**, *136*, 9521-9523.

[65] R. B. Bedford, P. B. Brenner, E. Carter, T. Gallagher, D. M. Murphy, D. R. Pye, *Organometallics* **2014**, *33*, 5940-5943.

[66] W. Yao, H. Fang, S. Peng, H. Wen, L. Zhang, A. Hu, Z. Huang, *Organometallics* **2016**.

[67] T. C. Atack, S. P. Cook, *J. Am. Chem. Soc.* **2016**, *138*, 6139-6142.

[68] E. Yamamoto, K. Izumi, Y. Horita, H. Ito, *J. Am. Chem. Soc.* **2012**, *134*, 19997-20000.

[69] E. Yamamoto, K. Izumi, Y. Horita, S. Ukigai, H. Ito, *Top. Catal.* **2014**, *57*, 940-945.

[70] E. Yamamoto, S. Ukigai, H. Ito, *Chem. Sci.* **2015**, *6*, 2943-2951.

[71] R. Uematsu, E. Yamamoto, S. Maeda, H. Ito, T. Taketsugu, *J. Am. Chem. Soc.* **2015**, *137*, 4090-4099.

[72] J. Zhang, H.-H. Wu, J. Zhang, *Eur. J. Org. Chem.* **2013**, 6263-6266.

[73] D. G. Hall, *Boronic Acids: Preparation and Applications in Organic Synthesis, Medicine and Materials (Volume 1 and 2)*, 2nd ed., Wiley-VCH, Weinheim, **2011**.

[74] N. Miyaura, A. Suzuki, *J. Chem. Soc., Chem. Commun.* **1979**, 866-867.

[75] N. Miyaura, K. Yamada, A. Suzuki, *Tetrahedron Lett.* **1979**, *20*, 3437-3440.

[76] N. Miyaura, A. Suzuki, *Chem. Rev.* **1995**, *95*, 2457-2483.

[77] W. K. Chow, O. Y. Yuen, P. Y. Choy, C. M. So, C. P. Lau, W. T. Wong, F. Y. Kwong, *RSC Adv.* **2013**, *3*, 12518-12539.

[78] C.-T. Yang, Z.-Q. Zhang, H. Tajuddin, C.-C. Wu, J. Liang, J.-H. Liu, Y. Fu, M. Czyzewska, P. G. Steel, T. B. Marder, L. Liu, *Angew. Chem. Int. Ed.* **2012**, *51*, 528-532.

[79] S. L. Zultanski, G. C. Fu, *J. Am. Chem. Soc.* **2013**, *135*, 624-627.

[80] S. Pietsch, E. C. Neeve, D. C. Apperley, R. Bertermann, F. Y. Mo, D. Qiu, M. S. Cheung, L. Dang, J. B. Wang, U. Radius, Z. Y. Lin, C. Kleeberg, T. B. Marder, *Chem. Eur. J.* **2015**, *21*, 7082-7098.

[81] C. A. Tolman, *Chem. Rev.* **1977**, *77*, 313-348.

[82] L. Z. Chen, A. J. Poe, *Coord. Chem. Rev.* **1995**, *143*, 265-295.

[83] W. A. Henderson, C. A. Streuli, *J. Am. Chem. Soc.* **1960**, *82*, 5791-5794.

[84] A. J. Poe, D. H. Farrar, Y. Zheng, *J. Am. Chem. Soc.* **1992**, *114*, 5146-5152.

[85] J. R. Sowa, R. J. Angelici, *Inorg. Chem.* **1991**, *30*, 3534-3537.

[86] P. Dierkes, P. van Leeuwen, *J. Chem. Soc., Dalton Trans.* **1999**, 1519-1529.

[87] R. D. Dewhurst, E. C. Neeve, H. Braunschweig, T. B. Marder, *Chem. Commun.* **2015**, *51*, 9594-9607.

[88] W. Reeve, C. M. Erikson, P. F. Aluotto, *Can. J. Chem.* **1979**, *57*, 2747-2754.

[89] M. B. Smith, J. March, in *March's Advanced Organic Chemistry*, 6th ed., John Wiley & Sons, Inc., Hoboken, New Jersey (USA), **2006**.

[90] P. C. J. Kamer, P. W. N. van Leeuwen, J. N. H. Reek, *Acc. Chem. Res.* **2001**, *34*, 895-904.

[91] P. van Leeuwen, P. C. J. Kamer, J. N. H. Reek, P. Dierkes, *Chem. Rev.* **2000**, *100*, 2741-2769.

[92] L. A. van der Veen, P. H. Keeven, G. C. Schoemaker, J. N. H. Reek, P. C. J. Kamer, P. van Leeuwen, M. Lutz, A. L. Spek, *Organometallics* **2000**, *19*, 872-883.

[93] R. Thorwirth, F. Bernhardt, A. Stolle, B. Ondruschka, J. Asghari, *Chem. Eur. J.* **2010**, *16*, 13236-13242.

[94] X. F. Zhou, Y. D. Wu, J. J. Dai, Y. J. Li, Y. Huang, H. J. Xu, *RSC Adv.* **2015**, *5*, 46672-46676.

[95] Y. Isomura, T. Narushima, H. Kawasaki, T. Yonezawa, Y. Obora, *Chem. Commun.* **2012**, *48*, 3784-3786.

[96] H. Yi, A. Jutand, A. Lei, *Chem. Commun.* **2015**, *51*, 545-548.

[97] D. S. Laitar, P. Muller, J. P. Sadighi, *J. Am. Chem. Soc.* **2005**, *127*, 17196-17197.

[98] K. Semba, M. Shinomiya, T. Fujihara, J. Terao, Y. Tsuji, *Chem. Eur. J.* **2013**, *19*, 7125-7132.

[99] C. Borner, C. Kleeberg, *Eur. J. Inorg. Chem.* **2014**, 2486-2489.

[100] C. M. Wyss, J. Bitting, J. Bacsa, T. G. Gray, J. P. Sadighi, *Organometallics* **2016**, *35*, 71-74.

[101] T. Tsuda, T. Saegusa, Hashimot.T, *J. Am. Chem. Soc.* **1972**, *94*, 658-659.

[102] J. Huang, J. Chan, Y. Chen, C. J. Borths, K. D. Baucom, R. D. Larsen, M. M. Faul, *J. Am. Chem. Soc.* **2010**, *132*, 3674-3635.

[103] K. Semba, T. Fujihara, T. Xu, J. Terao, Y. Tsuji, *Adv. Synth. Catal.* **2012**, *354*, 1542-1550.

[104] P. Aslanidis, P. J. Cox, A. Kaltzoglou, A. C. Tsipis, *Eur. J. Inorg. Chem.* **2006**, 334-344.

[105] A. Tsuboyama, K. Kuge, M. Furugori, S. Okada, M. Hoshino, K. Ueno, *Inorg. Chem.* **2007**, *46*, 1992-2001.

[106] F. G. Moers, P. H. Op Het Veld, *J. Inorg. Nucl. Chem.* **1970**, *32*, 3225-3228.

[107] G. A. Bowmaker, S. E. Boyd, J. V. Hanna, R. D. Hart, P. C. Healy, B. W. Skelton, A. H. White, *J. Chem. Soc., Dalton Trans.* **2002**, 2722-2730.

[108] O. Moudam, A. Kaeser, B. Delavaux-Nicot, C. Duhayon, M. Holler, G. Accorsi, N. Armaroli, I. Seguy, J. Navarro, P. Destruel, J. F. Nierengarten, *Chem. Commun.* **2007**, 3077-3079.

[109] K. Rueck-Braun, B. Priewisch, *Sci. Synth.* **2007**, *31b*, 1401-1424.

[110] A. Béchamp, *Annales de Chimie et de Physique* **1854**, 186-196.

[111] M. Eck, S. Würtemberger-Pietsch, A. Eichhorn, J. H. Berthel, R. Bertermann, U. S. Paul, H. Schneider, A. Friedrich, C. Kleeberg, U. Radius, T. B. Marder, *Dalton Trans* **2017**, *46*, 3661-3680.

[112] Y. G. Lawson, M. J. G. Lesley, T. B. Marder, N. C. Norman, C. R. Rice, *Chem. Commun.* **1997**, 2051-2052.

[113] N. J. Bell, A. J. Cox, N. R. Cameron, J. S. O. Evans, T. B. Marder, M. A. Duin, C. J. Elsevier, X. Baucherel, A. A. D. Tulloch, R. P. Tooze, *Chem. Commun.* **2004**, 1854-1855.

[114] H. Ito, H. Yamanaka, J. Tateiwa, A. Hosomi, *Tetrahedron Lett.* **2000**, *41*, 6821-6825.

[115] K. Takahashi, T. Ishiyama, N. Miyaura, *Chem. Lett.* **2000**, 982-983.

[116] K. Takahashi, T. Ishiyama, N. Miyaura, *J. Organomet. Chem.* **2001**, *625*, 47-53.

[117] V. Lillo, A. Bonet, E. Fernández, *Dalton Trans.* **2009**, 2899-2908.

[118] A. Bonet, H. Gulyás, E. Fernández, *Angew. Chem. Int. Ed.* **2010**, *49*, 5130-5134.

[119] J. Cid, H. Gulyás, J. J. Carbó, E. Fernández, *Chem. Soc. Rev.* **2012**, *41*, 3558-3570.

[120] C. Pubill-Ulldemolins, A. Bonet, C. Bo, H. Gulyás, E. Fernández, *Chem. Eur. J.* **2012**, *18*, 1121-1126.

[121] I. Ibrahem, P. Breistein, A. Córdova, *Chem. Eur. J.* **2012**, *18*, 5175-5179.

[122] B. W. Liu, M. Gao, L. Dang, H. T. Zhao, T. B. Marder, Z. Y. Lin, *Organometallics* **2012**, *31*, 3410-3425.

[123] L. Dang, Z. Lin, T. B. Marder, *Organometallics* **2008**, *27*, 4443-4454.

[124] J. E. Lee, J. Yun, *Angew. Chem. Int. Ed.* **2008**, *47*, 145-147.

[125] A. D. J. Calow, A. Whiting, *Org. Biomol. Chem.* **2012**, *10*, 5485-5497.

[126] E. La Cascia, X. Sanz, C. Bo, A. Whiting, E. Fernández, *Org. Biomol. Chem.* **2015**, *13*, 1328-1332.

[127] S. Mun, J. E. Lee, J. Yun, *Org. Lett.* **2006**, *8*, 4887-4889.

[128] H. Chea, H. S. Sim, J. Yun, *Adv. Synth. Catal.* **2009**, *351*, 855-858.

[129] S. Lee, J. Yun, in *Synthesis and Application of Organoboron Compounds* (Eds.: E. Fernández, A. Whiting), Springer International Publishing, Cham (Switzerland), **2015**, pp. 73-92.

[130] K. S. Lee, A. R. Zhugralin, A. H. Hoveyda, *J. Am. Chem. Soc.* **2009**, *131*, 7253-7255.

[131] K. S. Lee, A. R. Zhugralin, A. H. Hoveyda, *J. Am. Chem. Soc.* **2010**, *132*, 12766-12766.

[132] H. Wu, S. Radomkit, J. M. O'Brien, A. H. Hoveyda, *J. Am. Chem. Soc.* **2012**, *134*, 8277-8285.

[133] H. Wu, J. M. Garcia, F. Haeffner, S. Radomkit, A. R. Zhugralin, A. H. Hoveyda, *J. Am. Chem. Soc.* **2015**, *137*, 10585-10602.

[134] P. Nguyen, C. Y. Dai, N. J. Taylor, W. P. Power, T. B. Marder, N. L. Pickett, N. C. Norman, *Inorg. Chem.* **1995**, *34*, 4290-4291.

[135] W. Clegg, C. Y. Dai, F. J. Lawlor, T. B. Marder, P. Nguyen, N. C. Norman, N. L. Pickett, W. P. Power, A. J. Scott, *J. Chem. Soc., Dalton Trans.* **1997**, 839-846.

[136] C. Y. Dai, S. M. Johnson, F. J. Lawlor, P. Lightfoot, T. B. Marder, N. C. Norman, A. G. Orpen, N. L. Pickett, M. J. Quayle, C. R. Rice, *Polyhedron* **1998**, *17*, 4139-4143.

[137] W. Clegg, T. B. Marder, S. Nlate, A. J. Scott, *Acta Cryst.* **2007**, *C63*, o603-o605.

[138] M. Gao, S. B. Thorpe, W. L. Santos, *Org. Lett.* **2009**, *11*, 3478-3481.

[139] S. B. Thorpe, X. Guo, W. L. Santos, *Chem. Commun.* **2011**, *47*, 424-426.

[140] M. Gao, S. B. Thorpe, C. Kleeberg, C. Slebodnick, T. B. Marder, W. L. Santos, *J. Org. Chem.* **2011**, *76*, 3997-4007.

[141] I. A. Cade, W. Y. Chau, I. Vitorica-Yrezabal, M. J. Ingleson, *Dalton Trans.* **2015**, *44*, 7506-7511.

[142] G. Palau-Lluch, X. Sanz, E. La Cascia, M. G. Civit, N. Miralles, A. B. Cuenca, E. Fernández, *Pure Appl. Chem.* **2015**, *87*, 181-193.

[143] J. M. O'Brien, A. H. Hoveyda, *J. Am. Chem. Soc.* **2011**, *133*, 7712-7715.

[144] H. Ito, Y. Horita, E. Yamamoto, *Chem. Commun.* **2012**, *48*, 8006-8008.

[145] T. Mita, J. Y. Chen, M. Sugawara, Y. Sato, *Org. Lett.* **2012**, *14*, 6202-6205.

[146] C. Kleeberg, C. Borner, *Eur. J. Inorg. Chem.* **2013**, 2799-2806.

[147] C. Kleeberg, A. G. Crawford, A. S. Batsanov, P. Hodgkinson, D. C. Apperley, M. S. Cheung, Z. Lin, T. B. Marder, *J. Org. Chem.* **2012**, *77*, 785-789.

[148] C. Kleeberg, IMEboronXIV, Niagara Falls, Canada, **2011**.

[149] T. B. Marder, Euroboron 5, Edinburgh, U.K., **2010**.

[150] X. Sanz, G. M. Lee, C. Pubill-Ulldemolins, A. Bonet, H. Gulyás, S. A. Westcott, C. Bo, E. Fernández, *Org. Biomol. Chem.* **2013**, *11*, 7004-7010.

[151] A. Bonet, C. Solé, H. Gulyás, E. Fernández, *Org. Biomol. Chem.* **2012**, *10*, 6621-6623.

[152] A. Bonet, C. Solé, H. Gulyás, E. Fernández, *Chem. Asian J.* **2011**, *6*, 1011-1014.

[153] C. Pubill-Ulldemolins, A. Bonet, H. Gulyás, C. Bo, E. Fernández, *Org. Biomol. Chem.* **2012**, *10*, 9677-9682.

[154] J. Cid, J. J. Carbó, E. Fernández, *Chem. Eur. J.* **2012**, *18*, 12794-12802.

[155] C. Solé, H. Gulyás, E. Fernández, *Chem. Commun.* **2012**, *48*, 3769-3771.

[156] J. Cid, J. J. Carbó, E. Fernández, *Chem. Eur. J.* **2014**, *20*, 3616-3620.

[157] D. Schmidt, J. H. J. Berthel, S. Pietsch, U. Radius, *Angew. Chem. Int. Ed.* **2012**, *51*, 8881-8885.

[158] M. Arrowsmith, M. S. Hill, G. Kociok-Kohn, D. J. MacDougall, M. F. Mahon, *Angew. Chem. Int. Ed.* **2012**, *51*, 2098-2100.

[159] M. Arrowsmith, M. S. Hill, G. Kociok-Kohn, *Organometallics* **2015**, *34*, 653-662.

[160] S. M. I. Al-Rafia, R. McDonald, M. J. Ferguson, E. Rivard, *Chem. Eur. J.* **2012**, *18*, 13810-13820.

[161] D. Franz, S. Inoue, *Chem. Asian J.* **2014**, *9*, 2083-2087.

[162] T. Wang, D. W. Stephan, *Chem. Eur. J.* **2014**, *20*, 3036-3039.

[163] K. J. Iversen, D. J. D. Wilson, J. L. Dutton, *Dalton Trans.* **2013**, *42*, 11035-11038.

[164] M. R. Momeni, E. Rivard, A. Brown, *Organometallics* **2013**, *32*, 6201-6208.

[165] K. J. Iversen, D. J. D. Wilson, J. L. Dutton, *Organometallics* **2013**, *32*, 6209-6217.

[166] K. J. Iversen, D. J. D. Wilson, J. L. Dutton, *Dalton Trans.* **2014**, *43*, 12820-12823.

[167] R. Fang, L. Z. Yang, Q. Wang, *Organometallics* **2014**, *33*, 53-60.

[168] M. D. Su, *Inorg. Chem.* **2014**, *53*, 5080-5087.

[169] K. J. Iversen, D. J. D. Wilson, J. L. Dutton, *Dalton Trans.* **2015**, *44*, 3318-3325.

[170] S. Pietsch, U. Paul, I. A. Cade, M. J. Ingleson, U. Radius, T. B. Marder, *Chem. Eur. J.* **2015**, *21*, 9018-9021.

[171] S. Würtemberger-Pietsch, U. Radius, T. B. Marder, *Dalton Trans.* **2016**, *45*, 5880-5895.

[172] S. Würtemberger-Pietsch, H. Schneider, T. B. Marder, U. Radius, *Chem. Eur. J.* **2016**, *22*, 13032-13036.

[173] A. B. Cuenca, N. Zigon, V. Duplan, M. Hoshino, M. Fujita, E. Fernández, *Chem. Eur. J.* **2016**, *22*, 4723-4726.

[174] T. Ishiyama, M. Murata, T. Ahiko, N. Miyaura, *Org. Synth.* **2000**, *77*, 176-185.

[175] P. Nguyen, G. Lesley, N. J. Taylor, T. B. Marder, N. L. Pickett, W. Clegg, M. R. J. Elsegood, N. C. Norman, *Inorg. Chem.* **1994**, *33*, 4623-4624.

[176] S. A. Westcott, H. P. Blom, T. B. Marder, R. T. Baker, J. C. Calabrese, *Inorg. Chem.* **1993**, *32*, 2175-2182.

[177] G. Lesley, P. Nguyen, N. J. Taylor, T. B. Marder, A. J. Scott, W. Clegg, N. C. Norman, *Organometallics* **1996**, *15*, 5137-5154.

[178] W. G. Henderson, M. J. How, G. R. Kennedy, E. F. Mooney, *Carbohydr. Res.* **1973**, *28*, 1-12.

[179] J. A. Blau, W. Gerrard, M. F. Lappert, *J. Chem. Soc.* **1957**, 4116-4120.

[180] J. A. Blau, W. Gerrard, M. F. Lappert, *J. Chem. Soc.* **1960**, 667-670.

[181] A. J. Hubert, B. Hargitay, J. Dale, *J. Chem. Soc.* **1961**, 931-936.

[182] S. H. Rose, S. G. Shore, *Inorg. Chem.* **1962**, *1*, 744-748.

[183] S. Würtemberger-Pietsch, PhD thesis, Institute of Inorganic Chemistry, University of Würzburg **2016**.

[184] D. Curtis, M. J. G. Lesley, N. C. Norman, A. G. Orpen, J. Starbuck, *J. Chem. Soc., Dalton Trans.* **1999**, 1687-1694.

[185] A. J. Arduengo, III, R. Krafczyk, R. Schmutzler, H. A. Craig, J. R. Goerlich, W. J. Marshall, M. Unverzagt, *Tetrahedron* **1999**, *55*, 14523-14534.

[186] X. Bantreil, S. P. Nolan, *Nature Protocols* **2011**, *6*, 69-77.

[187] N. Kuhn, T. Kratz, *Synthesis* **1993**, *1993*, 561-562.

[188] T. Schaub, M. Backes, U. Radius, *Organometallics* **2006**, *25*, 4196-4206.

[189] T. Schaub, U. Radius, A. Brucks, M. P. Choules, M. T. Olsen, T. B. Rauchfuss, *Inorg. Synth.* **2010**, *35*, 78-83.

[190] J. Rohonczy, SOLA – Solid Lineshape Analysis Version 2.2.4, Bruker Biospin, Rheinstetten, Germany **2013**.

[191] R. P. van Summeren, S. J. W. Reijmer, B. L. Feringa, A. J. Minnaard, *Chem. Commun.* **2005**, 1387-1389.

[192] J. W. Clary, T. J. Rettenmaier, R. Snelling, W. Bryks, J. Banwell, W. T. Wipke, B. Singaram, *J. Org. Chem.* **2011**, *76*, 9602-9610.

[193] N. Sakai, K. Fujii, S. Nabeshima, R. Ikeda, T. Konakahara, *Chem. Commun.* **2010**, *46*, 3173-3175.

[194] B. A. Baker, Z. V. Bokovic, B. H. Lipshutz, *Org. Lett.* **2008**, *10*, 289-292.

[195] N. J. Farrer, R. McDonald, T. Piga, J. S. McIndoe, *Polyhedron* **2010**, *29*, 254-261.

[196] D. Stalke, *Chem. Soc. Rev.* **1998**, *27*, 171-178.

[197] A. Altomare, G. Cascarano, C. Giacovazzo, A. Guagliardi, *J. Appl. Crystallogr.* **1993**, *26*, 343-350.

[198] G. M. Sheldrick, *Acta Cryst.* **2008**, *A64*, 112-122.

[199] G. M. Sheldrick, *Acta Cryst.* **2015**, *A71*, 3-8.

[200] A. L. Spek, PLATON - A Multipurpose Crystallographic Tool, Utrecht University, Utrecht, The Netherlands **1998**.

[201] Diamond Version 4.2.2. - Crystal and Molecular Structure Visualization, Crystal Impact - Dr. H. Putz and Dr. K. Brandenburg GbR, Kreuzherrenstr. 102, 53227 Bonn, Germany.

[202] L. J. Farrugia, *J. Appl. Crystallogr.* **1999**, *32*, 837-838.

[203] C. F. Macrae, I. J. Bruno, J. A. Chisholm, P. R. Edgington, P. McCabe, E. Pidcock, L. Rodriguez-Monge, R. Taylor, J. van de Streek, P. A. Wood, *J. Appl. Crystallogr.* **2008**, *41*, 466-470.

[204] A. Addamiano, *J. Phys. Chem.* **1958**, *62*, 1018-1020.

APPENDIX

APPENDIX

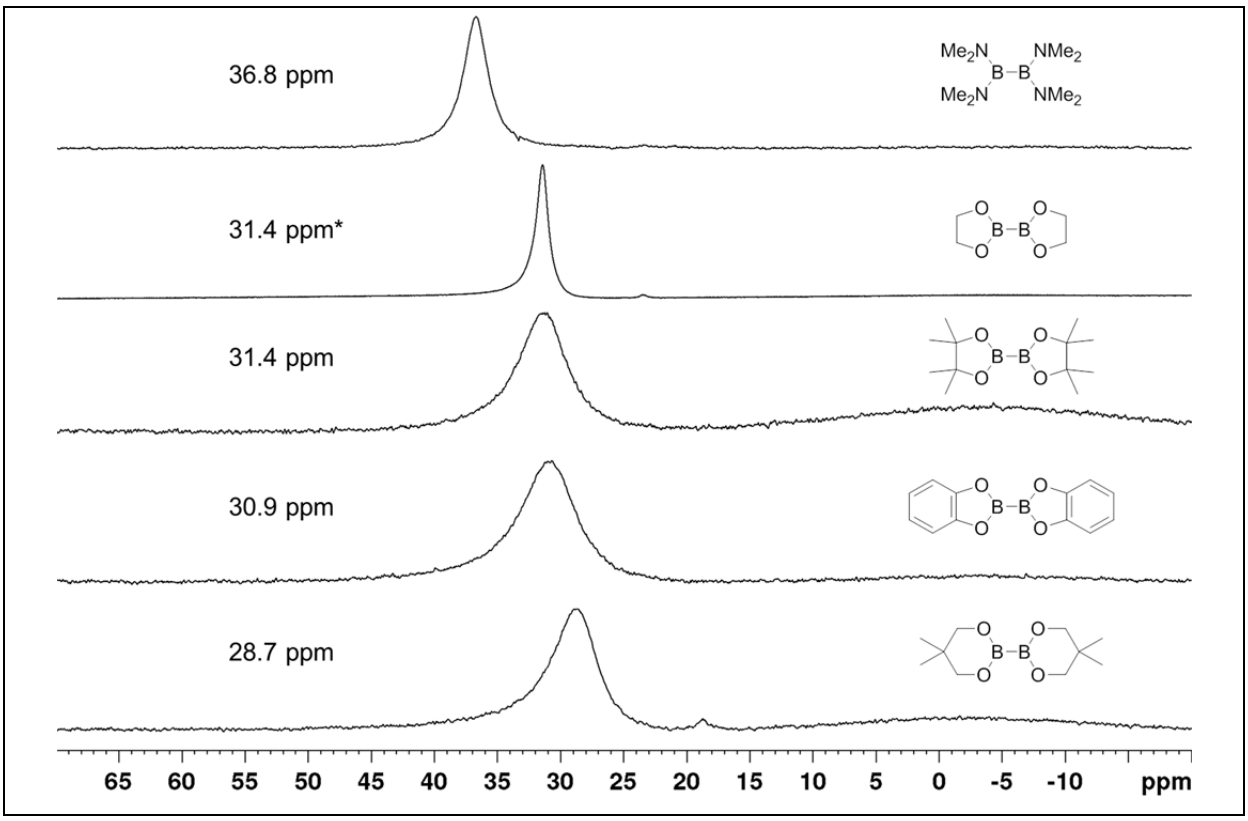

Figure A1.1: $^{11}B\{^{1}H\}$ NMR spectra of selected diboron(4) compounds in C_6D_6 (64 MHz, *96 MHz, 25 °C).

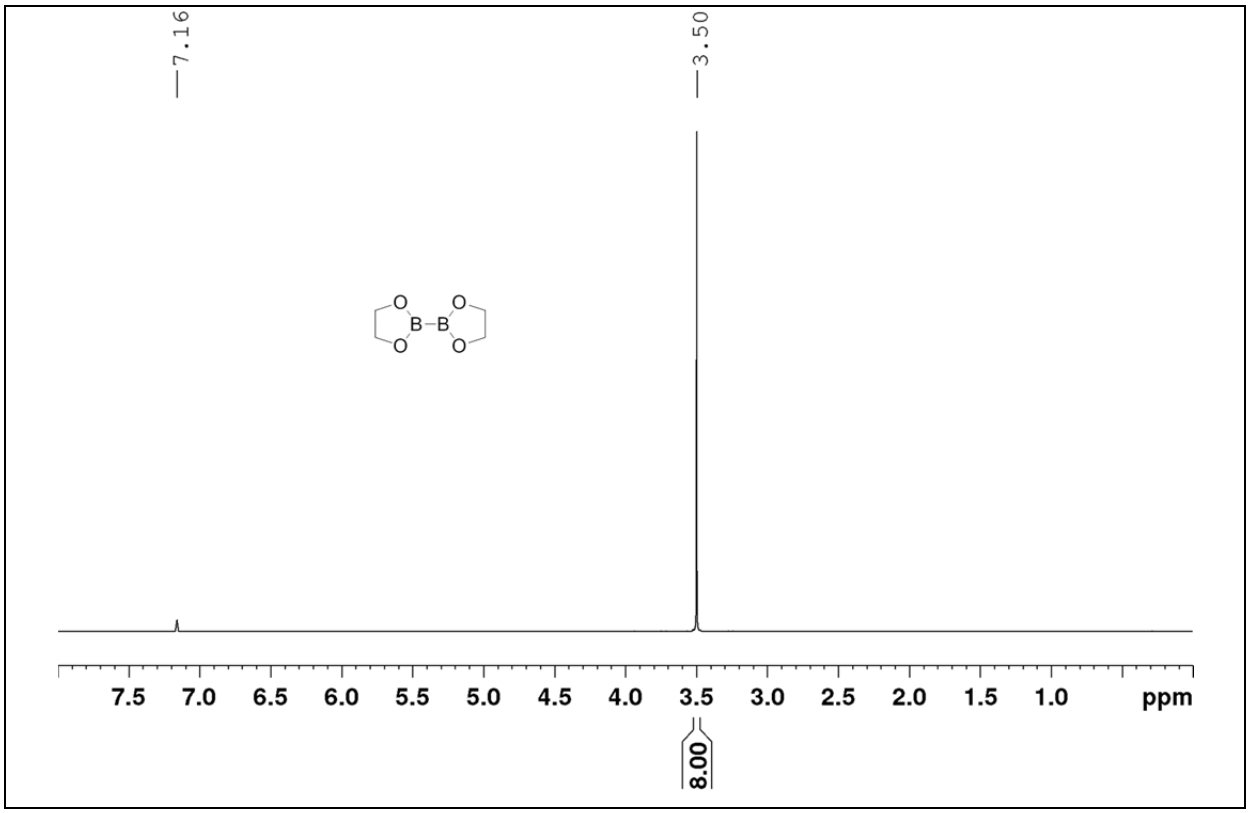

Figure A2.1: ^{1}H NMR spectrum of compound **110** in C_6D_6 (300 MHz, 25 °C).

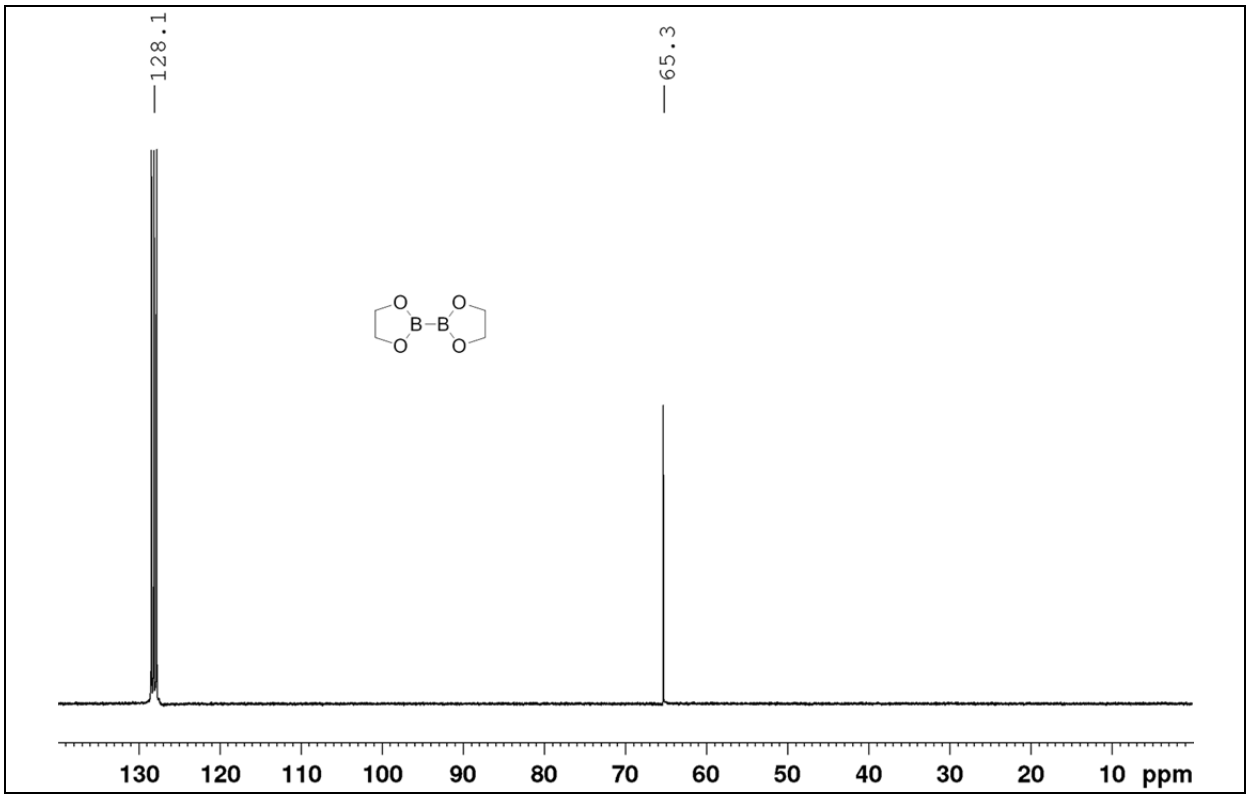

Figure A2.2: ^{13}C{^{1}H} NMR spectrum of compound **110** in C_6D_6 (75 MHz, 25 °C).

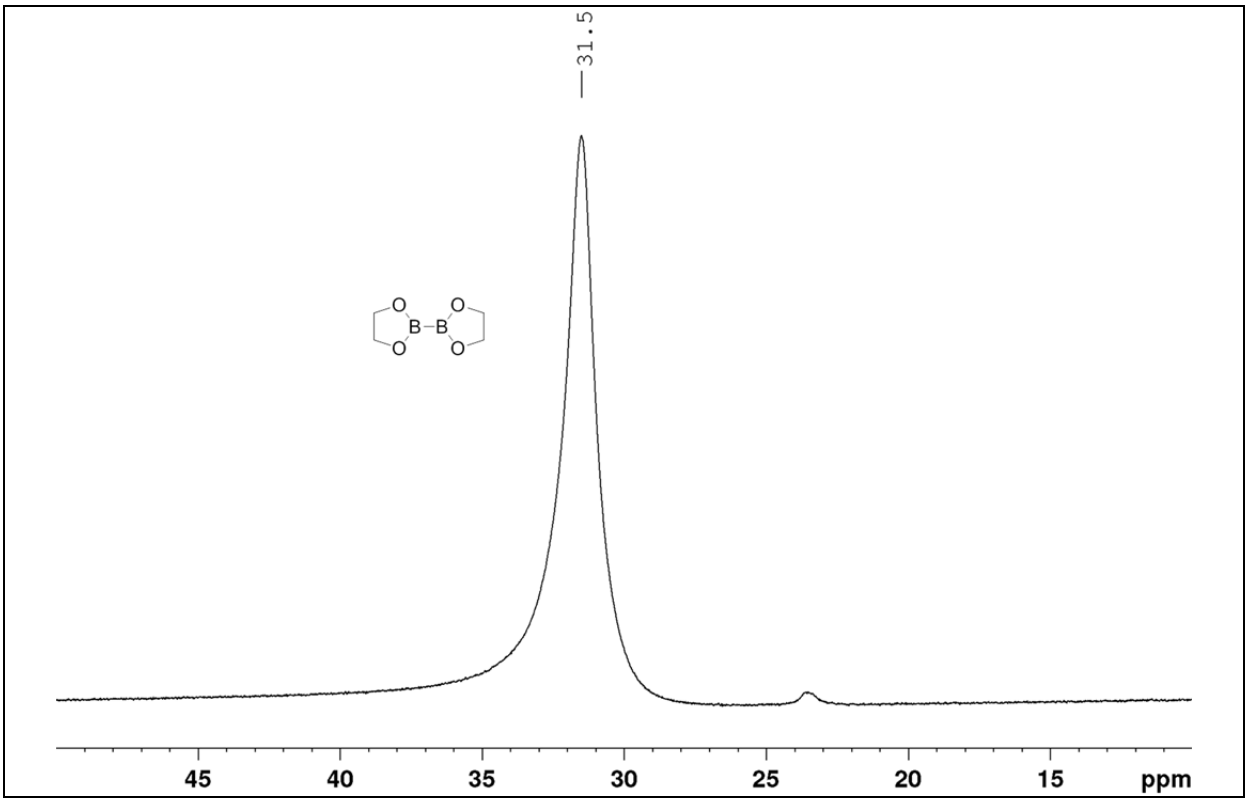

Figure A2.3: $^{11}B\{^{1}H\}$ NMR spectrum of compound **110** in C_6D_6 (96 MHz, 25 °C).

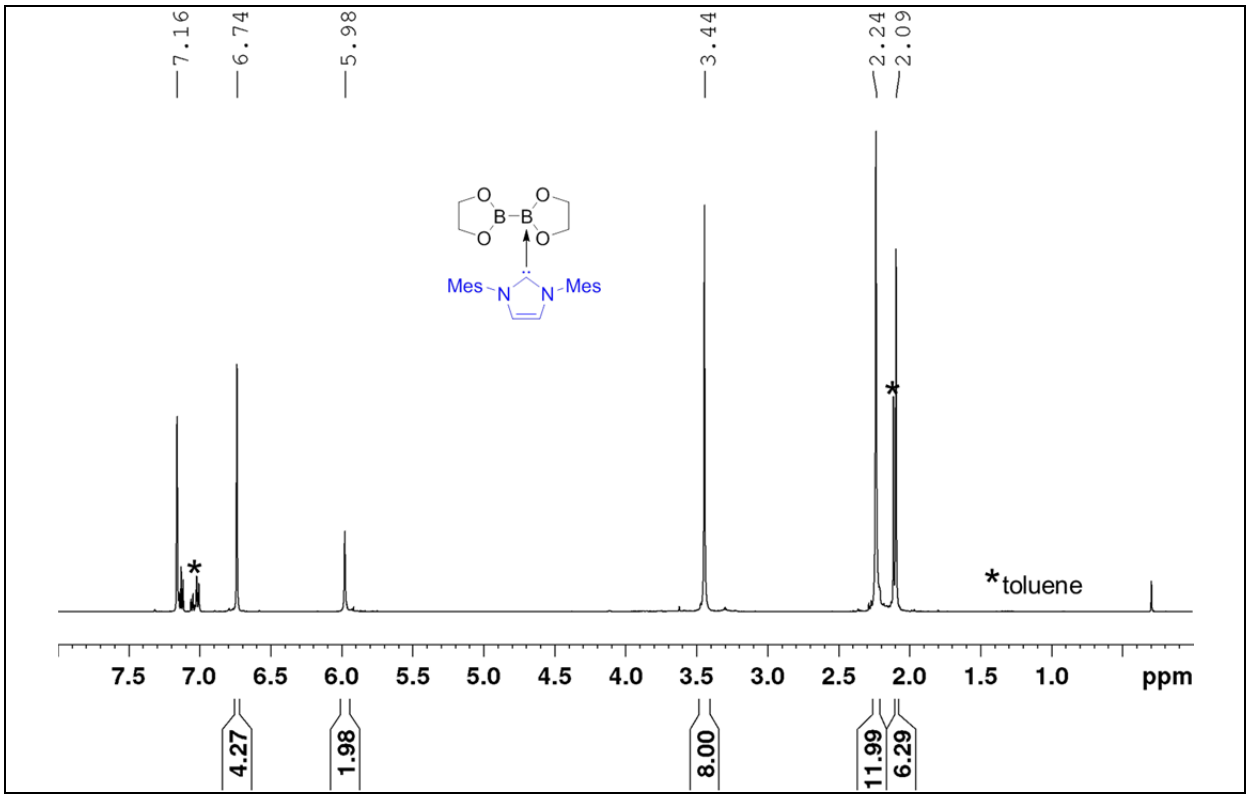

Figure A3.1: ^{1}H NMR spectrum of compound **118** in C_6D_6 (500 MHz, 25 °C).

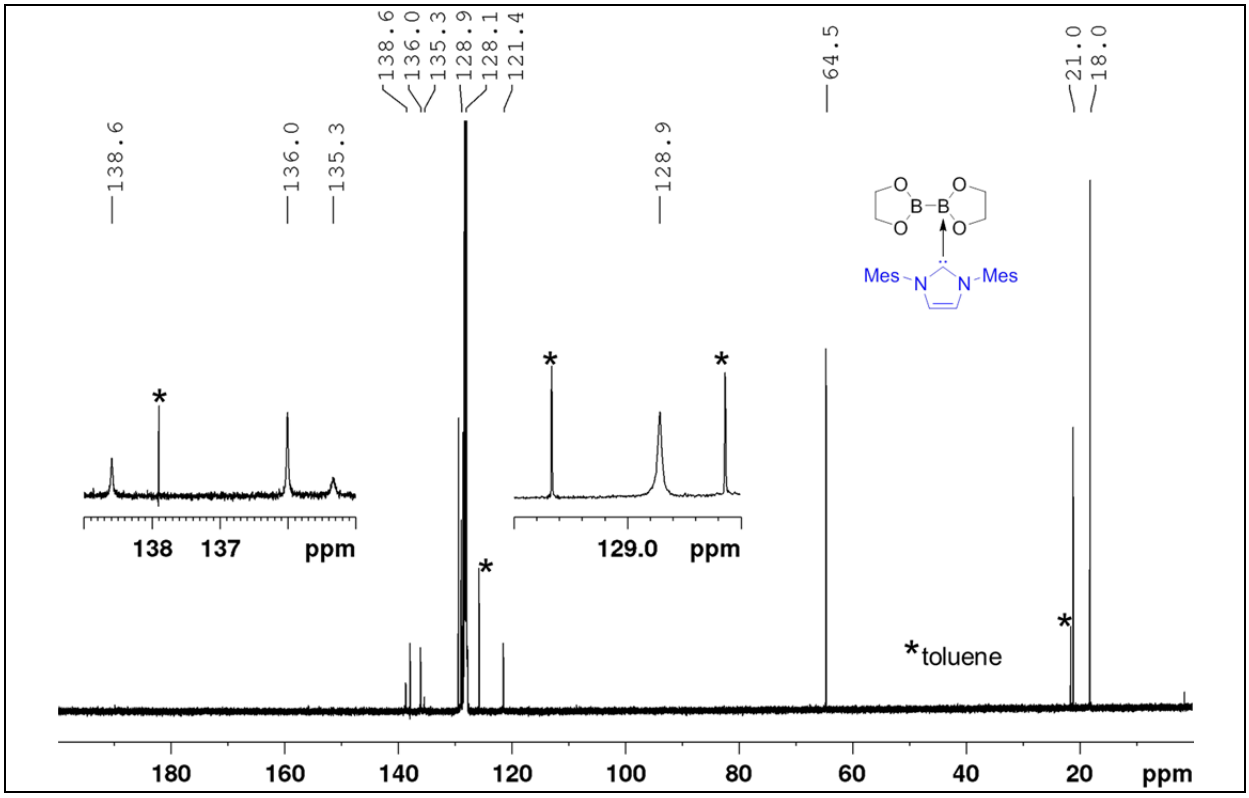

Figure A3.2: ^{13}C{^{1}H} NMR spectrum of compound **118** in C_6D_6 (125 MHz, 25 °C).

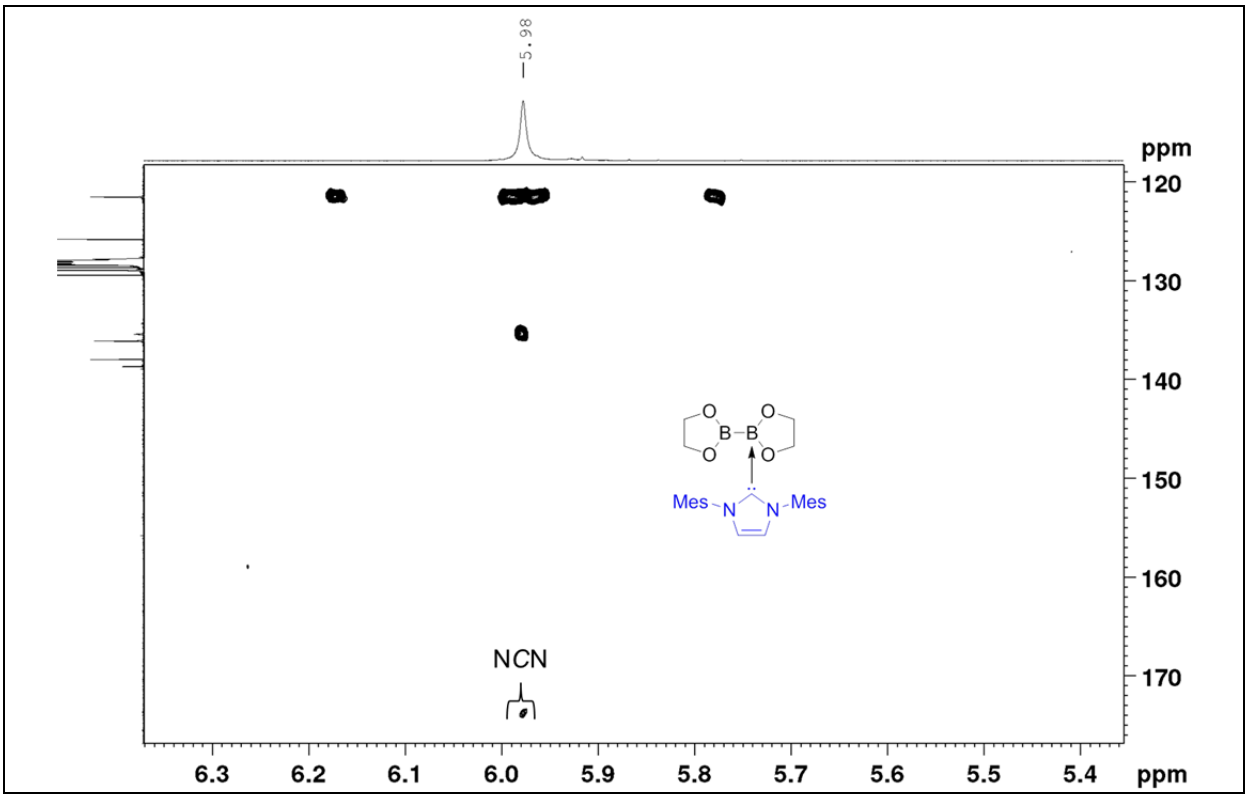

Figure A3.3: $^{13}C,^{1}H$ HMBC NMR spectrum of compound **118** in C_6D_6 (125 MHz, 25 °C).

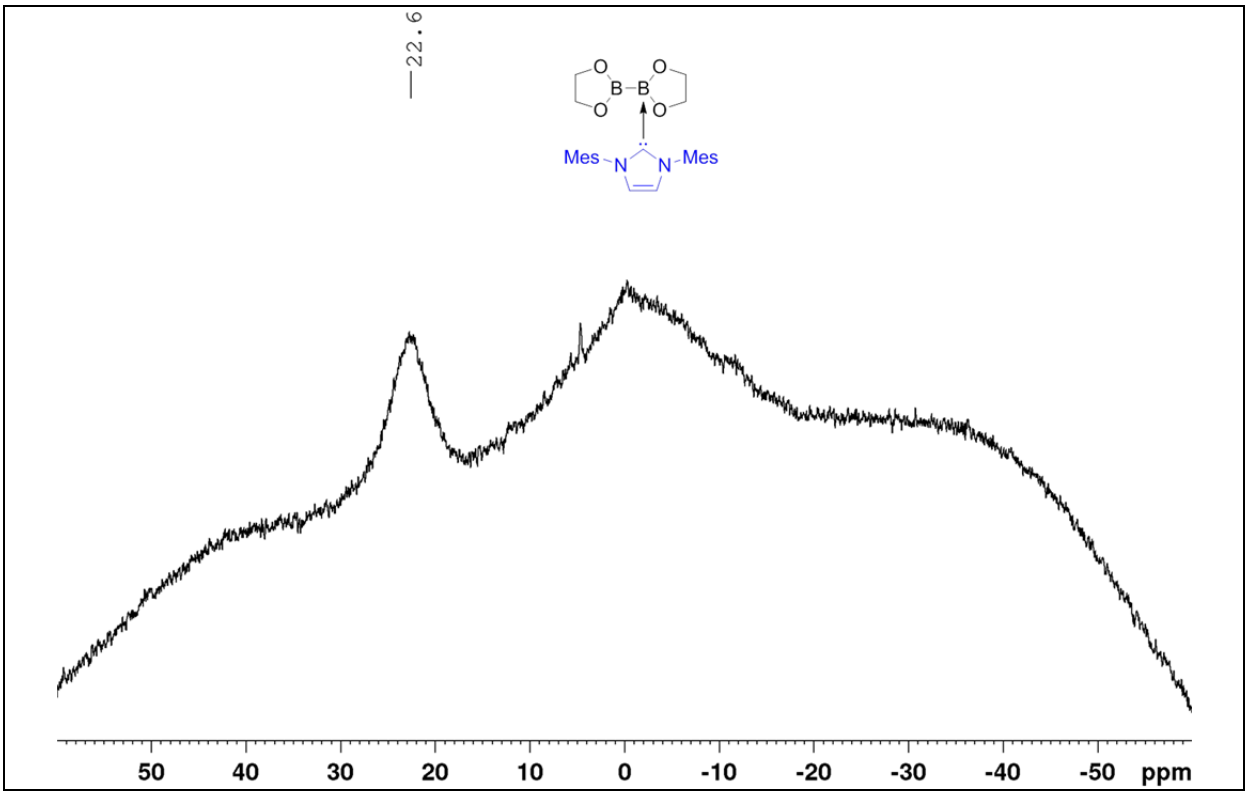

Figure A3.4: $^{11}B\{^{1}H\}$ NMR spectrum of compound **118** in C_6D_6 (96 MHz, 25 °C).

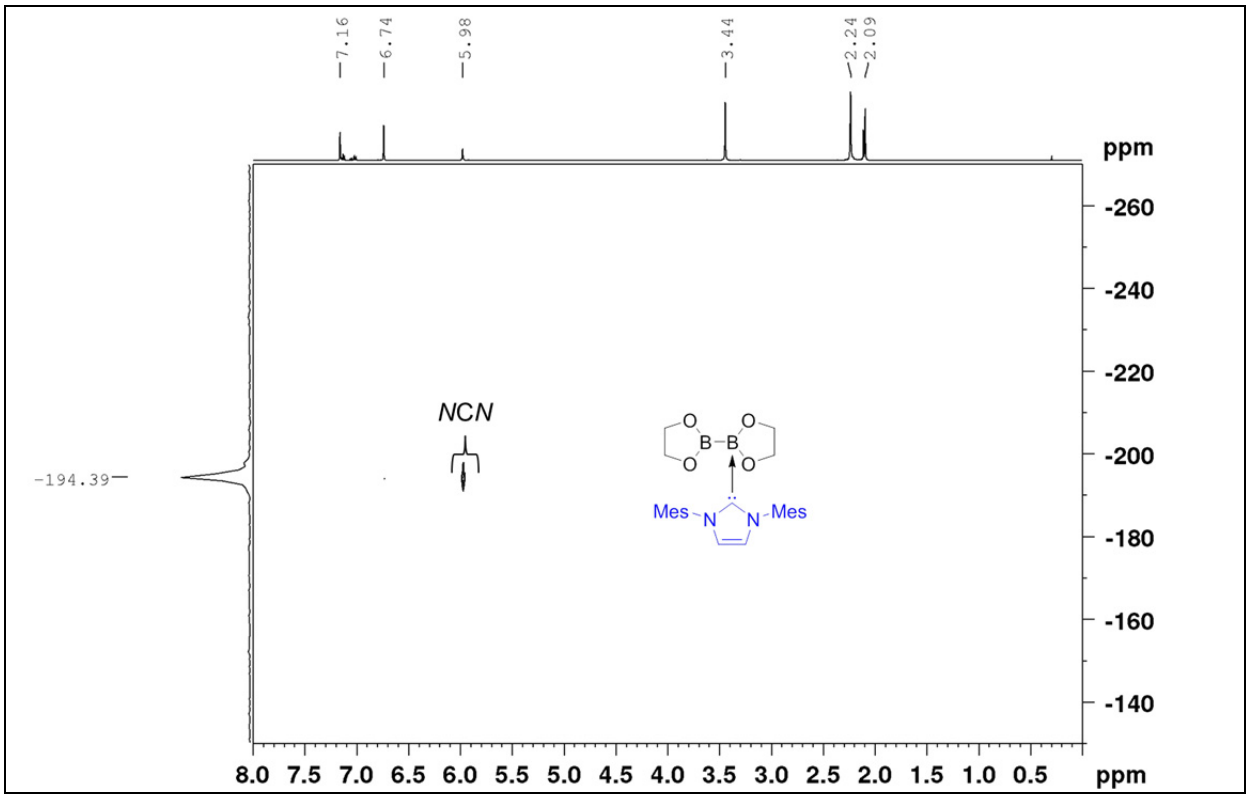

Figure A3.5: $^{15}N,^{1}H$ HMBC NMR spectrum of compound **118** in C_6D_6 (51 MHz, 25 °C).

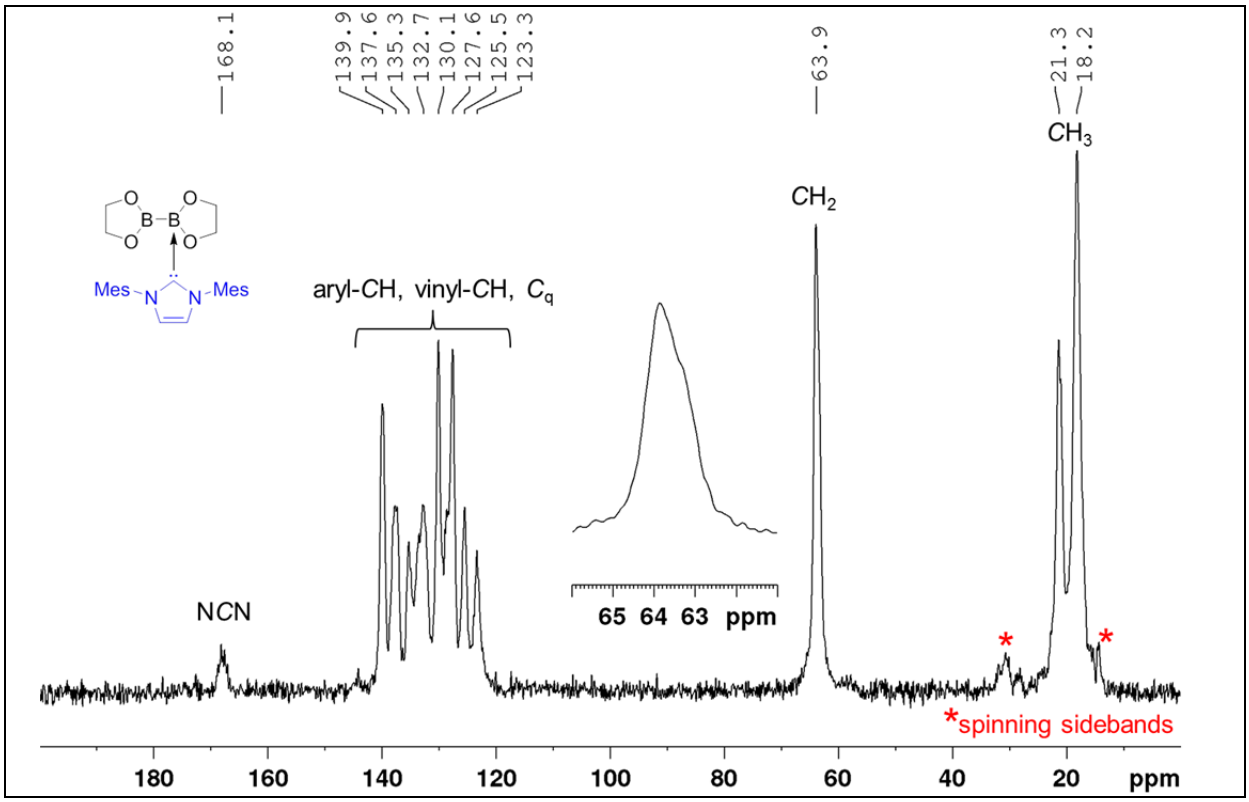

Figure A3.6: ^{13}C CP/MAS NMR spectrum of compound **118** (101 MHz, 22 °C, ν rot = 11000 Hz).

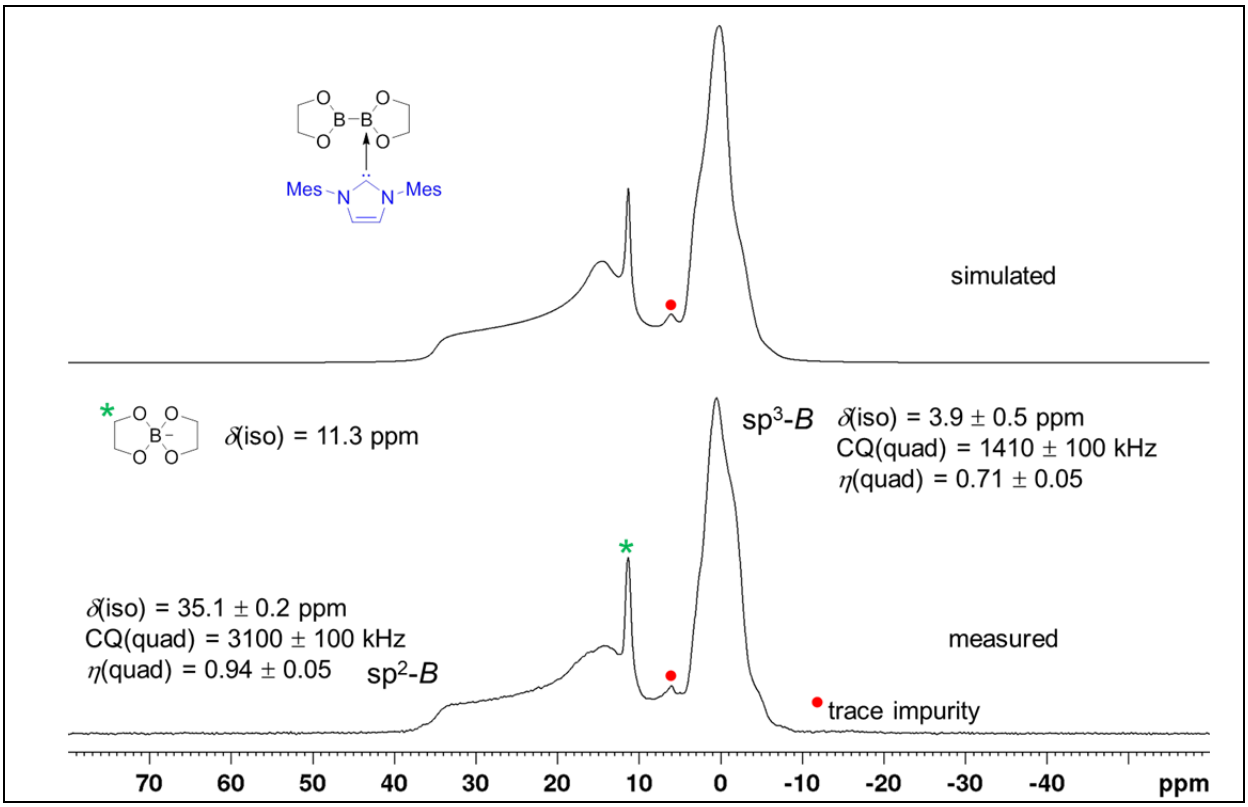

Figure A3.7: ^{11}B RSHE/MAS NMR spectrum of compound **118** (128 MHz, 22 °C, ν rot = 15000 Hz).

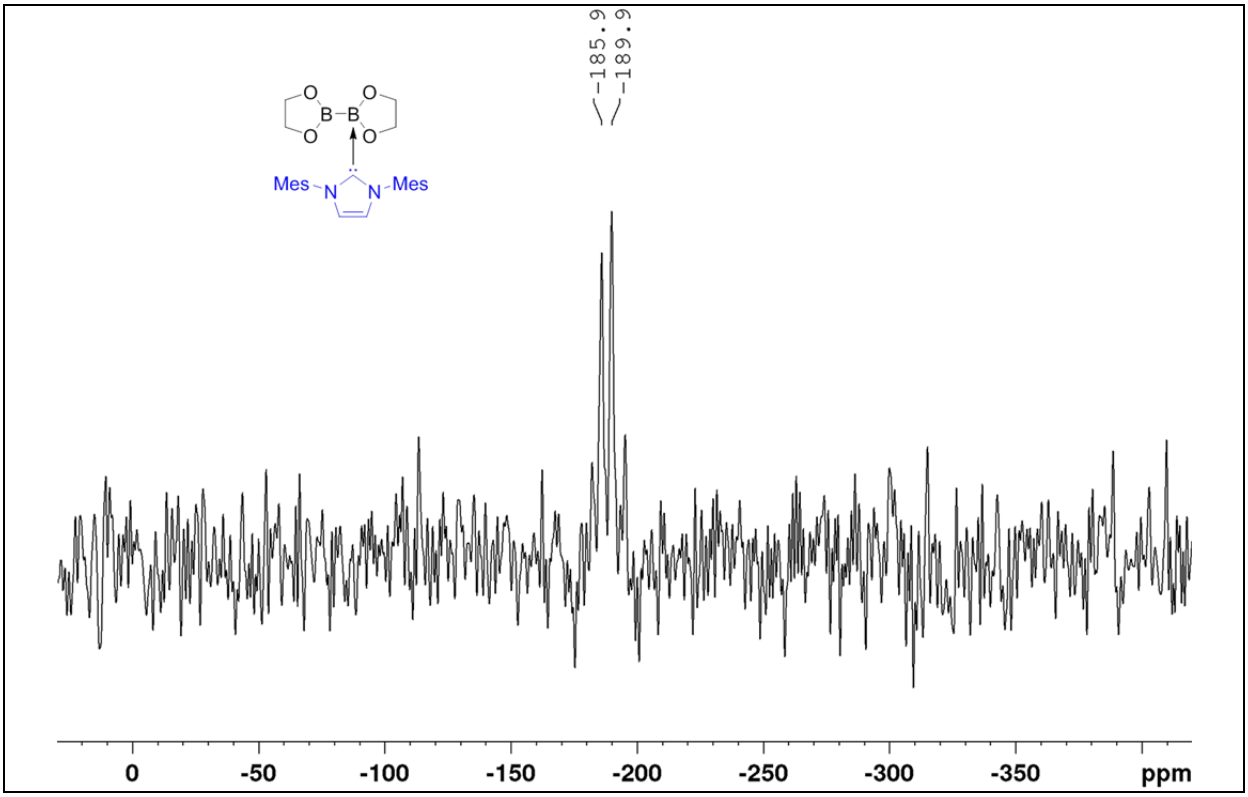

Figure A3.8: ^{15}N CP/MAS NMR spectrum of compound **118** (41 MHz, 22 °C, ν rot = 7000 Hz).

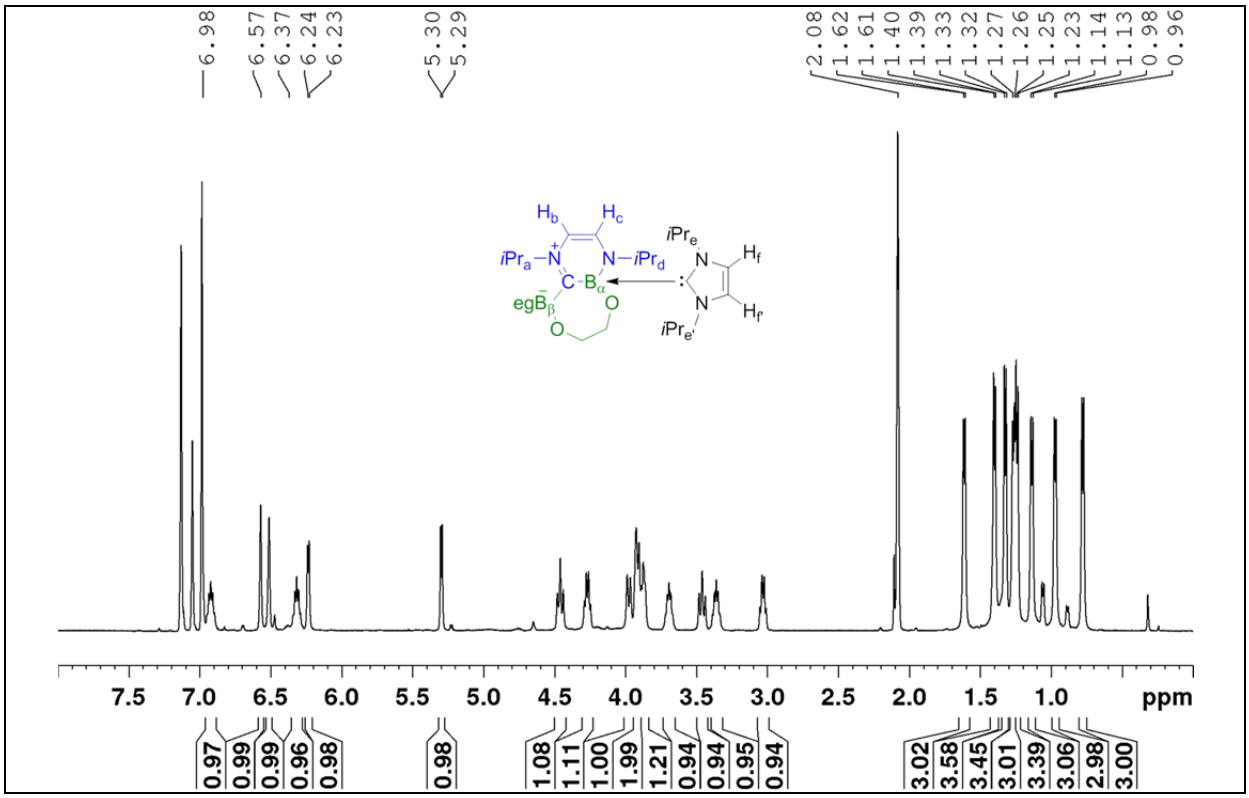

Figure A4.1: ^{1}H NMR spectrum of compound **120** in d_8-toluene (500 MHz, -40 °C).

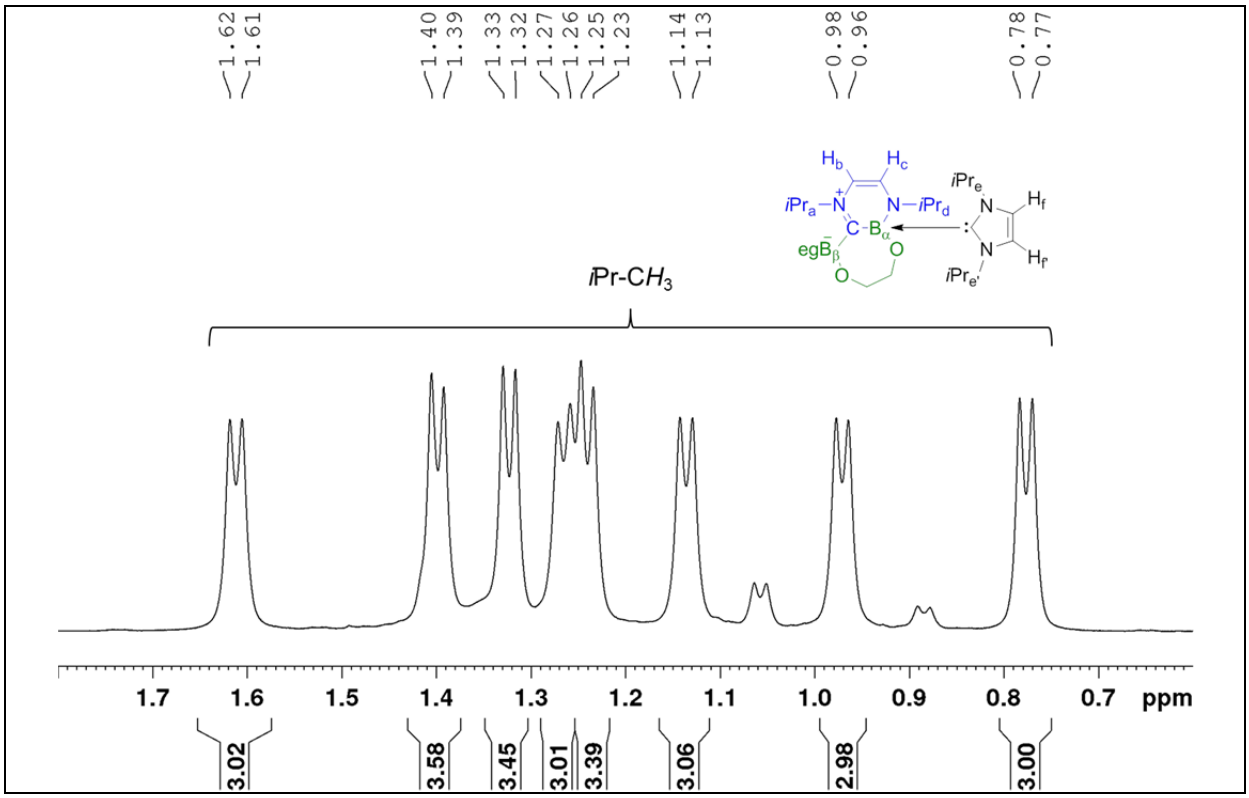

Figure A4.2: ^{1}H NMR spectrum of compound **120** in d_8-toluene (500 MHz, -40 °C).

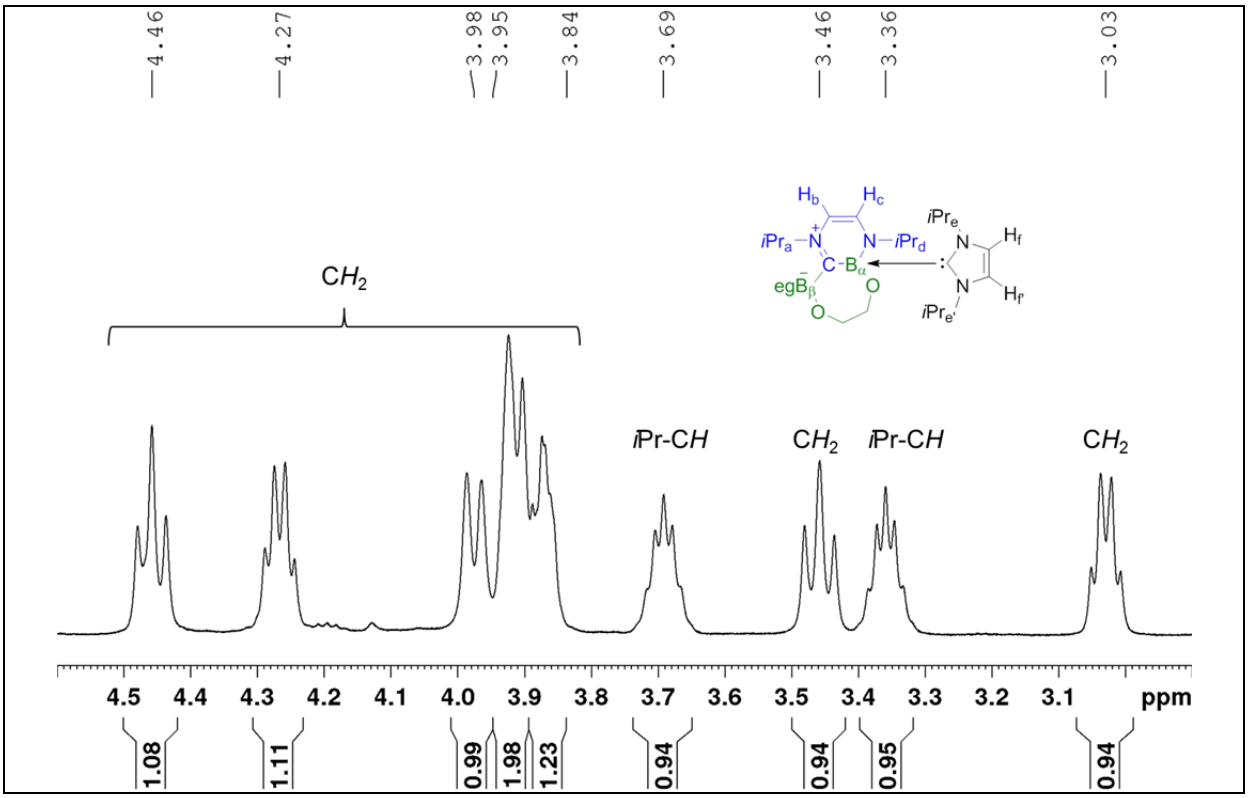

Figure A4.3: ^{1}H NMR spectrum of compound **120** in d_8-toluene (500 MHz, -40 °C).

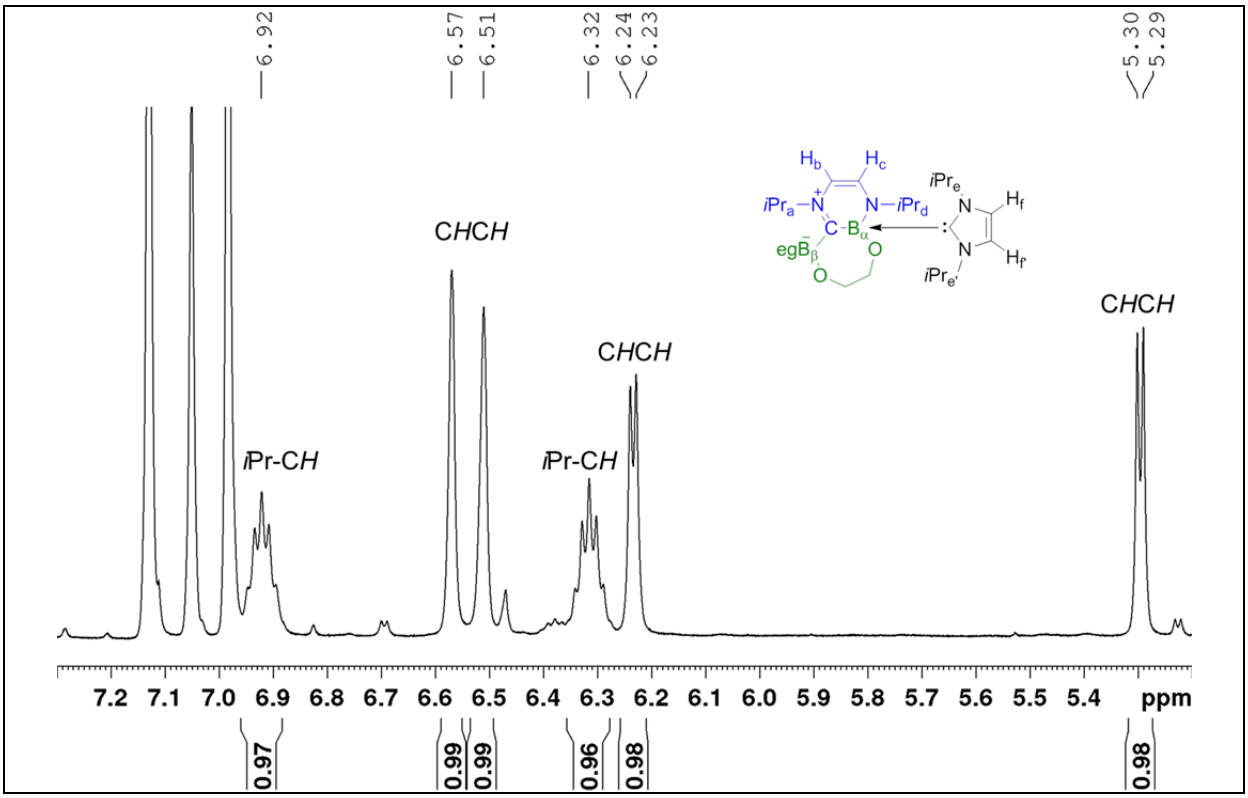

Figure A4.4: ^{1}H NMR spectrum of compound **120** in d_8-toluene (500 MHz, -40 °C).

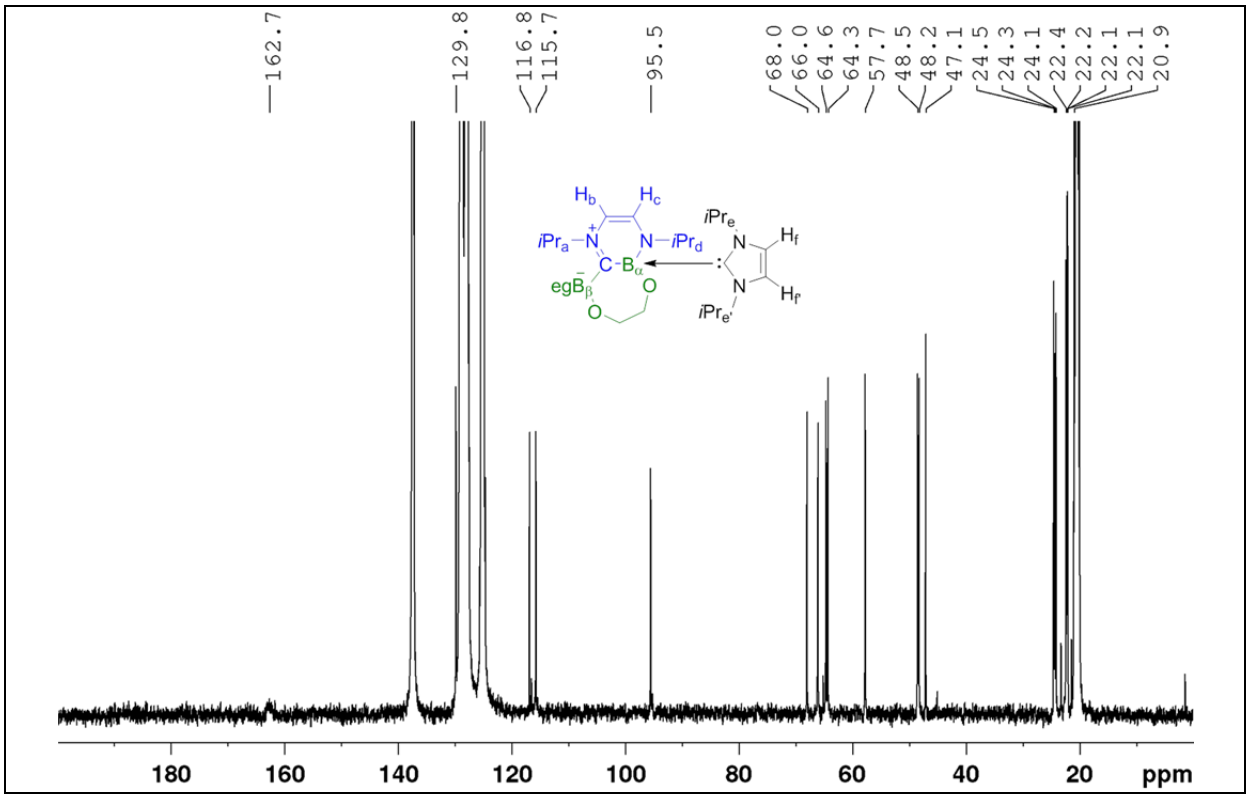

Figure A4.5: $^{13}C\{^{1}H\}$ NMR spectrum of compound **120** in d_8-toluene (125 MHz, -40 °C).

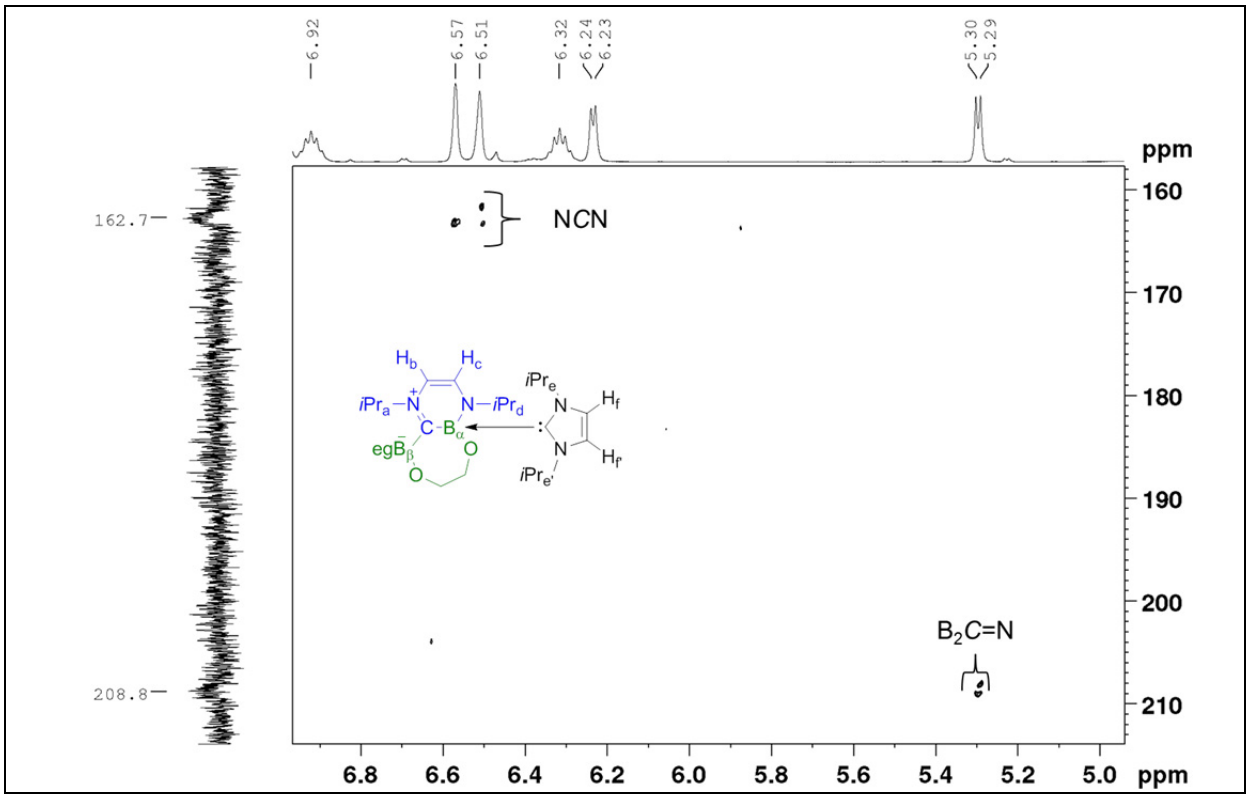

Figure A4.6: $^{13}C,^{1}H$ HMBC NMR spectrum of compound **120** in d_8-toluene (125 MHz, -40 °C).

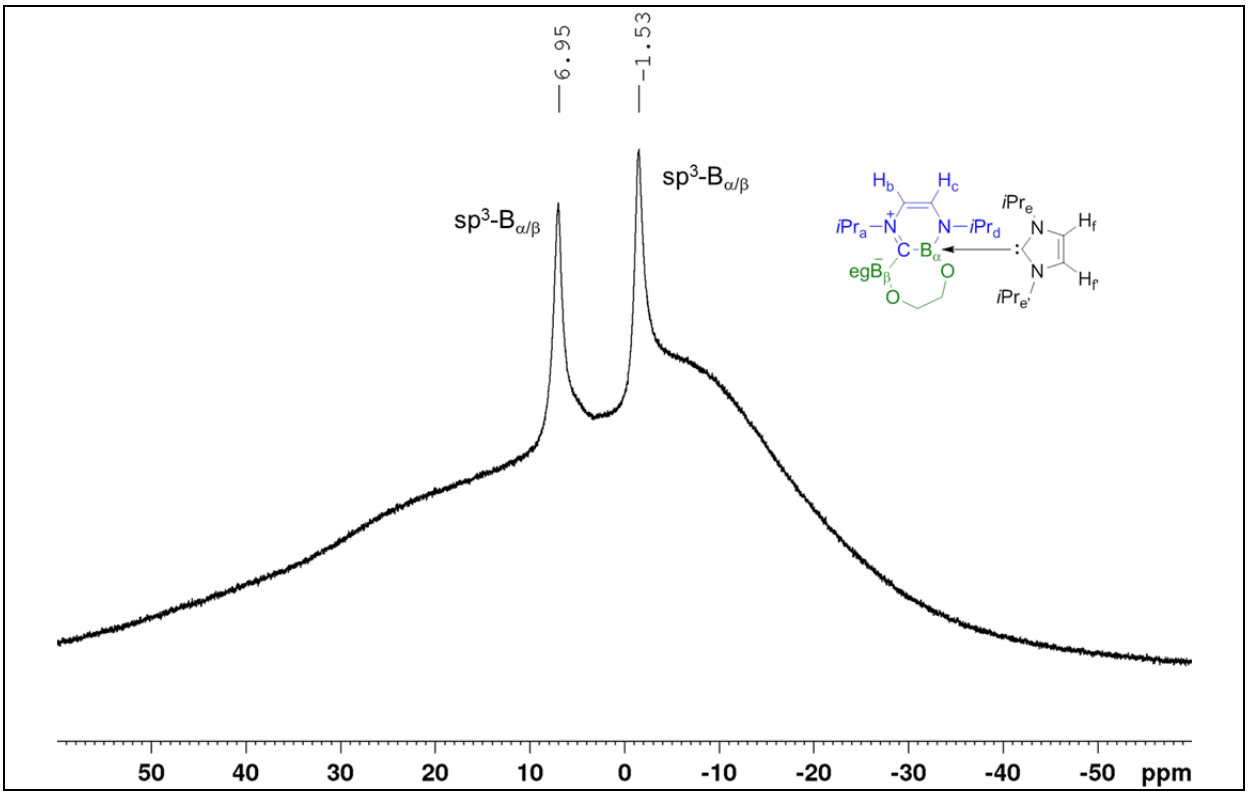

Figure A4.7: $^{11}B\{^{1}H\}$ NMR spectrum of compound **120** in d_8-toluene (160 MHz, -40 °C).

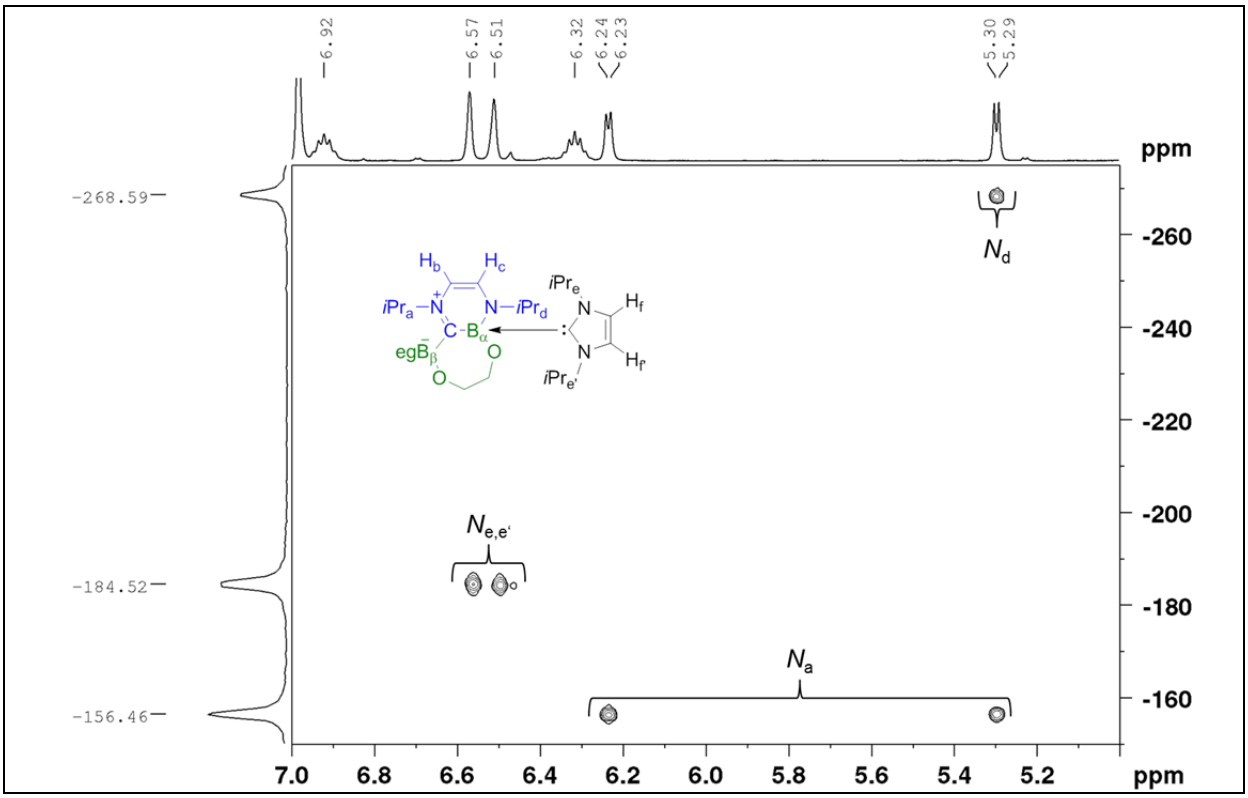

Figure A4.8: $^{15}N,^{1}H$ HMBC NMR spectrum of compound **120** in d_8-toluene (51 MHz, -40 °C).

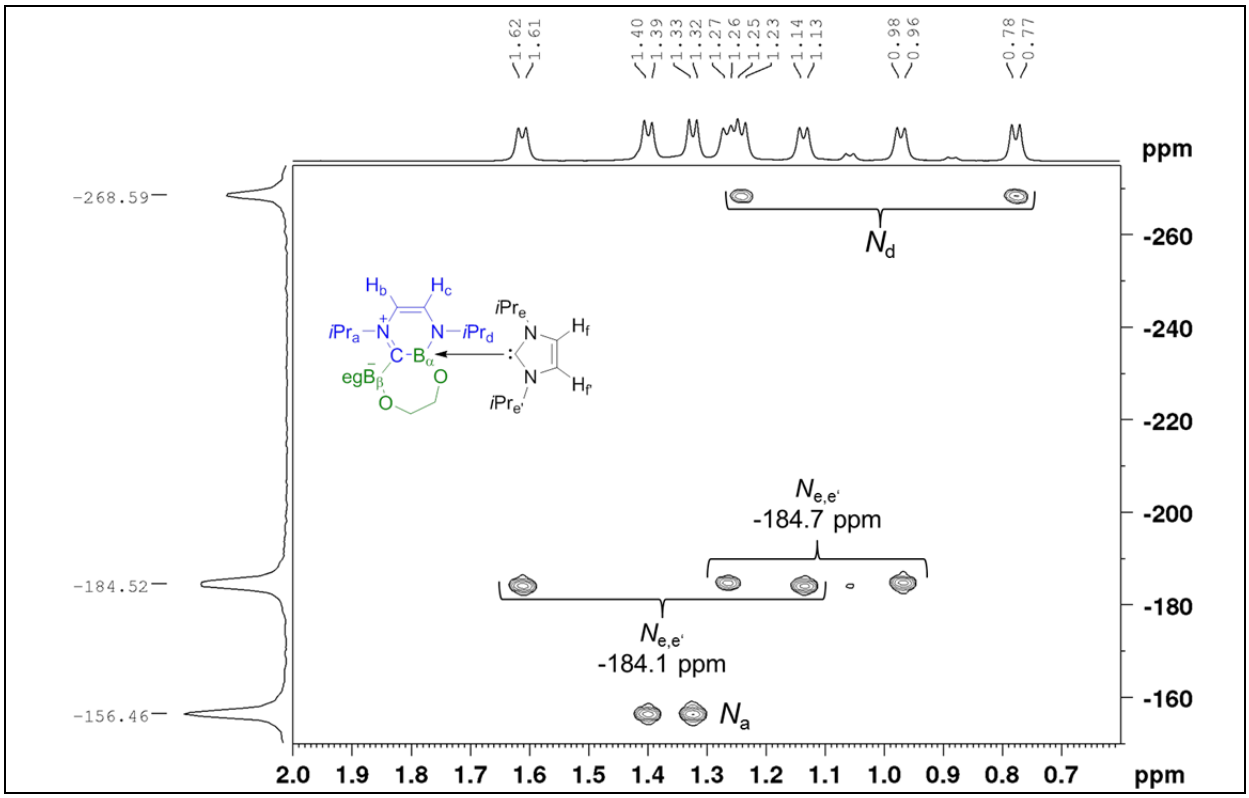

Figure A4.9: $^{15}N,^{1}H$ HMBC NMR spectrum of compound **120** in d_8-toluene (51 MHz, -40 °C).

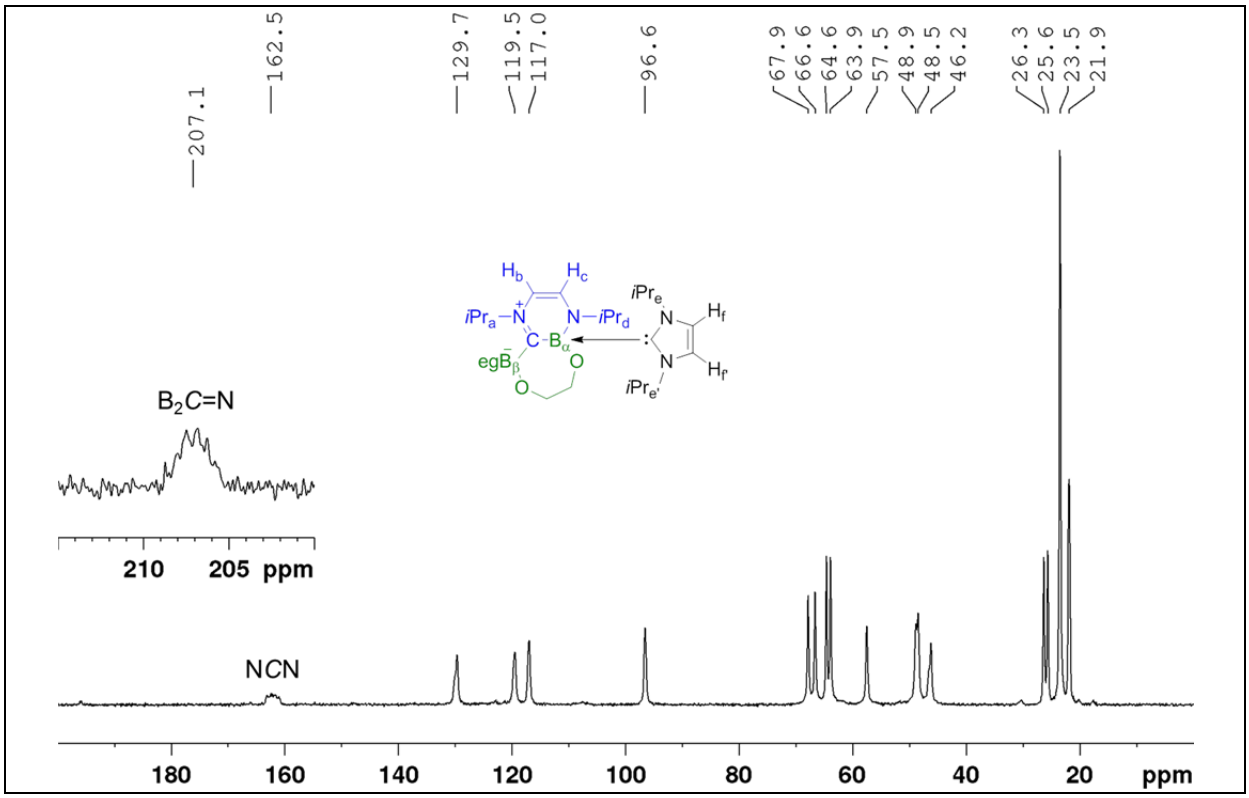

Figure A4.10: ^{13}C CP/MAS NMR spectrum of compound **120** (101 MHz, 22 °C, ν rot = 10000 Hz).

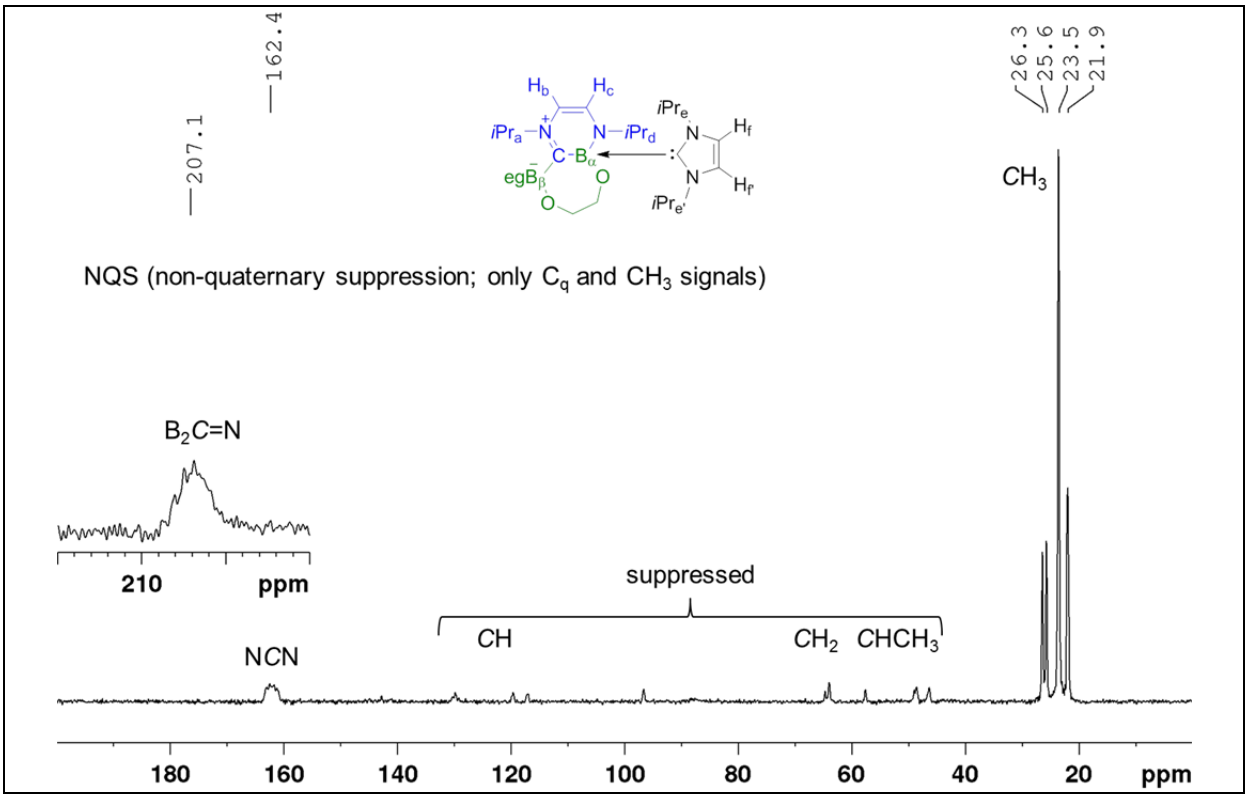

Figure A4.11: ^{13}C CP/NQS/MAS NMR spectrum of compound **120** (101 MHz, 22 °C, ν rot = 12000 Hz).

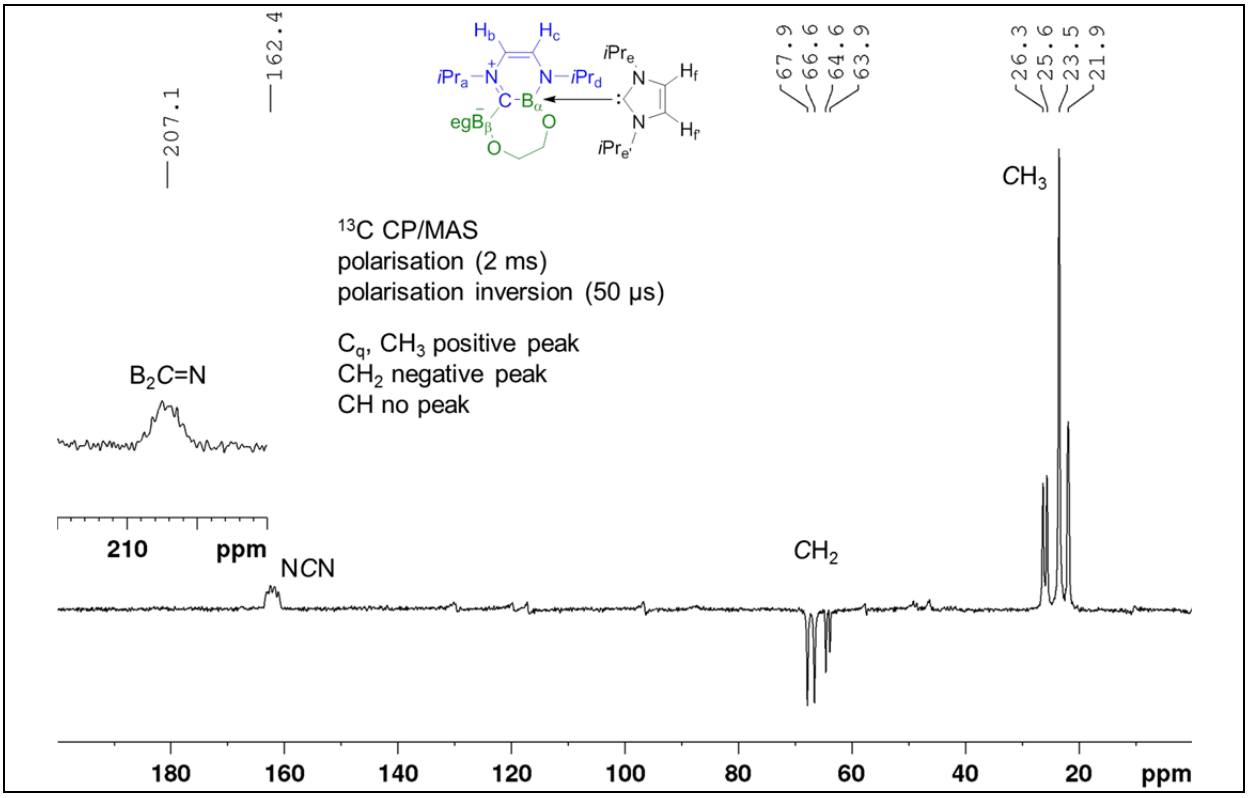

Figure A4.12: ^{13}C CP/PI/MAS NMR spectrum of compound **120** (101 MHz, 22 °C, ν rot = 12000 Hz).

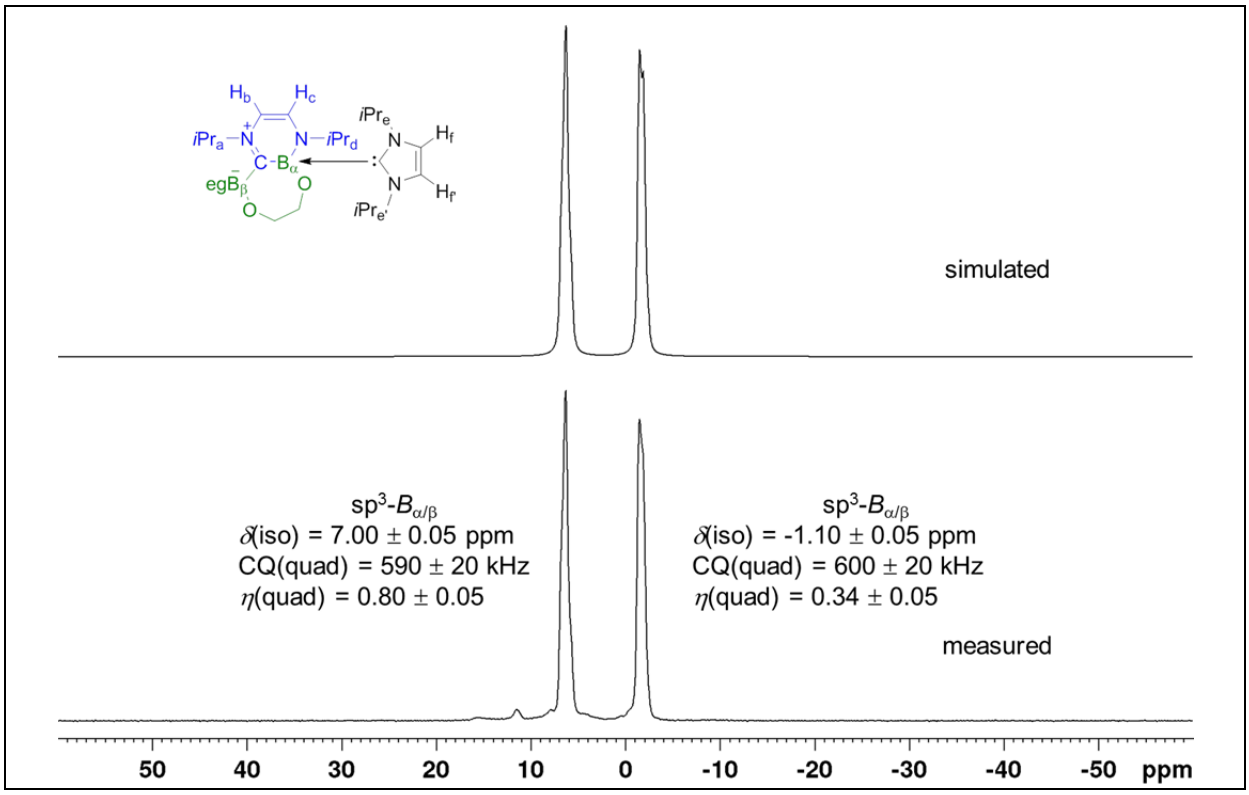

Figure A4.13: ^{11}B RSHE/MAS NMR spectrum of compound **120** (128 MHz, 22 °C, ν rot = 15000 Hz).

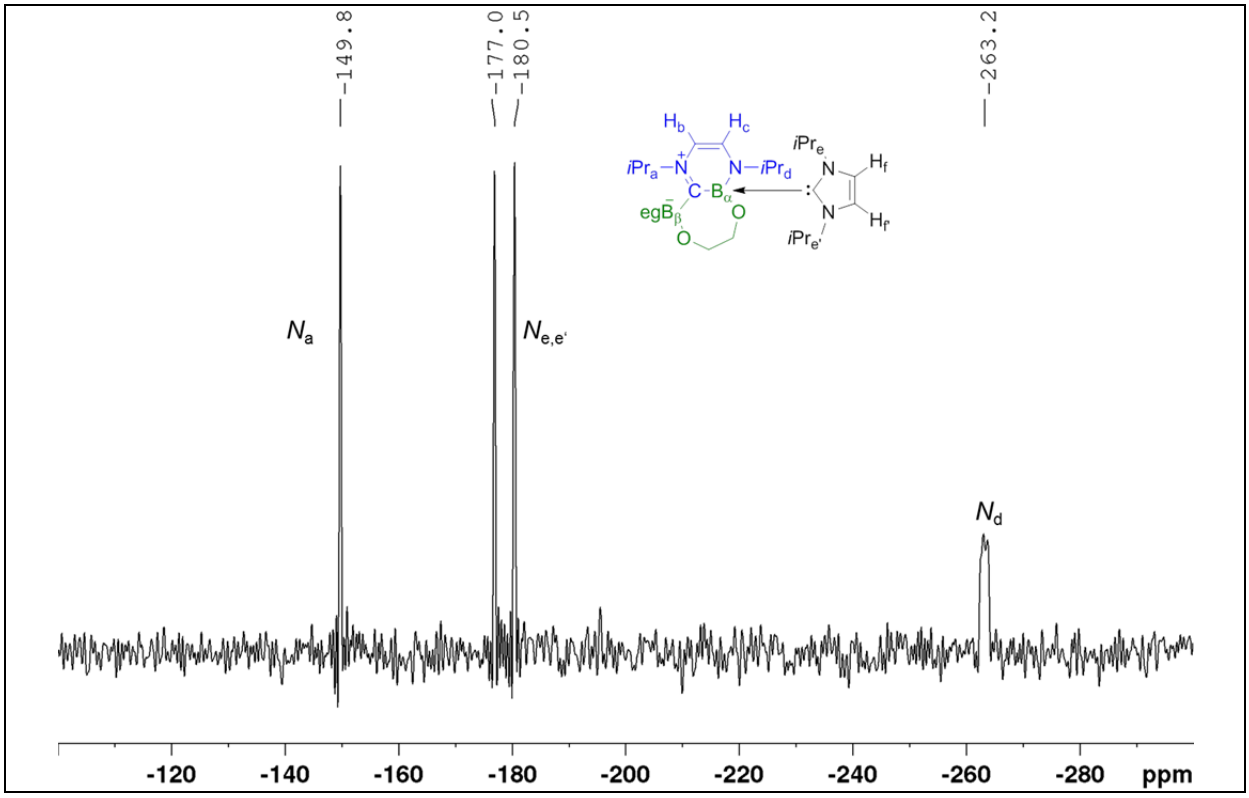

Figure A4.14: ^{15}N CP/MAS NMR spectrum of compound **120** (41 MHz, 22 °C, ν rot = 8000 Hz).

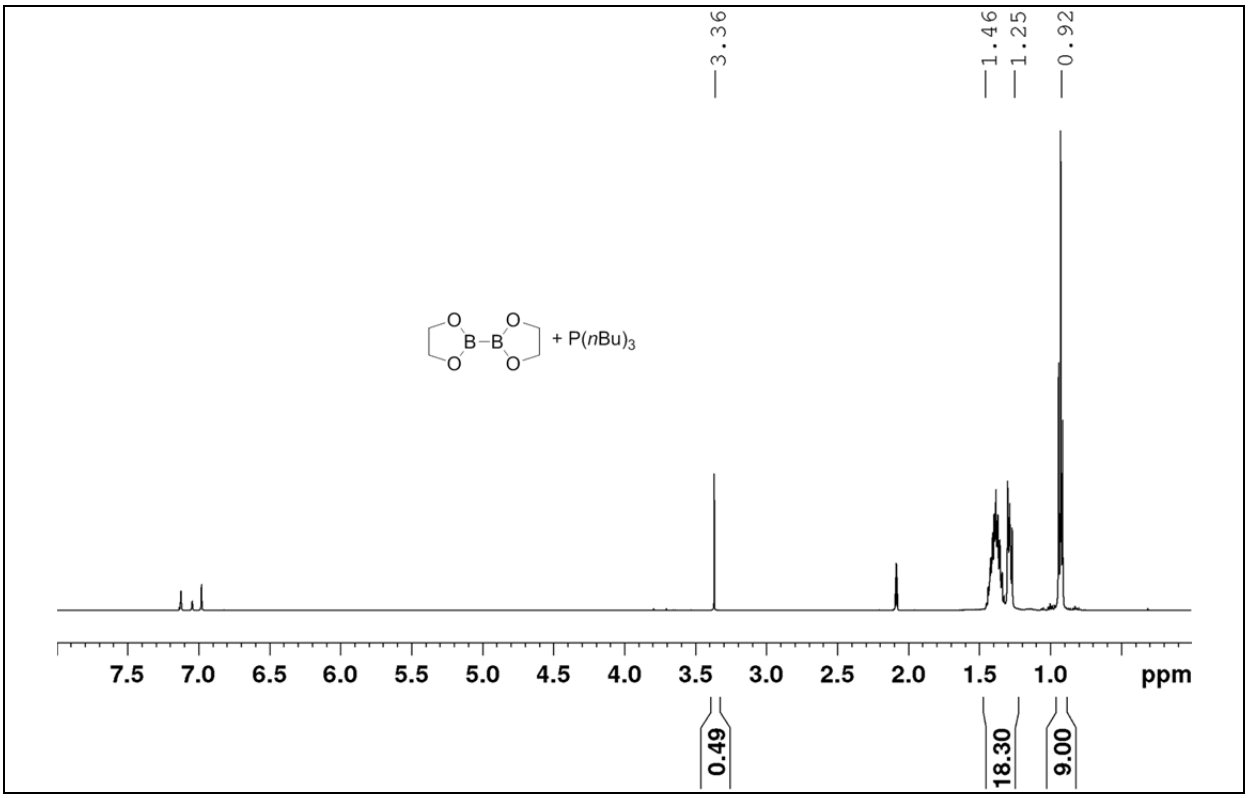

Figure A5.1: *In situ* ^{1}H NMR spectrum of the reaction of B_2eg_2 with P(*n*Bu)$_3$ in d_8-toluene (500 MHz, -40 °C).

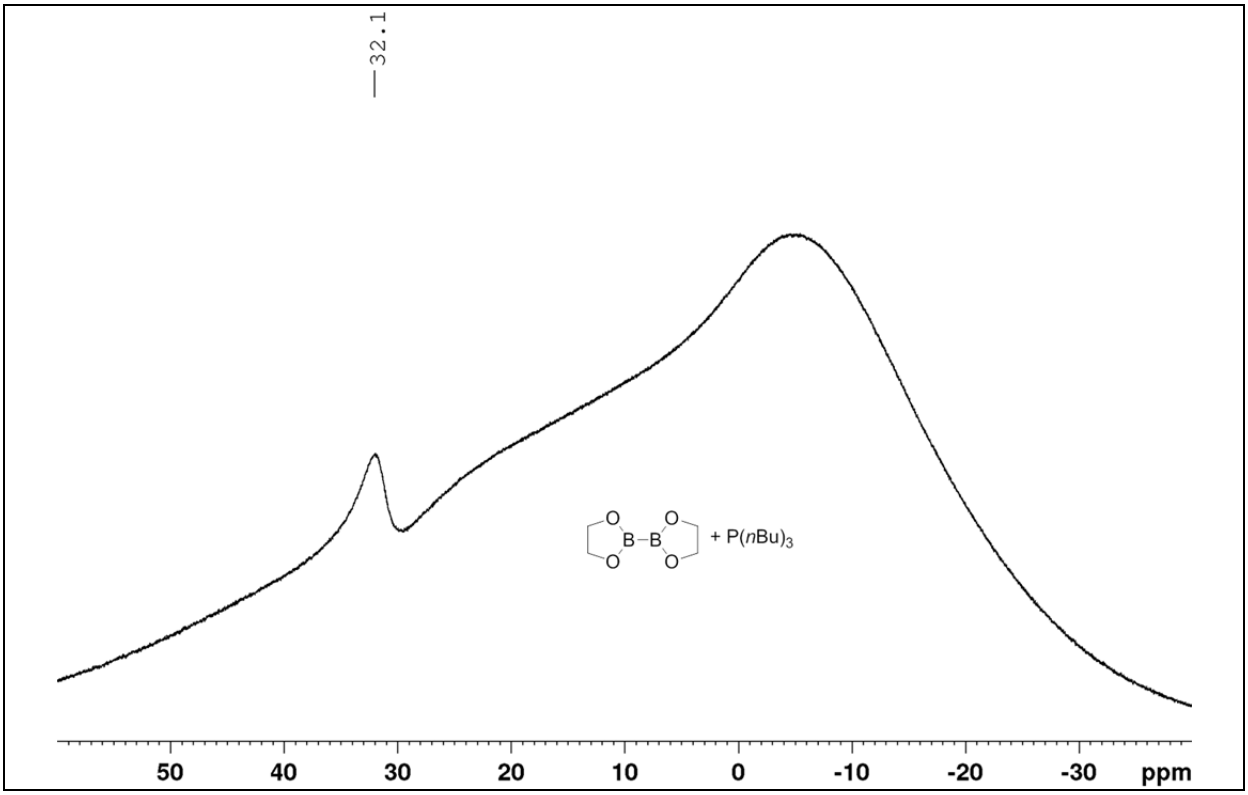

Figure A5.2: *In situ* ^{11}B{^{1}H} NMR spectrum of the reaction of B_2eg_2 with P(*n*Bu)$_3$ in d_8-toluene (160 MHz, -40 °C).

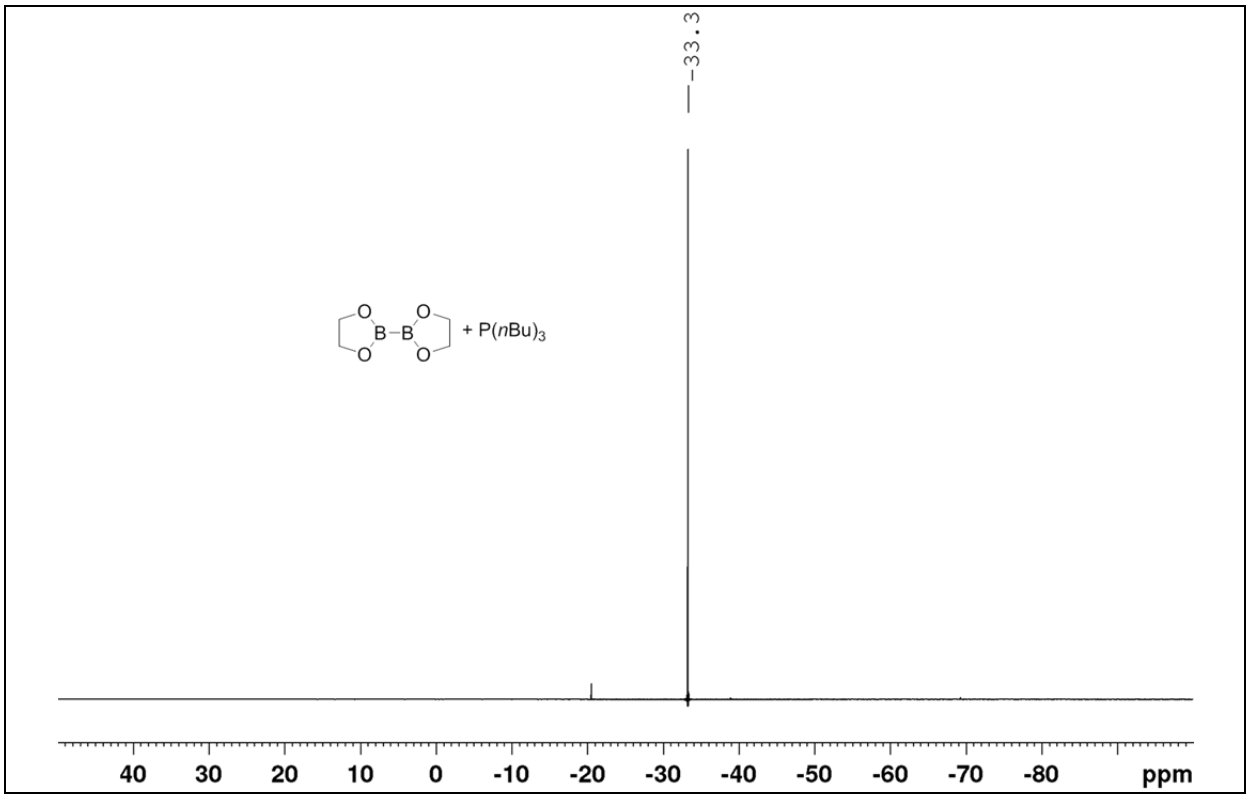

Figure A5.3: *In situ* $^{31}P\{^{1}H\}$ NMR spectrum of the reaction of B_2eg_2 with $P(nBu)_3$ in d_8-toluene (202 MHz, -40 °C).

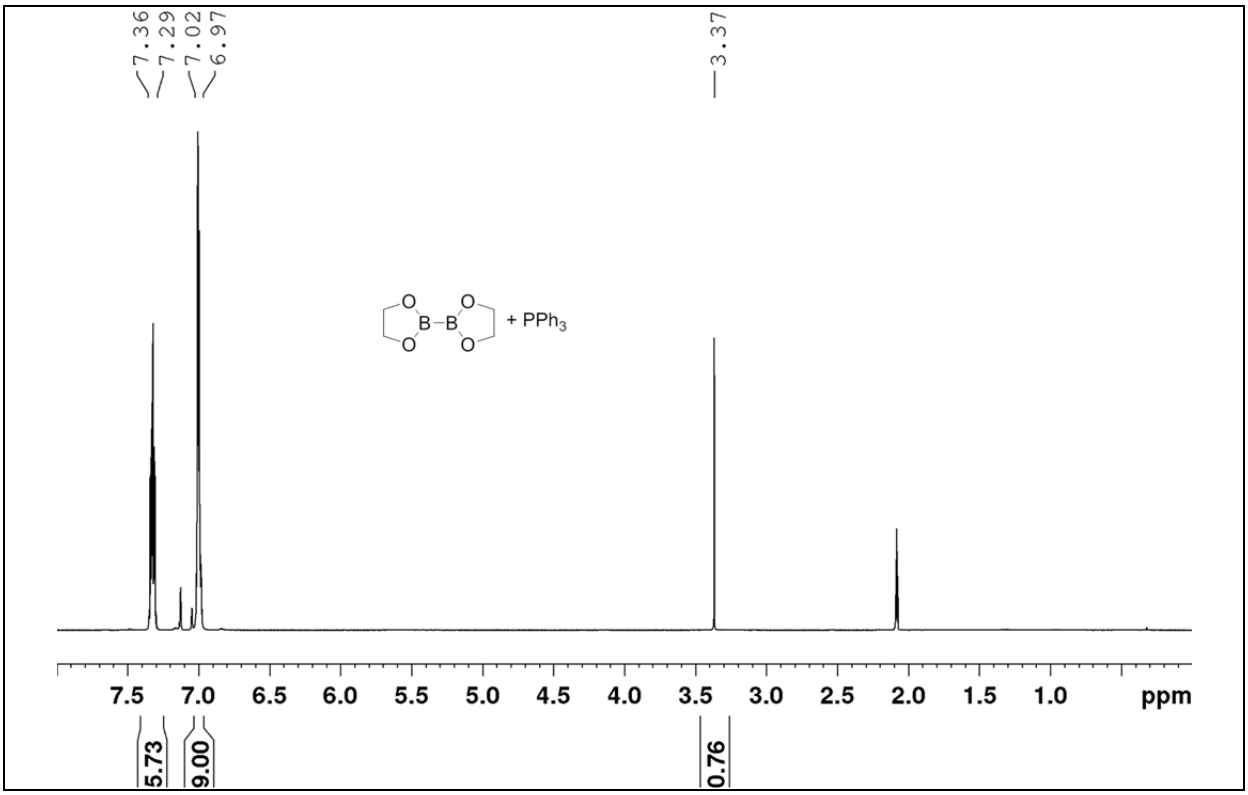

Figure A6.1: *In situ* ^{1}H NMR spectrum of the reaction of B_2eg_2 with PPh_3 in d_8-toluene (500 MHz, -40 °C).

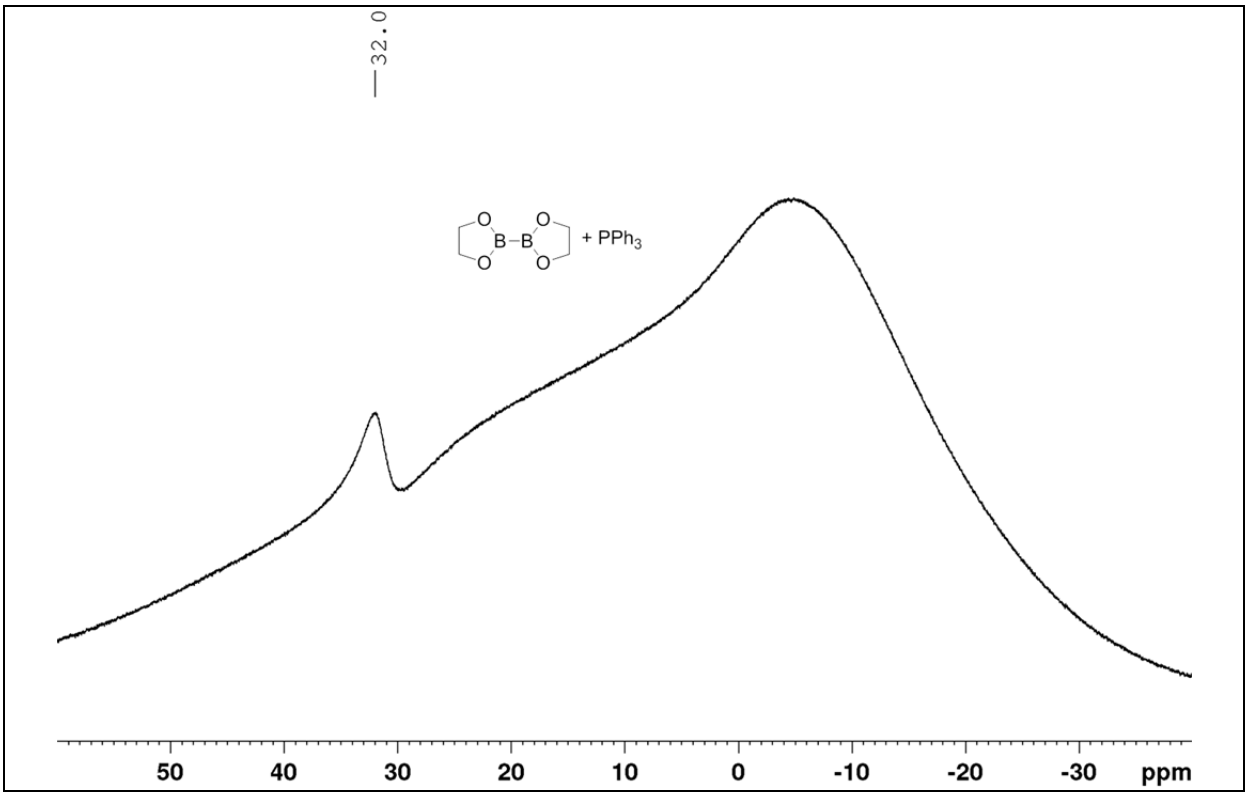

Figure A6.2: *In situ* ^{11}B{^{1}H} NMR spectrum of the reaction of B_2eg_2 with PPh_3 in d_8-toluene (160 MHz, -40 °C).

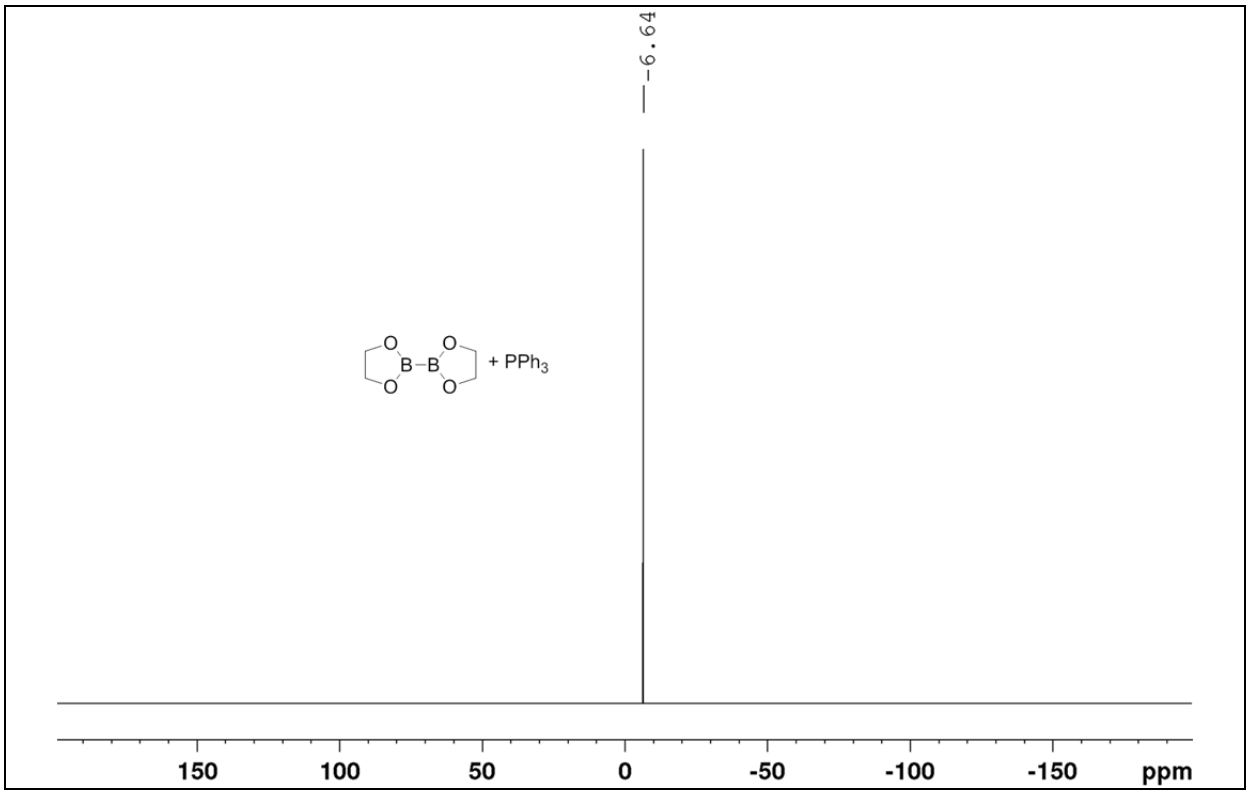

Figure A6.3: *In situ* $^{31}P\{^{1}H\}$ NMR spectrum of the reaction of B_2eg_2 with PPh_3 in d_8-toluene (202 MHz, -40 °C).

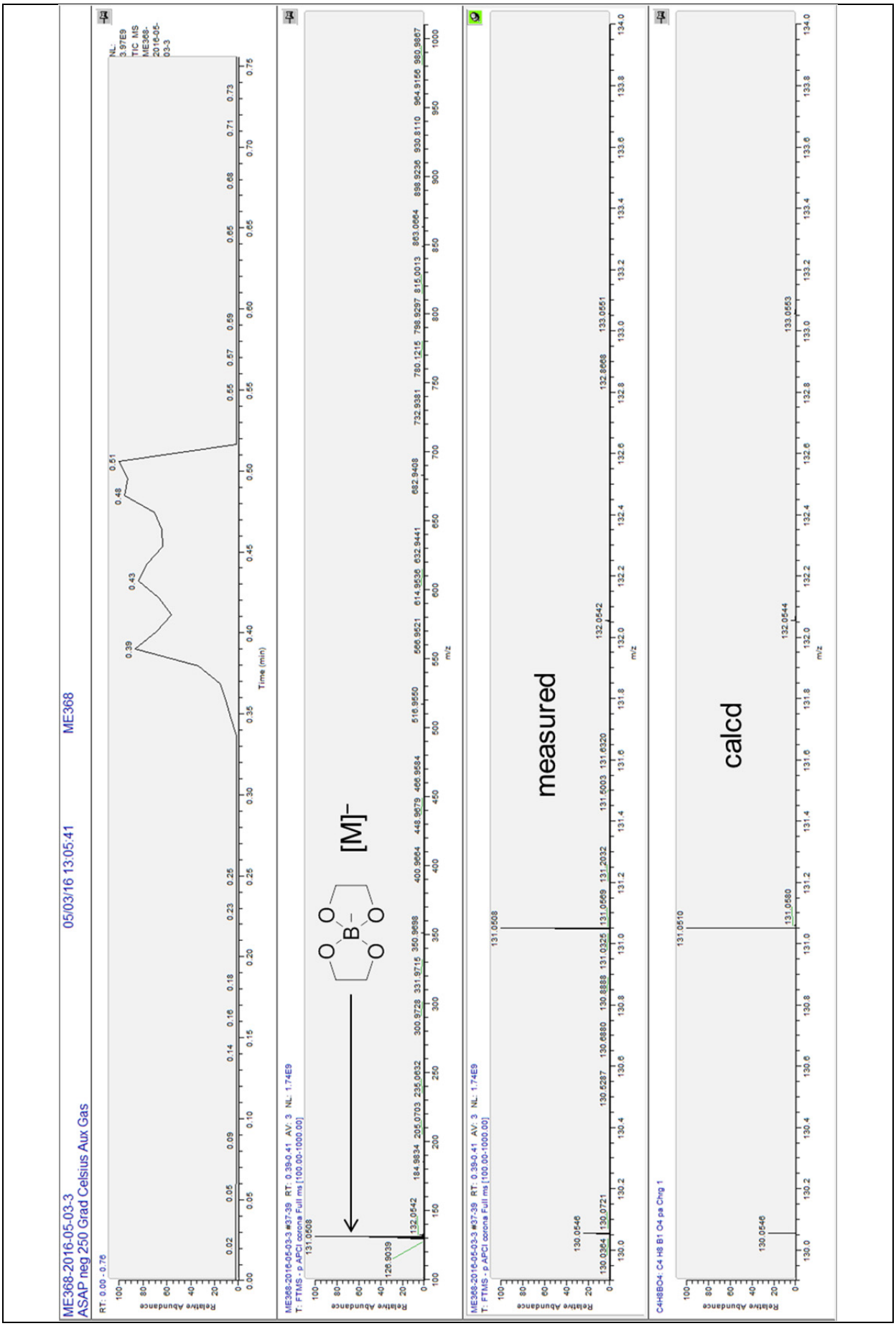

Figure B1.1: HRMS of the obtained solid from the reaction of B_2eg_3 with *i*Pr_2Im; ASAP neg, 250 °C.

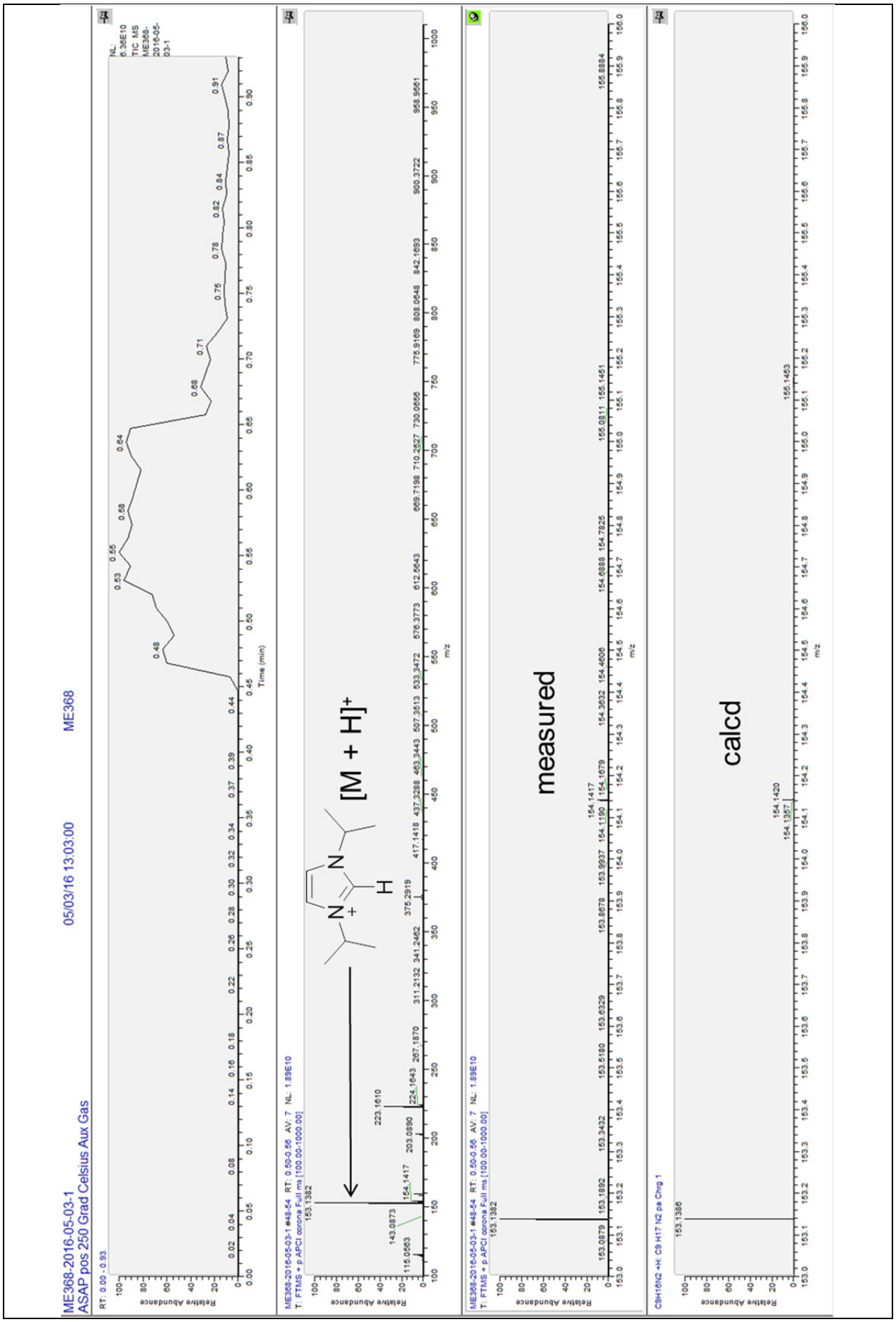

Figure B1.2: HRMS of the obtained solid from the reaction of B_2eg_3 with *i*Pr_2Im; ASAP pos, 250 °C.

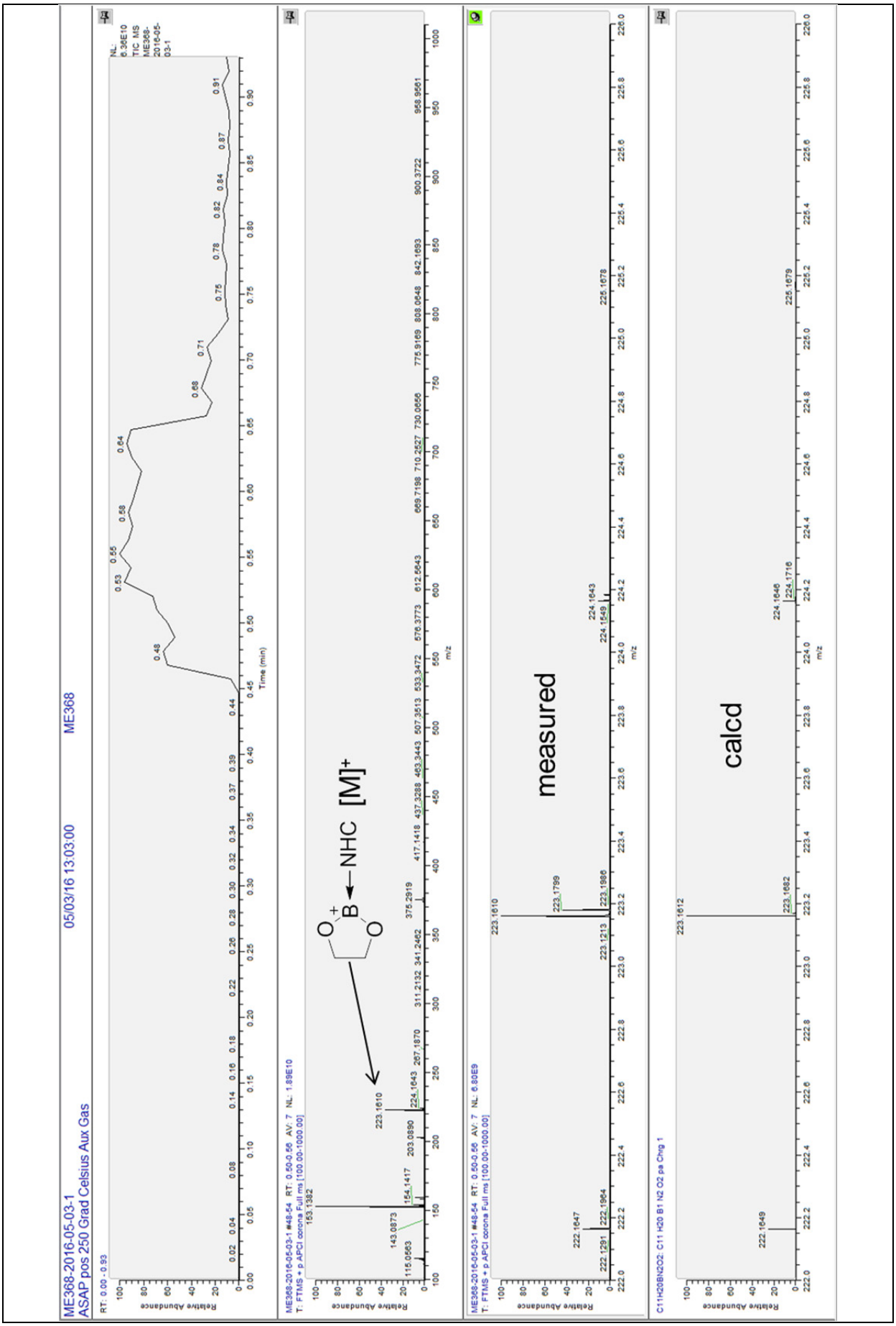

Figure B1.3: HRMS of the obtained solid from the reaction of B_2eg_3 with *i*Pr_2Im; ASAP pos, 250 °C.

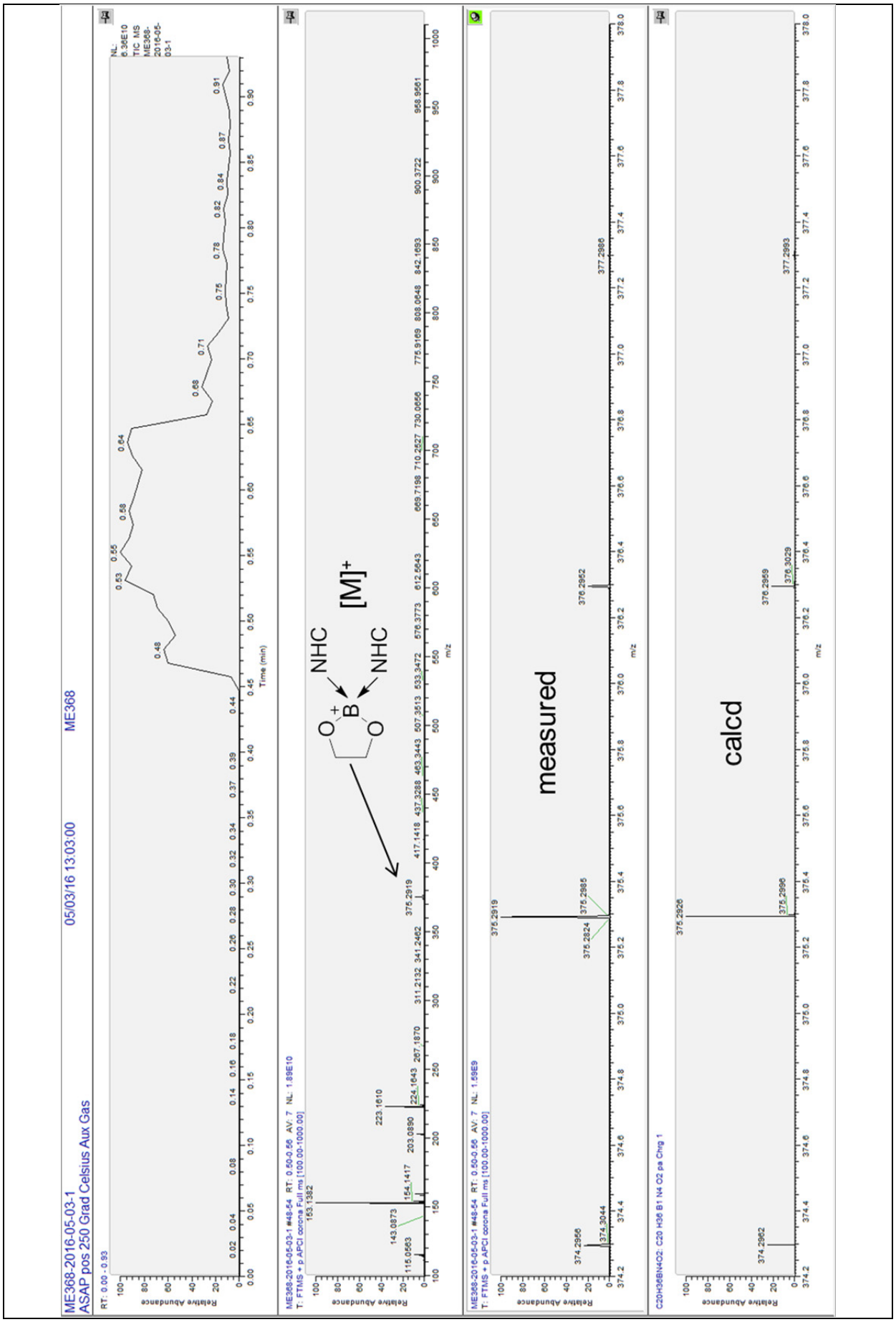

Figure B1.4: HRMS of the obtained solid from the reaction of B_2eg_3 with *i*Pr_2Im; ASAP pos, 250 °C.

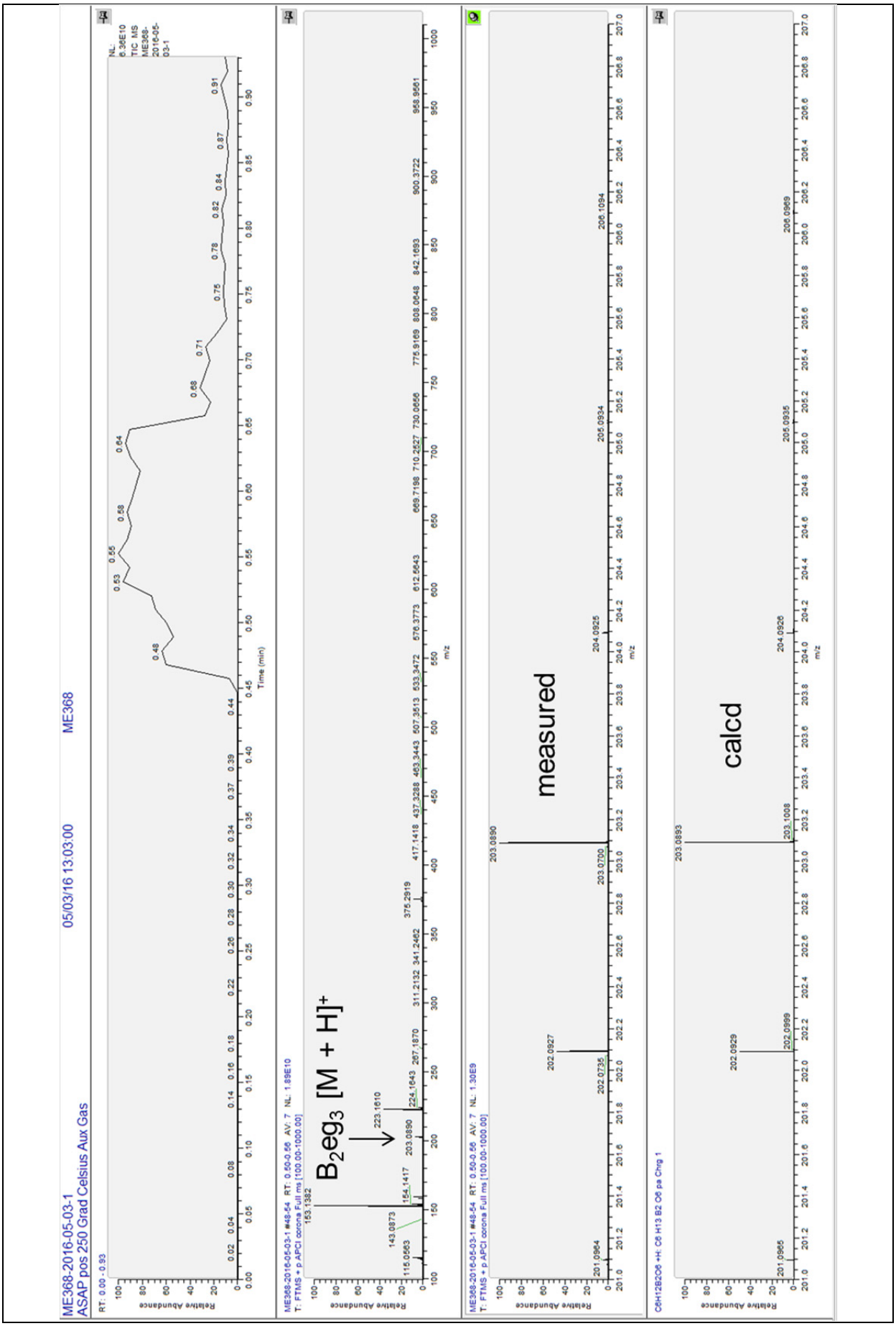

Figure B1.5: HRMS of the obtained solid from the reaction of B_2eg_3 with *i*Pr_2Im; ASAP pos, 250 °C.

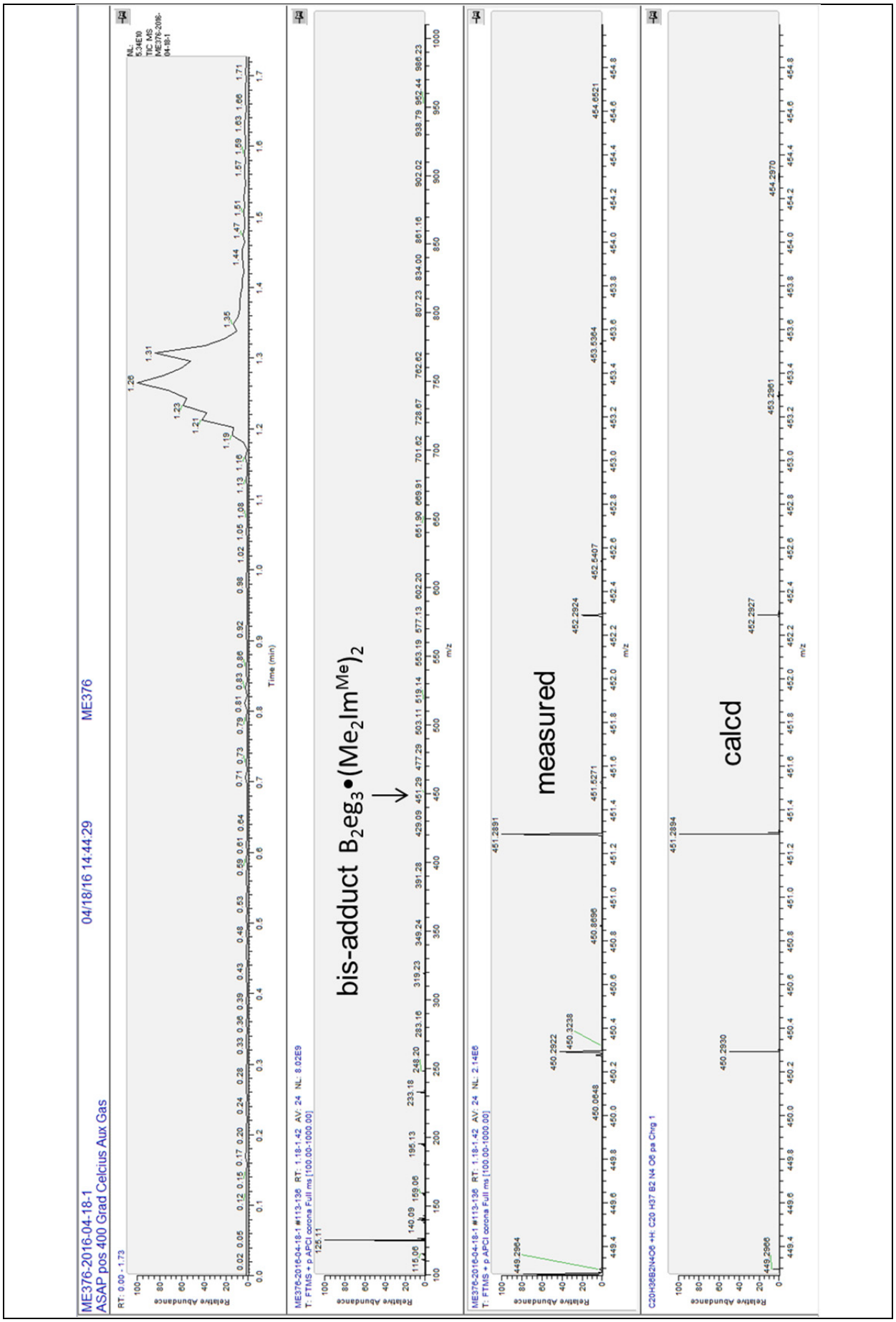

Figure B2.1: HRMS of the obtained solid from the reaction of B_2eg_3 with Me_2Im^{Me}; ASAP pos, 400 °C.

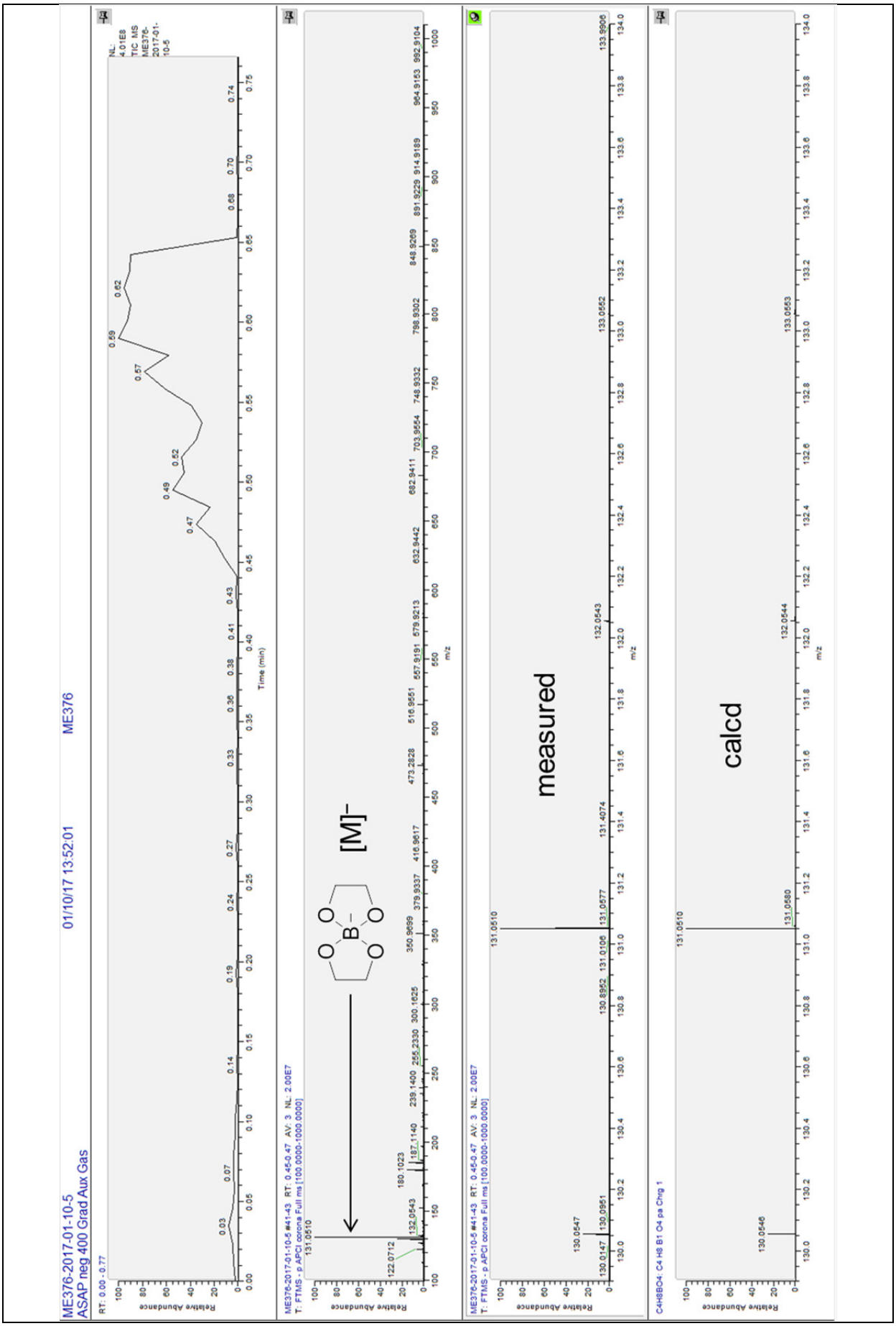

Figure B2.2: HRMS of the obtained solid from the reaction of B_2eg_3 with Me_2Im^{Me}; ASAP neg, 400 °C.

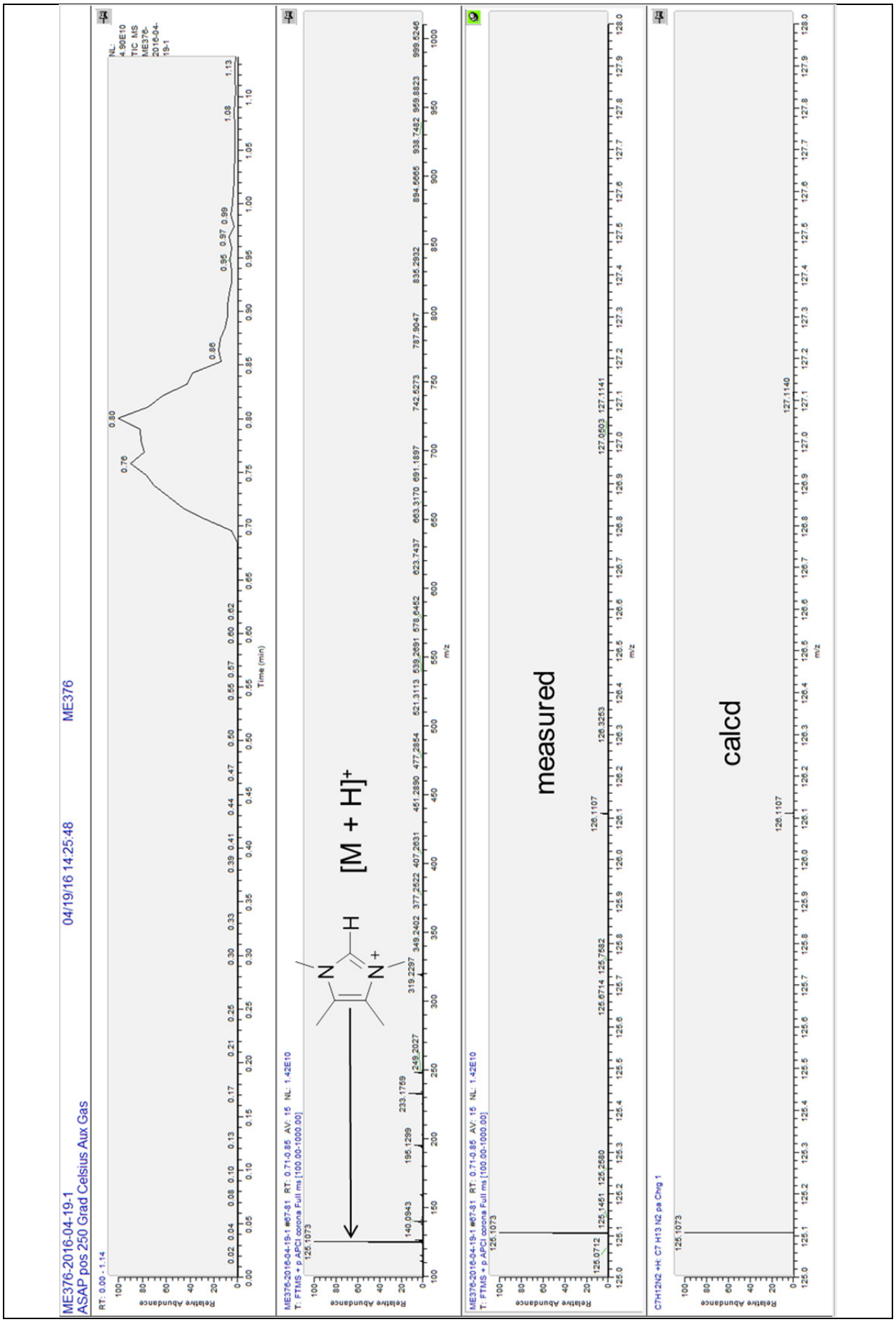

Figure B2.3: HRMS of the obtained solid from the reaction of B_2eg_3 with Me_2Im^{Me}; ASAP pos, 250 °C.

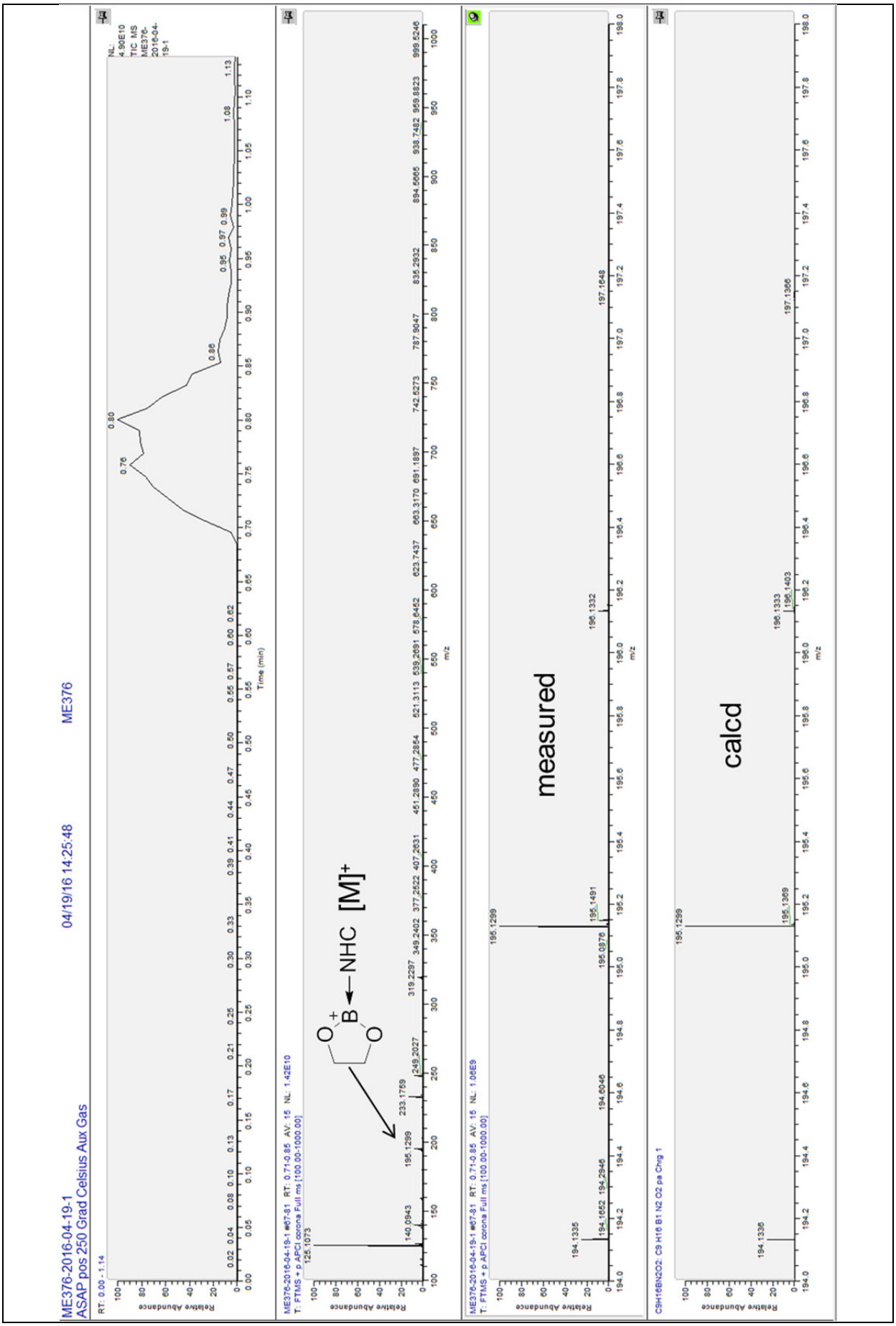

Figure B2.4: HRMS of the obtained solid from the reaction of B_2eg_3 with Me_2Im^{Me}; ASAP pos, 250 °C.

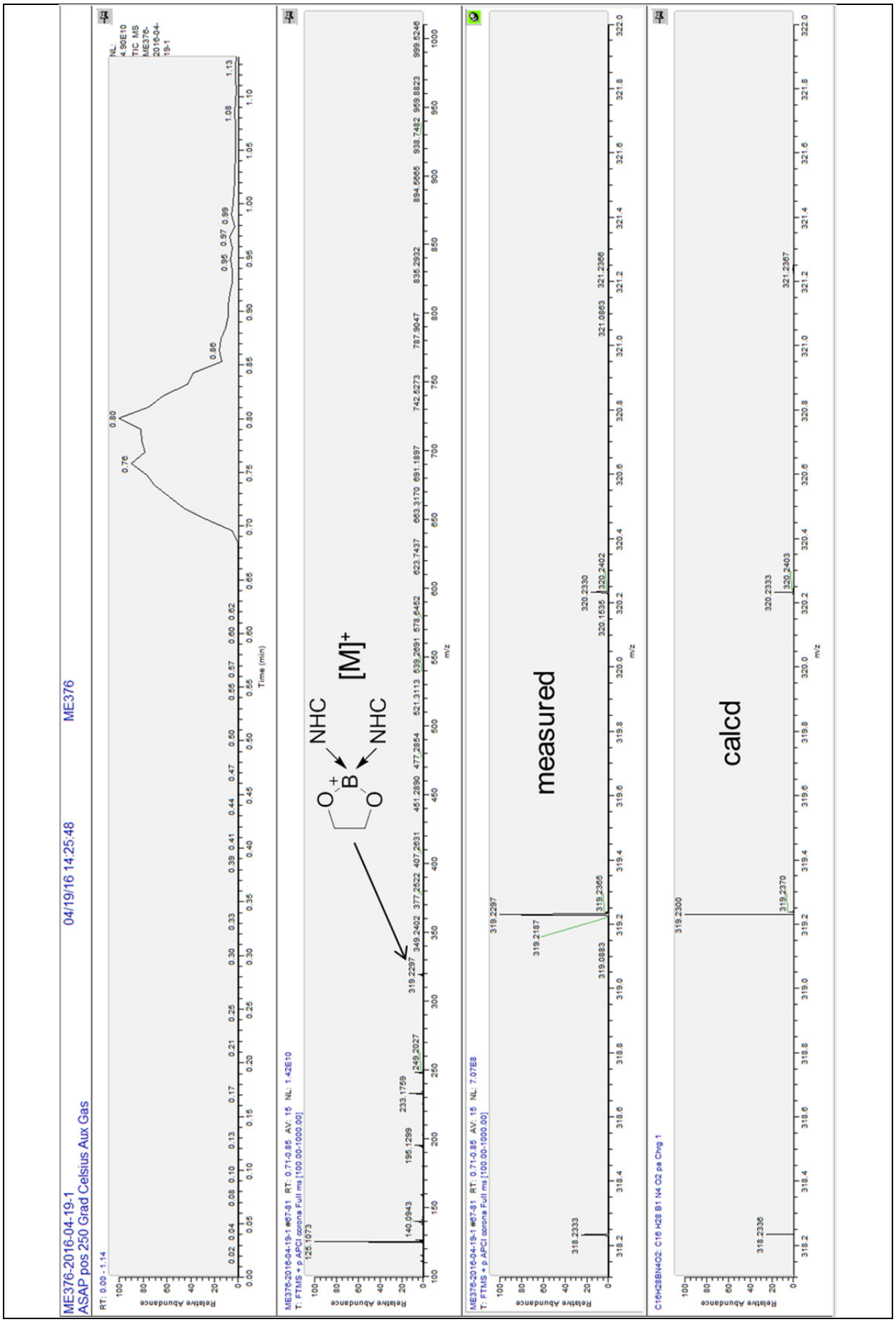

Figure B2.5: HRMS of the obtained solid from the reaction of B_2eg_3 with Me_2Im^{Me}; ASAP pos, 250 °C.

SIGMA-ALDRICH®

sigma-aldrich.com

3050 Spruce Street, Saint Louis, MO 63103, USA
Website: www.sigmaaldrich.com
Email USA: techserv@sial.com
Outside USA: eurtechserv@sial.com

Certificate of Analysis

Product Name:
Iron(II) chloride - anhydrous, beads, -10 mesh, 99.99%

$FeCl_2$

Product Number:	**450936**
Lot Number:	**MKBJ5163V**
Brand:	ALDRICH
CAS Number:	7758-94-3
Formula:	Cl2Fe
Formula Weight:	126.75 g/mol
Quality Release Date:	21 DEC 2011

Test	Specification	Result
Appearance (Color)	Conforms to Requirements	Brown
Light Brown to Brown or Dark Grey		
Appearance (Form)	Beads	Beads
ICP Major Analysis	Confirmed	Conforms
Confirms Iron Component		
Trace Metal Analysis	≤ 200.0 ppm	187.9 ppm
Sodium (Na)		1.6 ppm
Nickel (Ni)		48.7 ppm
Magnesium (Mg)		1.0 ppm
Calcium (Ca)		5.7 ppm
Copper (Cu)		2.9 ppm
Barium (Ba)		0.2 ppm
Yttrium (Y)		0.7 ppm
Zinc (Zn)		0.8 ppm
Aluminum (Al)		0.2 ppm
Cerium (Ce)		0.3 ppm
Silicon (Si)		5.0 ppm
Chromium (Cr)		13.6 ppm
Tungsten (W)		0.1 ppm
Lead (Pb)		0.5 ppm
Manganese (Mn)		98.4 ppm
Cobalt (Co)		<7.7 ppm
Europium (Eu)		0.5 ppm
Purity	Meets Requirements	Meets Requirements
99.99% Based on Trace Metals Analysis		

SIGMA-ALDRICH®

sigma-aldrich.com

3050 Spruce Street,Saint Louis,MO 63103,USA
Website: www.sigmaaldrich.com
Email USA: techserv@sial.com
Outside USA: eurtechserv@sial.com

Certificate of Analysis

Product Name:
Iron(III) chloride - anhydrous, powder, ≥99.99% trace metals basis

Product Number:	**451649**	$FeCl_3$
Lot Number:	**MKBF3598V**	
Brand:	ALDRICH	
CAS Number:	7705-08-0	
Formula:	Cl3Fe	
Formula Weight:	162.20 g/mol	
Quality Release Date:	31 JAN 2011	

Test	Specification	Result
Appearance (Color)	Brown to Black	Brown
Appearance (Form)	Conforms to Requirements	Powder
Powder or Crystalline Powder		
Titration by Na2S2O3	33.9 - 34.9 %	34.7 %
% Fe		
ICP Major Analysis	Confirmed	Conforms
Confirms Iron Component		
Trace Metal Analysis	≤ 100.0 ppm	41.8 ppm
Lithium (Li)		0.2 ppm
Sodium (Na)		5.7 ppm
Potassium (K)		0.6 ppm
Cesium (Cs)		0.3 ppm
Calcium (Ca)		2.4 ppm
Copper (Cu)		24.1 ppm
Zinc (Zn)		1.1 ppm
Hafnium (Hf)		0.2 ppm
Aluminum (Al)		2.0 ppm
Gallium (Ga)		1.3 ppm
Molybdenum (Mo)		0.1 ppm
Lead (Pb)		0.1 ppm
Manganese (Mn)		2.7 ppm
Selenium (Se)		1.0 ppm
Purity	Conforms	Conforms
> = 99.99% Based On Trace Metals Analysis		

SIGMA-ALDRICH® ALDRICH Chemistry

Riedstrasse 2, D-89555 Steinheim/Germany
Tel: +49 73 2997 2550 Fax: +49 73 2997 2557

Certificate of Analysis

Product Name:	POTASSIUM METHOXIDE 95 %
Product Number:	292788
Product Brand:	Aldrich
Molecular Formula:	CH_3KO
Molecular Mass:	70.13
CAS Number:	865-33-8

TEST	SPECIFICATION	LOT STBC3538V RESULTS
APPEARANCE (COLOR)	WHITE	WHITE
APPEARANCE (FORM)	POWDER	POWDER
TITRATION (T) HCL 0.1M	≥ 94.0%	96.3 %
	≤ 6.0% TOTAL K2CO3 AND KOH IMPURITIES	< 3.0 %
INFRARED SPECTRUM	CONFORMS TO STRUCTURE	CONFORMS
QC RELEASE DATE	14/SEP/11	

Claudia Mayer, Manager
Quality Control
Steinheim, Germany

Certificate of Analysis

Alfa Aesar
A Johnson Matthey Company

Product Number:	12887
Product:	Cesium carbonate 99 % (metals basis)
Lot no:	61200333

Assay Cs_2CO_3	99.9 %
Li	< 0.2 mg / kg
Na	65 mg / kg
K	150 mg / kg
Rb	140 mg / kg
Ca	0.7 mg / kg
Mg	< 0.1 mg / kg
Sr	1.0 mg / kg
Ba	3 mg / kg
Al	0.3 mg / kg
Fe	0.9 mg / kg
Cr	0.8 mg / kg
P_2O_5	< 0.5 mg / kg
SO_4	11 mg / kg
NO_3	< 5 mg / kg
Cl	48 mg / kg
SiO_2	5 mg / kg
Loss of weight / 500 °C	< 0.1 %
CsOH	< 0.1 %

This document has been electronically generated and does not require a signature.

www.alfa.com

NORTH AMERICA
Tel: +1-800-343-0660 or +1-978-521-6300
Fax: +1-800-322-4757
Email: info@alfa.com

GERMANY
Tel: 00800 4566 4566 or +49 721 84007 280
Fax: 00800 4577 4577 or +49 721 84007 300
Email: Eurosales@alfa.com

UNITED KINGDOM
Tel: 0800-801812 or +44 (0)1524-850506
Fax: +44 (0)1524-850608
Email: UKsales@alfa.com

FRANCE
Tel: 0800 03 51 47 or +33 (0)3 8862 2690
Fax: 0800 10 20 67 or +33 (0)3 8862 6864
Email: frventes@alfa.com

INDIA
Tel: +91 8008 812424 or +91 8008 812525 or +91 8008 812626
Fax: +91 8418 260060
Email: India@alfa.com

CHINA
Tel: +86 (010) 8567-8600
Fax: +86 (010) 8567-8601
Email: salechina@alfa-asia.com

KOREA
Tel: +82-2-3140-6000
Fax: +82-2-3140-6002
Email: salekorea@alfa-asia.com

Certificate of Analysis

Alfa Aesar
A Johnson Matthey Company

Lithium tert-butoxide, 99.9% (metals basis)

Stock Number: 44133
Lot Number: B09X005

Analysis

Appearance	White powder
Assay (acidimetric)	99.9 %
$LiOH + Li_2CO_3$ (K.F.)	0.1 % as LiOH
Cl (wet test)	< 300 ppm

Ba	< 50
Ca	< 50
Fe	< 10
K	65
Mg	< 50
Na	350
Zn	< 10

Values given in ppm unless otherwise stated
Trace impurities determined by FE/ICP

Certified by:

Quality Control

This document has been electronically generated and does not require a signature.

www.alfa.com

NORTH AMERICA
Tel: +1-800-343-0660 or +1-978-521-6300
Fax: +1-800-322-4757
Email: info@alfa.com

GERMANY
Tel: 00800 4566 4566 or +49 721 84007 280
Fax: 00800 4577 4577 or +49 721 84007 300
Email: Eurosales@alfa.com

UNITED KINGDOM
Tel: 0800-801812 or +44 (0)1524-850506
Fax: +44 (0)1524-850608
Email: UKsales@alfa.com

FRANCE
Tel: 0800 03 51 47 or +33 (0)3 8862 2690
Fax: 0800 10 20 67 or +33 (0)3 8862 6864
Email: frventes@alfa.com

INDIA
Tel: +91 8008 812424 or +91 8008 812525 or +91 8008 812626
Fax: +91 8418 260060
Email: India@alfa.com

CHINA
Tel: +86 (010) 8567-8600
Fax: +86 (010) 8567-8601
Email: salechina@alfa-asia.com

KOREA
Tel: +82-2-3140-6000
Fax: +82-2-3140-6002
Email: salekorea@alfa-asia.com

B–B bond activation and NHC ring-expansion reactions of diboron(4) compounds, and accurate molecular structures of $B_2(NMe_2)_4$, B_2eg_2, B_2neop_2 and B_2pin_2

M. Eck, S. Würtemberger-Pietsch, A. Eichhorn, J. H. J. Berthel, R. Bertermann, U. S. D. Paul, H. Schneider, A. Friedrich, C. Kleeberg, U. Radius and T. B. Marder, *Dalton Trans.*, 2017, **46**, 3661
DOI: 10.1039/C7DT00334J